# TECHNISCHE UNIVERSITÄT MÜNCHEN

## Institute for Advanced Study

# Synthesis of Mono- and Divalent Integrin Antagonists for Surface Coating and Imaging

Alexander Dominic Bochen

Vollständiger Abdruck der von der Fakultät für Chemie der Technischen Universität München zur Erlangung des akademischen Grades eines

Doktors der Naturwissenschaften

genehmigten Dissertation.

Vorsitzender: Univ.-Prof. Dr. Steffen Glaser

Prüfer der Dissertation:

1. Univ.-Prof. Dr. Dr. h.c. Horst Kessler
2. Univ.-Prof. Dr. Aphrodite Kapurniotu

Die Dissertation wurde am 10.10.2012 bei der Technischen Universität München eingereicht und durch die Fakultät für Chemie am 20.03.2013 angenommen.

Die vorliegende Arbeit wurde im Zeitraum von April 2008 bis September 2012 am Department Chemie der Technischen Universität München unter Anleitung von Prof. Dr. Horst Kessler angefertigt.

*meinen Eltern*

An expert is a person who has made all mistakes that can be made in a very narrow field.
*(Niels Bohr)*

Wer nie einen Fehler gemacht hat, hat nie etwas Neues probiert.
*(Albert Einstein)*

# Danksagungen

Meinem Doktorvater Prof. Dr. Horst Kessler danke ich für die interessante Themenstellung, die ausgezeichneten Arbeitsbedingungen und die weitreichenden Freiheiten bei der Ausgestaltung der Arbeit. Weiter gilt mein Dank seinem Interesse an meiner Arbeit und seiner steten Unterstützung.

Mein weiterer Dank gilt:

Meinen Laborkollegen Dr. Lucas Doedens, Dr. Dominik Heckmann, Dr. Carles Mas-Moruno, Dr. Elke Otto, Markus Bollinger, Tobias Knapp, Stefanie Neubauer und Florian Rechenmacher für die gute Zusammenarbeit.

Dr. Johannes Beck und Dr. Udaya Kiran Marelli für die Zusammenarbeit bei Struktur- und NMR-Fragestellungen.

Für den hochinteressanten Aufenthalt am Max-Planck Institute for Intelligent Systems, Stuttgart, Prof. Dr. Joachim Spatz & Dr. Heike Böhm für die herzliche Aufnahme in ihren Arbeitskreis, sowie der gesamten Gruppe für den angenehmen Aufenthalt.

Dr. Diego Pallarola für die hervorragende Zusammenarbeit auf dem Gebiet der nanostrukturierten Goldoberflächen und den offenen wissenschaftlichen Austausch.

Dr. Iina Laitinen für interessante Gespräche und die gute Zusammenarbeit auf dem Gebiet des *Rat Myocardial Infarction Models*.

Meinen zahlreichen Studenten für die geleistete Arbeit.

Für schöne Bergtouren Dr. Timo Huber, Dr. Franz Hagen und Dr. Florian Manzenrieder.

Großer Dank gilt auch meinen Freunden mit denen ich in den letzten Jahren viel erleben durfte und so die nötige Abwechslung vom Laboralltag bekommen konnte.

Meinen Eltern bin ich unendlich dankbar für ihre stete Unterstützung während des Studiums und der Promotion und dass sie mir meine Entwicklung in diesem Maße ermöglicht haben.

Zuletzt gebührt mein außerordentlicher Dank meiner Freundin Kathrin Steib für die Unterstützung, Verständnis und Rückhalt in allen Höhen und Tiefen die es während des Studiums und Promotionsvorhabens zu durchleben gilt.

# Scientific Record

## Publications

**A. Bochen**, D. Pallarola, H. Böhm, J.P. Spatz, H. Kessler. Impact of RGD-functionalized Poyproline Spacers on Integrin Mediated Cell Adhesion to Gold Nanoparticle Coated Surfaces. *Manuscript in preparation,* September **2012**.

M. Bollinger, B. H. Yousefi, **A. Bochen**, I. Laitinen, T. Petzold, M. Schwaiger, H. Kessler, H.-J. Wester. Direct One-Step $^{18}$F-Labeling of a New Highly Active αIIbβ3 Integrin Antagonist via Nucleophilic Aromatic Substitution, *Manuscript in preparation,* September **2012.**

**A. Bochen**, U. K. Marelli, E. Otto, D. Pallarola, C. Mas-Moruno, F. S. Di Leva, H. Boehm, J. P. Spatz, E. Novellino, H. Kessler, L. Marinelli. Biselectivity of *iso*DGR Peptides for Fibronectin Binding Integrin Subtypes α5β1 and αvβ6: Conformational Control through Flanking Amino Acids. Manuscript submitted to *Journal of Medicinal Chemistry*, August **2012**.

M. Bollinger, F. Manzenrieder, R. Kolb, **A. Bochen**, S. Neubauer, L. Marinelli, V. Limongelli, E. Novellino, G. Moessmer, R. Pell, W. Lindner, J. Fanous, A. Hoffman, H. Kessler. Tailoring of Integrin Ligands: Probing the Charge Capability of the Metal-Ion-Dependent Adhesion Site. *Journal of Medicinal Chemistry* **2012**, *55*, 871-882.

A.O. Frank, E. Otto, C. Mas-Moruno, H.B. Schiller, L. Marinelli, S. Cosconati, **A. Bochen**, D. Vossmeyer, G. Zahn, R. Stragies, E. Novellino, H. Kessler. Conformational Control of Integrin Subtype Selectivity in *iso*DGR Peptide Motives: A Biological Switch. *Angewandte Chemie International Edition* **2010**, *49*, 9278-9281.

## Oral Presentations

“Polyproline based spacers linking *cyclo*-RGDfE to nano-structured gold surfaces for investigation of integrin mediated cell adhesion” 22$^{nd}$ American Peptide Symposium 2011, June 26$^{th}$ **2011**, San Diego, USA.

## Poster Presentations

**A. Bochen**, D. Pallarola, H. Böhm, J.P. Spatz, H. Kessler, „Polyproline based spacers of different lengths linking *cyclo*-RGDfE by “click-chemistry” for attachment to nanostructured gold surfaces to improve cell adhesion”, 22$^{nd}$ American Peptide Symposium 2011, June 25$^{th}$-30$^{st}$ **2011**, San Diego, USA.

M. Bollinger, F. Manzenrieder, **A. Bochen**, G. Mössmer, H.Kessler, „Platelet Aggregation Inhibition by a new class of Glycoprotein IIb/IIIa Inhibitors“, 22nd American Peptide Symposium 2011, June 25th – 30st **2011**, San Diego, USA.

F. Rechenmacher, S. Neubauer, C. Mas-Moruno, **A. Bochen**, P. Kleiner, R. Burgkart, A. Schwede, J.P. Spatz, H. Kessler, „Functionalization of Peptidomimetic Integrin Ligands with Thiols and Phosphonates for Surface Coating“, 5th International Peptide Symposium 2010, December 4th – 9th **2010**, Kyoto, Japan.

M. Bollinger, F. Manzenrieder, R. Kolb, **A. Bochen**, L. Marinelli, V. Limongelli, R. Pell, W. Lindner, H. Kessler, „Probing the Charge Capability of the MIDAS: Phosphinic and Phosphonic acid containing compounds as new potent αIIbβ3 Integrin Antagonists”, 5th International Peptide Symposium 2010, December 4th – 9th **2010**, Kyoto, Japan.

**A. Bochen**, H. Kessler, „RGD-containing mono- and oligomeric polyprolines as large molecular rulers”, 31st European Peptide Symposium 2010, September 5th – 9th **2010**, Copenhagen, Denmark.

S. Neubauer, F. Rechenmacher, C. Mas-Moruno**, A. Bochen**, P. Kleiner, A. Schwede, J.P. Spatz, H. Kessler, „Highly active and selective Integrin Ligands and their Application for surface coating via thiol anchoring”, 31st European Peptide Symposium 2010, September 5th – 9th **2010**, Copenhagen, Denmark.

# Abbreviations

| | |
|---|---|
| AA | Amino acid |
| ACN | Acetonitrile |
| $Ac_2O$ | Acetic acid anhydride |
| AcOH | Acetic acid |
| ADMIDAS | Adjacent metal ion-dependent adhesion site |
| Ahx | Aminohexanoic acid |
| Alloc | Allyloxycarbonyl |
| Bn | Benzyl |
| BOC | *tert*-Butyloxycarbonyl |
| $^{t}$Bu | *tert*-Butyl |
| $^{t}$BuOH | *tert*-Butanol |
| BSA | Bovine serum albumin |
| Cbz | Carboxybenzyl |
| Cl-TCP | Tritylchloridpolystyrene |
| COMU | (1-Cyano-2-ethoxy-2-oxoethylidenaminooxy)dimethylamino-morpholino-carbenium hexafluorophosphate |
| Cta | Cystamine |
| DAPI | 4',6-diamidino-2-phenylindole |
| DCC | Dicyclohexylcarbodiimide |
| DCM | Dichlormethane |
| DDTC | *N*,*N*-Diethyldithiocarbamate |
| DIEA | Diisopropylethylamine |
| DMA | *N,N*-Dimethylacetamid |
| DMF | *N,N*-Dimethylformamid |
| DMSO | Dimethylsulfoxide |
| DPPA | Diphenylphosphoryl azide |
| ECM | Extracellular matrix |
| ELISA | Enzyme linked immune sorbent assay |
| equiv. | Equivalent |
| ESI | Electrospray ionization |
| EtOH | Ethanol |

| | |
|---|---|
| $Et_2O$ | Diethyl ether |
| Fbg | Fibrinogen |
| Fmoc | 9-Fluorenylmethyloxycarbonyl |
| Fn | Fibronectin |
| HATU | *N,N,N′,N′*-Tetramethyl-*O*-(7-azabenzotriazol-1-yl)uronium hexafluorophosphate |
| Hegas | Heptaethylene glycol amino acid |
| HFIP | Hexafluorisopropanol |
| HOAt | 1-Hydroxy-7-azabenzotriazole |
| HOBt | 1-Hydroxybenzotriazol |
| $IC_{50}$ | Inhibition constant 50 |
| ITC | Isothiocyanate |
| ivDde | 1-(4,4-Dimethyl-2,6-dioxocyclohex-1-ylidene)-3-methyl-butyl |
| LAP | Latency associated peptide |
| LIMBS | Ligand induced metal binding site |
| MD | Molecular dynamics |
| MeOH | Methanol |
| MIDAS | Metal ion-dependent adhesion site |
| MPA | Mercaptopropionic acid |
| MS | Mass spectrometry |
| NaAsc | Sodium ascorbate |
| NF-31 | 4-Nitrophenyl-5-[*N*-ethyl-*N*-[4-(4-Nitrophenyl)azo]phenyl]-amino-3-oxapentanoate |
| NHS | *N*-Hydroxysuccinimide |
| NMP | *N*-Methylpyrrolidone |
| NMR | Nuclear magnetic resonance |
| NODAGA | 2-(4,7-*bis*(carboxymethyl)-1,4,7-triazonan-1-yl)pentanedioic acid |
| Oxyma | Ethyl (hydroxyimino)cyanoacetate |
| Pbf | 2,2,4,6,7-Pentamethyldihydrobenzofuran-5-sulfonyl |
| PBS | Phosphate buffered saline |
| PBST | Phosphate buffered saline tween-20 |
| PEG | Polyethylene glycol |
| PET | Positron emission tomography |
| PP | Polypropylene |

| | |
|---|---|
| PyAOP | (7-Azabenzotriazol-1-yloxy)tripyrrolidinophosphonium hexafluorophosphat |
| PyBOP | benzotriazol-1-yl-oxytripyrrolidinophosphonium hexafluorophosphate |
| RP-HPLC | Reversed phase high performance liquid chromatography |
| SPPS | Solid phase peptide synthesis |
| TBTU | *O*-(1H-Benzotriazol-1-yl)-*N,N,N′,N′*-tetramethyluronium-tetrafluoroborat |
| TCP | Tritylchlorid polystyrene |
| TFA | Trifluoracetic acid |
| TFE | Trifluorethanol |
| TIPS | Triisopropylsilan |
| TM | Transmembrane |
| TMB | 3,3′,5,5′-tetramethylbenzidine |
| Trt | Trityl |
| Vn | Vitronectin |

# Table of Contents

# 1. Introduction

In every living being the essential information about the generation of all proteins is encoded by nucleic acids, like DNA, RNA or plasmids. In this way, the information is stored rather safely with regards to unwanted modifications, but needs to be transcribed and translated into the structure it encodes. These encoded structures are proteins which can interact with other proteins or modify substrates in terms of creating a use for the organism. The building blocks for proteins are 20 (or 22 including selenocysteine, Sec/U and pyrrolysine, Pyl/O) amino acids with varying side-chains featuring different entities, e.g. functional groups for diverse chemical interactions or hydrophilic and lipophilic groups for physical interactions. Proteins are long chains of amide bond connected amino acids and their sequence is termed *primary structure*, forming defined spatial structures via interactions of their amino acid side-chains, resulting in a *secondary structure*. Even higher orders (*tertiary and quartary structures*) are formed. Spatial alignment is crucial for the biological function of a protein. Short amino acid sequences (≤ 50 aa) are called peptides, with only the larger ones being big enough to align in defined *secondary structures*. Short, linear peptides are flexible, thus lacking a defined *secondary structure.* Consequently, these peptides adopt several conformations. Some of these conformations might be more biologically active than others. Conformational space of a short amino acid sequence can be restricted by cyclization of the linear peptide (Figure 1, left). Depending on the cyclization method (side-chain-to-side-chain or head-to-tail), on the position of the cycle formed within the total sequence of the linear precursor and on the hydrogen bond interaction pattern, an active conformation or inactive conformation can be fixed (Figure 1, right).

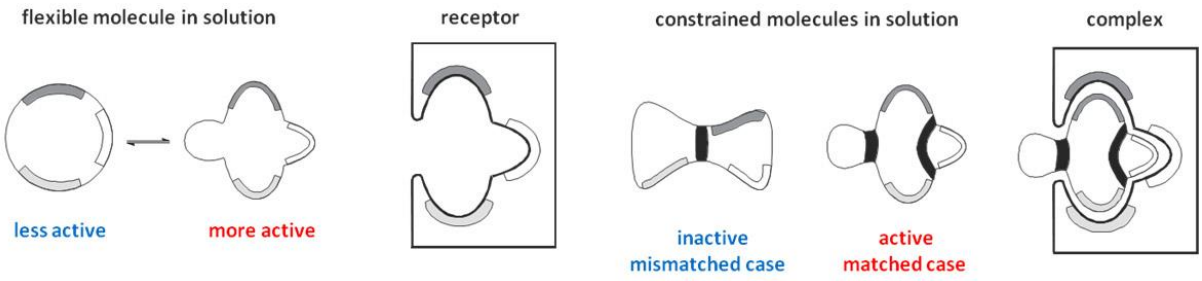


**Figure 1:** Comparison of a flexible and constraint cyclic molecule in solution. Flexible, cyclic molecules can adopt more or less active conformations (left). Further restriction of flexibility within the cyclic molecule by intramolecular interactions, e.g. hydrogen bonds can yield an inactive (mismatched case) conformation, if the fixed conformation is not matching the target's binding pocket (right). A fixed active (matched case) conformation, creates a highly active ligand (right).[1]

The underlying general principle was discovered by *Paul Ehrlich* and *Emil Fischer*, known as the *key-lock-principle*.[2, 3]

A very successful example of conformational restriction by cyclization improving ligand binding affinity was demonstrated by the cyclization of the Arg-Gly-Asp (RGD) amino acid sequence within penta- or hexapeptides.[4, 5] This tripeptidic sequence was recognized as the essential three amino acids facilitating binding of extracellular matrix (ECM) proteins to a class of cell adhesion proteins, termed integrins.[6] Therefore, the RGD sequence was grafted onto cyclic penta- or hexapeptides, which are conformational restricted in their peptide backbone flexibility by intramolecular hydrogen bonds.[4] Conformational control induced by this interaction pattern aligns the arginine and aspartic acid side-chains in an optimized position, forming key interactions with the protein.

Increasing binding affinity of a ligand by exhibiting more than one binding entity is another strategy to create active and selective interaction patterns, thereby enabling multivalent interactions.[7] Highly specific and highly active ligands exist in nature, which use this concept, to fine-tune the ligand-protein interaction. Artificially mimicking the polyvalent approach seems to be straightforward to improve avidity of a designed ligand towards its receptor. To achieve this goal, a key feature is the type of connection (spacer) between the binding entities. Chemists already have explored a full plethora of spacer types in the design of multivalent ligands, including aliphatic or polyether based spacers. A commonly observed disadvantage of these ligands is a decreased avidity of the ligand towards the targeted receptor upon dimerization. This disadvantage can be circumvented by the synthesis of ligands containing higher valences (tetravalent, octavalent etc.). These, in terms of avidity improved molecules possess other disadvantages which are even increasing with the number of binding entities. These disadvantages can be a difficult synthesis and purification or unfavorable properties in regard to pharmacodynamics and pharmacokinetics of these bulky molecules.[8-12] One reason for the decreased binding affinity of divalent ligands could be the interference of ligands with themselves or their interference in other unfavorable mode, by this reducing their overall binding affinity.

The previous paragraph focused on binding entities, connected by a spacer to each other, forming multivalent ligands. Besides connecting two or more binding motifs, a spacer can also be used to connect a ligand to a surface. This concept increases biocompatibility of these surfaces, which is important for several medical applications.[13] Using spacers between surface and binding motif is crucial for integrin ligands, to

mediate cell adhesion to these surfaces.[14, 15] The design of spacers fostering an optimal ligand-receptor interaction is of great relevance to further improve biocompatibility of surfaces.

This thesis focuses primarily on the effect of polyproline spacers, functionalized by integrin ligands, towards integrin binding affinity of these ligands and its implication on biological processes. The results of two projects have already been included in manuscripts for publication in peer-reviewed journals. One manuscript was submitted to the *Journal of Medicinal Chemistry* (chapter 4.1) and the other manuscript is in preparation for submission to the *Journal of the American Chemical Society* (chapter 4.2.1). Within these chapters, the results are only briefly summarized. The full manuscripts can be found in the appendix (chapter 8).

Chapter 4.1 describes the systematic screening of a cyclic *iso*DGR lead structure to increase its selectivity and activity towards integrins α5β1 and αvβ6. In addition, its modification for coating of gold nanostructured surfaces and its effect on cell adhesion to these surfaces is described.
Chapter 4.2 depicts the modification of selective and active integrin ligands of the RGD type and *iso*DGR type by polyproline spacers suitable for surface coating. In addition to investigate the effect of polyproline spacers of different lengths, also the implication of the connection type between integrin ligand and spacer (click chemistry ligation or amide bond formation) as well as differences between monovalent and divalent integrin ligands are explored.
Chapter 4.3 shows the adaption of monovalent and divalent RGD integrin ligands connected by polyproline spacers to tracers or probes to make these compounds suitable for *ex vivo* and *in vivo* imaging.
Chapter 4.4 comprises RGD ligands, connected by the polyproline spacer to isothiocyanate surface anchors, which are developed to improve the biocompatibility of stent surfaces.

# 2. Integrin Biology

## 2.1. Integrins: Structure and Biological Context

Cell surface receptors of the integrin protein family regulate multicellular interactions at a key position. Consequently, these proteins are expressed in all cells of multicellular animals, mediating cell-matrix interactions and cell-cell interactions.[16] They were recognized as central receptors for cell adhesion, platelet aggregation, homing of leucocytes and immune response during the 1980's. *Tamkun* and *Hynes* introduced the term "integrin" in 1986 to emphasize their central function as an integral membrane complex, linking the extracellular matrix to the cytoskeleton across the cell membrane.[17] Since then, they became one of the most intensively studied families of cell adhesion receptors. Currently, involvement of integrins in many biological and pathological processes such as cell migration, thrombosis, restenosis, bone resorption, cardiovascular disorders, inflammation, auto immune diseases, cancer invasion, metastasis and tumor induced angiogenesis is known.[18-22] The discovery by *Pierschbacher* and *Ruoslahti* in 1984, showing that ECM protein fibronectin is mediating integrin cell adhesion by a short sequence of the four amino acids Arg-Gly-Asp-Ser (RGDS), was a major breakthrough for the later rational design of natural integrin ligand mimics.[6] Today, many recognition motifs are known and the serine in RGDS sequence turned out to be not crucial for binding, leaving the RGD sequence as a pivotal recognition motif for integrin binding.[23] Up to now, 24 different integrins existing in humans could be identified, which can be classified in four subfamilies: Collagen-, Leukocyte-, Laminin- and RGD-receptors (Figure 2).

Integrins are αβ heterodimeric, type I transmembrane glycoproteins with a large extracellular and short cytoplasmic domain (700-1100 and 30-50 residues respectively), linked by a short transmembrane helix.[24] Each integrin subfamily recognizes a distinct set of protein ligands. They have different binding affinities to these ligands, enabling them to precisely fine-tune their biological function.[25] Revealing the integrin αvβ3 extracellular segment's crystal structure and shortly later its state bound to artificial ligand Cilengitide as well as ECM protein fibronectin, *Arnout et al*. were able to precisely determine the integrin ectodomain and the interface between integrin α- and β-subunit.[26-29] The ligand binding site is located at the tip of the extracellular domains. Precisely, it is located at the

interface of the β-propeller domain of the αv subunit and the βI-domain of the β3 subunit. The β-propeller domain is formed by seven radially arranged “blades” each consisting of about 60 amino acids. Each blade forms a four stranded antiparallel sheet. A consensus sequence of all blades, formed by three aromatic residues, is pointing to the center of the propeller. Thereby formed hydrophobic cavity is occupied by $Arg^{261}$ of the β-subunit, thus stabilizing the αβ-heterodimer by a cation-π interaction.

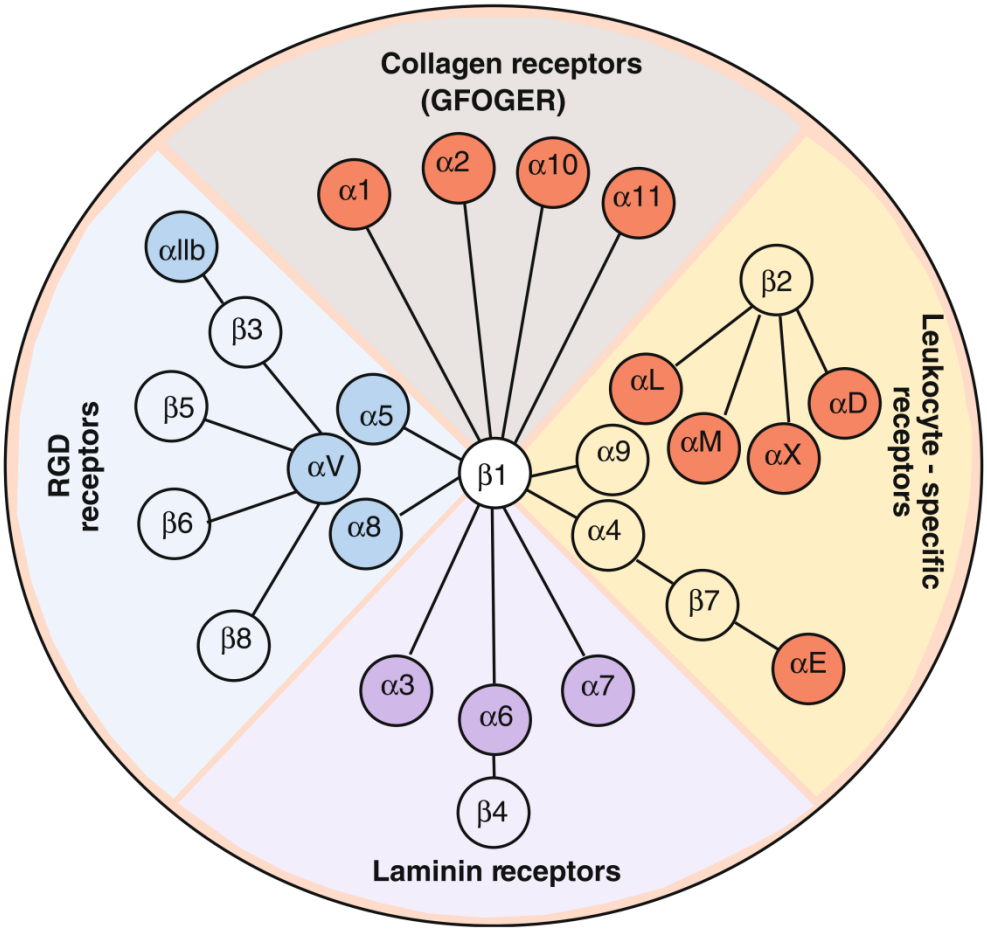


**Figure 2:** Representation of the integrin family. In humans, the integrin family contains 24 heterodimers which can be divided into four subgroups: Collagen-, Leucocyte-, Laminin- and RGD-(Arg-Gly-Asp) receptors.[23]

The βI-domain of the β-subunit forms a *Rossmann*-fold by formation of six-stranded β-sheets, surrounded by eight α-helices and three binding sites for divalent cations ($Ca^{2+}$, $Mg^{2+}$ or $Mn^{2+}$). Cations incorporated are dependent on the used buffer. One out of these three metal ion binding sites is located at the top of the central β-strand and is indispensable for ligand binding, consequently termed *metal ion-dependent adhesion site* (MIDAS). Although this site is not occupied in the unbound state of the integrin the adjacent MIDAS (ADMIDAS) is occupied by a metal ion in both, the unbound and bound integrin state. The last metal ion binding site is occupied after ligand binding and stabilizes the bound conformation (*ligand induced metal binding site*, LIMBS). An

illustration of integrin structure and conformational changes induced by intra- and extra cellular ligand binding can be found in Figure 3.

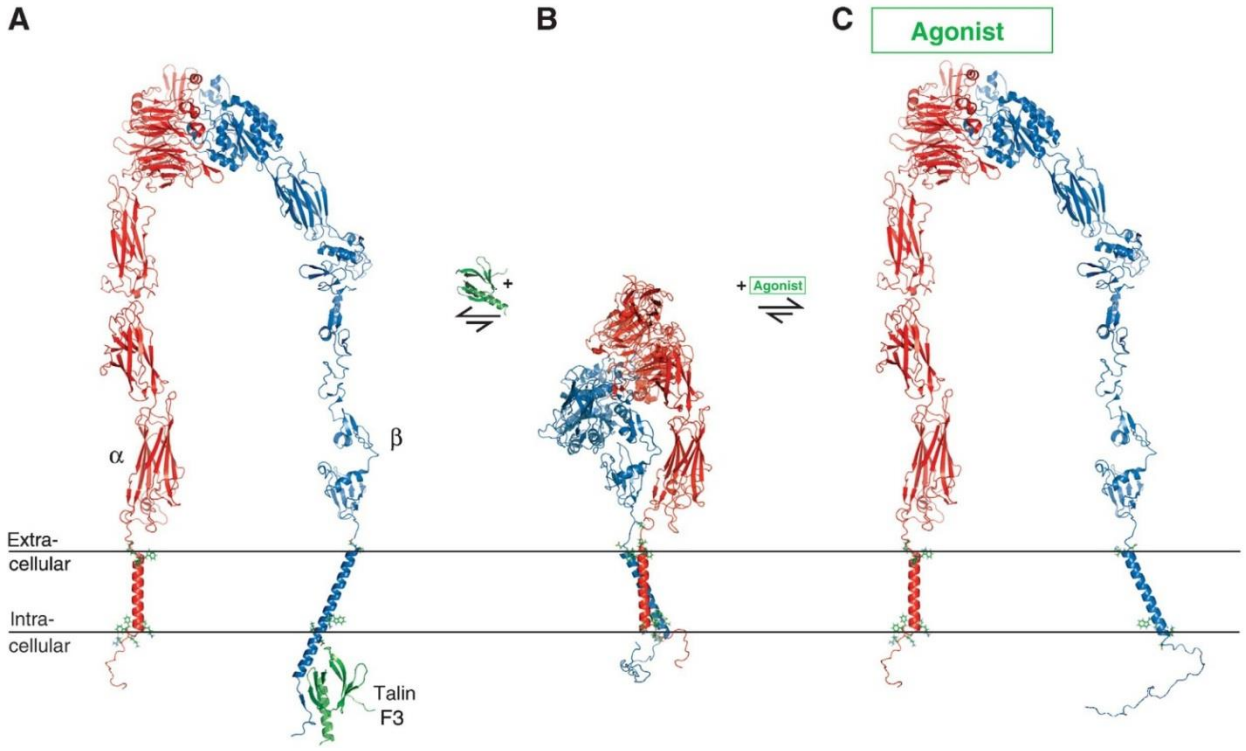


**Figure 3:** Illustration of proposed integrin receptor functional states. (**A**) Inside-out activated integrin composed of an activated extracellular headpiece[30] (PDB ID 2vdn), extended I-EGF1-2 domains[31] (PDB ID 2p28) and modeled tailpiece, fused to the monomeric αIIb and β3 TM structures (PDB ID 2k1a and 2mrz), and connected to the activating β-cytosolic tail–talin F3 complex (PDB ID 2h7e).[32] Talin F3 domain binding stabilizes α-helical structure subsequent to the β-TM helix. (**B**) Resting integrin composed of the bent integrin αvβ3/αIIbβ3 structure[27, 29, 33] (PDB ID 1jv2), the αIIbβ3 TM complex (PDB ID 2k9j), and dynamically unstructured cytosolic tails.[34, 35] (**C**) Outside-in activated integrin composed of an activated extracellular headpiece[30] (PDB ID 2vdn), extended I-EGF1-2 domains[31] (PDB ID 2p28) and modeled tailpiece, fused to the monomeric αIIb and β3 TM structures (PDB ID 2k1a and 2mrz), and connected to dynamically unstructured cytosolic tails.[34, 35] As no high-resolution structures of an entire, activated ectodomain exist, the depicted domain–domain orientations only serve to illustrate a presumed extended geometry.[33, 36, 37] In each functional transition, the TM helices have been rotated in addition to their dissociation. During both inside-out and outside-in signaling, additional ectodomain intermediates are likely to exist[30, 33, 37] and some debate regarding the structural rearrangement of the ectodomain on activation remains.[33, 38-40] Reprinted by permission from Macmillan Publishers Ltd: *EMBO J* **2009**, *28*, 1351-1361, copyright (2009).[41]

Besides their function as mechanical linkers, integrins are bidirectional signaling receptors, transducing signals either from the outside of a cell to its inside or vice versa.[42, 43] These signaling events provide additional information for the cell, complementing information transmitted by growth-factors or G-protein coupled receptors. But also on its own, integrin signaling provokes cellular responses like survival, growth, proliferation, motility, spreading and migration. Analyzing literature about the diverse and

complex integrin signaling, a network of 156 proteins linked via 690 interactions could be revealed.[44] The most important ones directly interacting with integrins or directly related to integrins are summarized in Figure 4.

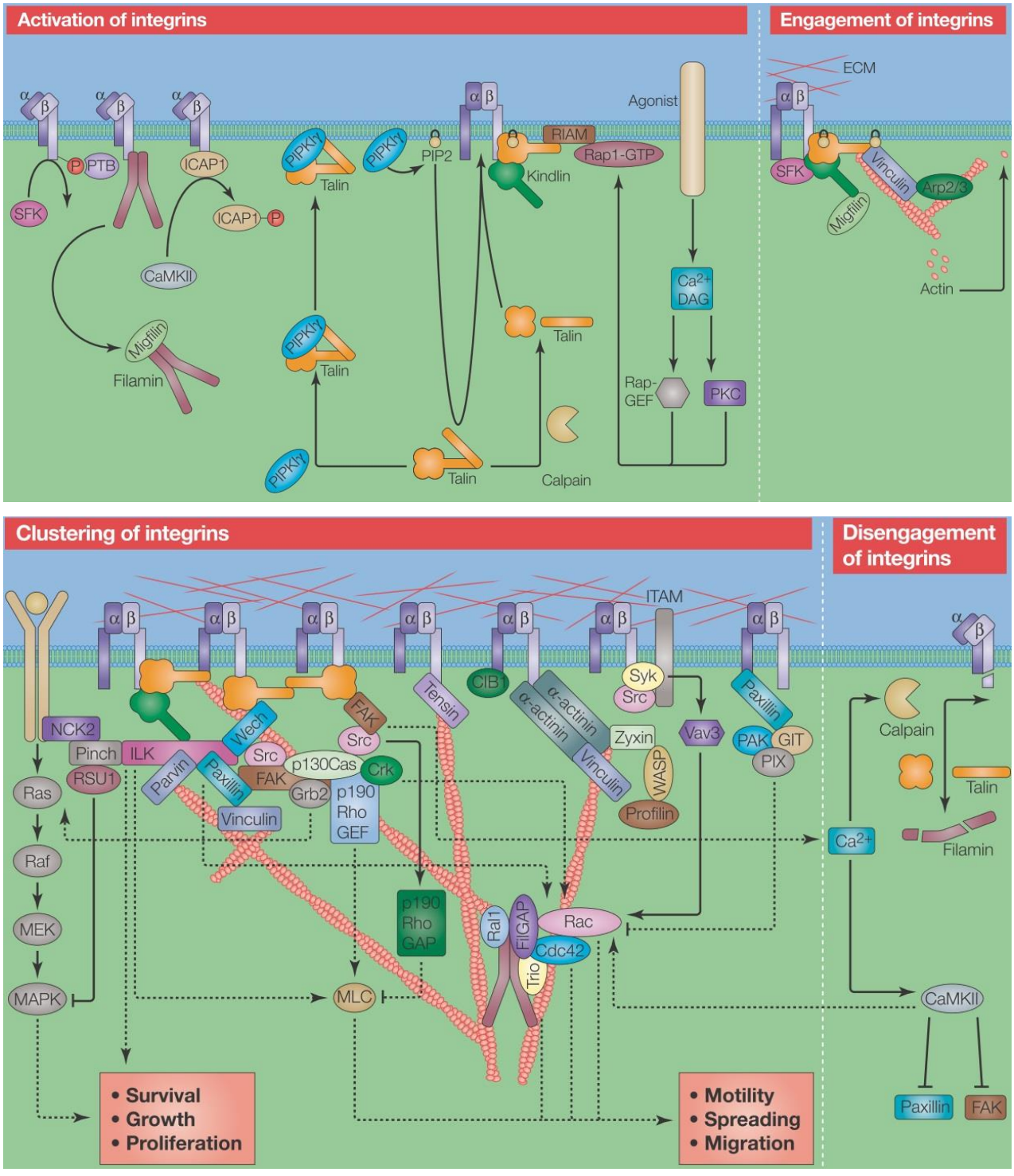


**Figure 4:** Integrin signaling at a glance. Upon integrin activation and first engagement of integrins forming nascent focal adhesions, integrin clustering induces mature focal adhesions and stable cell adhesion. By the short cytoplasmic tail of the integrin α- and β-domain several different proteins of the cytosol can be recruited inducing manifold signaling events.[43]

Clustering of activated integrins in focal adhesion points and binding to ligands of the ECM recruits several proteins of the cytosol like talin, paxilin, zyxin and vinculin. This protein cluster links integrins to the actin filaments of the cytoskeleton. Moreover, various tyrosine kinases can be activated by integrins, e.g. focal adhesion kinase (FAK) and integrin-linked kinase (ILK). This triggers signaling cascades influencing cell cycle, cell growth and survival or apoptosis. To make things even more complex, integrin pattern expressed by a cell at a certain time point can result in a “cross talk” of integrin signaling pathways influencing each other, thus making it difficult to selectively influence integrin induced signaling.[45]

## 2.2. Integrins as Therapeutic Targets in Medicinal Chemistry

Integrin mediated adhesion and signaling plays a pivotal role in diverse human diseases, including autoimmune disorders, thrombosis, inflammation and cancer (Table 1). Being exposed on the cell surface and sensitive to blockade by artificial inhibitors, they are pharmacological targets of great interest. Although many efforts have been made to develop integrin targeting inhibitors, only four are approved drugs today, three of them targeting the same integrin (α4βx: Tysabri; αIIbβ3: Tirofiban, Intrifiban and Abciximab).[25] This might be related to the functional complexity of integrin signaling cascades, the incomplete understanding of the role of integrins in the formation of diseases, as well as a lack of knowledge of the precise role integrins play within progression of these diseases.

Nevertheless, about 260 integrin targeting drugs are in all stages of clinical phases these days.[25] A promising candidate, currently in clinical phase III for the treatment of glioblastomas and phase II for other cancer types is the anti-angiogenic small pentapeptide *cyclo*(-RGDf(*N*Me)V-), targeting RGD recognizing integrins αvβ3, αvβ5 and α5β1.[26, 46] It could be developed due to the discovery of the RGD sequence as a natural binding motif of some integrins and the successive improvement of activity and selectivity towards the targeted angiogenic integrins. To achieve this objective, a novel "spatial screening" strategy was developed.[47] Using peptide cyclization, incorporation of D-amino acids and *N*-methylation of amide bonds, activity and selectivity was improved by several orders of magnitude compared to the starting sequence.

Although many peptidomimetic integrin inhibitors have been designed, only Tirofiban has made it to the market.[25] Others struggled by usual pharmacological issues of bioavailability, specificity or off-target effects.[22] Notably, all RGD targeted integrin ligands (peptides or peptidomimetics) feature the same two pharmacophoric groups being responsible for interactions crucial for integrin binding. The first one is the basic guanidyl group of the Arg side chain or a basic mimic, setting up a salt bridge to residues of the α-subunit's β-propeller. The second one is the Asp carboxylic acid, interacting with the MIDAS site.[48] For a long time it was thought to be impossible to replace the carboxylic acid within integrin ligands. During the last years, it could be demonstrated that this conserved functional group can be replaced by hydroxamic acids[49] as well as phosphinates and monomethyl phosphonates.[50] This might offer further possibilities to medicinal chemists for the design of integrin ligands for the future.

**Table 1:** Integrin subfamilies cluster major therapeutic indications.[22, 23, 25, 42]

| Integrin class | Clinically targeted in | Main Ligands[a] |
|---|---|---|
| ***α4 Family*** | | |
| **α4β1** | MS, autoimmune, Crohn's, IBD | VCAM-1, FN |
| **α4β7** | MS, autoimmune, arthritis | MAd-CAM-1 |
| **α9β1** | Cancer | VCAM-1, Opn, VEGF-C, -D |
| ***Leukocyte cell adhesion*** | | |
| **αLβ2** | Inflammation, psoriasis, stroke, ischemia, fibrosis | ICAM-1,-2,-3 |
| **αMβ2** | Inflammation, autoimmune | iC3b, Fbg |
| **αXβ2** | Inflammation | iC3b, Fbg |
| **αDβ2** | Inflammation | ICAM-3, VCAM-1 |
| **αEβ7** | Inflammation | E-cadherin |
| ***LN binding*** | | |
| **α3β1** | None | LN-5 |
| **α6β1, α7β1** | None | LN-1, -2 |
| **α6β4** | None | LN-2, -4, -5 |
| ***RGD-binding*** | | |
| **αIIbβ3** | Thrombosis, stroke, myocardial ischemia | Fbg, vWf |
| **α5β1** | Cancer, AMD | FN |
| **α8β1** | None | Npn, FN, VN |
| **αvβ1** | Cancer | VN, FN |
| **αvβ3** | Cancer, osteoporosis | VN, Opn, vWf, FN, Fbg |
| **αvβ5** | Cancer | VN |
| **αvβ6** | Fibrosis, transplant rejection, cancer | FN, TGF-β1,-3 |
| **αvβ8** | Cancer | FN, TGF-β1,-3 |
| ***I domain: collagen binding*** | | |
| **α1β1** | Fibrosis, cancer | Col |
| **α2β1** | Fibrosis, cancer | Col |
| **α10β1, α11β1** | None | Col |

[a] Abbreviations: AMD, age-related macular degeneration; Col, Collagens; Fbg, fibrinogen; FN, Fibronectin; IBD, inflammatory bowel disease; ICAM, intercellular adhesion molecule; LN, laminin; Mad-CAM, mucosal vascular addressin cell adhesion molecule; MS, multiple sclerosis; Npn, nephronectin; Opn, osteopontin; TGF, transforming growth factor; VCAM, vascular cell adhesion molecule; VEGF, vascular endothelial growth factor; VN, vitronectin; vWF, von Willebrand factor. Reprinted from Trends in Pharmacological Sciences, 33/7, Goodman, S.L.; Picard, M., Integrins as Therapeutic Targets, 405-412, Copyright (2012), with permission from Elsevier.

# 3. Key Experimental Methods

This chapter briefly summarizes techniques used for the preparation of the compounds, their *in vitro* characterization, as well as the preparation of gold nanoparticle structured surfaces coated with these compounds. These techniques are not discussed in depth within the manuscripts included, but maybe helpful to gain additional insights into the projects discussed in chapter 4.

## 3.1. Solid Phase Peptide Synthesis

Peptides are short polymers of amino acid monomers. Each monomer is linked by an amide bond to its next monomer neighbor. Although small dipeptides, consisting out of only two amino acids, were already synthesized by chemists at the beginning of the 20$^{th}$ century,[51] synthesis was limited due to the fact of massive side product formation and difficult purification of a chemically similar crude product mixture. Hence, dipeptides consisting of amino acids containing only aliphatic side chains were the easiest peptides accessible. Incorporation of amino acids possessing reactive functional groups at their side chains needed adequate protecting groups to prevent unwanted side reactions. The benzyloxycarbonyl protecting group was the first one that was developed.[52] Nevertheless, synthesis of peptides was hampered till a solid phase supported synthesis strategy was introduced by *Merrifield* in 1963.[53-55] This major breakthrough allowed the synthesis of longer peptide sequences than before, due to the attachment of the first amino acid to an insoluble carrier polymer. Reagents and side products formed during the peptide synthesis could be removed from the resin bound peptide sequence by a simple thoroughly washing and filtering process of the polymer. Furthermore, temporary amino protecting groups and permanent side chain protecting groups were needed, which are orthogonal to each other. The temporary amino protecting group hinders the amine of the introduced amino acid from side reactions. The side chain protecting group does the same for the functional groups of the side chain. Up to now, a plethora of protecting groups was developed, complementing one another for all kinds of synthetic needs.[56] The two most prominent strategies using the orthogonal protecting concept are termed after their temporary protecting groups, the Boc-strategy (*tert.*-**B**utyl**o**xy**c**arbonyl)[53, 54] introduced by *Merrifield* and the later developed Fmoc-strategy (9-**F**luorenyl**m**ethyl**o**xy**c**arbonyl).[57, 58] Although the latter uses milder conditions

throughout the synthesis, still both methods are frequently used today, as the success of the synthesis strategy can depend on the peptide sequence desired to be synthesized.[59] A brief overview of synthesis steps for the Fmoc-based solid phase peptide synthesis (SPPS) of cyclic peptides is given in Scheme 1.

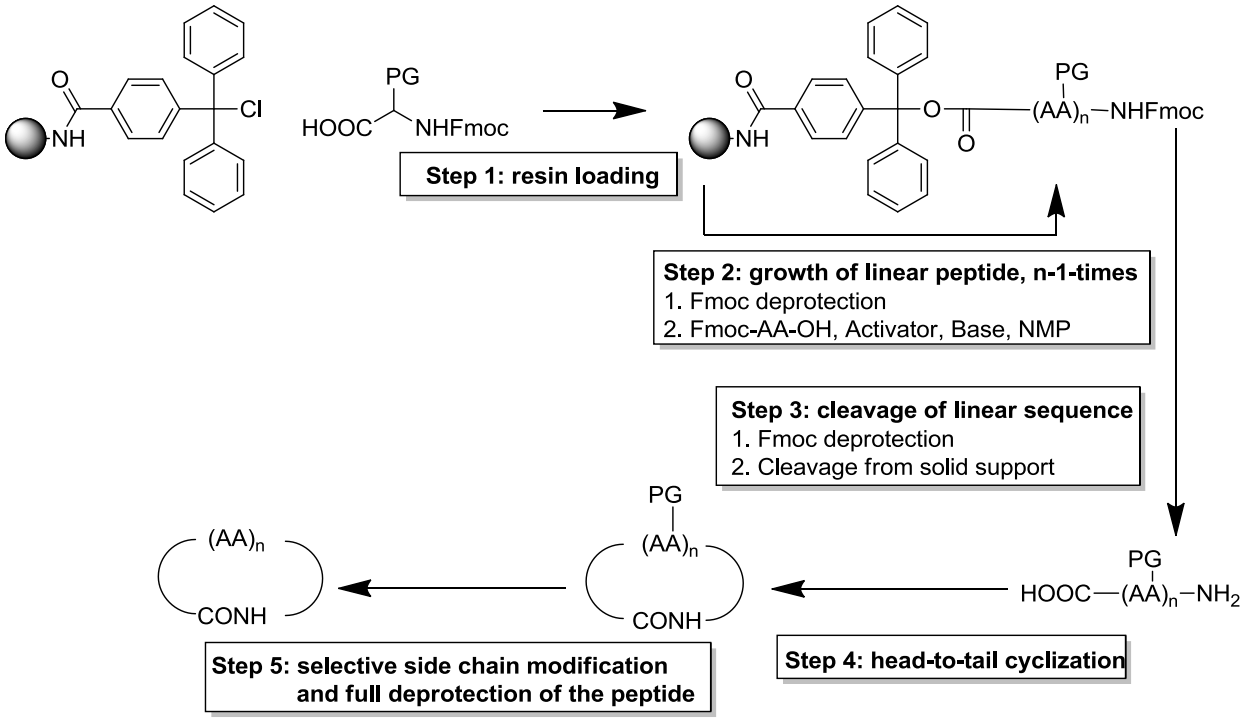


**Scheme 1:** Fmoc-based solid phase peptide synthesis (SPPS) of cyclic peptides. **Step 1:** An Fmoc-protected amino acid is attached to a linker bound to an insoluble polymer. **Step 2:** Desired amino acid sequence is synthesized *C*- to *N*-terminal by repetitive steps of Fmoc removal an attachment of the next amino acid. **Step 3:** Cleavage of the side chain protected peptide from the resin. **Step 4:** Successive head-to-tail cyclization. **Step 5:** Dependent on side chain protecting groups, selective chemical modification of a side chain is possible, followed by complete removal of all remaining protecting groups.

After overcoming these first major obstacles, many challenges remained. Unwanted deletion peptides, lacking one or more amino acids within the sequence can be avoided, if all primary amines of the resin bound peptide sequence are converted into the corresponding amide. This can be achieved, if the carboxylic acid of the next incorporated *N*-Fmoc protected amino acid is transformed into an activated ester, reacting easily with the primary amine of the resin bound peptide sequence. At first, activators of the carbodiimide type were used, like dicyclohexylcarbodiimide (DCC).[60] Today, they are not the best choice for most applications as the formed carbodiimide active ester is prone to many side-reactions like racemization at the $C^{\alpha}$ carbon of the activated amino acid as well as derivatization of the activated amino acid into unreactive side products.[61] Although additives like 1-hydroxybenzotriazole (HOBt)[62] and

7-aza-1-hydroxybenzotriazole (HOAt)[63] were developed to reduce racemization during DCC mediated peptide couplings, success of DCC couplings is still limited by its intrinsic tendency to form side products. In order to replace DCC, other classes of activators were developed. Derived from HOBt, amidinium salts are a common substance class widely applied today for this purpose. *O*-(7-Azabenzotriazol-1-yl)-*N*,*N*,*N´*,*N´*-tetramethyluronium-hexafluorophosphate (HATU)[63] or *O*-(1H-benzotriazol-1-yl)-*N*,*N*,*N´*,*N´*-tetramethyl-uroniumtetrafluoroborate (TBTU)[64] are just two examples. Phosphonium salts are an additional class of newer coupling reagents. Most prominent examples of this class are benzotriazol-1-yl-*N*-oxy-*tris*(pyrrolidino)phosphonium hexafluorophosphate (PyBob)[65] or (7-azabenzotriazol-1-yl-*N*-oxy)-*tris*(pyrrolidino)phosphonium hexafluorophosphate (PyAOP).[66] Coupling reagents of both classes are far less prone to induce racemization during activation of an amino acid compared to DCC. By addition of additives like HOBt, racemization can be further suppressed and consequently the efficiency of the synthesis is improved. However, both classes of activators have disadvantages as well.[61] For amidinium salt based reagents, guadinylation of the *N*-terminus of the peptide terminates the peptide chain elongation. During the slow activation of hindered amino acids, protected peptides or carboxylic acids involved in cyclizations, guadinylation as a side reaction may become important. Using phosphonium salt based reagents, a non-reactive carboxylic acid derivative might be formed by pyrrolidination during the activation reaction. The latest activator developed is (1-cyano-2-ethoxy-2-oxoethylidenaminooxy)-dimethylamino-morpholino-carbenium hexafluorophosphate (COMU)[67, 68] and its corresponding additive ethyl-(hydroxyimino)cyanoacetate (Oxyma).[69] Both have been reported to perform extremely well, at least comparable to HATU, known as the most efficient activator till now, without having any tendency to induce racemization. As an additional advantage these compounds are highly soluble in solvents typically applied during SPPS which allows more concentrated reagent solutions, thereby decreasing the reaction time and the formation of possible side products.[68, 70]

To activate the carboxylic acid of an amino acid, at least one equivalent of base is necessary for the formation of the activated ester, carbodiimide reagents as the only exception. Therefore, non-nucleophilic, sterically hindered bases like diisopropylethylamine (DIEA), 2,4,6-trimethylpyridine (*sym.*-collidine) or 1,8-diazabicycloundec-7-ene (DBU) are used, thus preventing unwanted side reactions with the activated amino acid. These reagents are mild bases ($pk_a$ 10-13) avoiding the

racemization at the $C^{\alpha}$ of the activated amino acid by a base catalyzed deprotonation and reprotonation process.

The solid support used in SPPS is required to be insoluble in all, during SPPS commonly used, solvents. Nevertheless, it should retain a high degree of polymer swelling in these solvents, resulting in a porous structure accessible for further chemical modifications. Throughout the peptide synthesis, the structure of the polymer carrier should be stable with no sign of polymer bead deterioration. This can be caused by an osmotic shock, if the type of solvent needs to be changed during the synthesis and the swelling parameters of the resin in both solvents differs too much. Furthermore, the polymer needs to be stable during conditions applied for the peptide cleavage from solid support.[71, 72] Commonly, polystyrene (PS), cross-linked by 1-2% divinylbenzene (DVB), is the polymer of choice. In recent years, polyethylene glycol based polymers (e.g. ChemMatrix resin) became increasingly important.[73] These newly developed resins offer advantages during peptide synthesis, especially for the synthesis of lipophilic peptide sequences.[74]

The connection between polymer and first amino acid is achieved by a wide range of suitable linkers. The linker should keep the synthesized peptide sequence bound to the solid support throughout the synthesis, but has to allow quantitative removal of the peptide from the solid support during the peptide cleavage step. Dependent on the chosen linker, *C*-terminal carboxylic acids, amides or other termini can be obtained upon cleavage. Peptides containing *C*-terminal carboxylic acids can be synthesized using tritylchlorid linker (TCP). For the synthesis of peptides containing *C*-terminal amides one prominent example is the rink-amide linker, although its need is currently questioned for some applications.[75, 76] A summary of reagents, additives, bases and linkers discussed is depicted in Figure 5.

During peptide synthesis, peptide micro cleavage and subsequent analysis by mass spectrometry (MS), ideally in combination with prior RP-HPLC, is nowadays the best way to monitor the completeness of peptide coupling. However, even by using an extremely soft ionization method for mass spectrometry, e.g. electron spray ionization (ESI), the analyte will likely show a fragmentation pattern caused by the ionization process. For most sequences, this pattern might not disturb analysis because side chain protection groups alter strongly the polarity of the analyte mixture, which enables a

chromatographic separation of possible deletion sequences. But within highly repetitive sequences, such as the polyproline sequence, it can be difficult to distinguish between fragmentation artifacts and deletion peptides.

**a) Activators**

**Carbodiimides**

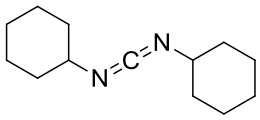

DCC

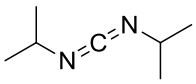

DIPCDI

**Ethyl-(oxyimino)-cyanoacetate**

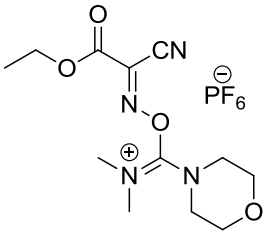

COMU

**Amidinium Salts**

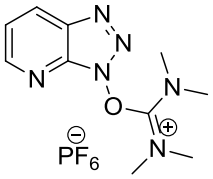

HATU

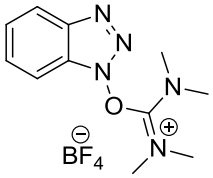

TBTU

**Phosphonium Salt**

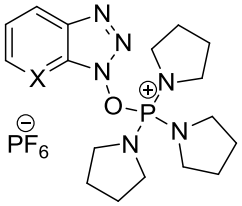

PyAOP X=N
PyBob X=CH

**b) Additives**

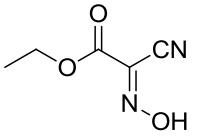

Oxyma

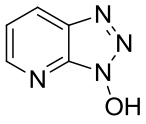

HOAt

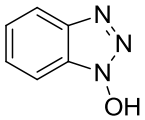

HOBt

**c) Bases**

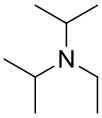

DIEA

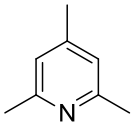

*sym.*-Collidin

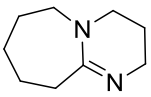

DBU

**d) Linker**

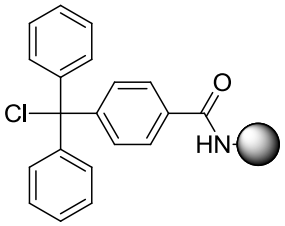

TCP

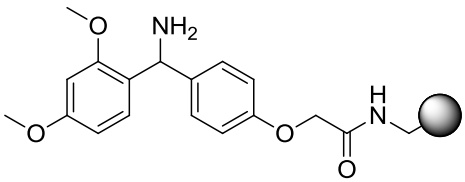

Rink Amide

**Figure 5: a)** Activators for the carboxylic acid used in peptide synthesis of the carbodiimide, oxyiminocyanoacetate, amidinium and phosphonium type. **b)** Additives to reduce racemization of the activated amino acid. **c)** Typical none-nucleophilic bases. **d)** Two commonly used scaffolds to link the peptide sequence to the solid support.

As a practical quick orthogonal method, colorimetric assessment of coupling completion can be an alternative. The NF-31 reagent (Figure 6) was developed for this purpose and stains resin beads clearly.[77] Its high reactivity permits monitoring of conversion of more than 98% by eye. Combined with HPLC-MS it improves distinguishing between ionization artifacts caused by MS ionization and deletion sequences. Benefits over older detection methods, e.g. the *Kaiser test,*[78] are the higher reactivity and thus lower detection limit. Another advantage of the NF-31 reagent is its reactivity with steric hindered amines, e.g. the secondary amine of proline residues. In this case, the *Kaiser test* would produce false negative results.

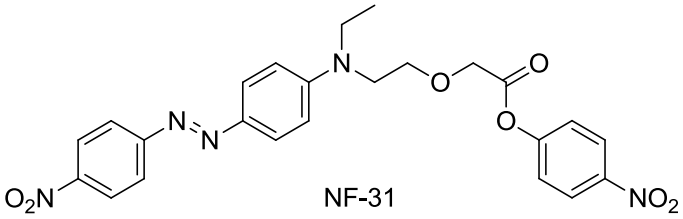


NF-31

**Figure 6:** NF-31 active ester for color assessment of peptide coupling completion during peptide couplings. This dye reacts with steric hindered amines, e.g. the secondary amine of proline. The *Kaiser test* would produce false negative results as it is not reacting with these steric hindered amines.

## 3.2. *In Vitro* Inhibition of Integrin Binding Using ELISA

Synthesized compounds are designed to bind the integrin of interest with high affinity. To determine the binding affinity, compounds are assessed in a competitive integrin binding assay of the ELISA type (**E**nzyme **L**inked **I**mmune **S**orbent **A**ssay) (Scheme 2).[50, 79]

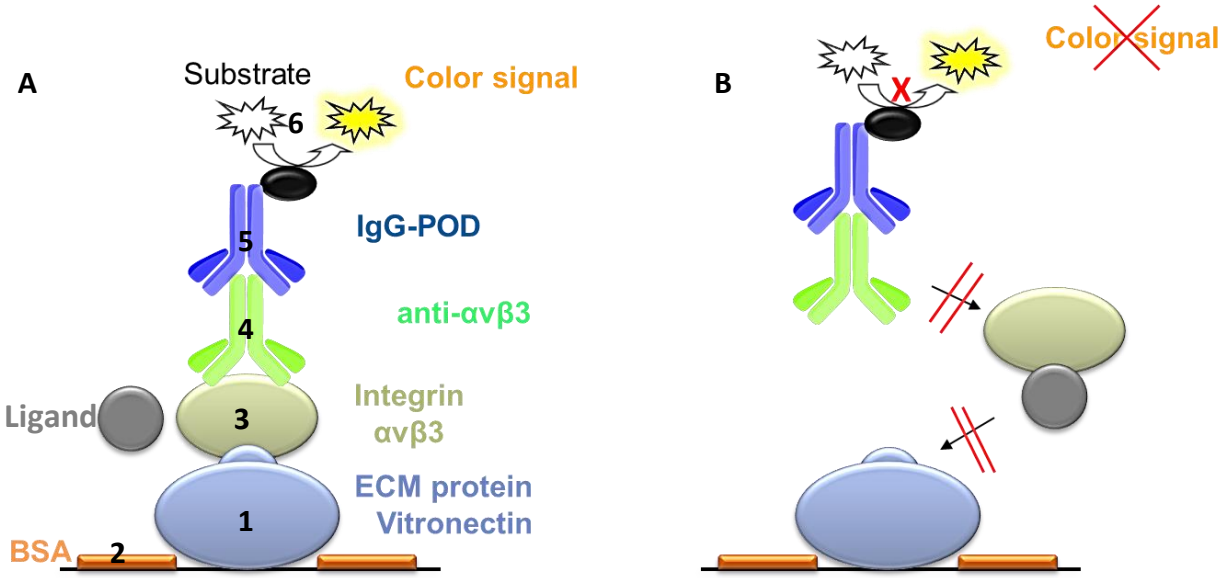


**Scheme 2:** Enzyme linked immune sorbent assay (ELISA). **A: 1.** Each well of a 96-well plate was coated by an ECM protein (e.g. vitronectin). **2.** Uncoated spots were blocked by bovine serum albumin (BSA). **3.** ECM protein competes with the tested ligand for binding to the soluble integrin (e.g. αvβ3). **4.** Integrin bound to ECM protein is detected by an integrin specific primary antibody **5.** Secondary antibody, coupled to a peroxidase (POD), detects bound primary antibody. **6.** Peroxidase converts a colorless substrate into a colored substrate (TMB, 3,3′,5,5′-tetramethylbenzidine). **B:** Ligand inhibits binding of the coated ECM protein to the integrin. Consequently, steps **3-6** are blocked and no color signal can be detected.

In contrast to a classic competitive ELISA, 96-well plates are coated with ECM integrin ligand in this case. As a next step, the soluble ligand of interest competes with coated ECM protein in the binding to the soluble integrin. The ligand is tested in a series of wells, using a different ligand concentration for each well. The tested ligand (partially) inhibits binding of the Integrin to the coated ECM protein. ECM bound integrin is detected by a primary antibody. A secondary antibody, coupled to a peroxidase, binds to the primary antibody. In the last step of the ELISA, a colorless substrate is the converted by the peroxidase into a colored compound (Scheme 3).

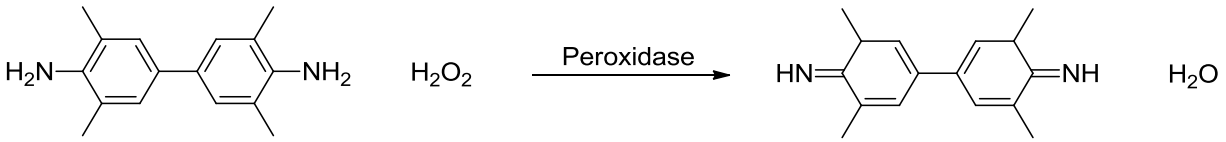


**Scheme 3:** Conversion of 3,3′,5,5′-Tetramethylbenzidine (TMB) by peroxidase.

The conversion is stopped to prevent signal saturation by addition of 3 M $H_2SO_4$, which induces a color change from blue to yellow (Figure 7, left and middle). The amount of conversion in each well is analyzed by photometrical measurement at 450 nm (Figure 7, middle). Measured absorption values of each well are correlated to the ligand concentration. The inflection point of the sigmoidal fitted curve describes the inhibition constant 50 ($IC_{50}$) (Figure 7, right).

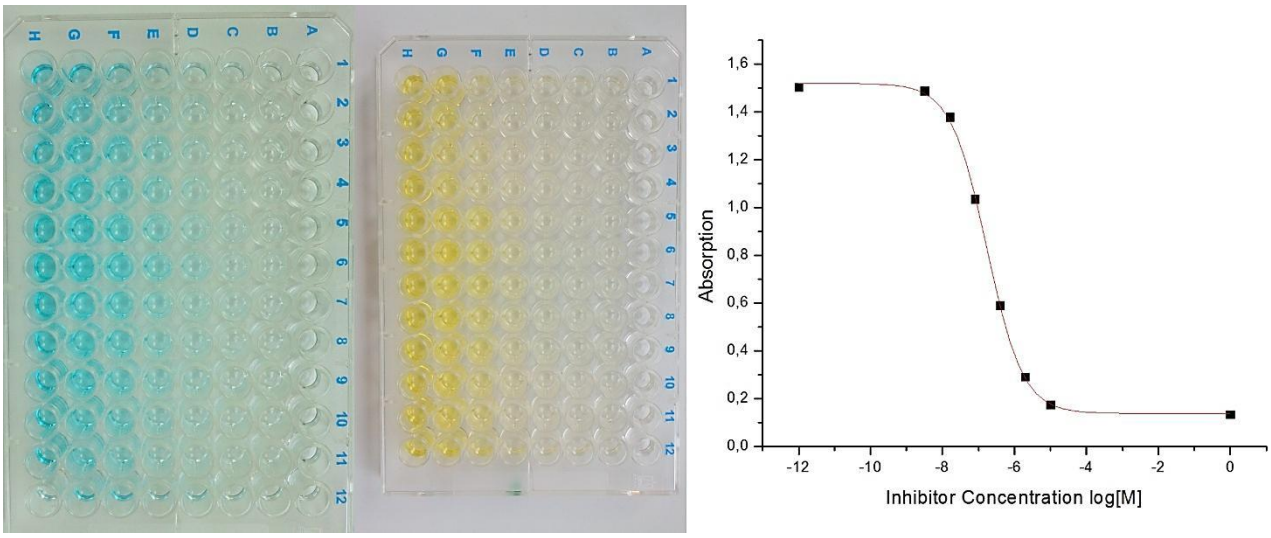


**Figure 7: Left:** 96-well plate with serial dilutions of several ligands in an ELISA after TMB conversion. Inhibitor (ligand) concentration increases from left to right. **Middle:** Peroxidase catalyzed TMB conversion is stopped by addition of 3 M $H_2SO_4$. Absorption of the yellow colored solution is analyzed by a photometer at 450 nm. **Right:** Measured absorption is correlated to ligand concentration. The inflection point of the sigmoidal fitted curve describes the inhibition constant 50 ($IC_{50}$).

## 3.3. Cell Adhesion Studies on Gold Nanoparticle Structured Surfaces

The preparation of gold nanoparticle structured surfaces by nanolithography was developed in the group of *J.P. Spatz*.[80] Briefly, a polymer consisting of a lipophilic block formed by polystyrene and a hydrophilic block formed by poly-2-vinylpyridine is used (diblock copolymer). Within an unpolar solvent such as *ortho*-xylene this polymer forms micelles, as soon as the polymer concentration is above the critical micelle concentration (cmc). Subsequently, micelle cores can be loaded with metal salts ($HAuCl_4$). Glass substrates (surfaces) are prepared by a treatment in Caro's acid (peroxomonosulfuric acid). Afterwards, substrates are spin coated (depicted in Scheme 4, or dip coated, not shown) with the metal salt loaded micelle solution. Onto the fast spinning substrate, a defined amount of the loaded micelle solution is added in the middle of the substrate and distributed evenly across the surface by centrifugal force. Micelles are self-organizing in a hexagonal alignment. The diblockcopolymer is removed and the metal salt reduced by plasma treatment. Bare metal dots remain on the substrate's surface. The interparticle distance is tunable by the number of repeats of each monomer in the diblockcopolymer, hence regulating the polymer composition and the size of the formed micelles. Quality of the aligned nanoparticles and their hexagonality can be controlled by scanning electron microscopy (SEM, Figure 8).[81]

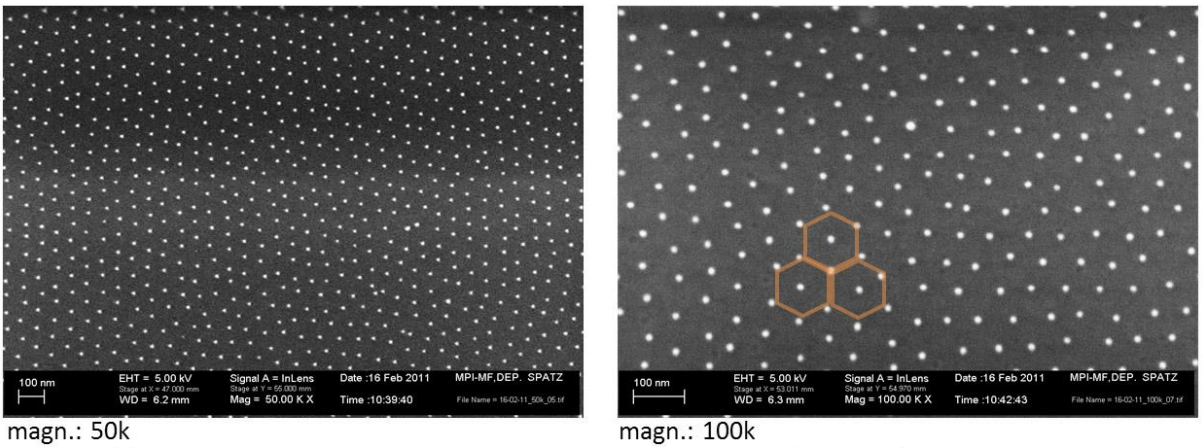


**Figure 8:** SEM (scanning electron microscopy) images of gold nanoparticle structured surfaces. **Left:** Alignment of gold nanoparticles in their long-range order (magnification: 50.000). **Right:** Alignment of gold nanoparticles in their short-range order (magnification: 100.000). Hexagonal alignment of the gold nanoparticles is emphasized by orange hexagons. Hexagonality of this pattern is determined to 77%.

To prevent non-specific cell adhesion on these surfaces, the area between gold nanoparticles is passivated by $PEG_{2000}$-triethoxysilane.[82] In the last step, passivated surfaces are functionalized by thiol containing RGD-peptides. Physisorbed peptide excess is removed by extensive rinsing. Cells adhere to these coated surfaces via their integrins (Scheme 4).

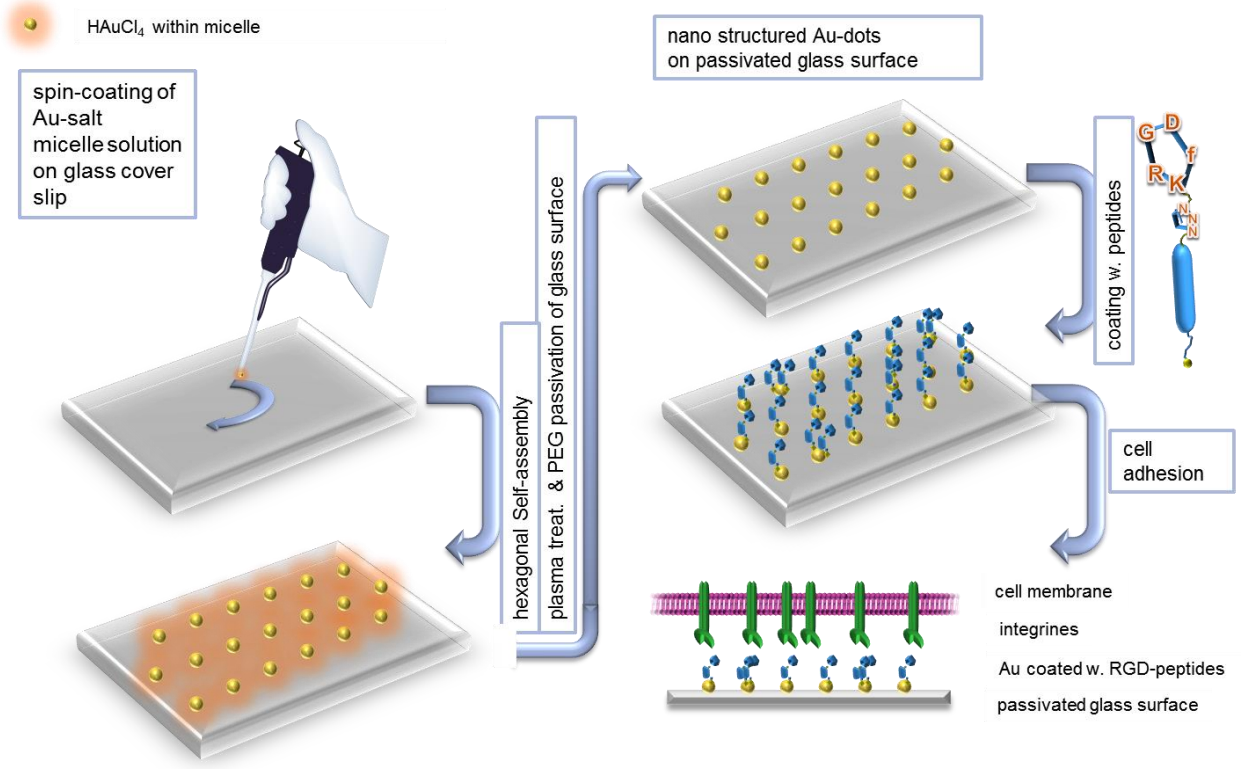


**Scheme 4:** Preparation of gold nanoparticle structured surfaces by nanolithography for cell adhesion studies. The glass substrate is spin-coated with gold salt loaded diblockcopolymer micelle solution. After hexagonal self-alignment of the micelles, the polymer is removed and the gold salt reduced by plasma treatment. After PEG passivation of the glass surface, gold nanoparticles are coated by thiol containing RGD-peptides. Cells adhere to this surface via their RGD recognizing integrins.

For cell adhesion studies, cells are incubated on the RGD-functionalized nanoparticle structured surface for a defined period of time. Afterwards cells are fixed by paraformaldehyde. Cellular nuclei are stained with DAPI to ensure only single cells are included in the analysis. Cell membranes and actin filaments are stained with wheat germ agglutinin (WGA) and phalloidin to determine the total area of the spread cells. Immunocytochemistry is used to analyze focal contacts, thus assessing the quality and quantity of formed focal adhesions. Size and shape of formed focal contacts are software

supported analyzed as they are a key characteristic to determine the quality of cell adhesion (Figure 9).

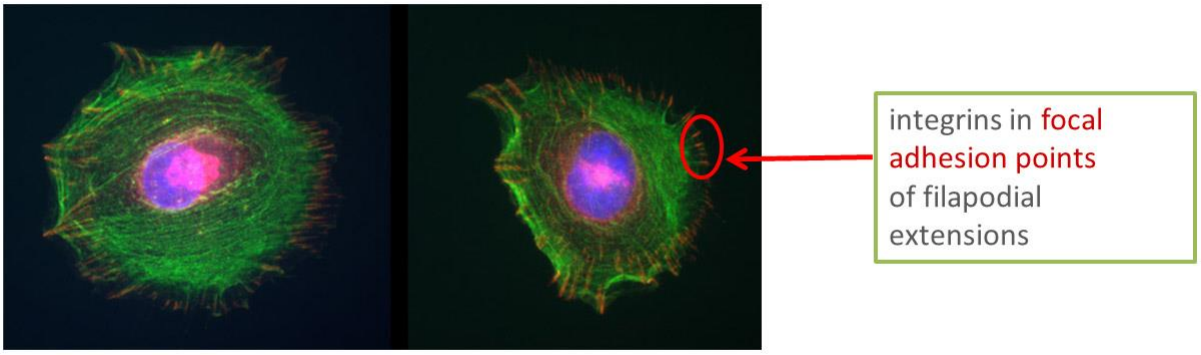


**Figure 9:** Rat embryonic fibroblast cells (cell line: REF52) with focal adhesion points (red) within the filapodial extensions. Size and shape of formed focal contacts are important characteristics to determine the quality of cell adhesion. Blue: nuclei (DAPI); Green: actin (phalloidin); Red: focal contacts (paxilin).

# 4. Integrin Ligands

## 4.1. *iso*DGR Peptides as Biselective Ligands for Integrins αvβ6 and α5β1

This chapter outlines a manuscript submitted to the *Journal of Medicinal Chemistry*. To avoid redundant information here the results are only briefly summarized. The full manuscript can be found in chapter 8.1.

**Biselectivity of *iso*DGR Peptides for Fibronectin Binding Integrin Subtypes α5β1 and αvβ6: Conformational Control through Flanking Amino Acids.**

**A. Bochen**, U. K. Marelli, E. Otto, D. Pallarola, C. Mas-Moruno, F. S. Di Leva, H. Boehm, J. P. Spatz, E. Novellino, H. Kessler, L. Marinelli.

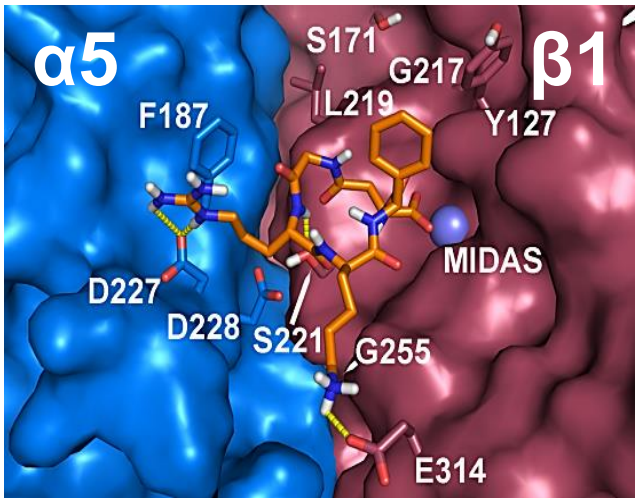


**Figure 10:** Optimized *c*(-phg-*iso*DGRk-) peptide docked into the binding pocket of integrin α5β1. It addresses integrin subtypes α5β1 and αvβ6, both are receptors of fibronectin. Binding to integrin αvβ3 and αIIbβ3 is completely suppressed.

In addition to the RGD sequence as an essential integrin binding motif, recent studies have proven that a naturally occurring NGR to *iso*DGR rearrangement within ECM proteins creates a new integrin binding site.[83, 84] Non-binding amino acid sequence Asn-Gly-Arg (NGR) is transformed by rearrangement and subsequent deamidation into an *iso*DGR motif. The *iso*DGR motif is recognized by the RGD binding integrins with different affinities.

This publication aimed to explore the *iso*DGR motif as a specific integrin binding sequence. Insights obtained by a previous publication of our group in the design of active, cyclic *iso*DGR pentapeptide integrin inhibitors[79] were used here for the synthesis of an, in terms of integrin affinity and selectivity, improved *iso*DGR peptide library. To be more precise, the previous publication demonstrated the necessity of the unnatural amino acid D-phenylglycine at the *N*-terminal position of the *iso*DGR motif for activity. Herein, the impact of the remaining site at the *C*-terminal position of the *iso*DGR motif within these cyclic pentapeptides, was systematically screened. Amino acids containing aliphatic side chains, aliphatic side chains with polar groups and aromatic side chains were incorporated at this position, either in their L- or D- amino acid configuration. The synthesized peptide library was tested for integrin α5β1 and αvβ3 binding inhibition in a competitive ELISA-type assay. The peptides showed low nanomolar affinities for integrin α5β1 and improved selectivity against integrin αvβ3, if a D-amino acid was used at the screened position. The most promising candidates were also evaluated in their binding behavior for integrin αvβ5, αvβ6 and αIIbβ3. In contrast to the other analyzed integrins, α5β1 and αvβ6 both bind *in vivo* primarily to fibronectin. Therefore it was quite likely to obtain also active ligands for αvβ6. The most active peptide for integrin α5β1, *c*(-phg-*iso*DGRw-), showed an activity of 5.5 nM for α5β1 and 92 nM for αvβ6 (αvβ3: >10000 nM, αvβ5: >10000 nM, αIIbβ3: >10000 nM). Almost as active for integrin α5β1, but also highly active for αvβ6, peptide *c*(-phg-*iso*DGRk-) was the best biselective compound for the both integrins (α5β1: 8.7 nM, αvβ6: 19 nM, αvβ3: >10000 nM, αvβ5: >10000 nM, αIIbβ3: >10000 nM). In contrast, the corresponding L-amino acid analogue, *c*(-phg-*iso*DGRK-), was only moderately active for α5β1 (94 nM), αvβ6 (140 nM) and by far less selective due to its activity towards integrin αvβ3 (516 nM).

For further insights on the binding mode and rationalization of these findings, the structure of the biselective compound, *c*(-phg-*iso*DGRk-), and the structure of its L-amino acid analogue were determined by NMR and molecular dynamics studies. Obtained structures were used for docking experiments of these ligands to integrin α5β1, αvβ3 and αvβ6 binding pockets. Structural differences induced by the different steric configurations were responsible for the observed activity and selectivity profile. Additionally, individual shape of the different integrin binding pockets contributed to additional ligand-integrin interactions or prevented such interactions.

Biological implications of these findings were studied by cell adhesion assays on gold nanoparticle structured surfaces. Therefore, *c*(-phg-*iso*DGRk-) was modified at the $N^{\varepsilon}$-lysine by a PEG spacer combined with a thiol anchor. The peptide was coated via its

thiol to the surface. Quality of cell adhesion was determined by analyzing the formed focal cell adhesions points. As a reference peptide within these cell experiments active, but less specific integrin ligand *c*(-RGDfK-) (αvβ3: 2.6 nM, αvβ6: 68 nM, α5β1: 133 nM, αvβ5: 310 nM, αIIbβ3: >10000 nM), functionalized by the same spacer and anchor as the *iso*DGR peptide, was used. As integrin αvβ3 is essential for the formation of focal complexes, an early step in the formation of focal adhesions, cell adhesion to the *iso*DGR coated surfaces was delayed in comparison to cell adhesion on surfaces coated with the reference peptide. In addition, geometrical shape of formed focal adhesions on *iso*DGR coated surfaces differed from the shape of adhesions formed on RGD coated surfaces. Focal adhesions formed on *iso*DGR coated surfaces were long and thin after 4 h, whereas focal adhesions formed on RGD coated surfaces were of a shorter and broader shape. Within 24 h this differences became smaller.

For more details the reader is referred to the full manuscript given in chapter 8.1.

# 4.2. Polyproline as a Spacer Connecting RGD and *iso*DGR Peptides to Gold Nanoparticle Structured Surfaces

## 4.2.1. Monovalent and Divalent Polyproline Spacers Functionalized by Click Chemistry with RGD Peptides for Coating of Gold Nanoparticle Structured Surfaces

This chapter outlines a manuscript which is prepared for submission to the *Journal of the American Chemical Society*. To avoid redundant information results are briefly summarized. The full manuscript can be found in chapter 8.2.

**Impact of RGD-functionalized Polyproline Spacers on Integrin Mediated Cell Adhesion to Gold Nanoparticle Coated Surfaces**

**Alexander Bochen**, Diego Pallarola, Heike Boehm, Joachim P. Spatz and Horst Kessler

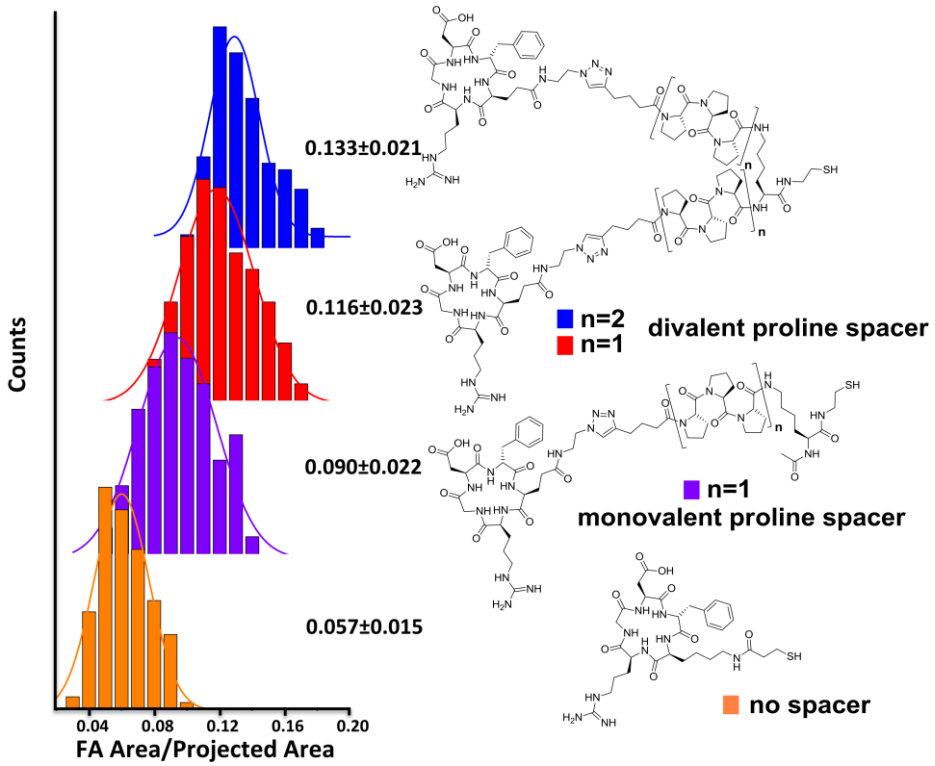


**Figure 11:** Quality of cell adhesion is determined by the ratio between the focal adhesion area and the projected cell area. The result of cell adhesion experiments to gold nanoparticle structured surfaces coated by the depicted peptides is shown. Integrin mediated cell adhesion is the lowest, if the RGD ligand is connected without a spacer by a thiol anchor to the surface (orange). Using a monovalent proline spacer (purple) or divalent proline spacer of different length (red & blue) further improves cell adhesion to this surface.

Functionalization of a surface with ligands mimicking the integrin binding motif within proteins of the extracellular matrix is a feasible approach to improve cell adhesion to these surfaces. However, these ligands cannot be directly connected to the surface via an anchor. A spacer in between the ligand and the anchor is crucial to for improved binding of cells to these coated surfaces.[14, 85, 86] Additionally, integrin mediated cell adhesion is also influenced by the topography of the surface, and its correlation to ligand coated surfaces has recently been investigated.[87] Nevertheless, in each of these studies flexible spacers of the aminohexanoic or polyethylenglycole type were used, possessing disadvantages like decreasing the integrin ligand's binding affinity as it was observed in several studies.[88, 89]

The focus of this publication was the evaluation of the polyproline sequence as a rigid spacer for the connection of integrin ligands to gold nanoparticle structured surfaces. The polyproline sequence forms rigid helices of the polyproline II type in aqueous media.[90-93] Cyclic RGD peptides of the *c*(-RGDfX-) type were linked using "click chemistry" and the polyproline sequences in different lengths to a thiol surface anchor. Besides monovalent ligands also the use of the polyproline sequence within divalent ligands was explored. Along with these rigid spacers, integrin ligands were linked with well-known flexible spacers of the ahx and PEG type in different lengths to thiol surface anchors. To compare results obtained for the rigid spacers, peptides using flexible spacers (PEG and ahx) were included. Influence of the spacer on ligand binding affinity was first assessed *in vitro* in an isolated receptor assay of the ELISA type. The binding affinity of the unmodified peptide *c*(-RGDfK-) towards integrin αvβ3 was 2.6 nM. Modification of the Lys side chain by mercaptopropionic acid as a thiol surface anchor just slightly altered the binding affinity (3.4 nM). Insertion of an aminohexanoic spacer between the Lys side chain and the thiol anchor reduced the integrin αvβ3 binding affinity of the ligand to 13.6 nM. Using a PEG spacer of similar length (triethylenglycole amino acid, trigas) as the ahx spacer, the integrin αvβ3 binding affinity of the ligand was only reduced to 8.4 nM. Increasing the length of the PEG spacer to heptaethylenglycol amino acid (Hegas) or double-Hegas further reduced the ligand's binding affinity to 13.6 nM and 16.5 nM respectively. In contrast, by using a triprolinehexanoic acid as a spacer, linked by the use of click chemistry to azido modified *c*(-RGDfE($N_3$)-) and connected with a lysine spacer to the thiol anchor, the integrin αvβ3 binding affinity of this ligand remained unaffected (2.4 nM), compared to the unmodified ligand. This is especially noteworthy as the total spacer length between the thiol and the cyclic peptide is already longer than it is

in the case of the Hegas modified compound. Even by further increasing the length of the proline spacer to six or nine residues, integrin αvβ3 binding affinity of these ligands was not altered (2.5 nM and 2.1 nM respectively). Divalent ligands, using the lysine as a linker between both polyproline spacers even increased the integrin αvβ3 binding affinity of these ligands ligand to the subnanomolar range (0.52 nM for the triproline spacer and 0.17 nM for the hexaproline spacer). The binding affinity of these divalent ligands was in the range of the super-potent integrin αvβ3 ligand Cilengitide (0.54 nM, *c*(-RGDf$^{Me}$V-)), while covering in solution longer distances with the spacer compared to the PEG or monovalent proline spacers.

Ligand binding affinity was determined in an isolated receptor assay using soluble integrin and soluble artificial integrin ligand. The next step was to use these peptides for coating of gold nanoparticle structured surfaces and subsequent cell adhesion studies to these coated surfaces to determine which peptide can foster cell adhesion best. The used rat embryonic fibroblast cells (REF52) are of globular shape, if not adhered to a surface and spread upon adhesion. The more spread the cells are, the better the adhesion to the surface is. During the cell spreading, filapodial extensions are formed possessing focal adhesion (FA) points in their tips. Therefore, the formed FAs of the cells were analyzed with regards to their size correlated to the total cell area. A clear trend was observed. Cell adhesion to surfaces with the integrin ligand without any spacer was the lowest, followed by the peptide using ahx spacer. The peptide using trigas PEG spacer gave better cell adhesion results than the peptide using ahx spacer and could be further increased the longer the PEG spacer was (Hegas and double-Hegas). The ligand using the shortest proline spacer was mediating cell adhesion better than the peptide using Hegas spacer. This trend further continued by increasing length of the proline spacer. The two divalent ligands containing the proline spacer were mediating cell adhesion best within the compared 10 peptides.

As a second criterion, adhesion dynamics was investigated. As observed before, also dynamics analyses revealed, that the surfaces coated with peptides without a spacer or using an ahx spacer were the ones with the slowest adhesion rate. The adhesion rate measured for surfaces coated by PEG spacers was higher and increased by increasing spacer length. The same trend was observed for monovalent and divalent proline spacers. Peptides with proline spacers showed the fastest adhesion rate, followed by PEG and ahx spacer peptides.

For more details the reader is referred to the full manuscript given in chapter 8.2.

### 4.2.2. Monovalent Polyproline Spacers Linking RGD and *iso*DGR Peptides to Gold Nanoparticle Structured Surfaces

Polyproline spacer compounds described in chapter 4.2.1 were all ligated to RGD peptides using click chemistry, which is especially important for the synthesis of divalent compounds. Consequently, a flexible alkyl section remains on both sides of the triazole formed during this ligation reaction. This joint breaks the rigidity introduced by the polyproline sequence. The influence of this flexible section next to the more rigid polyproline sequence on ligand integrin binding affinity was investigated by shortening the length of this flexible section to a minimum. Therefore, a set of peptides using polyproline spacers in two different lengths (3 or 6 prolines) were synthesized and functionalized by integrin ligands using peptide couplings. Integrin ligands *c*(-RGDfK-) (αvβ3, αvβ6 and α5β1), *c*(-phg-*iso*DGRk-) (α5β1 and αvβ6; chapter 4.1) and its azido-lysine derivative *c*(-phg-*iso*DGR-k($N_3$)-) were used. The latter one was ligated to the same monovalent polyproline spacer systems used in chapter 4.2.1 to allow further comparison. All synthesized peptides were additionally functionalized at the polyproline spacer with a thiol group, for coating of the peptides to gold nanoparticle structured surfaces and subsequent cell adhesion studies.

The amine of the last proline residue within the polyproline spacer was functionalized by mercaptopropionic acid (MPA). An amide bond was formed between the carboxylic acid of the first proline within the polyproline spacer and the $N^{\varepsilon}$-Lysine within peptide *c*(-RGDfK-) resulting in compounds **1** and **2** (Figure 12).

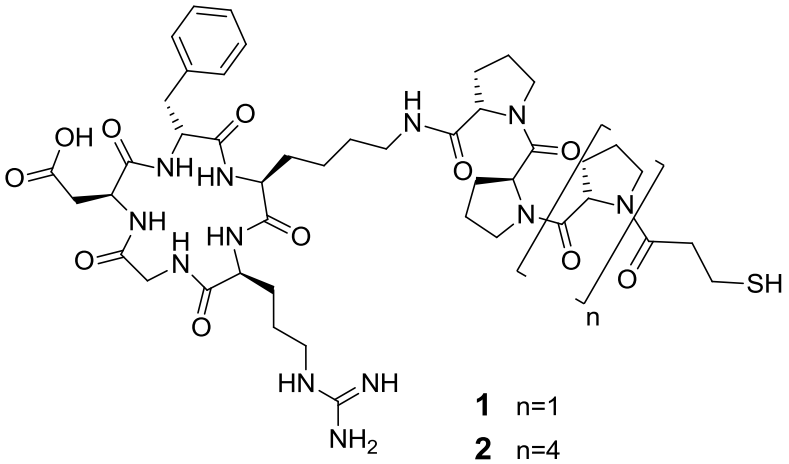


**Figure 12:** Peptide *c*(-RGDfK[MPA-PPP]-) **1** and hexaproline analog **2**. Proline spacer and cyclic peptide are directly connected by an amide bond. MPA: mercaptopropionic acid.

For the synthesis of **1** and **2**, TCP resin was loaded with Fmoc-Pro-OH, the triproline or hexaproline sequence synthesized as described in chapter 4.2.1 (COMU, Oxyma, DIEA) and the polyproline spacer functionalized by Trt-mercaptopropionic acid. The amide bond between the proline spacer and $N^{\varepsilon}$-Lysine of *c*(-RGDfK-) was formed by using the same coupling reagents as for the synthesis of the polyproline sequence.

The integrin α5β1/ αvβ6 biselective peptide *c*(-phg-*iso*DGRk-) was modified by MPA-polyproline spacers using the same methods as described for RGD-peptides (**1** and **2**) resulting in peptides **3** and **4** (Figure 13).

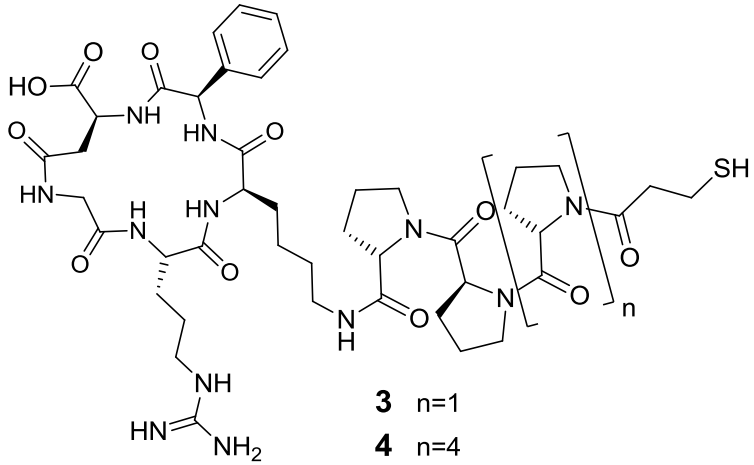


**Figure 13:** Peptide *c*(-phg-*iso*DGRk[MPA-PPP]-) **3** and hexaproline analog **4**. Proline spacer and cyclic peptide are directly connected by an amide bond. MPA: mercaptopropionic acid; phg: D-phenylglycine.

To compare integrin α5β1/ αvβ6 biselective *iso*DGR ligands (**3** and **4**) to RGD ligands described in chapter 4.2.1, the lysine azido-derivative, *c*(-phg-*iso*DGRk($N_3$)-), of the isoDGR peptide was synthesized. This ligand was ligated by click chemistry to two alkynyl containing, monovalent polyproline spacers (3 or 6 prolines, chapter 4.2.1). This peptide was functionalized with Trt-cystamine using the same methods as described in chapter 4.2.1, resulting in peptides **5** and **6** (Figure 14).

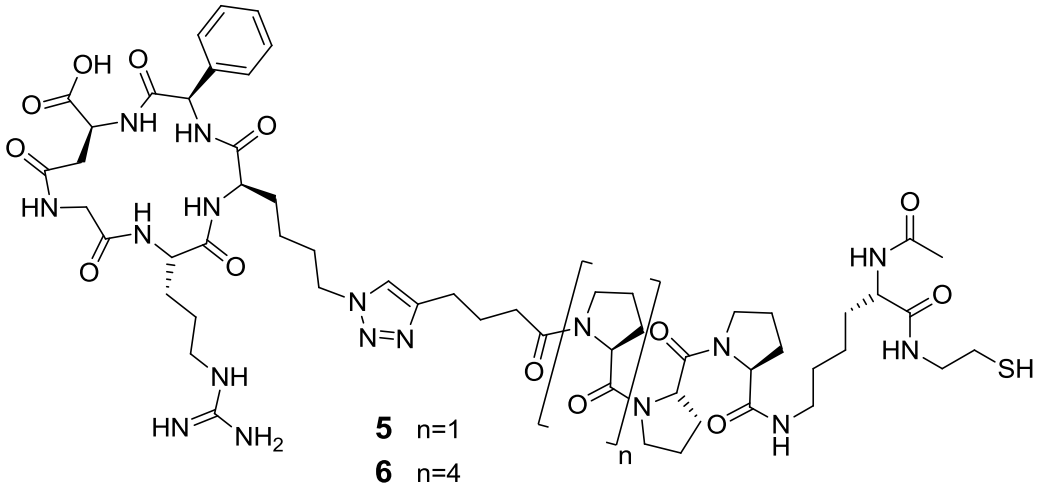


**Figure 14:** Peptide Ac-K[*c*(-phg-*iso*DGRk[HexPPP]-)]-cta **5** and hexaproline analog **6**. Proline spacer and cyclic peptide were ligated using click chemistry. cta: cystamine, Hex: 5-(1-alkyl-1*H*-1,2,3-triazol-4-yl)pentanoic acid, D-phenylglycine.

To determine the $IC_{50}$ of the synthesized peptides for integrin α5β1 and αvβ3, the previously described isolated receptor assay of the ELISA type was used (chapter 3.2). Results are summarized below (Table 2).

**Table 2:** Inhibition of integrin binding to vitronectin (αvβ3) or fibronectin (α5β1) by *c*(-RGDfK-), *c*(-phg-*iso*DGRk-) or *c*(-phg-*iso*DGRk($N_3$)-) peptides functionalized at the lysine side chain by a proline spacer and thiol anchor group. In compounds **1**-**4** spacer and binding motif were connected via an amide bond, in compounds **5** and **6** spacer and binding motif were connected via an amide bond mimic, the 1,2,3-triazole formed by a click chemistry ligation reaction.

| Peptide | $IC_{50}$ [a] αvβ3 [nM] | IC50 [a] α5β1 [nM] |
|---|---|---|
| **1** *c*(-RGDfK[MPA-PPP]-) | 1.6 (± 0.3) | 262 (± 62) |
| **2** *c*(-RGDfK[MPA-PPPPPP]-) | 2.1 (± 0.3) | 232 (± 34) |
| **3** *c*(-phg-*iso*DGRk[MPA-PPP]-) | 1045 (± 198) | 17.3 (± 1.0) |
| **4** *c*(-phg-*iso*DGRk[MPA-PPPPPP]-) | 1319 (± 448) | 27.0 (± 5.4) |
| **5** Ac-K[*c*(-phg-*iso*DGRk[HexPPP]-)]-cta | 479 (± 93) | 6.4 (± 1.1) |
| **6** Ac-K[*c*(-phg-*iso*DGRk[HexPPPPPP]-)]-cta | 434 (± 109) | 12.5 (± 0.8) |
| *c*(-RGDfK-) | 2.6 (± 0.6) | 133 (± 23) |
| *c*(-phg-*iso*DGRk-) | >10000 | 8.7 (± 0.7) |
| Cilengitide[b] | 0.54 (± 0.15) | 15.4 (± 3.0) |

[a]$IC_{50}$ values were derived from a competitive ELISA using immobilized fibronectin and soluble integrin α5β1 or vitronectin and integrin αvβ3 respectively. [b]The highly active, cyclic pentapeptide Cilengitide, *c*(-RGDf$^{Me}$V-) was used in ELISA as a control αvβ3 and α5β1 inhibitor. cta: cystamine, Hex: 5-(1-alkyl-1*H*-1,2,3-triazol-4-yl)pentan-2-one, MPA: mercapto-propionic acid, phg: D-phenylglycine.

The $IC_{50}$ of spacer peptides containing *c*(-RGDfK-) integrin ligand (**1** and **2**) on integrin αvβ3 remained unaffected (1.6 nM and 2.1 nM) compared to the unmodified cyclic peptide (2.6 nM, chapter 4.1). This is consistent with the results previously observed for compounds ligated by click chemistry (chapter 4.2.1). Affinities of the compounds for α5β1 were reduced (262 nM and 232 nM) compared to the unmodified cyclic peptide (133 nM, chapter 4.1). Notably, this effect is slightly stronger compared to the Hegas modified cyclic peptide (197 nM, chapter 4.1). For *iso*DGR peptides that are directly connected to the proline spacer (**3** and **4**), the integrin α5β1 binding affinity (**3**: 17.3 nM; **4**: 27.0 nM) remained similar to the binding affinity of the Hegas modified *iso*DGR peptide (27.0 nM, chapter 4.1) to integrin α5β1. In comparison, unmodified peptide *c*(-phg-*iso*DGRk-) (chapter 4.1) had a binding affinity of 8.7 nM towards integrin α5β1. Integrin αvβ3 binding affinity of these peptides was not as low as expected (**3**: 1045 nM; **4**: 1319 nM), demonstrating that these peptides are less selective compared to the stem peptide, *c*(-phg-*iso*DGRk-) ($IC_{50}$ integrin αvβ3: >10000 nM, chapter 4.1). Remarkably, the binding affinity was increased to the level of the unmodified *iso*DGR peptide, if the azido-derivative, ligated to alkynyl-functionalized polyproline spacers was used (**5**: 6.4 nM and **6**: 12.5 nM). However, integrin αvβ3 binding affinity was increased as well (**5**: 479 nM and **6**: 434 nM).

These findings indicate the strong influence of the formed triazole as an amide bond mimic on the binding affinity.[94, 95] Summarizing these results, the use of the polyproline sequence as a spacer between the RGD-ligand and surface anchor, did not influence the binding affinity towards integrin αvβ3, if compared to the binding affinity of the unmodified RGD-ligand. Using *iso*DGR integrin ligands, the binding affinity towards integrin α5β1 was decreased about the same amount as observed for more flexible spacers. However, the affinity of the unmodified *iso*DGR peptide was regained by connecting the *iso*DGR peptide by click chemistry to the proline spacer. Thus, the polyproline sequence can be used as a spacer system performing at least as well as the more flexible Hegas spacer.

In conclusion, using the polyproline sequence as a spacer, improvements towards retained binding affinity of the ligand can be achieved. Performance of this spacer depends on the type of connection formed between ligand and spacer (amide or 1,2,3-triazol), as well as on the targeted integrin (α5β1or αvβ3).

Biological implications of these findings are currently investigated in a cell adhesion assay on gold nanoparticle structured surfaces coated with these peptides. This assay is performed by *Dr. Diego Pallarola* from the group of *Prof. Dr. J.P. Spatz* at the MPI for Intelligent Systems (Stuttgart, Germany).

## 4.3. RGD Peptides Connected by Polyproline Spacer to a Label Suitable for Fluorescence or PET Imaging

Summarizing results from chapter 4.2, the polyproline spacer sequence is not influencing the binding affinity of a cyclic RGD peptide grafted onto this spacer sequence, hence it remains as active as the unmodified *c*(-RGDfK-). This chapter describes the redesign of these ligands for two, in preclinical or clinical settings, commonly used imaging methods.

The first imaging method, the peptide was adapted to, was fluorescence microscopy. By introduction of a fluorescence imaging label to the RGD peptide, the targeted integrin expressing tissues of interest can be visualized using an appropriate microscopy technique. Widely used Cy5.5 label has been chosen as an exemplary label for this class of imaging probes.
As a second imaging method, PET imaging (*positron emission tomography*) was chosen due to its wide utilization in clinical practice, both in research and as an established imaging method for the diagnosis of several severe diseases. NODAGA chelates efficiently radionuclides suitable for PET, such as $^{68}$Ga, and is used here as an exemplary tracer for PET imaging.
In order to synthesize these compounds, the synthesis strategy used for azido-RGD and the polyproline spacer scaffold was adapted, which is described in chapter 4.3.2.

### 4.3.1. Background

Imaging of biological processes is a fundamental requirement for an in depth understanding of disease progression. *Positron emission tomography* and *fluorescence microscopy* are two widely used techniques enabling scientists to track biological processes. Using PET *in vivo,* these processes can be visualized and followed using an appropriate tracer. Several different radionuclides suitable for PET imaging exist, e.g. $^{11}$C, $^{13}$N, $^{18}$F or $^{68}$Ga. Visualization of glucose metabolism by $^{18}$F-2-Deoxy-2-fluoro-D-glucose (FDG) was one of the first experiments demonstrating the potential of the PET technique.[96] Expression of biomarkers (e.g. protein) in different tissues can also be tracked by appropriate ligands. Therefore, the ligand is functionalized by a radionuclide suitable for PET imaging. This can be done for some nuclei by covalent binding of the radionuclide to the ligand. Besides FDG for glucose metabolism visualization, $^{18}$F is also covalently bound to the ligand in $^{18}$F-Galacto-RGD, which is the most prominent example

as a ligand used for PET imaging of integrin αvβ3 expression *in vivo*.[97-99] A second approach is the introduction of the radionuclide by a chelator, which is linked covalently to the ligand. DOTA (1,4,7,10-tetraazacyclododecane-1,4,7,10-tetraacetic acid), NOTA (1,4,7-triazacyclononane-*N,N',N''*-triacetic acid) and its latest derivative NODAGA[100] (2-(4,7-*bis*(carboxymethyl)-1,4,7-triazonan-1-yl)pentanedioic acid) are most commonly applied.[101] A comprehensive illustration of the basic physical processes involved in PET imaging is given in Figure 15.

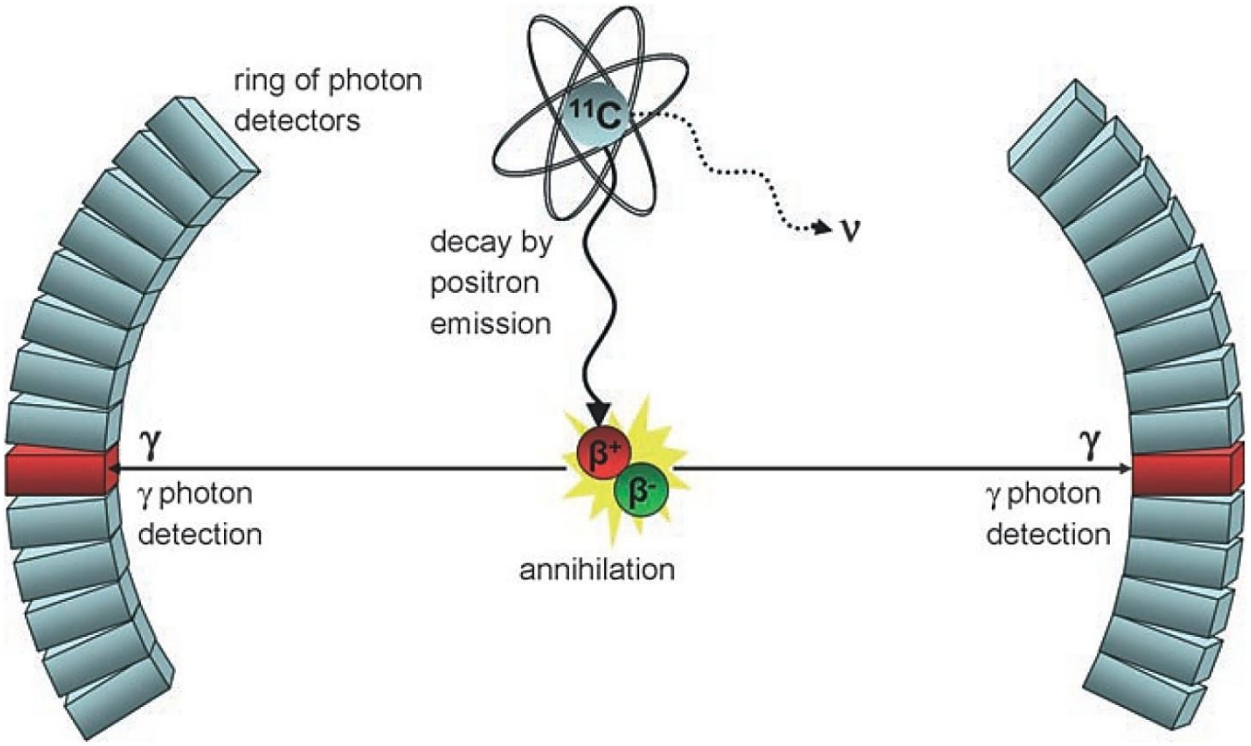


**Figure 15:** Schematic representation of the physical processes involved in PET imaging. The positron decay of the radionuclide and its subsequent annihilation by collision with an electron emits two γ-quanta of 511 keV. Both γ-quanta are emitted in the opposite direction, respectively. The quanta are detected by a circular array of photon detectors around the positron source. A PET image can be generated by computer assisted processing of the detected signals. Several radionuclides like $^{11}C$, $^{13}N$, $^{18}F$ or $^{68}Ga$ can be used as a positron source. Reprinted with permission, Copyright © 2008 WILEY-VCH Verlag GmbH & Co. KGaA, Weinheim.[102]

While PET improved spatial resolution compared to other methods, e.g. MRI (*magnetic resonance imaging*), spatial resolution is still low in comparison to optical imaging methods like near infrared (NIR) fluorescence imaging. The latter method allows determination of biological processes on a cellular level. Although it is developed towards an *in vivo* imaging method, it is usually used for *ex vivo* and cell culture analysis.[103, 104] Similar as for PET, a ligand targeting the biomarker of interest is covalently attached to a fluorophore. An orbital electron of the fluorophore is excited electronically and vibronically from its ground state ($S_0$) to its first electronically excited state ($S_1$) by photons of an external light source (absorption). The excitation energy transferred to the fluorophore is transformed upon relaxation to its ground state by vibronic transitions (non-radiative) and the emission of a photon (fluorescence). Emitted photons have a lower energetic value than photons used for excitation (*Stokes* shift), hence a longer wavelength (Jablonski diagram, Figure 16). Fluorescence labels consist of conjugated π-electron systems which are expanded by aromatic moieties. As these molecular structures are of lipophilic character, their solubility in aqueous media is limited. Solubility is increased by functional groups, which are charged under physiological conditions. Fluorescence imaging allows cellular resolution and complements histopathologic staining of tissue samples. Combing all methods, a plethora of information about a biological process, both in time and space can be obtained.

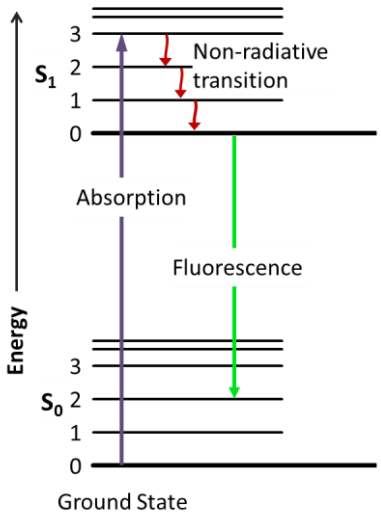


**Figure 16:** Jablonski diagram. After an electron absorbs a high energy photon the system is excited electronically and vibrationally. The system relaxes vibrationally, and fluoresces at a longer wavelength.

One pathological condition in which imaging methods can help to reveal underlying biological processes is the acute myocardial infarction (MI), which is the ischemia of the myocardium after occlusion of a coronary artery (Figure 17). The healing process is accompanied by stages of necrosis, apoptosis, inflammation, fibroblast proliferation, agiogenesis and scar formation.[105, 106] Inadequate healing leads to left ventricle remodeling and heart failure.

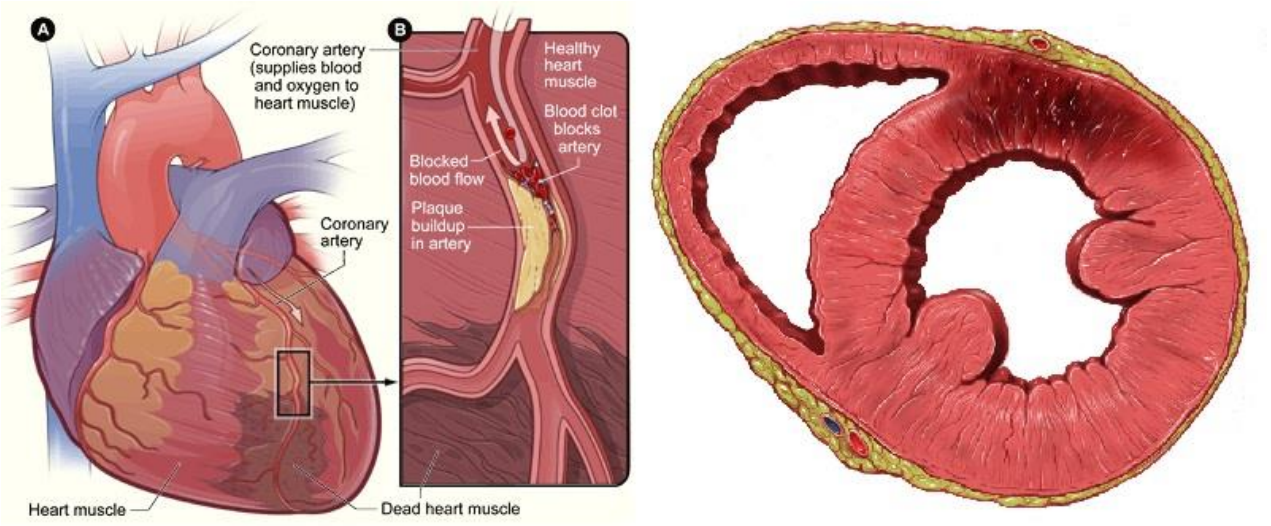


**Figure 17: Left: A)** Heart with dead heart muscle caused by lack of oxygen after coronary artery occlusion. **B)** Longitudinal cut of a coronary artery with plaque buildup and a blood clot. (http://www.nhlbi.nih.gov/health/health-topics/topics/heartattack) **Right:** Heart posterior left ventricle wall infarction (dark red: dead heart muscle cells). ©Patrick J. Lynch, medical illustrator; C. Carl Jaffe, MD, cardiologist.

Integrin αvβ3, which is highly important for angiogenesis, is one of the integrins up-regulated on endothelial cells and myofibroblasts within the infarcted area.[107] Tracking the healing process within the infarcted area by imaging of integrin αvβ3 expression has been shown to be feasible by RGD based PET tracers.[108-110] Expression level of integrin αvβ3 and uptake of integrin αvβ3 tracers within the myocardium is highest one week after infarct.[111] These PET tracers allow an assessment of the healing processes within the infarcted area. However, to gain more detailed information about the healing process on a cellular level, NIR fluorescence imaging is more valuable.

### 4.3.2. Modifications of the Stem Peptide, Synthesis Strategy and *In Vitro* Evaluation

Since incorporating azido modified amino acids in cyclic peptides, standard procedures for their synthesis became more complicated in terms of purification and yield. Consequently, the critical step of *c*(-R(Pbf)GD(O$^t$Bu)fE-) modification in solution by 2-azidoethylamine was avoided by incorporation of Fmoc-Lys($N_3$)-OH instead of Fmoc-Glu(Bn)-OH during the solid phase peptide synthesis of the linear precursor. This was combined by on resin head-to-tail peptide backbone cyclization. To achieve this, Fmoc-Asp-OAllyl was attached onto TCP resin via its side chain and the linear precursor synthesized using standard Fmoc SPPS conditions. During SPPS, the azido group is inert to the applied reaction conditions. After cyclization, the Pbf-protected peptide is cleaved from the solid support and can be used for click chemistry ligation reactions without further purification.

Imaging agents such as Cy5.5 or NODAGA are commonly ligated to the molecule of interest by an amide bond formation and are consequently commercially available as active esters of the *N*-hydroxysuccinimide (NHS) type. For the ligation of NHS-activated imaging agents to the RGD-polyproline spacer ligands, a primary amine is indispensable. The introduction of an additional lysine into the sequence offered a modification site for the imaging agent at the lysine-$N^{\varepsilon}$. By this, any label of the NHS-type can easily be introduced. Therefore, Fmoc-Lys(Alloc)-OH was coupled to resin bound Fmoc-Lys(ivDde)-OH, offering an orthogonal protecting group (Alloc) and a semi-orthogonal protecting group (ivDde) at the lysine-$N^{\varepsilon}$ during Fmoc SPPS. Fmoc-Lys(Alloc)-OH was incorporated as a linker for the synthesis of divalent spacer peptides and its $N^{\alpha}$ was acetylated during the synthesis of the monovalent spacer peptide (analog as described in chapter 4.2.1). After the synthesis of the polyproline spacer peptide was completed, the ivDde protecting group of the lysine-$N^{\varepsilon}$ was removed and the imaging label was introduced at this position during the last step of the synthesis. To avoid unnecessary functional groups, these spacer systems were synthesized on ChemMatrix RinkAmide solid support, resulting in a *C*-terminal amide after peptide cleavage. All these modifications are summarized in Figure 18.

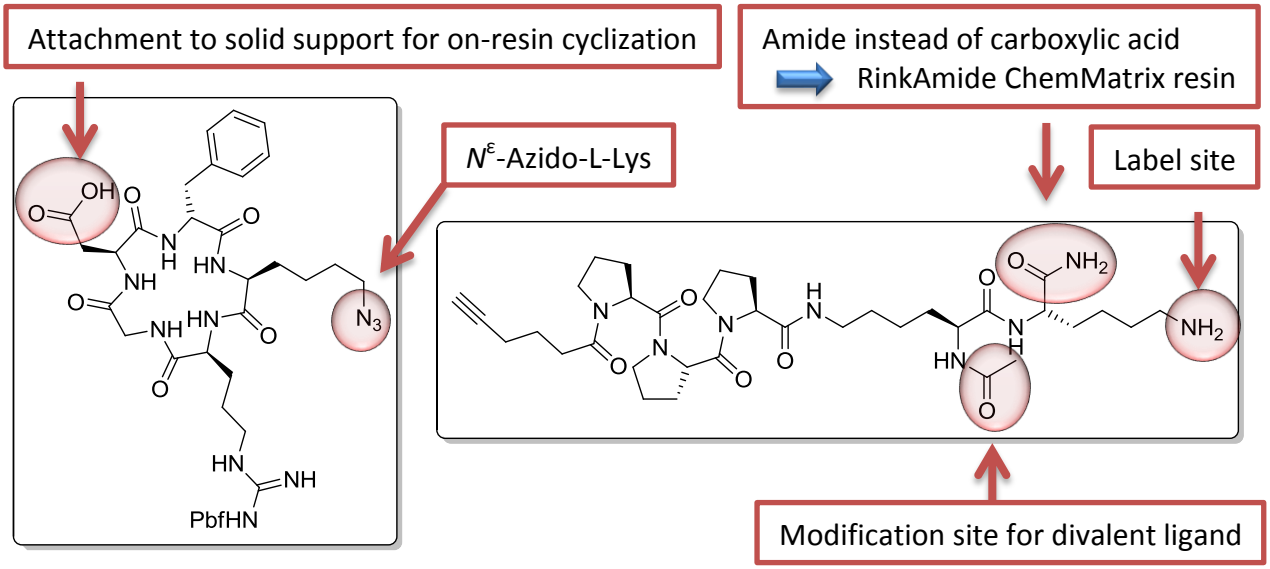


**Figure 18:** RGD-polyproline peptide building blocks described in chapter 4.2.1 were adapted to be suitable for different imaging methods by the introduction of several modifications. Due to improper precipitation of azido-modified *c*(-R(Pbf)GD(O$^t$Bu)fE-) (chapter 4.2), synthesis of azide modified cyclic peptide was improved by incorporation of $N^{\varepsilon}$-azido-lysine into the sequence in combination with cyclization of the linear precursor on solid support. Therefore, Fmoc-Asp-OAllyl was attached to the solid support via its side-chain. RinkAmide resin was used for the synthesis of the proline spacer resulting in a *C*-terminal amide after cleavage from solid support. $N^{\varepsilon}$ amino group of the first lysine within the polyproline spacer peptide was used to for the imaging label ligation reaction. For the synthesis of a divalent compound, a second polyproline spacer was synthesized at the position of the acetyl group.

Four different peptides (**7**-**10**) were synthesized in order to compare the influence of the two imaging labels (NODAGA and Cy5.5) on the binding affinity of RGD peptides using the polyproline sequence as a spacer between both fragments. Two monovalent RGD peptides containing a triproline spacer were combined with Cy5.5 or NODAGA imaging labels as well as their two divalent analogues (Figure 19).

Binding affinities of the synthesized peptide probes towards integrin αvβ3 were determined by an isolated receptor assay as described in chapter 3.2. Monovalent Cy5.5 peptide (**7**) showed a significant reduced binding affinity towards integrin αvβ3 (20.3 nM) compared to the unmodified *c*(-RGDfK-). In this case, the short polyproline sequence was not able to retain the binding affinity around the 2.6 nM of the unmodified peptide, as it was observed before for other modifications (chapter 4.2). In contrast, divalent Cy5.5-peptide (**8**) obtained subnanomolar binding affinity (0.3 nM) towards integrin αvβ3 and was within the same subnanomolar affinity range as observed for all divalent polyproline peptides synthesized (chapter 4.2.1).

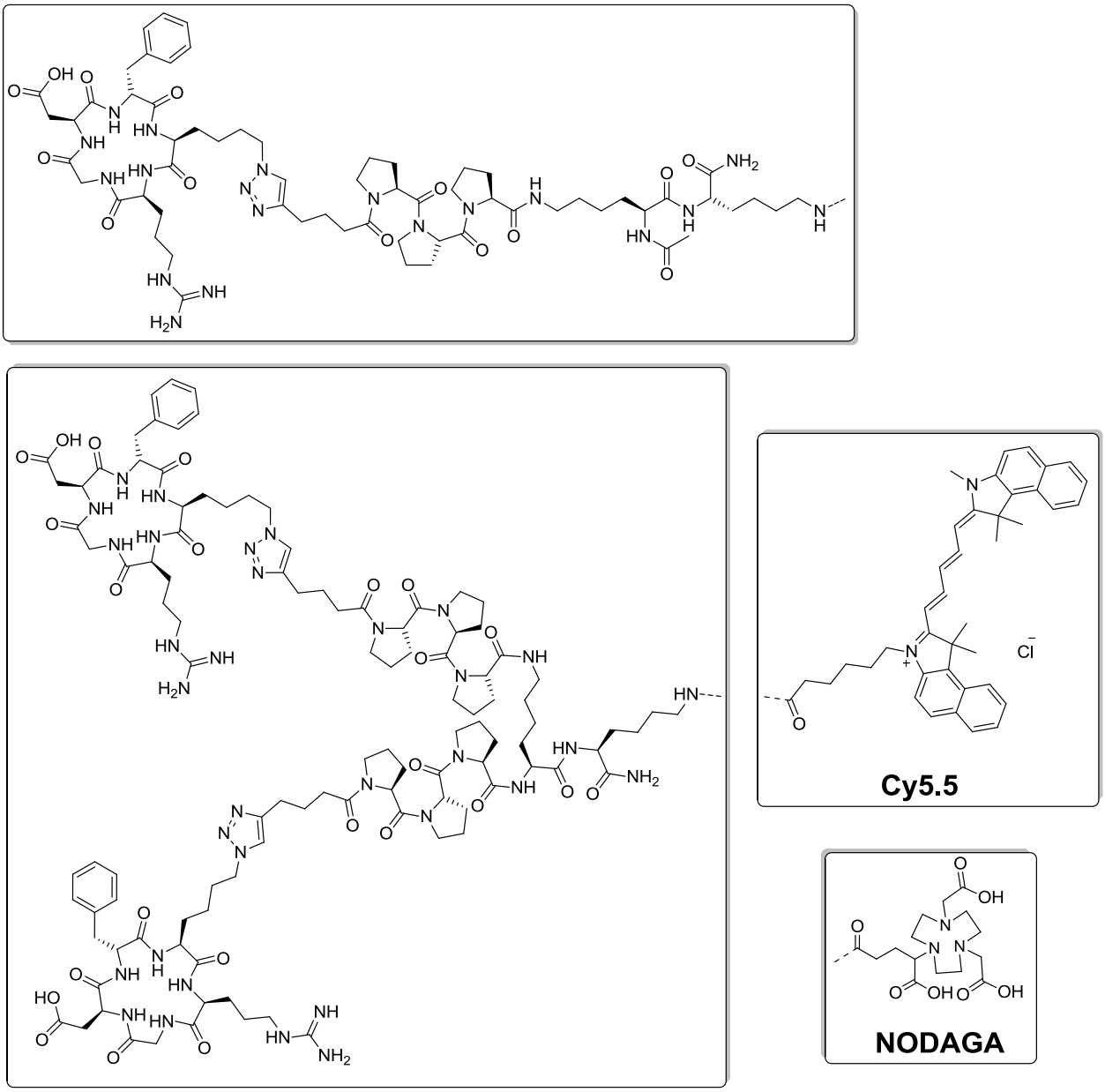


**Figure 19:** Monovalent and divalent peptides modified either with Cy5.5 (**7**, **8**) or NODAGA (**9**, **10**) for *ex vivo* fluorescence imaging and *in vivo* PET imaging.

Monovalent NODAGA-peptide (**9**) retained the integrin αvβ3 binding affinity (1.8 nM) of the stem peptide. This might rely on the smaller size of the NODAGA imaging label compared to Cy5.5. By using divalent NODAGA peptide (**10**), binding affinity improved to the subnanomolar range (0.6 nM), which was consistent with the results obtained for **8** and in chapter 4.2.1. Binding affinities towards integrin α5β1 remained unaffected for compounds **8**-**10** compared to the unmodified cyclic peptide (125 nM), with compound **7** as the only exception. Results of integrin αvβ3 and α5β1 ELISAs are summarized below (Table 3).

**Table 3:** Inhibition of integrin binding to vitronectin (αvβ3) or fibronectin (α5β1) by monovalent and divalent cyclic RGD compounds ligated to a proline spacer using click chemistry. The spacer system is either functionalized by Cy5.5 or NODAGA imaging agents for fluorescence- and PET-imaging.

| Peptide | $IC_{50}$ [a] αvβ3 [nM] | $IC_{50}$ [a] α5β1 [nM] |
|---|---|---|
| **7** Ac-K-[*c*(-RGDfK[HexPPP]-)]-K(Cy5.5)-$CONH_2$ | 20.3 (± 3.2) | 205 (± 12) |
| **8** [*c*(-RGDfK[HexPPP]-)]$_2$K-K(Cy5.5)-$CONH_2$ | 0.3 (± 0.06) | 114 (± 19) |
| **9** Ac-K-[*c*(-RGDfK[HexPPP]-)]-K(NODAGA)-$CONH_2$ | 1.8 (± 0.3) | 111 (± 14) |
| **10** [*c*(-RGDfK[HexPPP]-)]$_2$K-K(NODAGA)-$CONH_2$ | 0.6 (± 0.1) | 121 (± 17) |
| *c*(-RGDfK-) | 2.6 (± 0.6) | 133 (± 23) |
| Cilengitide[b] | 0.54 (± 0.15) | 15.4 (± 2.7) |

[a]$IC_{50}$ values are derived from a competitive ELISA using immobilized fibronectin and soluble integrin α5β1 or vitronectin and integrin αvβ3 respectively. [b]The highly active, cyclic pentapeptide Cilengitide, *c*(-RGDf$^{Me}$V-) is used in ELISA as a αvβ3 and α5β1 control inhibitor. Hex: 5-(1-alkyl-1*H*-1,2,3-triazol-4-yl)pentanoic acid.

### 4.3.3. Evaluation of Peptides for Fluorescence Imaging in the *Rat Myocardial Infarction Model*

Peptides **7** and **8** are currently investigated for their imaging properties in comparison to commercially available fluorescence imaging agent Anaspec *c*(-RGDyK[HiLyte$^{TM}$ 750]-) in a rat model of *myocardial infarct* (MI) by *Dr. Iina Laitinen* (Department of Nuclear Medicine), *Dr. Stefan Stangl* (Department of Radiotherapy and Radiological Oncology) and *Dr. Martina Rudelius* (Department of Pathology) at the Klinikum rechts der Isar der TUM (Munich, Germany).

Briefly, MI was induced in healthy male Wistar rats by ligation of the coronary artery. One week after the infarct, the animals (n=10) were anaesthetized and injected intravenously with 20 nmol of either Cy5.5 labeled RGD peptide **7** or **8**, and sacrificed 4 h after. In order to study the specificity of the integrin binding of peptides **7** and **8**, two animals received also an injection 1 µmol of an integrin αvβ3 specific compound **sn242** ($IC_{50}$: 0.86 nM (αvβ3) and 127 nM (α5β1), synthesized in our group by *Stefanie Neubauer*) 2.5 h before the peptide injection as a negative control. The heart, spleen and muscle were dissected and processed to cross sections. The Cy5.5 signal was visualized from the sections using an optical camera system with appropriate filters. Thin sections were processed for immunohistochemical stainings.

In most of the animals studied, a clear signal accumulation was seen in the infarcted area. In the reference tissues spleen and muscle showed positive and weak background signal respectively. When integrin αvβ3 was blocked by the specific compound (**sn242**), no signal was detected in the heart and muscle sections, and only very weak signal in the spleen (Figure 20).

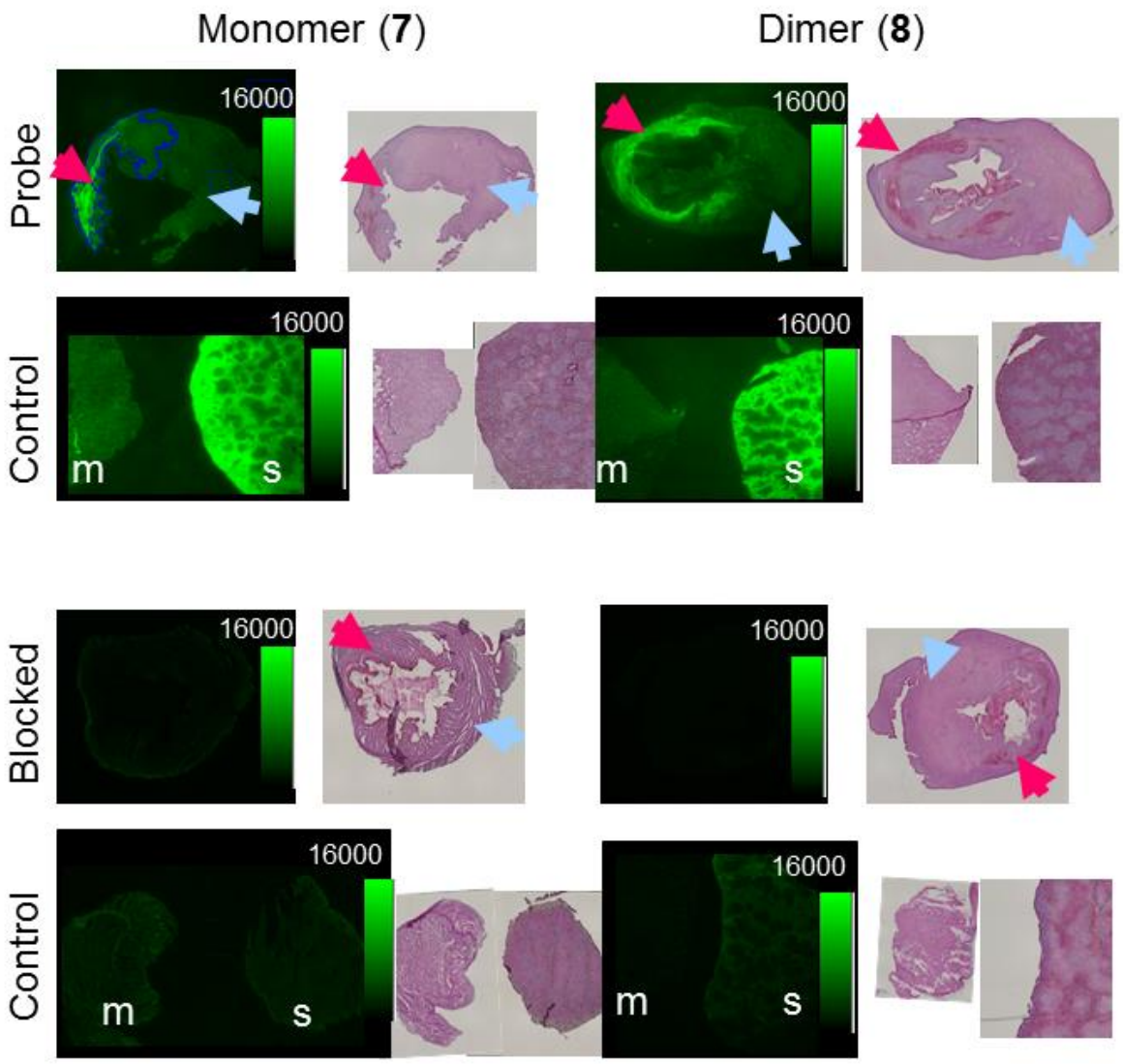


**Figure 20:** Cy5.5 signal of the myocardial, muscle (m) and spleen (s) cross sections *ex vivo* 4 h after *in vivo* injection of either monovalent or divalent RGD-Cy5.5 compound, and HE staining of same or adjacent section. Red arrowhead: infarct; blue arrowhead: remote myocardium, m: muscle (negative control), s: spleen (positive control). Blocking performed with 1 µmol of αvβ3 specific compound (**sn242**) injected 2 h prior Cy5.5-RGD compound injection.

Immunohistological analysis showed colocalisation of Cy5.5 signal in F4/80 positive cells (macrophages) and not in CD31 positive neovessels (Figure 21). Further studies are ongoing to verify the result, as well as the quantification of the signal in order to study potential benefits of the divalent probe over the monovalent probe with regards to an improved target to background ratio.

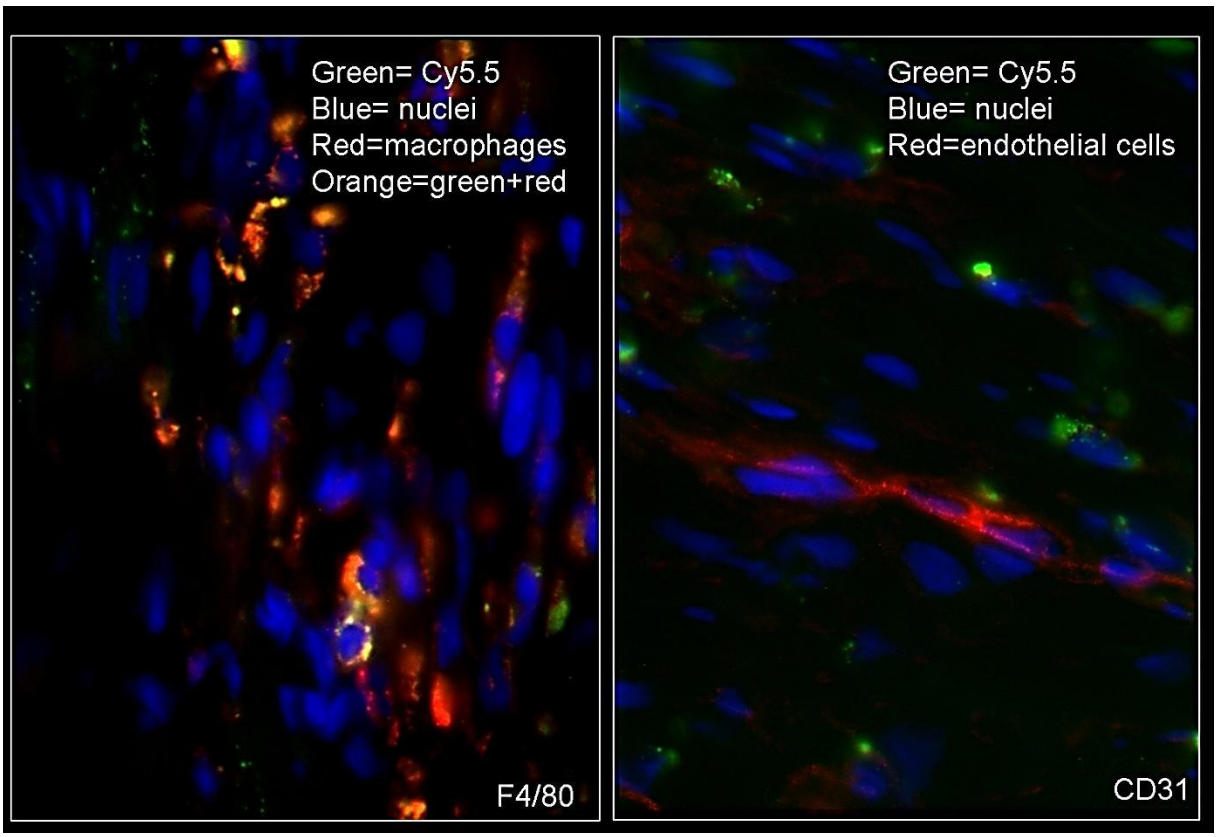


**Figure 21:** Fluorescence microscopy images of infarct borderzone after *in vivo* injection of compound **8** and further immunohistochemical staining with F4/80 (macrophages) or CD31 (endothelial cells). Sections were counterstained with DAPI (nuclei). Cy5.5 signal colocalizes with F4/80 positive cells.

## 4.4. RGD Peptide Coating of Stents Using Isothiocyanate Functionalized Polyproline Spacers

Vascular stents are expandable metal mesh tubes dilated into blood vessels to counteract local, disease induced flow constriction. Coating of stents with a *c*RGD-based peptide, connected by aminohexanoic acid (Ahx) spacer and an anchor moiety to the stent, facilitates vascular healing and endothelization of newly implanted stents.[112] Based on the knowledge gained by the study comparing Ahx, polyethyleneglycole (PEG) and polyproline spacers (chapter 4.2.1) it could be feasible to further improve endothelization and wound healing after stenting by using other than Ahx spacers. Isothiocyanate (ITC) functionalized *c*RGD-PEG spacers of different length have been synthesized by *Dr. Carles Mas-Moruno* in our group. RGD-peptides which are linked by polyproline spacers of different lengths to the ITC anchor could not be synthesized using the same synthesis strategy as for PEG spacer compounds due to *Edman* degradation during the synthesis. Successfully applied synthesis strategy and *in vitro* results are discussed in this chapter.

### 4.4.1. Background

Arteriosclerosis is a chronic disease induced by lipid-rich inflammatory plaque formation in the inner layers of the artery wall. The formed plaque restricts the blood flow in the arteries and in consequence to the heart muscle cells inducing hypoxia. Late stage atherosclerotic plaques are prone to ruptures causing thrombotic material to enter the artery lumen and in worst case to totally occlude the artery. Semi- or total occlusions cause angina pectoris or acute myocardial infarction. Several therapeutic strategies are existent to circumvent this disease. One of them is to dilate the affected vessel by catheter-based coronary intervention, i.e. percutaneous transluminal coronary intervention (PTCA). In the beginning, this was achieved by dilating a plain balloon at the target site. However, this technology had the major draw-back of vessel wall recoil in the short-term making repeated interventions necessary. The use of bare metal stents (BMS) has drastically improved this situation by grafting a metal strut into the artery to withstand vessel recoil and to keep it permanently open.[113] Nevertheless, proliferating vascular smooth muscle cells (VSMCs) resulted in an in-stent neointima growth reducing vessel diameter again (restenosis, Figure 22). Therefore, drug eluting stents (DES) were developed to prevent restenosis. These stent types successfully reduce neointima growth by eluting antiproliferative drugs like paclitaxel, sirolimus or everolimus.[114-116] The

disadvantage of DES is that its antiproliferative drugs not only affect VSMCs but also have a negative influence on endothelial cells as well. These cells play a major role in many aspects of vascular biology as they provide a non-thrombogenic surface and are involved in vasoconstriction and vasodilation. Antiproliferative drugs thus prevent endothelial cell growth on the stent surface which inhibits a normal function of the artery within the stented area. Additionally, incomplete endothelial cell coverage of the stent may induce late stent thrombosis.[117] Further improvements in stenting technology are a current research topic of great relevance and several approaches are explored.[112, 118, 119] One of these strategies is the coating of stent material by RGD peptides, improving endothelial cell coverage of the stent via integrin mediated cell adhesion.[112] However, what is the best spacer between RGD peptide and isothiocyanate surface anchor still needs to be explored.

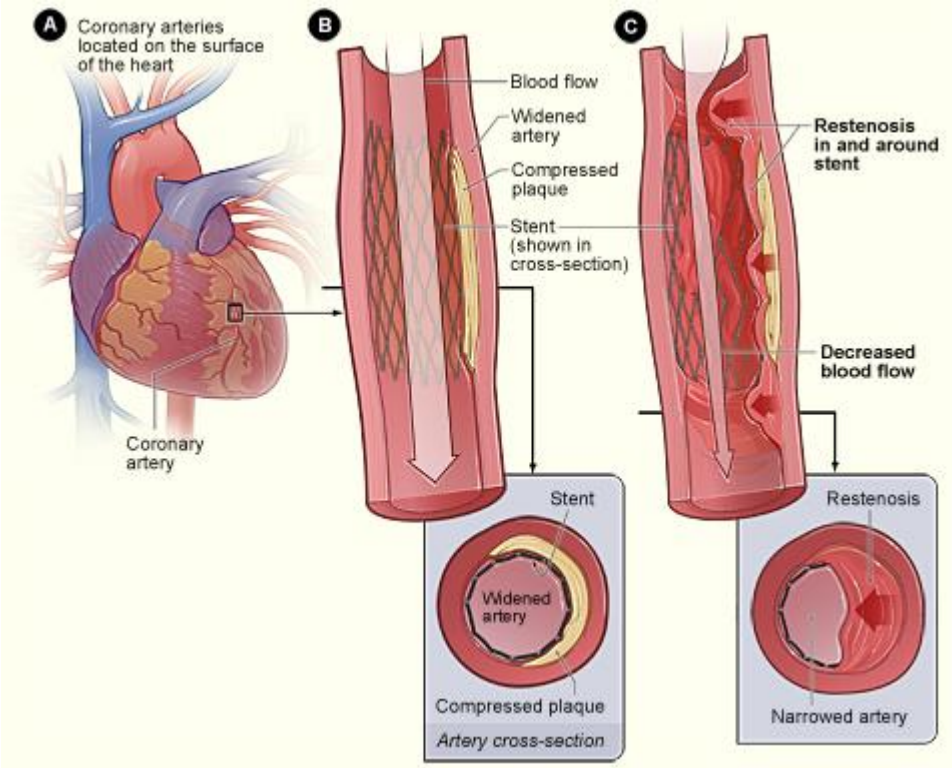


**Figure 22: A)** Coronary arteries located on the surface of the heart. **B)** Stented artery with normal blood flow. The inset image shows a cross-section of the stented artery. The plaque within the artery wall is compressed by the stent. **C)** Tissue growth in and around the stent. Neointima tissue growth causes re-narrowing of the artery and restricted blood flow. The inset image shows a cross-section of the tissue growth behind the stent (http://www.nhlbi.nih.gov/health/health-topics/topics/angioplasty/).

### 4.4.2. Isothiocyanate Functionalized Polyproline Spacers Connecting RGD Peptides to Stent Surfaces

ITC react under mild basic conditions with primary amines forming a thiourea. This ligation reaction is hereby used to coat amino-functionalized stent surfaces with RGD peptides linked by an ITC functionalized amino acid spacer to the surface. Phenyl-1,4-diisothiocyanate (DITC) reacts with the amine of the spacer and can be ligated in a following step via its second isothiocyanate to the amino-functionalized surface. Therefore, PEG spacers were attached to TCP-resin and functionalized on resin by DITC, subsequently cleaved from the resin and coupled by amide bond formation to the Lys-$N^{\varepsilon}$ within the *c*(-RGDfK-).

Using the same synthesis strategy for DITC functionalized polyproline spacers as for PEG spacers, *Edman* degradation occurred during the acidic cleavage from the solid support (Scheme 5).

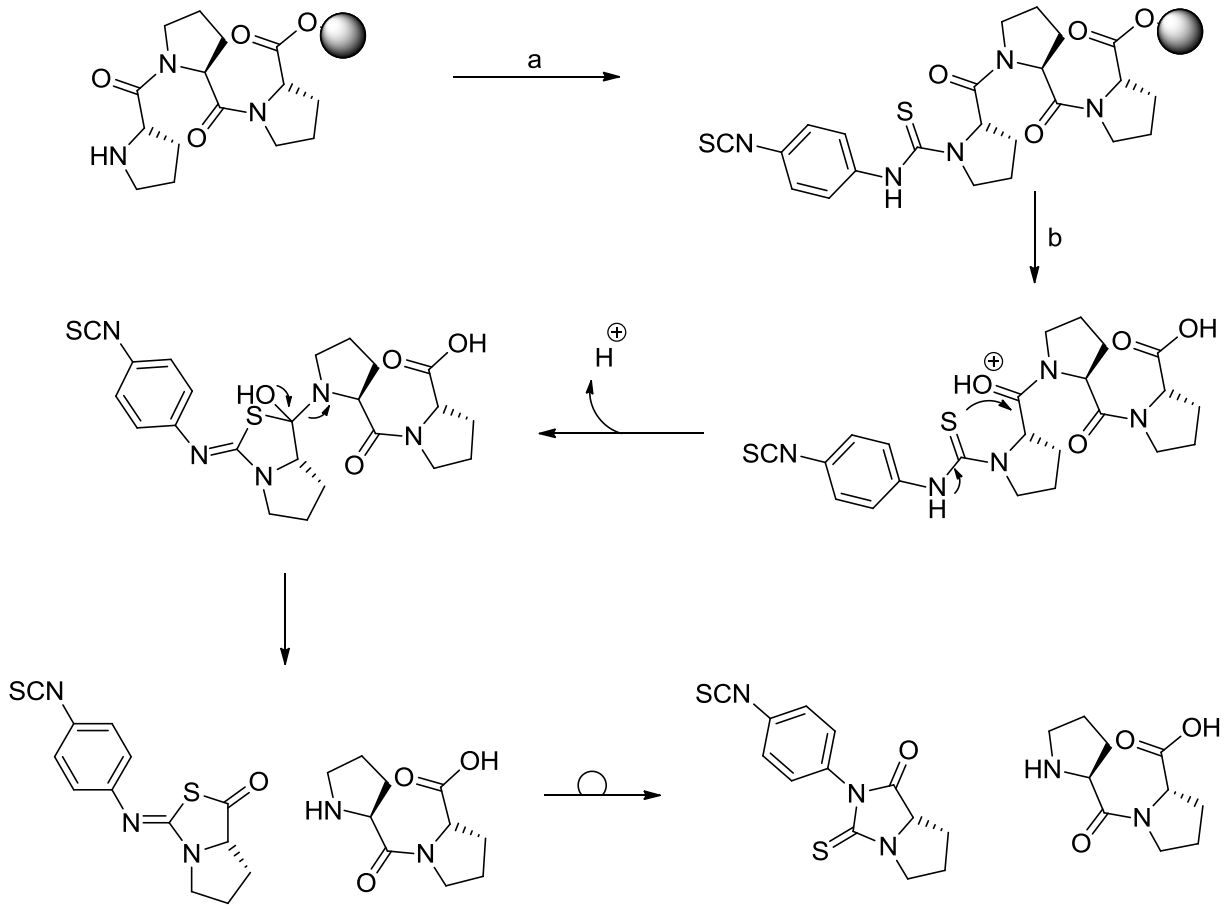


**Scheme 5: a)** Functionalization of an unprotected triproline peptide sequence on solid support by DITC (4.0 equiv.) and DIEA (5.0 equiv.), NMP, 1 h; **b)** During the cleavage of the ITC-polyproline sequence from solid support using 20% HFIP/DCM (3×20 min), an *in situ Edman* degradation occurs due to the acidic cleavage conditions.

Consequently, a different synthesis strategy avoiding acidic conditions after introduction of the DITC to the polyproline spacer was necessary (Scheme 6).

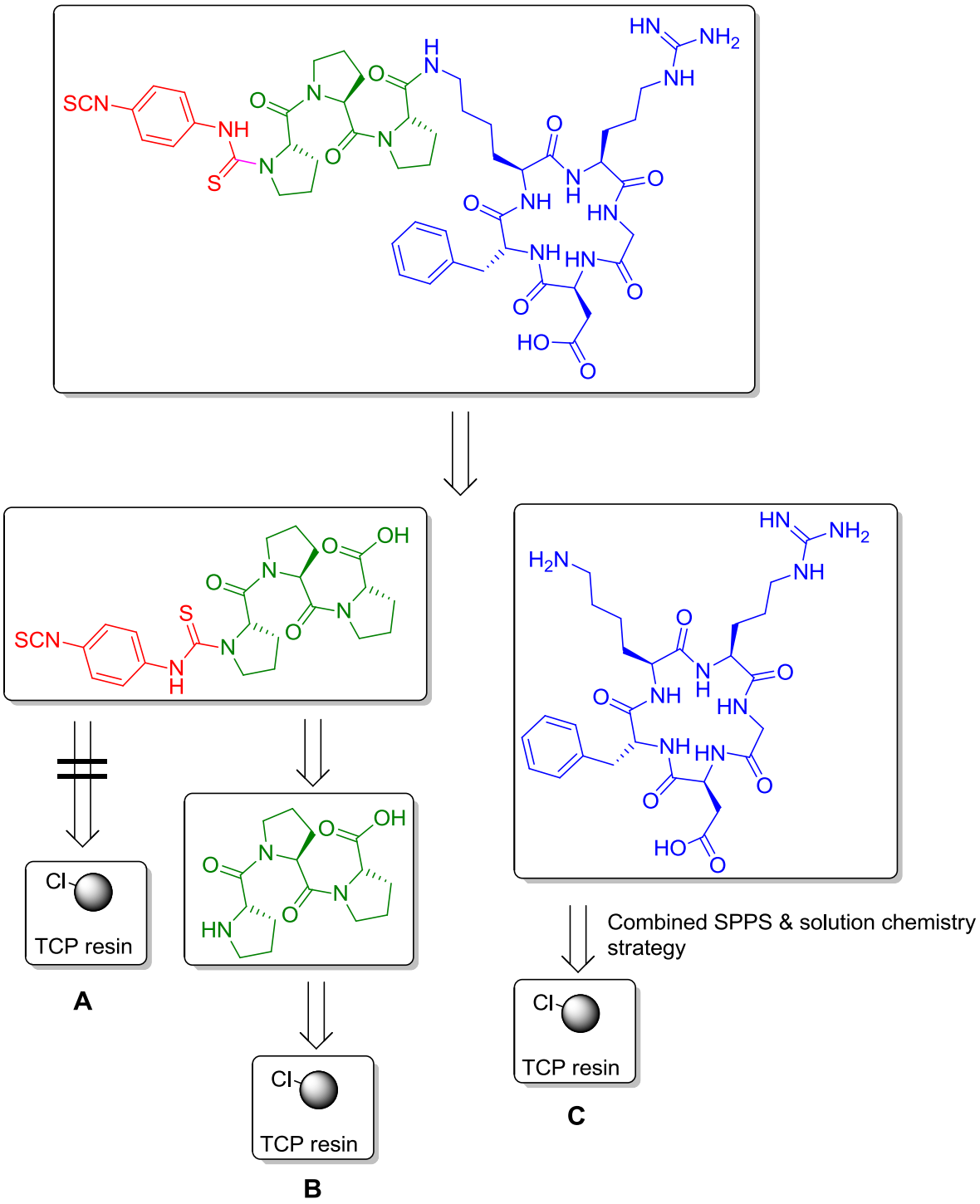


**Scheme 6:** Retrosynthesis analysis for the synthesis of isothiocyanate (ITC) functionalized polyproline spacers. **A)** ITC functionalization on solid phase failed due to acid catalyzed *Edman* degradation during the peptide cleavage from solid support (Scheme 5). **B)** Synthesis of the proline sequence on solid phase and its functionalization by DITC in solution. **C)** Already completely deprotected *c*(-RGDfK-) was used to functionalize the polyproline spacer at its carboxylic acid via an amide bond formation.

Therefore, TCP resin was loaded with Fmoc-Proline-OH and a polyproline sequence of 3, 6 or 9 proline residues was synthesized using the same coupling conditions as described in chapter 4.2.1. The unprotected polyproline sequence was cleaved from the solid support, reacted with DITC in solution and was purified by RP-HPLC. The functionalized spacer was coupled via an amide bond formation between carboxylic acid of the ITC-polyproline spacer and the $N^{\varepsilon}$-Lys of the unprotected *c*(-RGDfK-).

To suppress side-reactions, the carboxylic acid was transformed first into an activated ester using HATU/HOAt as coupling reagents and afterwards the cyclic peptide was added in a slight excess to favor an attack of the more nucleophilic $N^{\varepsilon}$-Lys over the guanidinium attack of the Arg side-chain. The product was purified by RP-HPLC. Compounds were synthesized in high yields of 46% for the ITC-proline spacer and 88% for the final ligation reaction (Scheme 7).

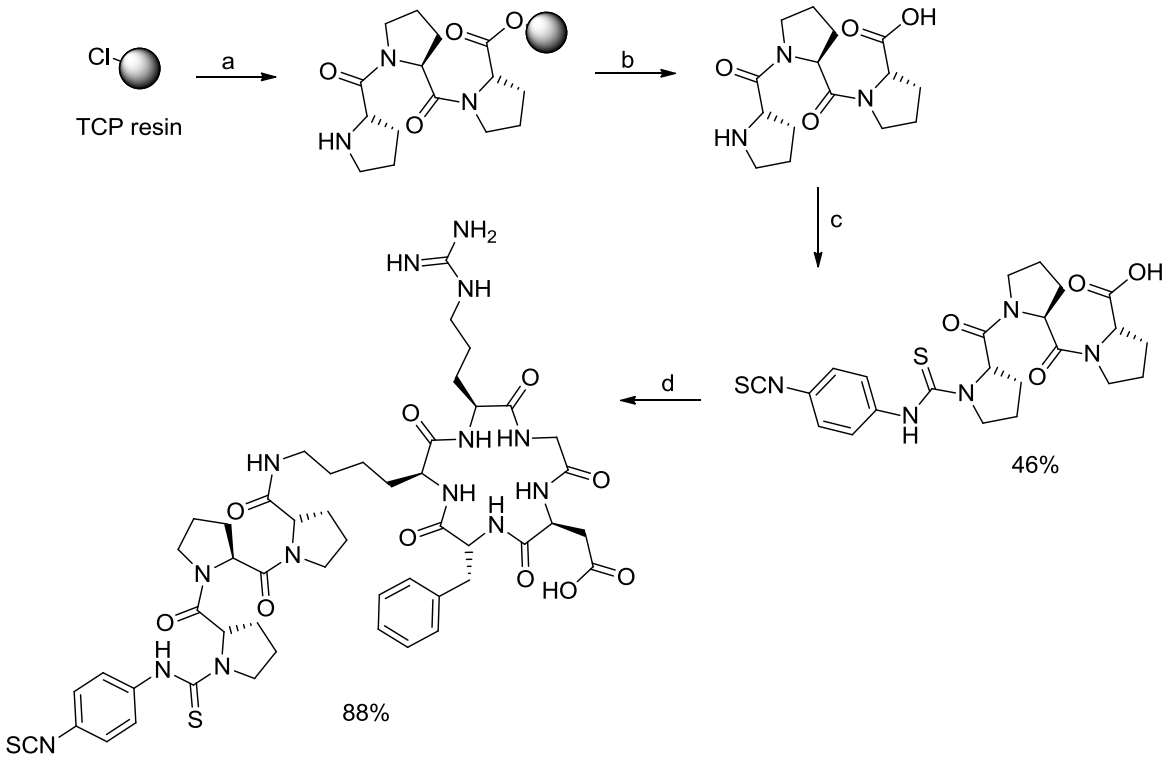


**Scheme 7:** Synthesis of isothiocyanate and *c*(-RGDfK-) functionalized proline spacers. Proline spacers synthesized consisted of 3, 6 and 9 proline residues. Reagents and conditions used: **a)** *i)* Fmoc-Pro-OH (1.2 equiv.), DIEA (3.0 equiv.), DCM, 1 h; *ii)* 20% piperidine/NMP (3×5 min); *iii)* Fmoc-Pro-OH (3.0 equiv.), COMU (3.0 equiv.), Oxyma (3.0 equiv.), DIEA (6.0 equiv.), NMP, 1 h; **b)** 20% HFIP/DCM (3×20 min); **c)** *i)* DITC (4.0 equiv.), DIEA (5.0 equiv.), DMF, 1 h; *ii)* RP-HPLC, YMC Basic, yield: 46%; **d)** *i)* HATU (1.0 equiv.), HOAt (1.0 equiv.), DIEA (5.0 equiv.), *c*(-RGDfK-) (1.05 equiv.), DMF, 1 h; *ii)* RP-HPLC, YMC Basic, yield: 88%.

To determine the effect of the ITC functionalized proline spacer on *c*(-RGDfK-) binding affinity towards integrin αvβ3, inhibition of vitronectin binding to integrin αvβ3 was determined by an isolated receptor assay as described in chapter 3.2. All compounds exhibited binding affinities between 1.8 nM and 2.7 nM (Table 4). This is comparable to the binding affinity of the unmodified *c*(-RGDfK-) peptide (2.6 nM) and to binding affinities obtained for other monovalent RGD-polyproline spacer conjugates (chapter 4.2 and 4.3).

**Table 4:** Inhibition of integrin binding to vitronectin (αvβ3) by *c*(-RGDfK-) peptides directly functionalized at the lysine side chain by a proline spacer containing an isothiocyanate anchor group for coating of stent surfaces.

| Peptide | $IC_{50}$ [a] αvβ3 [nM] |
|---|---|
| **11** *c*(-RGDfK[ITC-PPP]-) | 1.8 (± 0.3) |
| **12** *c*(-RGDfK[ITC-PPPPPP]-) | 2.7 (± 0.3) |
| **13** *c*(-RGDfK[ITC-PPPPPPPPP]-) | 2.0 (± 0.4) |
| *c*(-RGDfK-) | 2.6 (± 0.6) |
| Cilengitide[b] | 0.54 (± 0.15) |

[a]$IC_{50}$ values are derived from a competitive ELISA using immobilized vitronectin and soluble integrin αvβ3. [b]The highly active, cyclic pentapeptide Cilengitide, c(-RGDf$^{Me}$V-) was used in ELISA as an αvβ3 control inhibitor. ITC: isothiocyanate.

RGD-peptides containing PEG and polyproline spacers of different lengths are currently investigated to improve cell adhesion to surfaces coated with these peptides by *Li Liang* in the group of *Dr. M. Joner*, Translational Cardiology at the German Heart Center (Munich, Germany).

# 5. Summary

The scope of this work mainly focuses on the design, synthesis and *in vitro* evaluation of integrin binding peptides containing the polyproline sequence as a spacer to connect integrin ligands to surface anchors and imaging labels. The integrin binding affinity of these ligands was compared to the same ligands using other types of spacers, e.g. Ahx or PEG spacers.

The first topic was the development of *iso*DGR peptides, binding integrins αvβ6 and α5β1 with high affinity while being selective (non-binding) towards integrin αvβ3, αvβ5 and αIIbβ3 (Figure 23).

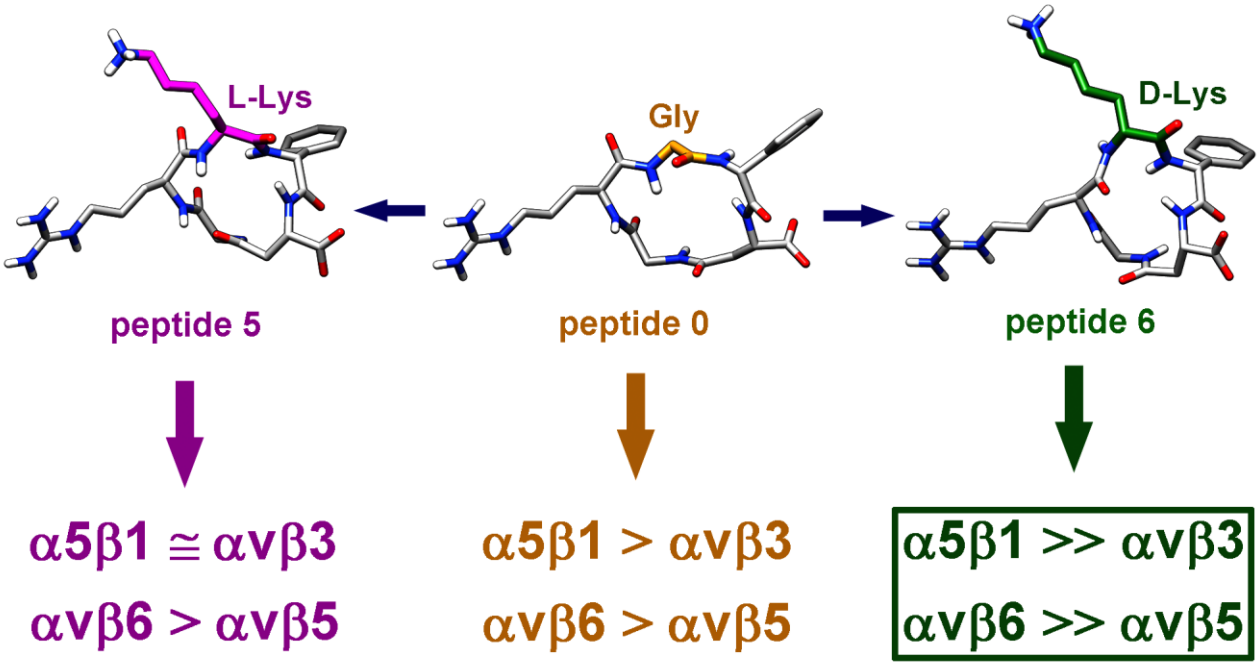


**Figure 23:** The 5th amino acid (X) within cyclic penta-peptides of the *c*(-phg-*iso*DGR-X-) type was screened on its influence of the peptide binding affinity towards different integrins. Starting with previously published stem peptide **0**, *c*(-phg-*iso*DGR-G-),[79] glycine was replaced by different amino acids in their L- or D- configuration. Binding affinity and selectivity towards integrins α5β1 and αvβ6, both binding fibronectin with high affinity *in vivo*, could be improved by the incorporation of D-Lys at the 5th position. Incorporation of L-Lys at this position decreased both, activity and selectivity of the peptide towards the targeted integrins.

Therefore, the previously published peptide *c*(-phg-*iso*DGR-G-)[79] (**0**) served as a template and the position five (glycine) within this peptide was screened on its influence on integrin binding behavior. Therefore, glycine was exchanged by amino acids with

aliphatic side chains, aliphatic side chains with under physiological conditions charged groups or aromatic side chains, both in their L-configuration and D-configuration. Within the synthesized library all peptides bound to integrin α5β1 with higher affinity as peptide **0**, if a D-amino acid was incorporated at the 5$^{th}$ position, while being selective towards integrin αvβ3. In contrast, using an L-amino acid at the 5$^{th}$ position, all peptides showed a lower binding affinity towards integrin α5β1 than the starting peptide **0**. In addition, these peptides gained binding affinity towards integrin αvβ3, making them less selective than the starting compound. The structure of the peptide *c*(-phg-*iso*DGR-k-) (**6**), binding integrins αvβ6 and α5β1 with the highest affinity, while being selective towards the other mentioned integrins, was determined using NMR and MD simulations. Additionally, the structure of its L-configured analog, *c*(-phg-*iso*DGR-K-) (**5**) was determined using the same methods. Subsequently, these structures were docked to the different integrin binding pockets revealing an additional interaction of the side chain of D-Lys which is responsible for the enhanced binding affinity towards integrins α5β1 and αvβ6 of **5**. Modification of peptide **5** by a PEG spacer/ thiol anchor for coating to a gold nanoparticle structured surface and subsequent cell adhesion studies, confirmed the activity and selectivity profile of the peptide observed before *in vitro* and in docking simulations. Integrin αvβ3 is known to be crucial during the initial steps of cell adhesion, while integrin α5β1 becomes important in later stages. A delayed cell adhesion to this surface was observed compared to a less specific reference peptide, which demonstrates the importance of integrin αvβ3 during the initial formation of focal complexes.
Using this specific peptide as a tool will allow further studies on cell-matrix interactions, on the precise role of integrin α5β1 and αvβ6 during cell adhesion as well as on the design of precisely fine-tuned artificial extracellular matrices for diverse applications.

The second topic was the design and synthesis of the polyproline sequence as a spacer between integrin ligands of the *c*(-RGDfX-) type and a thiol anchor for coating of these peptides to gold nanoparticle structured surfaces. Monovalent and divalent ligands of this type were synthesized using spacers of different lengths. Peptides using Ahx or PEG as a spacer were additionally included and the influence of the spacer type and length on integrin binding affinity of these ligands was assessed in an *in vitro* isolated receptor assay of the ELISA type. It was demonstrated that the integrin binding affinity of the ligand was reduced by the use of Ahx or PEG spacers compared to the unmodified ligand. This observed effect correlated to the spacer length. By increasing spacer length, the binding affinity was increasingly affected. In contrast, this effect was not observed, if

the polyproline sequence was used as a spacer. Independent on the spacer length, the integrin binding affinity of the ligand remained unaffected. Using divalent RGD peptides which are connected by the polyproline sequence, the ligand binding affinity was increased 5-fold and more. All ligands were functionalized by a thiol anchor group for coating to gold nanoparticle structured surfaces and for subsequent cell adhesion to these surfaces (Figure 24). Cell adhesion experiments could confirm the influence of the spacer type, on the ligand's binding affinity as well as the importance of the spacer length on the quality of formed cell adhesions.

It was demonstrated that the polyproline sequence has exceeding properties as a spacer with regards to retained ligand binding affinity. This offers a new general method to enhance the affinity of a ligand coated to a surface towards its target and will consequently stimulate the future design surface coatings for improved biocompatibility.

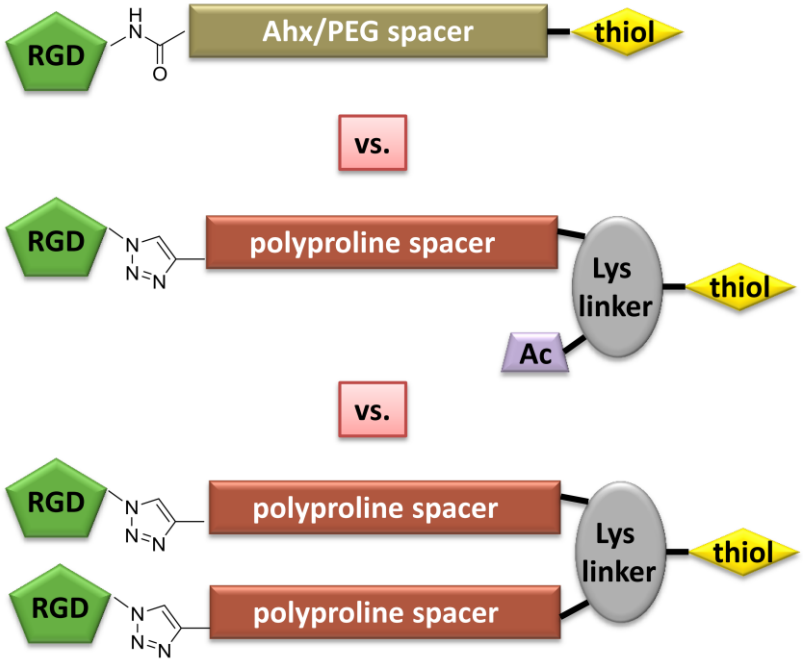


**Figure 24:** Comparative study on the influence of the spacer type and length on the integrin binding affinity of cyclic RGD penta-peptides. Aminohexanoic (Ahx), polyethylenglycole (PEG) and polyproline spacers of different length were compared to each other. The latter one was also modified to a divalent RGD peptide and its implication on integrin binding affinity compared to the monovalent RGD-peptide. All compounds contain a thiol group for coating the peptides to gold nanoparticle structured surfaces and subsequent cell adhesion studies on these modified surfaces.

The third topic combined the two first topics by grafting the *iso*DGR sequence onto the polyproline spacer. Amide bond formation and click chemistry ligation were used to connect the integrin ligand to polyproline spacers of different lengths and compared on

their influence on the ligand binding affinity. All peptides possess a thiol anchor for coating of gold nanoparticle structured surfaces and for subsequent cell adhesions experiments. These peptides were compared in their integrin binding properties to a RGD reference integrin ligand which was connected via a polyproline spacer to a thiol anchor as well (Figure 25).

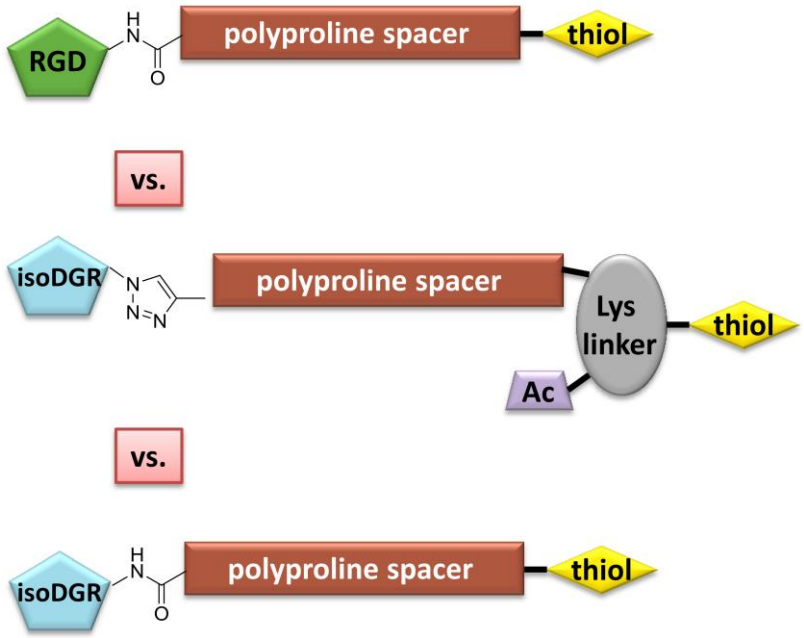


**Figure 25:** Integrin α5β1 and αvβ6 selective *iso*DGR binding motif was attached to polyproline spacers of different length connected by either click chemistry (1,2,3-triazol) or amide bond formation. As a reference peptide, non-specific ligand for integrins αvβ3, αvβ6 and α5β1, cyclic peptide *c*(-RGDfK-) was included. All compounds contain a thiol group for coating the peptides to gold nanoparticle structured surfaces and subsequent cell adhesion studies on these modified surfaces.

Ligating the *iso*DGR sequence by click chemistry to the polyproline spacer proved to be the most efficient method for the formation of the connection between integrin ligand and polyproline spacer while retaining integrin binding affinity. This finding strengthens the general applicability of the polyproline sequence to improve the binding affinity also for other than RGD integrin ligands.

The fourth topic was the adaption of monovalent and divalent RGD-triproline ligands as suitable probes or tracers for fluorescent and PET imaging respectively (Figure 26). Therefore, RGD ligands were ligated by click chemistry to the triproline sequence, connecting the ligand to a fluorescence imaging label (Cy5.5) or PET imaging label (NODAGA). *In vitro* determination of the binding affinities using ELISA revealed that the

monovalent ligand binds to integrin αvβ3 with a 10-fold decreased affinity (Cy5.5) compared to the unmodified RGD ligand. Using NODAGA as a label, the binding affinity was not altered compared to the unmodified RGD ligand. Binding affinity of divalent ligands increased to the subnanomolar range in both cases (Cy5.5 and NODAGA). The observed subnanomolar binding affinity is consistent to the results obtained for divalent ligands described in the second topic. *Ex vivo* determination of beneficial properties of these probes for optical imaging are currently on going in the rat model of *myocardial infarct* (MI) by *Dr. Iina Laitinen* (Department of Nuclear Medicine), *Dr. Stefan Stangl* (Department of Radiotherapy and Radiological Oncology) and *Dr. Martina Rudelius* (Department of Pathology) at the Klinikum rechts der Isar der TUM (Munich, Germany).

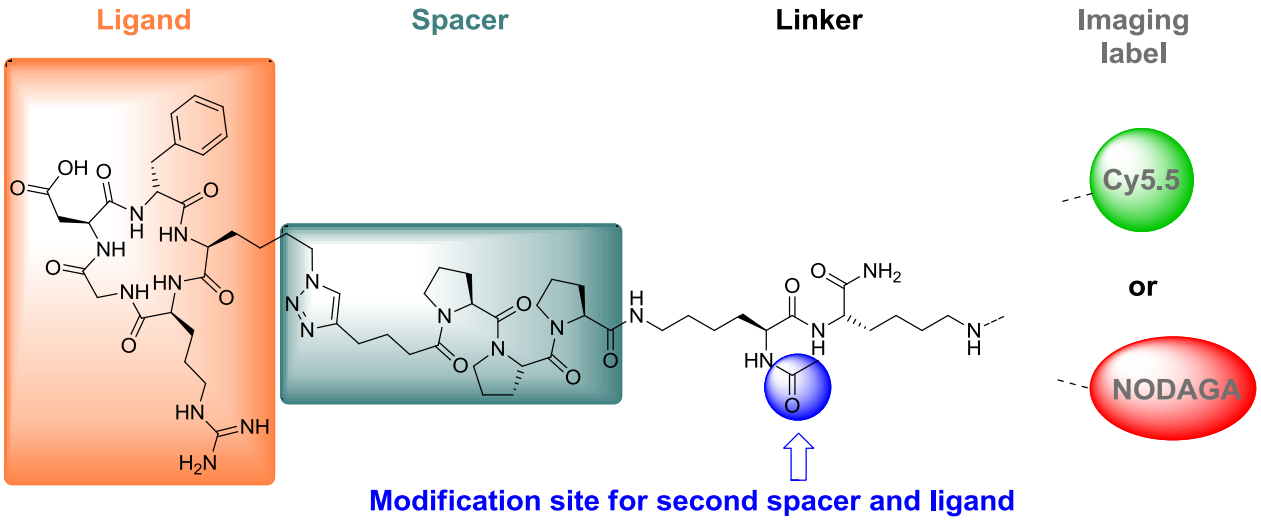


**Figure 26:** Monovalent and divalent RGD integrin ligands connected by a triproline spacer and lysine linker to imaging labels suitable for fluorescence (Cy5.5) or PET (NODAGA) imaging.

The use of the polyproline sequence with the improved properties in retaining integrin ligand binding affinity could be expanded to imaging applications. The general benefit by using the polyproline spacer was demonstrated *in vitro* and their implication in optical imaging is currently investigated *in vivo*.

The fifth topic of this thesis was the adaption of the polyproline spacer sequence to allow connection of a RGD ligand to amine functionalized surfaces by an isothiocyanate anchor. Therefore, ligands were connected with polyproline spacers of three different lengths to the ITC anchor (Figure 27, **11**-**13**). *In vitro* ELISA experiments confirmed an unaltered integrin binding affinity of the RGD integrin ligand, independent of the applied polyproline spacer length. Coating of surfaces with these peptides and subsequent

endothelial cell adhesion studies are currently ongoing as well as the comparison of the polyproline spacer in this application to analog ligands containing PEG spacers of different lengths. PEG spacer peptides were synthesized in our group by *Dr. Carles Mas-Moruno* and the endothelial cell adhesion experiments are performed by *Li Liang* in the group of *M. Joner*, Translational Cardiology, German Heart Center (Munich, Germany).

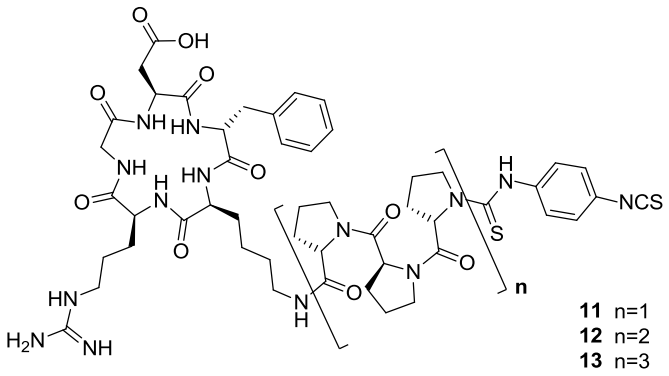


**Figure 27:** Isothiocyanate (ITC) functionalized polyproline spacers of different lengths connected to the peptidic integrin ligand *c*(-RGDfK-) for coating of amine functionalized stent surfaces. Endothelial cell adhesion to these surfaces is investigated and compared to surfaces coated with similar compounds using polyethylenglycole (PEG) as a spacer.

# 6. Experimental Section

## 6.1. Materials and Methods

**Mass spectra** were obtained by *electron spray ionization* (ESI)

**HPLC-ESI-MS** analysis were performed on a *Hewlett Packard HP 1100* system combined with a *Finnigan LCQ* mass spectrometer using *YMC-Hydrosphere $C_{18}$* column (12 nm pore size, 3 µm particle size, 125 mm × 2.1 mm, 9 min gradient elution, flow rate 0.55 mL/min), *YMC-Octyl $C_8$* column (20 nm pore size, 5 µm particle size, 150 mm × 2.1 mm, 30 min gradient elution, flow rate of 0.2 mL/min) or *YMC-basic* column (proprietary pore size, 5 µm particle size, 250 mm × 2.1 mm, 30 min gradient elution, flow rate of 0.35 mL/min). The system uses $H_2O$ (0.1% formic acid) and MeCN (0.1% formic acid) as eluents.

**Analytical HPLC** was performed using *Amersham Pharmacia Biotech Äkta Basic 10F* equipment, a P900 pump system, and reversed phase *YMC-ODS-A $C_{18}$* column (12 nm pore size, 5 µm particle size, 250 mm × 4.6 mm) and UV-detection (UV900; 220 nm and 254 nm). The system was run at a flow rate of 1.0 mL/min over 30 min using $H_2O$ (0.1% TFA) and MeCN (0.1% TFA) as solvents.

**Semipreparative HPLC** was performed on *Waters System Breeze* equipment. *Pump system 1525*, UV-*detector 2487 dual* (220 nm and 254 nm); Driver software Breeze version 3.20; column material *YMC-ODS-A $C_{18}$* (12 nm pore size, 5 µm particle size, 250 mm × 20 mm), *YMC-ODS-AQ $C_{18}$* (12 nm pore size, 5 µm particle size, 250 mm × 20 mm), or *YMC Basic* (proprietary, 5 µm particle size, 250 mm × 20 mm).

**$^1$H-NMR** and **$^{13}$C-NMR** were recorded at 298 K on a 250 MHz *Bruker AC spectrometer*. Chemical shifts (δ) are given in *parts per million* (ppm) relative to trimethylsilane (TMS). Following solvent peaks were used as internal standard: DMSO-$d_5$: 2.50 ppm ($^1$H-NMR) and 39.46 ppm ($^{13}$C-NMR). The spectra data was processed using MestReNova 8.0.0.

As a **Centrifuge** a Rotina 48 (Hettich Labtechnology) was used.

For simultaneous **heating and shaking** of small reaction volumes an *IKA KS130 Basic* equipped with a *Watlow* Temperature Controller was used.

**Air/water-sensitive reactions** were performed in flame-dried flasks under an atmosphere of argon (99.996%).

**Solid phase peptide synthesis** up to 1 g resin were performed in syringes (*Becton-Dickinson*) equipped with a polypropylene frit (*Vetter Labortechnik*) and canula (*Braun*). The loaded syringes were stuck into a rubber stopper connected to a rotary evaporator and mixed by gentle rotation. Dissolved crude products were filtered through a *Pall Acrodisc* (0.45 µm GHP membrane) syringe filter before RP-HPLC purification.

All technical solvents were distilled prior to use. Dry solvents were purchased from *Sigma-Aldrich*, *Fluka* or *Merck*. Fmoc-protected amino acids, building blocks and coupling reagents were purchased from *Orphregen* (Heidelberg, Germany), *Iris Biotech GmbH* (Marktredwitz, Germany), *Sigma-Aldrich* (Taufkirchen, Germany), *NovaBioChem* (Schwalbach, Germany), *Alfa Aesar* (Karlsruhe, Germany), Bachem (Weil am Rhein, Germany), and *Medalchemy S.L.* (Alicante, Spain). Resins for solid phase peptide synthesis were purchased from *Intavis PepChem* (Tübingen, Germany) or *Sigma-Aldrich* (Taufkirchen, Germany). Imaging labels were purchased from CheMatech (Dijon, France) and LumiProbe Corp. (Hallandale Beach, FL, USA). Proteins and antibodies used in ELISA experiments are described in the corresponding chapter 6.4. All other chemicals and organic solvents were purchased from commercial suppliers at the highest purity available and used without further purification.

## 6.2. General Procedures

### GP 1 - Loading of Cl-TCP resin

Chloro-TCP resin (theoretical loading 0.94 mmol/g) was filled into a suitable syringe (20 mL/g resin) equipped with a PP-frit and cannula. The amino acid (1.2 equiv. referred to theoretical loading) was added to the resin. 3.0 equiv. DIEA (referred to theoretical loading) was mixed in dry DCM (8 mL/g resin). The solution was sucked into the syringe and rotated at ambient temperature for 1 h. 0.2 equiv. DIEA and MeOH (200 µL/g resin) were added into the syringe and rotated for additional 20 min to cap all remaining free sites. The loaded resin was washed with DCM (3×), NMP (3×), NMP/MeOH (1:1, 1×) and MeOH (3×) and dried afterwards overnight in an evacuated desiccator. The dry resin was weighted and the loading gravimetrically determined by the following equation:

$$c\left(\frac{mol}{g}\right) = \frac{m(total) - m(resin)}{(MW - 36.461) \times m(total)}$$

**Equation 1:** Calculation of the resin loading. m(total): mass of the loaded resin. m(resin): mass of the unloaded resin. MW: molecular weight of the immobilized amino acid.

### GP 2 - Removal of Fmoc protecting group on solid phase

The swollen resin was treated 3 × 5 min by a 20% piperidine/NMP (v/v) solution and washed thoroughly afterwards with NMP (5×).

### GP 3 - Peptide coupling with COMU/Oxyma on solid phase

3.0 equiv. COMU (referring to resin loading) and Oxyma (3.0 equiv.) were dissolved in NMP (0.12 mM). DIEA (6.0 equiv.) was added and the resulting solution transferred to 3.0 equiv. of the AA. After complete dissolving the solution was sucked into the syringe containing the resin and rotated for 1 h at ambient temperature. The mixture was discarded and the resin thoroughly washed with NMP (5 × 10 mL/g resin).

### GP 4 - Solid phase peptide coupling with TBTU/HOBt

3.0 equiv. TBTU (referring to resin loading) and HOBt (3.0 equiv.) were dissolved in NMP (0.12 mM). DIEA (6.0 equiv.) was added and the resulting solution transferred to 3.0 equiv. of the AA. After complete dissolving, the solution was sucked into the syringe containing the resin and rotated for 1 h at ambient

temperature. The mixture was discarded and the resin thoroughly washed with NMP (5 × 10 mL/g resin).

**GP 5 - Removal of Alloc protecting group on solid phase**

The resin was washed three times with DCM and three times with dry DCM. 0.25 equiv. of *tetrakis*(triphenylphosphin)palladium(0) was dissolved together with 10.0 equiv. phenylsilane in dry DCM. The solution was sucked into the syringe and rotated at ambient temperature for 1 h. Care had to be taken due to gas evolution and the pressure was released from time to time. The resin was washed 2 × 3 min with 0.5% DDTC/DMF and 2 × 3 min with 0.5% DIEA/DMF. The procedure was repeated once or twice, till the resin obtained its original color and washed 5 times with NMP as a last step.

**GP 6 - Removal of ivDde protecting group on solid phase**

A 5% solution of hydrazine-hydrate in NMP (v/v) was added to the resin for 2 × 30 min. The resin was washed 5 times with NMP and the completion of the reaction checked by MS (see **GP 19**).

**GP 7 - Loading of ChemMatrix® Rink-Amide resin**

ChemMatrix® H-Rink amide resin (theoretical loading 0.60 mmol/g) was filled into a suitable syringe (20 mL/0.8 g resin) equipped with a PP-frit and cannula. Note: Due to the swelling properties in different solvents, especially TFA, maximum amount of resin needs to be even lower in a 20 mL syringe, dependent on the synthesis (resin split). 5.0 equiv. PyBob were dissolved together with 5.0 equiv. Oxyma and 15.0 equiv. *sym.*-Collidin in DCM (10 mL/0.8 g resin). The solution was added to the amino acid and sucked onto the syringe after complete dissolving. After rotating the resin for 5 h at ambient temperature the mixture was discarded and the resin washed with DCM (5×), MeOH (3×) and $Et_2O$ (3×). The resin was dried overnight in a desiccator and weighted immediately afterwards. The loading of the resin was gravimetrically determined by the following equation:

$$c\left(\frac{mol}{g}\right) = \frac{m(total) - m(resin)}{(MW - 18.02) \times m(total)}$$

**Equation 2:** Calculation of the resin loading. m(total): mass of the loaded resin. m(resin): mass of the unloaded resin. MW: molecular weight of the immobilized amino acid.

The loaded and dry resin was transferred immediately after weighting into a new syringe for continuing the synthesis and unreacted free amines were capped before continuing with the next synthesis step by acetylation after swelling in NMP following **GP 18**.

**GP 8 - Cleavage of side-chain protected peptides from TCP-resin by HFIP**

The swollen resin was washed with DCM (3×), and 8 mL/g resin of 20% HFIP in DCM (v/v) solution was added to the resin. After rotation at ambient temperature for 20 min the mixture was transferred to a round bottom flask and the procedure repeated twice. The resin was washed with the HFIP/DCM solution (3×) and the collected mixtures were concentrated to dryness in vacuo. The crude product was dissolved in MeCN/$H_2O$ and freeze-dried for direct further modification or purified after filtration through a 0.45 µm PTFE filter by semi-preparative RP-HPLC.

**GP 9 - Cleavage of side-chain protected peptides from TCP-resin by acetic acid**

The swollen resin was washed 3 times with DCM and 8 mL/g resin of DCM/AcOH/TFE (7:2:1, v/v/v) mixture was added to the resin within the syringe. After rotating for 30 min the mixture was collected in a round bottom flask and the procedure repeated twice. The resin was washed with DCM (3×) and the washing solution added to the flask. The mixture was concentrated in vacuo and the acetic acid co-evaporated by addition of toluene. The crude product was dissolved in MeCN/$H_2O$, lyophilized and used without further purification.

**GP 10 - Cleavage and full deprotection from TCP/ChemMatrix® resin**

The resin was washed three times with DCM and a solution of TFA/$H_2O$/TIPS (95/2.5/2.5, v/v/v) was added to the resin. After 1 h of rotating at ambient temperature the resin was washed twice with the TFA-solution and the collected mixtures were concentrated in vacuo. The crude product was purified by RP-HPLC.

**GP 11 - Full deprotection of peptides in solution**

A solution of TFA/$H_2O$/TIPS (95/2.5/2.5, v/v/v) was added to the peptide and stirred for 1 h at ambient temperature. The solvent was removed by vacuo and the crude product purified by RP-HPLC.

**GP 12 – 1,3 dipolar cycloaddition (“click”-reaction) in solution**

1.0 equiv. of alkyne possessing peptide and 1.0 equiv. (per alkyne moiety) of azide containing peptide were dissolved separately in a mixture of warm $^{t}$BuOH/$H_2O$ (1:1–2:1). 1.0 equiv. (referred to the alkyne) of an aqueous 0.1 M $CuSO_4$ solution was added. The flask was flushed thoroughly by argon, and under argon flow 2.0 equiv. (referred to the azide) of freshly prepared aqueous 0.1 M sodium ascorbate solution was added to the mixture. The flask was sealed, equipped with a pressure outlet, heated to 70 °C and stirred for 3 h. The solvent was removed after completion of the reaction by freeze drying and the crude product purified by RP-HPLC.

**GP 13 - Removal of Bn/Cbz protecting group in solution**

The peptide was dissolved in DMA and 100 mg of the catalyst (10% Pd/C) per mmol peptide was added to the solution. The flask was flushed with hydrogen and the solution stirred at ambient temperature and 1 bar hydrogen atmosphere for 12 h (or 5 bar for 3 h). The solvent was removed in vacuo and the residue dissolved in MeCN/$H_2O$ (9:1), filtered through Celite® and the peptide was obtained by freeze drying.

**GP 14 - On-resin peptide cyclization using HATU/HOAt**

1.5 equiv. (referred to determined loading of the resin) of HATU and HOAt were dissolved in NMP together with 5.0 equiv. of *sym.*-Collidin. The solution was added to the resin and discarded after completion of the reaction, usually after 2 h. The resin was washed 5 times with NMP.

**GP 15 – Amide bond formation in solution using HATU/HOAt**

1.0 equiv. HATU, 1.0 equiv. HOAt and 5.0 equiv. DIEA were dissolved in DMF. The solution was added to the carboxylic acid and after complete dissolving transferred to the amine containing vial. After stirring for 1 h the solvent was removed in vacuo and the crude product purified by RP-HPLC.

**GP 16 - Peptide cyclization in solution using HATU/HOBt**

The linear, side-chain protected peptide was diluted in DMF to a 1 mM solution. After addition of HATU (2.0 equiv.), HOBt (2.0 equiv.) and DIEA (10.0 equiv.) the mixture was stirred until all starting material was consumed (HPLC/LC-MS monitoring), usually within 12 h. The solvent was removed under reduced

pressure and re-dissolved by addition of acetyl acetate. The organic phase was washed with sat. $NaHCO_3$ (2×), brine, dried over $MgSO_4$ which was filtered off afterwards. The solvent was removed in vacuo.

**GP 17 - Backbone peptide cyclization in solution using DPPA**

The linear, side-chain protected peptide was diluted with DMF to a 1 mM solution. After addition of DPPA (3.0 equiv.) and $NaHCO_3$ (5.0 equiv.) the mixture was stirred until all starting material was consumed (HPLC/LC-MS monitoring), usually within 12 h. The solvent was removed under reduced pressure and the cyclic peptide precipitated by addition of diethyl ether. The peptide was spun down in a centrifuge, washed twice with water and dried in a desiccator.

**GP 18 - Acetylation of primary amines on solid phase**

The swollen resin was treated 2 × 5 min by a mixture of $Ac_2O$, DIEA and NMP (1:2:7, v/v/v) and washed 5 times with NMP.

**GP 19 - Micro cleavage of a peptide from the resin for HPLC-MS analysis**

A small amount of the resin was transferred into a 2 mL syringe equipped with a PP-frit and cannula. The resin was washed 3 times with DCM and transferred to a micro tube. Dependent on the resin linker two different cleavage protocols were applied:

a) 8 drops of a solution of 95% TFA, 2.5% $H_2O$ and 2.5% TIPS (v/v/v) were added to the ChemMatrix® Rink-Amide resin. After 10 min at ambient temperature 1 mL of MeCN/$H_2O$ (9:1) was added and the resulting solution filtered through a 0.45 µm PTFE filter into a short thread vial.

b) 8 drops of 1% TFA in DCM were added to the TCP-resin. After 8 min at ambient temperature, 1 mL of MeCN/$H_2O$ (9:1) was added and the resulting solution filtered through a 0.45 µm PTFE filter into a short thread vial.

**GP 20 - Monitoring of peptide coupling success on solid phase by NF-31 staining**

A small amount of the resin was transferred into a micro tube. 100 µL of a 2 mM solution of NF-31 in DCM were added and heated to 30 °C for 10 min. The resin was transferred to a syringe equipped with a PP frit and washed with DCM (3×). Red colored beads indicated an incomplete coupling.

### GP 21 - Monitoring of peptide coupling success on solid phase by Kaiser-Test

A small amount of the resin was transferred into a 2 mL syringe equipped with a PP frit and cannula. The resin was washed 3 times with DCM and transferred to a micro tube. Consecutively, 2 drops of the following solutions were added to the resin.

1) 3% ninhydrine/EtOH
2) 5% phenol/EtOH
3) 1 mmol KCN in 98 mL pyridine

The mixture was heated to 60 °C for 2 min. A blue staining of the resin indicated remaining free amines.

# 6.3. Compound Preparation and Analytical Data

All peptides were synthesized according to Fmoc-based solid phase peptide synthesis (SPPS). Dependent on the desired product either Tritylchlorid polystyrene or Rink Amide ChemMatrix solid supports were used. (Intermediate-) peptide products were purified by RP-HPLC.

## 6.3.1. Monovalent Polyproline Spacers Linking RGD and *iso*DGR Peptides to Gold Nanoparticle Structured Surfaces

### 1 *c*(-RGDfK[MPA-PPP]-)

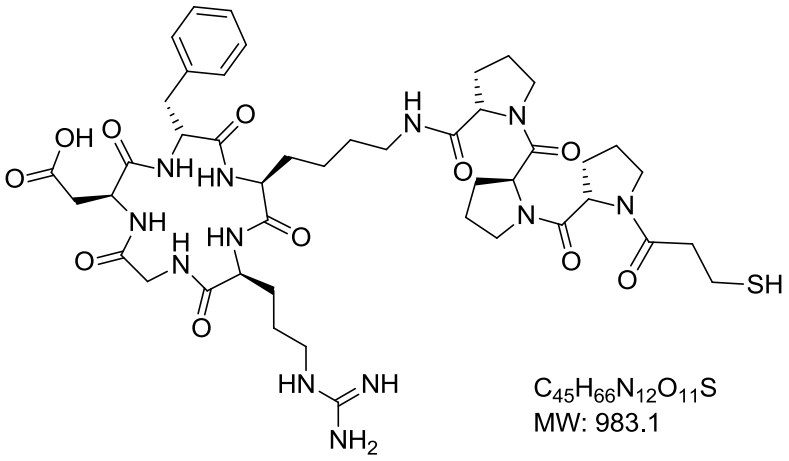


$C_{45}H_{66}N_{12}O_{11}S$
MW: 983.1

**14** (5.0 mg, 7.8 µmol, 1.0 equiv.) was mixed into a DMF solution containing COMU (4.2 mg, 9.8 µmol, 1.25 equiv.), Oxyma (1.4 mg, 9.8 µmol, 1.25 equiv.) and DIEA (6.8 µL, 39.0 µmol, 5.0 equiv.). The mixture was transferred into a vial containing *c*(-R(Pbf)GD(O$^t$Bu)fK-) (8.9 mg, 9.8 µmol, 1.25 equiv.) and stirred for 1 h. Solvent was removed in vacuo and the crude product purified by RP-HPLC. The peptide was deprotected (**GP 11**) and the crude product purified by RP-HPLC (1.6 mg, 1.5 µmol, 19%). **MS** (ESI): 983.5 $(M+H)^+$, 1005.5 $(M+Na)^+$, 1021.5 $(M+K)^+$. **RP-HPLC** (10-100%): 11.6 min.

## 2 *c*(-RGDfK[MPA-PPPPPP]-)

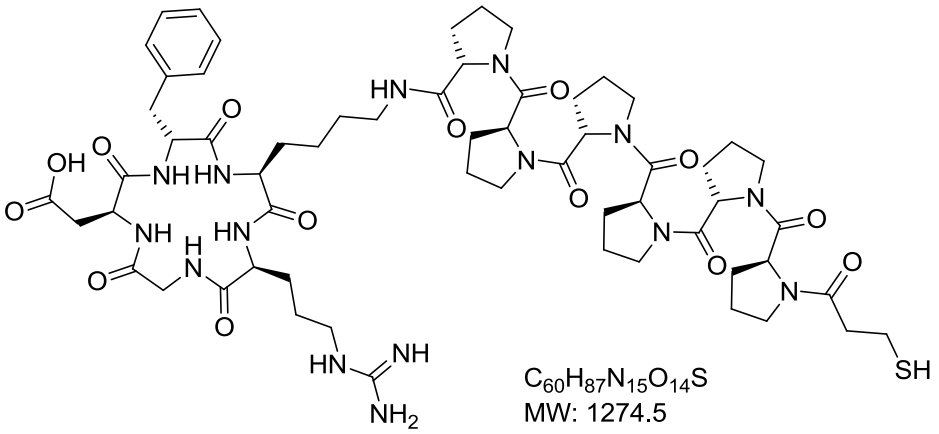


**15** (5.0 mg, 5.4 µmol, 1.0 equiv.) was mixed into a DMF solution containing COMU (2.9 mg, 6.7 µmol, 1.25 equiv.), Oxyma (1.0 mg, 6.7 µmol, 1.25 equiv.) and DIEA (4.7 µL, 26.9 µmol, 5.0 equiv.). The mixture was transferred into a vial containing *c*(-R(Pbf)GD(O$^t$Bu)fK-) (6.1 mg, 6.7 µmol, 1.25 equiv.) and stirred for 1 h. Solvent was removed in vacuo and the crude product purified by RP-HPLC. The peptide was deprotected (**GP 11**) and the crude product purified by RP-HPLC (0.9 mg, 0.7 µmol, 13%). **MS** (ESI): 1274.6 $(M+H)^+$, 1296.7 $(M+Na)^+$. **RP-HPLC** (10-100%): 11.0 min.

## 3 *c*(-phg-*iso*DGRk[MPA-PPP]-)

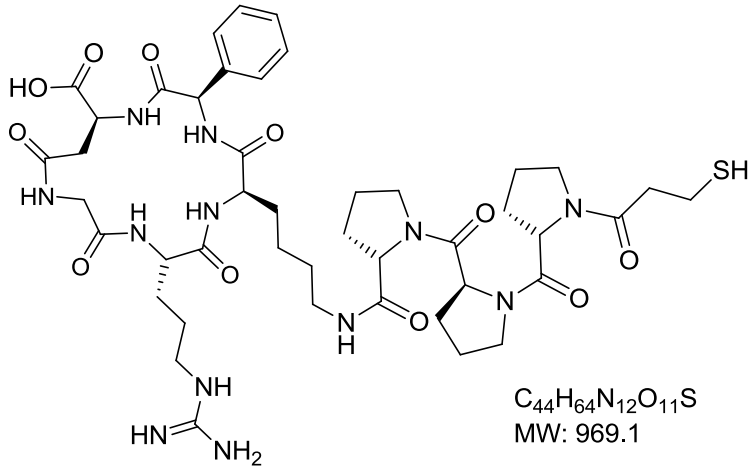


**14** (3.8 mg, 6.0 µmol, 1.0 equiv.) was mixed into a DMF solution containing HATU (2.3 mg, 6.0 µmol, 1.0 equiv.), HOAt (0.8 mg, 6.0 µmol, 1.0 equiv.) and DIEA (5.2 µL, 30.0 µmol, 5.0 equiv.). The mixture was stirred for 1 h at ambient temperature and *c*(-phg-*iso*DGR-k-) (3.5 mg, 6.0 µmol, 1.0 equiv.) dissolved in 500 µL DMF was added. After stirring for 1 h the solvent was removed in vacuo, the crude product was purified by RP-HPLC, the peptide deprotected (**GP 11**) and final product was purified by RP-HPLC

(3.2 mg, 3.3 µmol, 55%). **MS** (ESI): 969.5 $(M+H)^+$, 991.6 $(M+Na)^+$, 1007.5 $(M+K)^+$. **RP-HPLC** (10-100%): 10.3 min.

## 4 *c*(-phg-*iso*DGRk[MPA-PPPPPP]-)

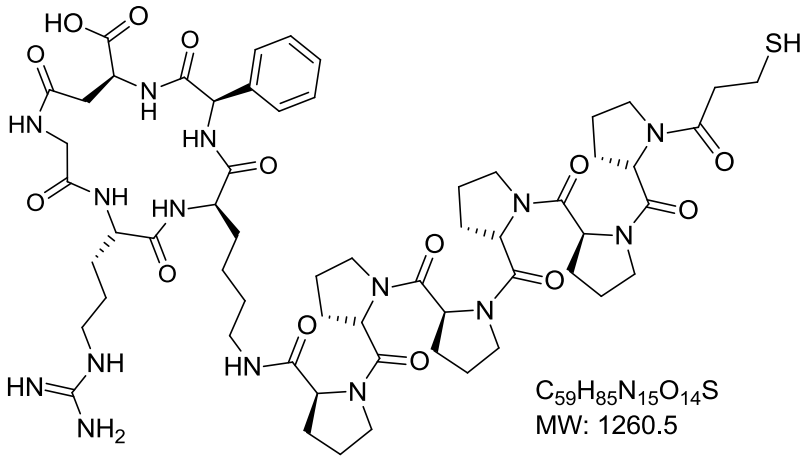


**15** (5.6 mg, 6.0 µmol, 1.0 equiv.) was mixed into a DMF solution containing HATU (2.3 mg, 6.0 µmol, 1.0 equiv.), HOAt (0.8 mg, 6.0 µmol, 1.0 equiv.) and DIEA (5.2 µL, 30.0 µmol, 5.0 equiv.). The mixture was stirred for 1 h at ambient temperature and *c*(-phg-*iso*DGR-k-) (3.5 mg, 6.0 µmol, 1.0 equiv.) dissolved in 500 µL DMF was added. After stirring for 1 h the solvent was removed in vacuo, the crude product purified by RP-HPLC, the peptide deprotected (**GP 11**) and final product purified by RP-HPLC (4.0 mg, 3.2 µmol, 53%). **MS** (ESI): 1260.7 $(M+H)^+$, 1282.7 $(M+Na)^+$. **RP-HPLC** (10-100%): 10.3 min.

## 5 Ac-K[*c*(-phg-*iso*DGRk[HexPPP]-)]-cta

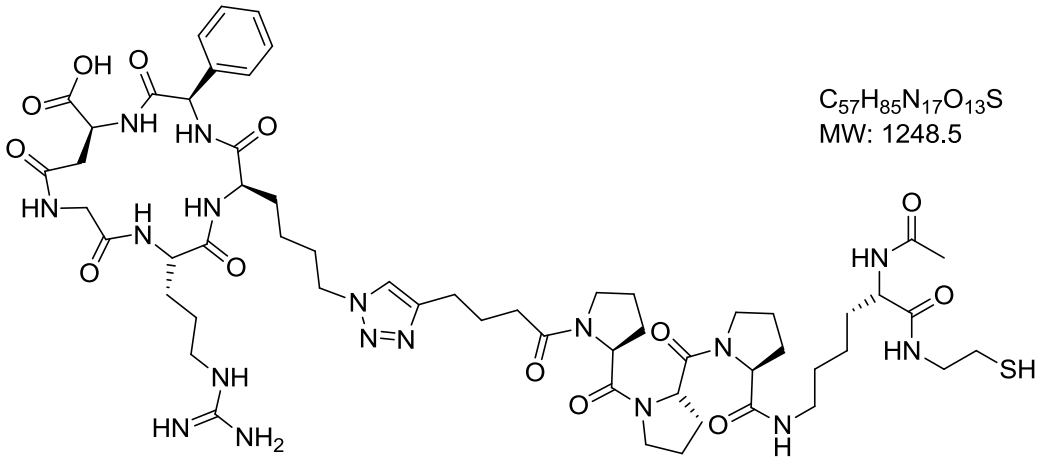


Ac-K(5-hexynoic acid-PPP)-OH (3.0 mg, 5.4 µmol, 1.0 equiv., s. chapter 8.2) and **23** (5.0 mg, 5.4 µmol, 1.0 equiv.) were ligated according to **GP 12**, the intermediate product reacted with Trt-cystamine (**GP 15**), purified by RP-HPLC and deprotected (**GP 11**) (1.7 mg, 1.3 µmol, 25%). **MS** (ESI): 1248.6 $(M+H)^+$, 1270.6 $(M+Na)^+$. **RP-HPLC** (10-100%): 10.4 min.

## 6 Ac-K[*c*(-phg-*iso*DGRk[HexPPPPPP]-)]-cta

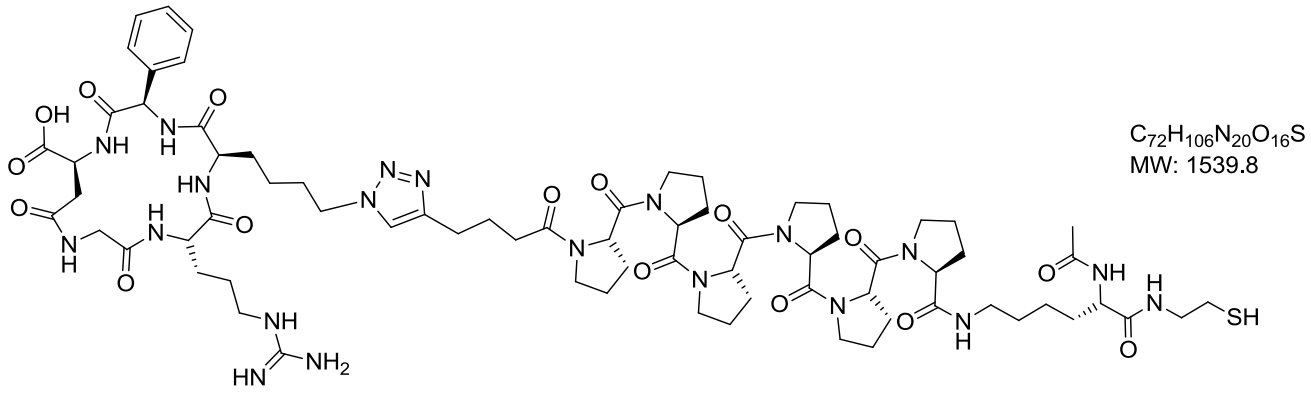


Ac-K(5-hexynoic acid-PPPPPP)-OH (4.7 mg, 5.4 µmol, 1.0 equiv., s. chapter 8.2) and **23** (5.0 mg, 5.4 µmol, 1.0 equiv.) were ligated according to **GP 12**, the intermediate product reacted with Trt-cystamine (**GP 15**), purified by RP-HPLC and deprotected (**GP 11**) (2.5 mg, 1.6 µmol, 30%). **MS** (ESI): 514.2 $(M+3H)^{3+}$, 770.6 $(M+2H)^{2+}$, 782.5 $(M+H+Na)^{2+}$, 1539.8 $(M+H)^+$, 1561.7 $(M+Na)^+$. **RP-HPLC** (10-100%): 10.4 min.

## 6.3.2. RGD Peptides Connected by Polyproline Spacers to a Label Suitable for Fluorescence or PET Imaging

### 7 Ac-K-[*c*(-RGDfK[HexPPP]-)]-K(Cy5.5)-CONH$_2$

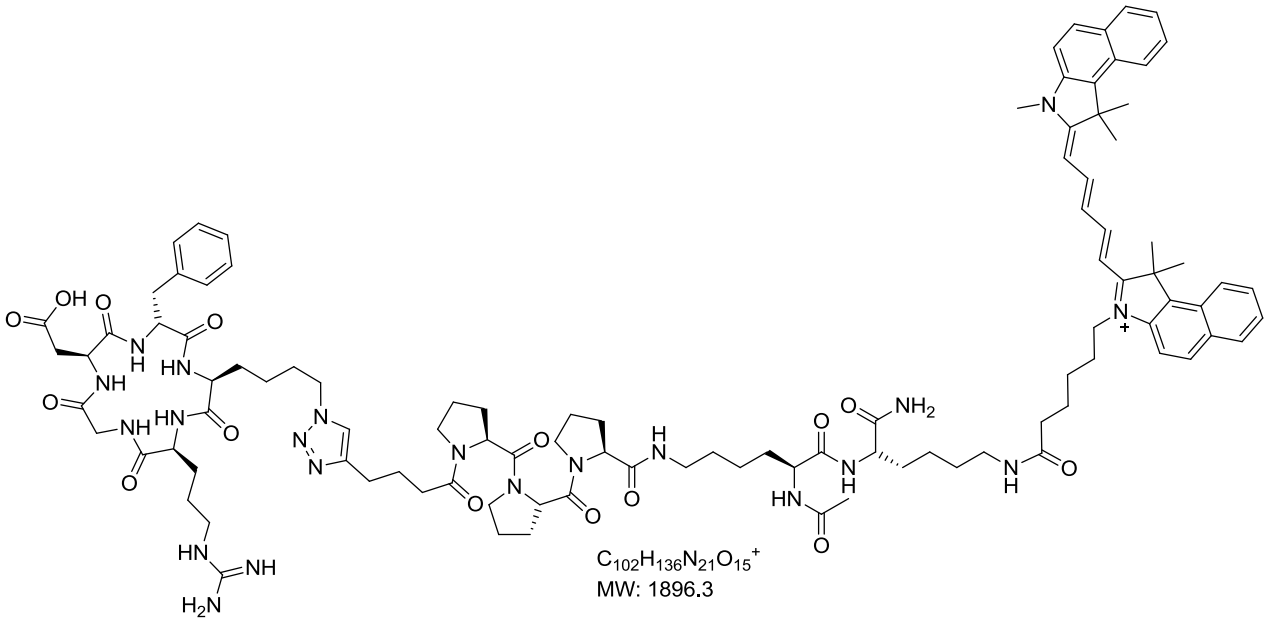


**16** (5.8 mg, 8.3 µmol, 1.0 equiv.) and **22** (7.3 mg, 8.3 µmol, 1.0 equiv.) were ligated according to **GP 12**, the intermediate product was dissolved in 1 mL dry DMF, Cy5.5-NHS ester (5.9 mg, 8.3 µmol, 1.0 equiv.) and DIEA (5.4 µL, 116 µmol, 14.0 equiv.) were added. After stirring for 12 h, the solvent was removed in vacuo and the crude product purified by RP-HPLC (2.7 mg, 1.2 µmol, 15%). The compound was deprotected (**GP 11**) and purified by RP-HPLC (1.6 mg, 0.8 µmol, 67%). **MS** (ESI): 948.4 $(M+2H)^{2+}$, 959.5 $(M+H+Na)^{2+}$, 967.5 $(M+H+K)^{2+}$, 1895.9 $(M+H)^{+}$, 1916.9 $(M+Na)^{+}$. **RP-HPLC** (10-100%): 20.1 min.

## 8 [*c*(-RGDfK[HexPPP]-)]$_2$K-K(Cy5.5)-CONH$_2$

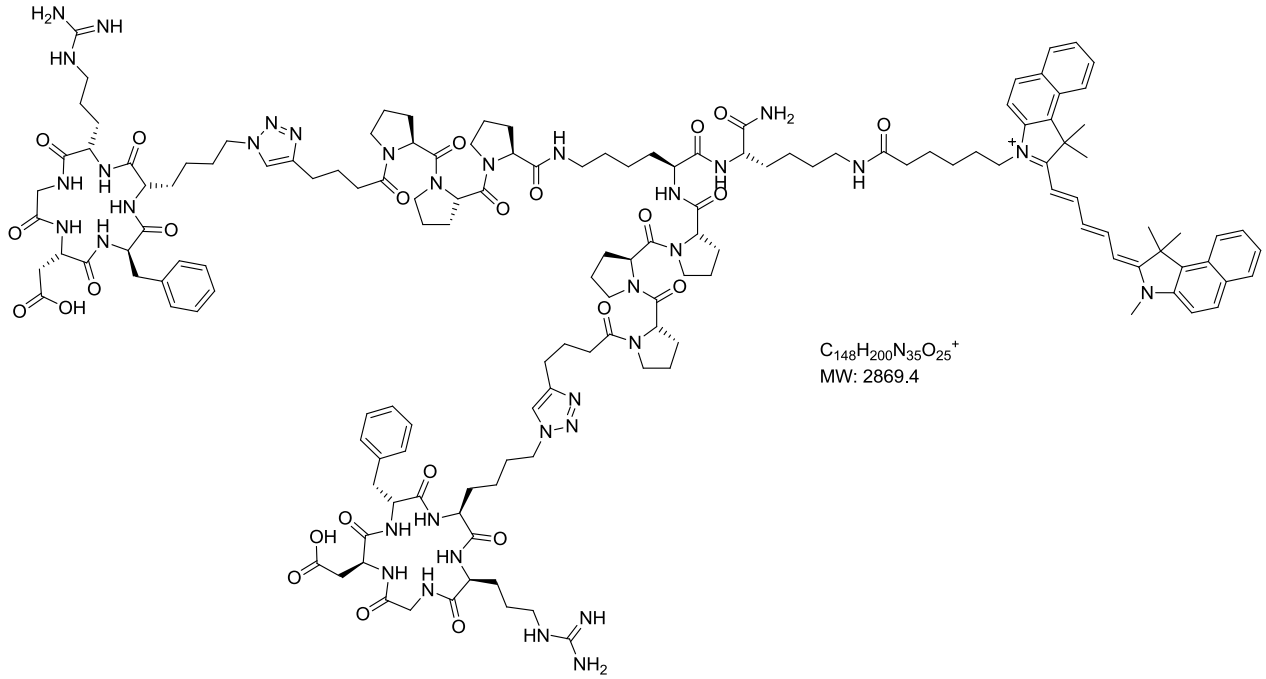


**17** (10.4 mg, 10.0 µmol, 1.0 equiv.) and **22** (17.6 mg, 20.0 µmol, 2.0 equiv.) were ligated according to **GP 12** (2.0 equiv. $CuSO_4$, 4.0 equiv. sodium ascorbate) and purified by RP-HPLC (8.8 mg, 3.1 µmol, 31%). The intermediate product (2.2 mg, 0.8 µmol, 1.0 equiv.) was dissolved in 1 mL dry DMF, Cy5.5-NHS ester (0.6 mg, 0.8 µmol, 1.0 equiv.) and DIEA (1.4 µL, 7.9 µmol, 10.0 equiv.) were added. After stirring for 12 h, the solvent was removed in vacuo and the crude product deprotected (**GP 11**) and purified by RP-HPLC (1.5 mg, 0.5 µmol, 66%). **MS** (ESI): 957.0 $(M+3H)^{3+}$, 964.4 $(M+2H+Na)^{3+}$, 1435.5 $(M+2H)^{2+}$, 1446.0 $(M+H+Na)^{2+}$, 1456.7 $(M+H+K)^{2+}$. **RP-HPLC** (10-100%): 18.8 min.

## 9 Ac-K-[*c*(-RGDfK[HexPPP]-)]-K(NODAGA)-CONH$_2$

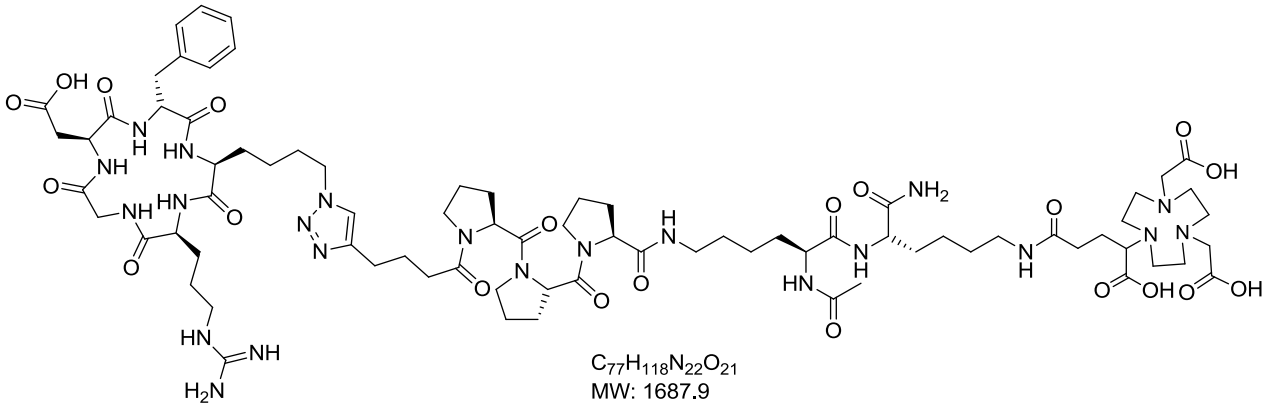


**16** (4.2 mg, 6.0 µmol, 1.0 equiv.) and **22** (5.3 mg, 6.0 µmol, 1.0 equiv.) were ligated according to **GP 12**, and purified by RP-HPLC (5.0 mg, 3.2 µmol, 53%). NODAGA($^t$Bu)$_3$ (1.7 mg, 3.2 µmol, 1.0 equiv.) was added to a solution of HATU (1.2 mg, 3.2 µmol, 1.0 equiv.) and DIEA (5.5 µL, 32.0 µmol, 10.0 equiv.) in 2 mL DMF and stirred for 1 h. The intermediate RGD product (5.0 mg, 3.2 µmol, 1.0 equiv.) was dissolved in 2 mL DMF, added to the mixture, stirred for 1 h and the solvent was removed in vacuo. The crude product was purified by RP-HPLC, the compound deprotected (**GP 11**) and purified by RP-HPLC (2.5 mg, 1.5 µmol, 48%). **MS** (ESI): 844.8 $(M+2H)^{2+}$, 856.5 $(M+H+Na)^{2+}$, 1687.8 $(M+H)^{+}$, 1709.8 $(M+Na)^{+}$. **RP-HPLC** (10-100%): 10.3 min.

## 10 [*c*(-RGDfK[HexPPP]-)]$_2$K-K(NODAGA)-CONH$_2$

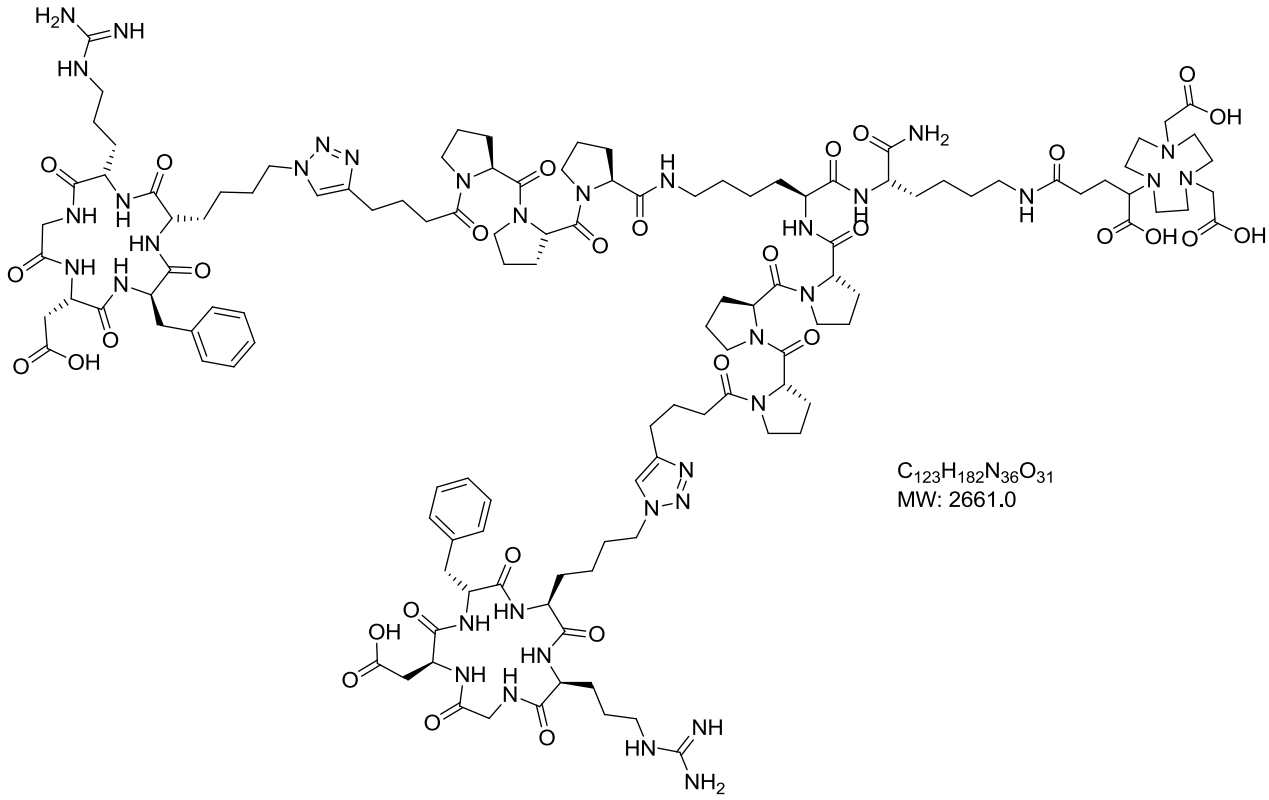


**17** (10.4 mg, 10.0 µmol, 1.0 equiv.) and **22** (17.6 mg, 20.0 µmol, 2.0 equiv.) were ligated according to **GP 12** (2.0 equiv. $CuSO_4$, 4.0 equiv. sodium ascorbate) and purified by RP-HPLC (8.8 mg, 3.1 µmol, 31%). NODAGA($^t$Bu)$_3$ (0.9 mg, 1.4 µmol, 1.0 equiv.) was added to a solution of HATU (0.6 mg, 1.4 µmol, 1.0 equiv.) and DIEA (1.2 µL, 14.0 µmol, 10.0 equiv.) in 2 mL DMF and stirred for 1 h. The intermediate RGD product (4.0 mg, 1.4 µmol, 1.0 equiv.) was dissolved in 2 mL DMF, added to the mixture, stirred for 12 h and the solvent removed in vacuo. The crude product was purified by RP-HPLC, the compound deprotected (**GP 11**) and purified by RP-HPLC (0.9 mg, 0.4 µmol, 29%). **MS** (ESI): 887.9 $(M+3H)^{3+}$, 895.4 $(M+2H+Na)^{3+}$, 1331.2 $(M+2H)^{2+}$, 1342.7 $(M+H+Na)^{2+}$. **RP-HPLC** (10-100%): 11.2 min.

### 6.3.3. RGD Peptide Coating of Stents Using Isothiocyanate Functionalized Polyproline Spacers

All peptides (**11**-**13**) containing an isothiocyanate-polyproline type spacer (**18**-**20**) were synthesized according to **GP 15** using cyclic peptide **21**. The reaction was followed by MS till the starting material was consumed. Analytical data is given in Table 5.

**Table 5:** Analytical data of *c*(-RGDfK-) peptides functionalized directly at the lysine side chain by a proline spacer and isothiocyanate anchor group.

| Peptide | Molecular formula | ESI-MS m/z = $[m+H]^+$ | RP-HPLC $t_R$ [min] (10-100%, 30 min) | Yield [%] |
|---|---|---|---|---|
| **11** *c*(-RGDfK[ITC-PPP]-) | MW = 1087.3<br>$C_{50}H_{66}N_{14}O_{10}S_2$ | 1087.4 | 17.1 | 72 |
| **12** *c*(-RGDfK[ITC-PPPPPP]-) | MW = 1378.6<br>$C_{65}H_{87}N_{17}O_{13}S_2$ | 1378.6 | 16.7 | 88 |
| **13** *c*(-RGDfK[ITC-PPPPPPPPP]-) | MW = 1670.0<br>$C_{80}H_{108}N_{20}O_{16}S_2$ | 1669.6 | 16.3 | 76 |

### 6.3.4. Preparation of Polyproline Spacers

**14 Trt-MPA-PPP-OH**

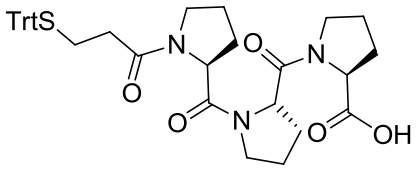


$C_{37}H_{41}N_3O_5S$
MW: 639.8

192 mg TCP resin was loaded with Fmoc-Pro-OH (**GP 1**) and the polyproline sequence synthesized according to **GP 2** and **GP 3**. The product was cleaved from the solid support (**GP 9**) and used without further purification (46.3 mg, 72.4 µmol, 63%). **MS** (ESI): 639.9 $(M+H)^+$, 662.2 $(M+Na)^+$, 678.2 $(M+K)^+$, 1279.0 $(2M+H)^+$, 1301.1 $(2M+Na)^+$. **RP-HPLC** (10-100%): 23.0 min.

## 15 Trt-MPA-PPPPPP-OH

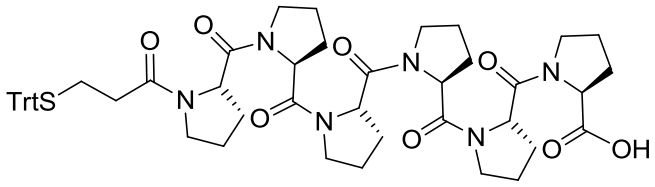


$C_{52}H_{62}N_6O_8S$
MW: 931.2

194 mg TCP resin was loaded with Fmoc-Pro-OH (**GP 1**) and the polyproline sequence synthesized according to **GP 2** and **GP 3**. The product was cleaved from the solid support (**GP 9**) and used without further purification (63.0 mg, 67.0 µmol, 59%). **MS** (ESI): 931.2 $(M+H)^+$, 953.4 $(M+Na)^+$, 975.3 $(M+K)^+$, 1861.2 $(2M+H)^+$, 1884.2 $(2M+Na)^+$. **RP-HPLC** (10-100%): 21.3 min.

## 16 Ac-K[(5-hexynoic acid)PPP]KK-CONH$_2$

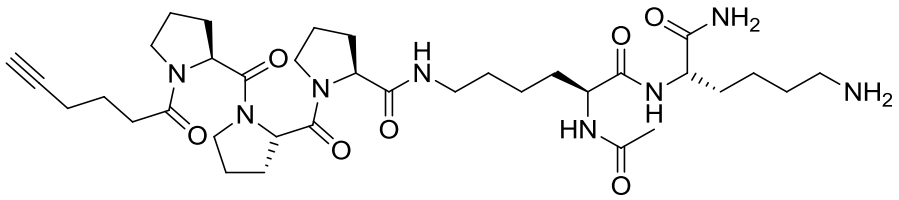


$C_{35}H_{56}N_8O_7$
MW: 700.9

RinkAmide ChemMatrix resin was loaded with Fmoc-Lys(ivDde)-OH (**GP 7**) (239 µmol, 1.0 equiv.) and the spacer peptide synthesized by following sequence: **GP 2**, **GP 3**, **GP 2**, **GP 18**, **GP 5**, **GP 3**, **GP 2**, **GP 3**, **GP 2**, **GP 3**, **GP 2**, **GP 3**, **GP 6** and **GP 10** (13.5 mg, 19.3 µmol, 8%). **MS** (ESI): 701.4 $(M+H)^+$, 723.5 $(M+Na)^+$, 739.5 $(M+K)^+$, 1401.2 $(2M+H)^+$, 1424.2 $(2M+Na)^+$.

## 17 [(5-hexynoic acid)PPP]$_2$-KK-CONH$_2$

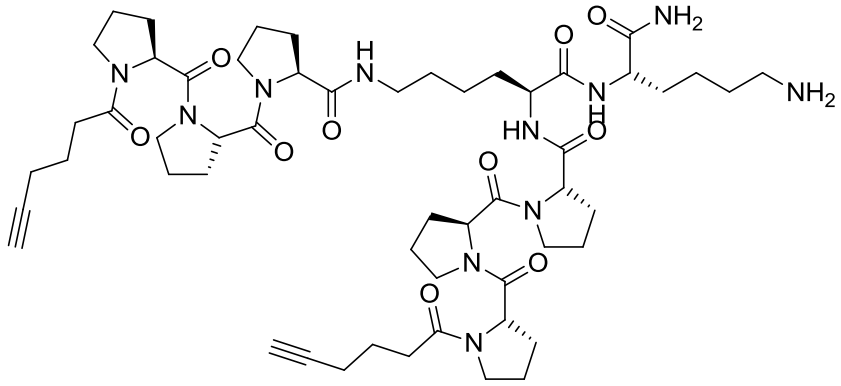


$C_{54}H_{81}N_{11}O_{10}$
MW: 1044.3

The peptide was synthesized using the same methods as described for **16** (239 µmol, 1.0 equiv.) except for the following modification: Instead of acetylation of the primary amine (**GP 18**), the first polyproline spacer was synthesized at this position as described

for **16** (24.2 mg, 23.2 µmol, 10%). **MS** (ESI): 1044.7 $(M+H)^+$, 1066.8 $(M+Na)^+$, 1082.6 $(M+K)^+$.

## 18 ITC-PPP-OH

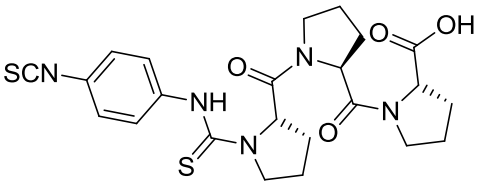


$C_{23}H_{27}N_5O_4S_2$
MW: 501.6

40 mg TCP resin was loaded with Fmoc-Pro-OH (**GP 1**) and the proline sequence synthesized according to **GP 2** and **GP 3**. The unprotected polyproline sequence was cleaved from the resin (**GP 8**) and added to a solution of 1,4-diisothiocyanatobenzene (4.0 equiv.), *sym.*-Collidin (5.0 equiv.) in DMF (0.2 M). The solution was stirred at ambient temperature for 3 h, DMF removed in vacuo and the crude product purified by RP-HPLC (5.42 mg, 10.8 µmol, 43%). **MS** (ESI): 501.9 $(M+H)^+$, 524.1 $(M+Na)^+$, 1002.7 $(2M+H)^+$, 1024.9 $(2M+Na)^+$. **RP-HPLC** (10-100%): 18.7 min.

## 19 ITC-PPPPPP-OH

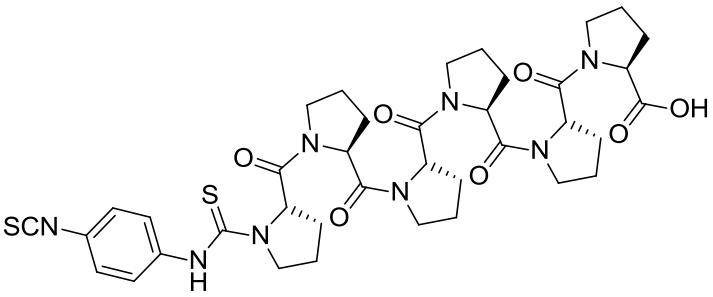


$C_{38}H_{48}N_8O_7S_2$
MW: 793.0

103 mg TCP resin was loaded with Fmoc-Pro-OH and the spacer peptide synthesized as described for **18** (25.4 mg, 32.0 µmol, 46%). **MS** (ESI): 504.3 $(M\text{-ITC-Pro}+H)^+$, 793.1 $(M+H)^+$, 815.2 $(M+Na)^+$, 1609.3 $(2M+Na)^+$. **RP-HPLC** (10-100%): 17.3 min.

**20 ITC-PPPPPPPPP-OH**

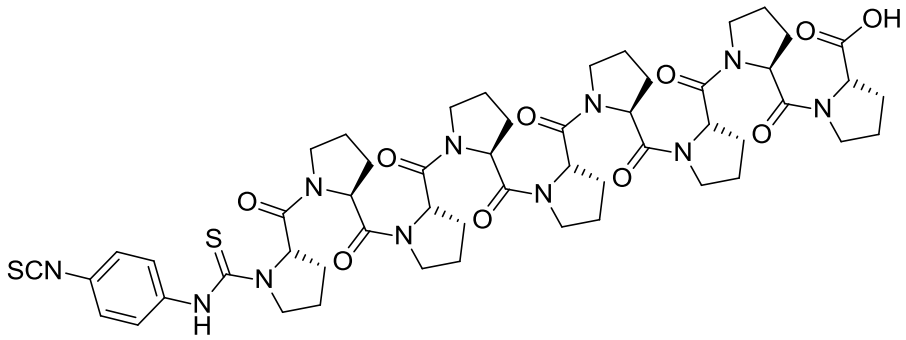


$C_{53}H_{69}N_{11}O_{10}S_2$
MW: 1084.3

136 mg TCP resin was loaded with Fmoc-Pro-OH and the spacer peptide synthesized as described for **18** (35.0 mg, 32.2 µmol, 46%). **MS** (ESI): 795.4 $(M\text{-ITC-Pro+H})^+$, 1084.2 $(M+H)^+$, 1106.4 $(M+Na)^+$. **RP-HPLC** (10-100%): 16.6 min.

## 6.3.5. Preparation of Cyclic Peptides

**21 *cyclo*[-RGDfK-]**

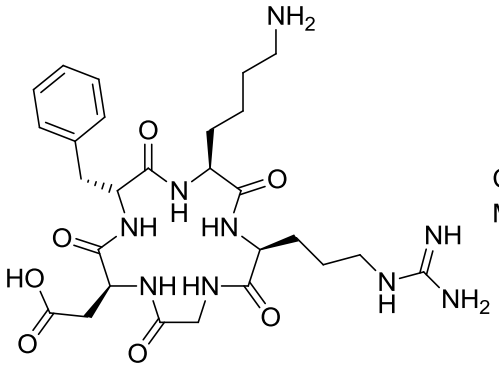


$C_{27}H_{41}N_9O_7$
MW: 603.7

TCP resin was loaded with Fmoc-Gly-OH (***GP 1***) and the peptide synthesized by following procedure: Repetitive steps of **GP 2** and **GP 4** were performed till the linear, Fmoc deprotected peptide was obtained. The linear peptide was processed using **GP 9**, **GP 16** and **GP 11**. **MS** (ESI): 604.5 $(M+H)^+$, 626.5 $(M+Na)^+$, 1207.3 $(2M+H)^+$, 1229.4 $(2M+Na)^+$, 1810.6 $(3M+H)^+$.

## 22 *cyclo*[-R(Pbf)GDfK($N_3$)-]

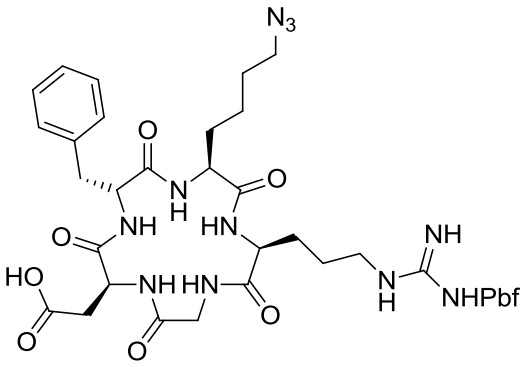

$C_{40}H_{55}N_{11}O_{10}S$
MW: 882.0

TCP resin was loaded with Fmoc-Asp-OAllyl (**GP 1**) and the Fmoc deprotected, linear sequence build up according to **GP 2** and **GP 3**. Allyl deprotection (**GP 5**) was followed by on resin cyclization (**GP 14**). The cyclic, Pbf protected peptide was cleaved from the solid support (**GP 8**) and was used for "click-chemistry" ligation reactions without further purification (usually about 58% crude product). **MS** (ESI): 882.4 $(M+H)^+$, 904.4 $(M+Na)^+$, 920.4 $(M+K)^+$, 1763.2 $(2M+H)^+$. **RP-HPLC** (10-100%): 18.5 min.

## 23 *cyclo*[-phg-*iso*D(O$^t$Bu)GR(Pbf)-k($N_3$)-]

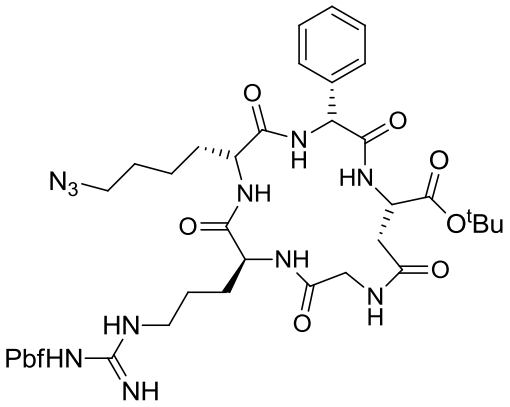

$C_{43}H_{61}N_{11}O_{10}S$
MW: 924.1

TCP resin was loaded with Fmoc-Arg(Pbf)-OH (**GP 1**). Following **GP 2** and **GP 3** Fmoc-Gly-OH, Fmoc-Asp-O$^t$Bu, Fmoc-phg-OH and Fmoc-lys($N_3$)-OH were attached stepwise. The linear peptide sequence was cleaved from the solid support (**GP 8**) and cyclized in solution (**GP 16**). The product could be used in "click chemistry" ligation reactions without further purification. **MS** (ESI): 868.4 $(M-^tBu+H)^+$, 924.3 $(M+H)^+$, 946.3 $(M+Na)^+$, 1847.5 $(2M+H)^+$, 1869.3 $(2M+Na)^+$.

## 6.4. Enzyme Linked Immuno Sorbent Assays (ELISA)

Integrin ligands were analyzed with regards to their integrin binding affinity in an ELISA-type assay using coated extracellular matrix proteins and soluble integrins. Binding of the integrin was detected by specific primary antibodies to which a secondary antibody, coupled to a peroxidase, binds. The peroxidase converts a colorless substrate into a colored substrate. The absorbance in each well was measured by a photometer.[120, 121]

### 6.4.1. ELISA Integrin αvβ3

*BRAND* flat-bottom 96-well ELISA plates were coated overnight at 4 °C with 100 µL/well of 1.0 µg/mL vitronectin from human plasma (*Sigma-Aldrich*, Taufkirchen, Germany) dissolved in carbonate buffer (15 mM $Na_2CO_3$, 35 mM $NaHCO_3$, 9.6 pH). Plates were subsequently washed three times with 200 µL/well PBST buffer (137 mM NaCl, 2.7 mM KCl, 10 mM $Na_2HPO_4$, 2 mM $KH_2PO_4$, 0.01% Tween20, pH 7.4) and free binding sites were blocked for 1 h at ambient temperature with 150 µL/well of TSB-buffer (TS-buffer containing 1% BSA, TS-buffer: 20 mM Tris-HCl, 150 mM NaCl, 1 mM $CaCl_2$, 1 mM $MgCl_2$, 1 mM $MnCl_2$, pH 7.5). After the plate was washed three times with PBST, controls or test compounds (0.006 to 20 µM in TSB, 50 µL/well) were added to the plate and mixed with human integrin αvβ3 (2.0 µg/mL, 50 µL/well, Millipore, Schwalbach/Ts., Germany). By addition of the integrin solution to the wells, the concentration of the integrin was diluted to 1.0 µg/mL and inhibitors were diluted to concentrations ranging from 0.003 µM to 10 µM. This mixture was incubated for 1 h at ambient temperature. The plate was washed three times with PBST buffer and 100 µL/well of 2.0 µg/mL integrin αvβ3 mouse anti-human antibody (anti-CD51/61, *BD Biosciences*, Heidelberg, Germany) in TSB-buffer was added and the plates were incubated for 1 h at ambient temperature. The plate was washed three times with PBST buffer. As a secondary antibody, anti-mouse IgG-POD (*Sigma-Aldrich*, Taufkirchen, Germany) at 100 µL/well of a 1.0 µg/mL solution in TSB-buffer was used. After incubation for 1 h at ambient temperature the plate was washed three times with PBST. Finally, 50 µL/well TMB solution (*Seramun Diagnostica GmbH*, Heidesee) was added and the plate was developed for 5 min in the dark. The reaction was stopped by addition of 50 µL/well of 3 M $H_2SO_4$, and the absorbance was measured at 450 nm with a POLARstar Galaxy plate reader (*BMG Labtechnologies*). For each concentration duplicates were measured. The measured

absorbance was correlated to the inhibitor concentration and analyzed by sigmoidal fitting using OriginPro 7.5G software. The inflection point describes the $IC_{50}$ value.

### 6.4.2. ELISA Integrin αvβ5

The experimental procedure was performed as described for αvβ3 assay, except for the following modifications: The plates were coated with 100 µL/well of 5.0 µg/mL vitronectin (*Sigma-Aldrich*, Taufkirchen, Germany) in carbonate buffer, washed and blocked as described for αvβ3. Soluble integrin αvβ5 (*Millipore,* Schwalbach/Ts., Germany) was mixed with equal amounts of serial diluted inhibitors or controls (0.006 to 20 µM in TSB, 50 µL/well) resulting in a final integrin concentration of 1.5 µg/mL (inhibitors: 0.003 to 10 µM). As a primary antibody 100 µL/well of 1:500 diluted mouse anti-human αv (*Millipore,* Schwalbach/Ts., Germany) was used. The secondary antibody was the same as in integrin αvβ3 assay, but 100 µL/well of 1.0 µg/mL were used. Visualization and analysis was performed as described for αvβ3.

### 6.4.3. ELISA Integrin αvβ6

The experimental procedure was as described for αvβ3 assay, except for the following modifications: The plates were coated with 100 µL/well of 0.4 µg/mL LAP (*R&D Systems*, Wiesbaden, Germany) in carbonate buffer, washed and blocked as described above. Soluble integrin αvβ6 (*R&D Systems*, Wiesbaden, Germany) was mixed with equal volume of serial diluted inhibitors or controls (0.006 to 20 µM in TSB, 50 µL/well) resulting in a final integrin concentration of 0.25 µg/mL (inhibitors: 0.003 to 10 µM). As a primary antibody 100 µL/well of 1:500 diluted mouse anti-human αv (*Millipore*, Schwalbach/Ts., Germany) was used. The secondary antibody was the same as in integrin αvβ3 assay, but 100 µL/well of 2.0 µg/mL were used. Visualization and analysis was performed as described for αvβ3.

### 6.4.4. ELISA Integrin α5β1

The experimental procedure was as described for αvβ3 assay, except for the following modifications: The plates were coated with 100 µL/well of 0.5 µg/mL fibronectin (*Sigma-Aldrich*, Taufkirchen, Germany) in carbonate buffer, washed and blocked as described above. Soluble integrin α5β1 (*R&D Systems*, Wiesbaden, Germany) was mixed with

equal volume of serial diluted inhibitors or controls (0.006 to 20 µM in TSB, 50 µL/well) resulting in a final integrin concentration of 1.0 µg/mL (inhibitors: 0.003 to 10 µM). As a primary antibody 100 µL/well of 1.0 µg/mL mouse anti-human CD49e (*BD Biosciences*, Heidelberg, Germany) was added to the plate. The secondary antibody was the same as in integrin αvβ3 assay, but 100 µL/well of 2.0 µg/mL were used. Visualization and analysis was performed as described for αvβ3.

### 6.4.5. ELISA Integrin αIIbβ3

The experimental procedure was as described for αvβ3 assay, except for the following modifications: The plates were coated with 100 µL/well of 10.0 µg/mL fibrinogen (*Millipore*, Schwalbach/Ts., Germany) in carbonate buffer, washed and blocked as described for αvβ3. Soluble integrin αIIbβ3 (*Millipore,* Schwalbach/Ts., Germany) was mixed with equal amounts of serial diluted inhibitors or controls (0.006 to 20 µM in TSB, 50 µL/well) resulting in a final integrin concentration of 2.5 µg/mL (inhibitors: 0.003 to 10 µM). As a primary antibody 100 µL/well of 2.0 µg/mL mouse anti-human CD41b (*BD Biosciences*, Heidelberg, Germany) was used. The secondary antibody was the same as in integrin αvβ3 assay, but 100 µL/well of 1.0 µg/mL were used. Visualization and analysis was performed as described for αvβ3.

# 7. References

1. Laufer, B. Synthesis of highly active and selective peptides and peptidomimetics. Technische Universität München, München, **2009**.

2. Fischer, E. Einfluss der Configuration auf die Wirkung der Enzyme. *Berichte der deutschen chemischen Gesellschaft* **1894,** 27, 2985-2993.

3. Ehrlich, P. Über den jetzigen Stand der Chemotherapie. *Berichte der deutschen chemischen Gesellschaft* **1909,** 42, 17-47.

4. Haubner, R.; Gratias, R.; Diefenbach, B.; Goodman, S. L.; Jonczyk, A.; Kessler, H. Structural and functional aspects of RGD-containing cyclic pentapeptides as highly potent and selective integrin avb3 antagonists. *Journal of the American Chemical Society* **1996,** 118, 7461-7472.

5. Gurrath, M.; Mueller, G.; Kessler, H.; Aumailley, M.; Timpl, R. Conformation/activity studies of rationally designed potent anti-adhesive RGD peptides. *European Journal of Biochemistry* **1992,** 210, 911-921.

6. Pierschbacher, M. D.; Ruoslahti, E. Cell attachment activity of fibronectin can be duplicated by small synthetic fragments of the molecule. *Nature* **1984,** 309, 30-33.

7. Mammen, M.; Choi, S.-K.; Whitesides, G. M. Polyvalent Interactions in Biological Systems: Implications for Design and Use of Multivalent Ligands and Inhibitors. *Angewandte Chemie International Edition* **1998,** 37, 2754-2794.

8. Thumshirn, G.; Hersel, U.; Goodman, S. L.; Kessler, H. Multimeric cyclic RGD peptides as potential tools for tumor targeting: solid-phase peptide synthesis and chemoselective oxime ligation. *Chemistry* **2003,** 9, 2717-2725.

9. Li, Z.-b.; Cai, W.; Cao, Q.; Chen, K.; Wu, Z.; He, L.; Chen, X. 64Cu-Labeled Tetrameric and Octameric RGD Peptides for Small-Animal PET of Tumor αvβ3 Integrin Expression. *Journal of Nuclear Medicine* **2007,** 48, 1162-1171.

10. Yim, C. B.; Dijkgraaf, I.; Merkx, R.; Versluis, C.; Eek, A.; Mulder, G. E.; Rijkers, D. T.; Boerman, O. C.; Liskamp, R. M. Synthesis of DOTA-conjugated multimeric [Tyr3]octreotide peptides via a combination of Cu(I)-catalyzed "click" cycloaddition and thio acid/sulfonyl azide "sulfo-click" amidation and their in vivo evaluation. *Journal of Medicinal Chemistry* **2010,** 53, 3944-3953.

11. Kubas, H.; Schäfer, M.; Bauder-Wüst, U.; Eder, M.; Oltmanns, D.; Haberkorn, U.; Mier, W.; Eisenhut, M. Multivalent cyclic RGD ligands: influence of linker lengths on receptor binding. *Nuclear Medicine and Biology* **2010,** 37, 885-891.

12. Wängler , C.; Maschauer, S.; Prante, O.; Schäfer, M.; Schirrmacher, R.; Bartenstein, P.; Eisenhut, M.; Wängler , B. Multimerization of cRGD Peptides by Click Chemistry: Synthetic Strategies, Chemical Limitations, and Influence on Biological Properties. *Chembiochem* **2010,** 11, 2168-2181.

13. Pérez, R. A.; Won, J.-E.; Knowles, J. C.; Kim, H.-W. Naturally and synthetic smart composite biomaterials for tissue regeneration. *Adv Drug Deliv Rev* **2012,** in press, 10.1016/j.addr.2012.03.009.

14. Kantlehner, M.; Finsinger, D.; Meyer, J.; Schaffner, P.; Jonczyk, A.; Diefenbach, B.; Nies, B.; Kessler, H. Selective RGD-Mediated Adhesion of Osteoblasts at Surfaces of Implants. *Angewandte Chemie International Edition* **1999,** 38, 560-562.

15. Kalinina, S.; Gliemann, H.; López-García, M.; Petershans, A.; Auernheimer, J.; Schimmel, T.; Bruns, M.; Schambony, A.; Kessler, H.; Wedlich, D. Isothiocyanate-functionalized RGD peptides for tailoring cell-adhesive surface patterns. *Biomaterials* **2008,** 29, 3004-3013.

16. Lowell, C. A.; Mayadas, T. N. Overview: Studying Integrins In Vivo. In *Integrin and Cell Adhesion Molecules*, Shimaoka, M., Ed. Humana Press: **2012**; Vol. 757, pp 369-397.

17. Tamkun, J. W.; DeSimone, D. W.; Fonda, D.; Patel, R. S.; Buck, C.; Horwitz, A. F.; Hynes, R. O. Structure of integrin, a glycoprotein involved in the transmembrane linkage between fibronectin and actin. *Cell* **1986,** 46, 271-282.

18. Shimaoka, M.; Springer, T. A. Therapeutic antagonists and conformational regulation of integrin function. *Nature Reviews Drug Discovery* **2003,** 2, 703-16.

19. Hwang, R.; Varner, J. The role of integrins in tumor angiogenesis. *Hematology/Oncology Clinics of North America* **2004,** 18, 991-1006.

20. Kim, S.; Bell, K.; Mousa, S. A.; Varner, J. A. Regulation of angiogenesis in vivo by ligation of integrin alpha5beta1 with the central cell-binding domain of fibronectin. *American Journal of Pathology* **2000,** 156, 1345-1362.

21. Clemetson, K. J.; Clemetson, J. M. Integrins and cardiovascular disease. *Cellular and Molecular Life Sciences* **1998,** 54, 502-513.

22. Cox, D.; Brennan, M.; Moran, N. Integrins as therapeutic targets: lessons and opportunities. *Nature Reviews Drug Discovery* **2010,** 9, 804-820.

23. Barczyk, M.; Carracedo, S.; Gullberg, D. Integrins. *Cell and Tissue Research* **2010,** Volume 339, 269-280.

24. Humphries, M. J.; McEwan, P. A.; Barton, S. J.; Buckley, P. A.; Bella, J.; Paul Mould, A. Integrin structure: heady advances in ligand binding, but activation still makes the knees wobble. *Trends in Biochemical Sciences* **2003,** 28, 313-320.

25. Goodman, S. L.; Picard, M. Integrins as therapeutic targets. *Trends in pharmacological sciences* **2012,** 33, 405-412.

26. Mas-Moruno, C.; Rechenmacher, F.; Kessler, H. Cilengitide: the first anti-angiogenic small molecule drug candidate design, synthesis and clinical evaluation. *Anticancer Agents in Medicinal Chemistry* **2010,** 10, 753-768.

27. Xiong, J.-P.; Stehle, T.; Diefenbach, B.; Zhang, R.; Dunker, R.; Scott, D. L.; Joachimiak, A.; Goodman, S. L.; Arnaout, M. A. Crystal Structure of the Extracellular Segment of Integrin αvβ3. *Science* **2001,** 294, 339-345.

28. Xiong, J.-P.; Stehle, T.; Zhang, R.; Joachimiak, A.; Frech, M.; Goodman, S. L.; Arnaout, M. A. Crystal Structure of the Extracellular Segment of Integrin αvβ3 in Complex with an Arg-Gly-Asp Ligand. *Science* **2002,** 296, 151-155.

29. Adair, B. D.; Xiong, J.-P.; Maddock, C.; Goodman, S. L.; Arnaout, M. A.; Yeager, M. Three-dimensional EM structure of the ectodomain of integrin αvβ3 in a complex with fibronectin. *The Journal of Cell Biology* **2005,** 168, 1109-1118.

30. Xiao, T.; Takagi, J.; Coller, B. S.; Wang, J.-H.; Springer, T. A. Structural basis for allostery in integrins and binding to fibrinogen-mimetic therapeutics. *Nature* **2004,** 432, 59-67.

31. Shi, M.; Foo, S. Y.; Tan, S.-M.; Mitchell, E. P.; Law, S. K. A.; Lescar, J. A Structural Hypothesis for the Transition between Bent and Extended Conformations of the Leukocyte β2 Integrins. *Journal of Biological Chemistry* **2007,** 282, 30198-30206.

32. Wegener, K. L.; Partridge, A. W.; Han, J.; Pickford, A. R.; Liddington, R. C.; Ginsberg, M. H.; Campbell, I. D. Structural Basis of Integrin Activation by Talin. *Cell* **2007,** 128, 171-182.

33. Zhu, J.; Luo, B.-H.; Xiao, T.; Zhang, C.; Nishida, N.; Springer, T. A. Structure of a Complete Integrin Ectodomain in a Physiologic Resting State and Activation and Deactivation by Applied Forces. *Molecular Cell* **2008,** 32, 849-861.

34. Ulmer, T. S.; Yaspan, B.; Ginsberg, M. H.; Campbell, I. D. NMR Analysis of Structure and Dynamics of the Cytosolic Tails of Integrin αIIbβ3 in Aqueous Solution. *Biochemistry* **2001,** 40, 7498-7508.

35. Li, R.; Babu, C. R.; Valentine, K.; Lear, J. D.; Wand, A. J.; Bennett, J. S.; DeGrado, W. F. Characterization of the Monomeric Form of the Transmembrane and Cytoplasmic Domains of the Integrin β3 Subunit by NMR Spectroscopy. *Biochemistry* **2002,** 41, 15618-15624.

36. Adair, B. D.; Yeager, M. Three-dimensional model of the human platelet integrin αIIbβ3 based on electron cryomicroscopy and x-ray crystallography. *Proceedings of the National Academy of Sciences* **2002,** 99, 14059-14064.

37. Takagi, J.; Strokovich, K.; Springer, T. A.; Walz, T. Structure of integrin alpha5beta1 in complex with fibronectin. *EMBO J* **2003,** 22, 4607-4615.

38. Arnaout, M. A.; Mahalingam, B.; Xiong, J.-P. Integrin Structure, Allostery, and Bidirectional Signaling. *Annual Review of Cell and Developmental Biology* **2005,** 21, 381-410.

39. Rocco, M.; Rosano, C.; Weisel, J. W.; Horita, D. A.; Hantgan, R. R. Integrin Conformational Regulation: Uncoupling Extension/Tail Separation from Changes in the Head Region by a Multiresolution Approach. *Structure* **2008,** 16, 954-964.

40. Ye, F.; Liu, J.; Winkler, H.; Taylor, K. A. Integrin αIIbβ3 in a Membrane Environment Remains the Same Height after Mn2+ Activation when Observed by Cryoelectron Tomography. *Journal of Molecular Biology* **2008,** 378, 976-986.

41. Lau, T. L.; Kim, C.; Ginsberg, M. H.; Ulmer, T. S. The structure of the integrin alphaIIbbeta3 transmembrane complex explains integrin transmembrane signalling. *EMBO J* **2009,** 28, 1351-1361.

42. Hynes, R. O. Integrins: Bidirectional, Allosteric Signaling Machines. *Cell* **2002,** 110, 673-687.

43. Harburger, D. S.; Calderwood, D. A. Integrin signalling at a glance. *Journal of Cell Science* **2009,** 122, 159-163.

44. Zaidel-Bar, R.; Itzkovitz, S.; Ma'ayan, A.; Iyengar, R.; Geiger, B. Functional atlas of the integrin adhesome. *Nature Cell Biology* **2007,** 9, 858-867.

45. Legate, K. R.; Wickstrom, S. A.; Faessler, R. Genetic and cell biological analysis of integrin outside-in signaling. *Genes Dev* **2009,** 23, 397-418.

46. Dechantsreiter, M. A.; Planker, E.; Matha, B.; Lohof, E.; Holzemann, G.; Jonczyk, A.; Goodman, S. L.; Kessler, H. N-Methylated cyclic RGD peptides as highly active and selective alpha(v)beta(3) integrin antagonists. *Journal of Medicinal Chemistry* **1999,** 42, 3033-3040.

47. Weide, T.; Modlinger, A.; Kessler, H. Spatial Screening for the Identification of the Bioactive Conformation of Integrin Ligands. In *Bioactive Conformation I*, Peters, T., Ed. Springer Berlin / Heidelberg: **2007**; Vol. 272, pp 1-50.

48. Heckmann, D.; Kessler, H. Design and Chemical Synthesis of Integrin Ligands. *Methods in Enzymology* **2007,** 426, 463-503.

49. Heckmann, D.; Laufer, B.; Marinelli, L.; Limongelli, V.; Novellino, E.; Zahn, G.; Stragies, R.; Kessler, H. Breaking the Dogma of the Metal-Coordinating Carboxylate Group in Integrin Ligands: Introducing Hydroxamic Acids to the MIDAS To Tune Potency and Selectivity. *Angewandte Chemie International Edition* **2009,** 48, 4436-4440.

50. Bollinger, M.; Manzenrieder, F.; Kolb, R.; Bochen, A.; Neubauer, S.; Marinelli, L.; Limongelli, V.; Novellino, E.; Moessmer, G.; Pell, R.; Lindner, W.; Fanous, J.; Hoffman, A.; Kessler, H. Tailoring of Integrin Ligands: Probing the Charge Capability of the Metal Ion-Dependent Adhesion Site. *Journal of Medicinal Chemistry* **2011,** 55, 871-882.

51. Fischer, E. Ueber einige Derivate des Glykocolls, Alanins und Leucins. *Berichte der deutschen chemischen Gesellschaft* **1902,** 35, 1095-1106.

52. Bergmann, M.; Zervas, L. Über ein allgemeines Verfahren der Peptid-Synthese. *Berichte der deutschen chemischen Gesellschaft (A and B Series)* **1932,** 65, 1192-1201.

53. Merrifield, R. B. Solid Phase Peptide Synthesis. I. The Synthesis of a Tetrapeptide. *Journal of the American Chemical Society* **1963,** 85, 2149-2154.

54. Merrifield, R. B. Solid Phase Synthesis (Nobel Lecture). *Angewandte Chemie International Edition in English* **1985,** 24, 799-810.

55. Merrifield, B. [1] Concept and early development of solid-phase peptide synthesis. In *Methods in Enzymology*, Gregg, B. F., Ed. Academic Press: **1997**; Vol. Volume 289, pp 3-13.

56. Isidro-Llobet, A.; Álvarez, M.; Albericio, F. Amino Acid-Protecting Groups. *Chemical Reviews* **2009,** 109, 2455-2504.

57. Carpino, L. A.; Han, G. Y. 9-Fluorenylmethoxycarbonyl amino-protecting group. *Journal of Organic Chemistry* **1972,** 37, 3404-3409.

58. Fields, G. B.; Noble, R. L. Solid phase peptide synthesis utilizing 9-fluorenylmethoxycarbonyl amino acids. *International Journal of Peptide and Protein Research* **1990,** 35, 161-214.

59. Wellings, D. A.; Atherton, E. [4] Standard Fmoc protocols. In *Methods in Enzymology*, Gregg, B. F., Ed. Academic Press: **1997**; Vol. Volume 289, pp 44-67.

60. Sheehan, J. C.; Hess, G. P. A New Method of Forming Peptide Bonds. *Journal of the American Chemical Society* **1955,** 77, 1067-1068.

61. Marder, O.; Albericio, F. Industrial application of coupling reagents in peptides. *Chemistry Today (Chimica Oggi)* **2003**, 6-11.

62. König, W.; Geiger, R. N-Hydroxyverbindungen als Katalysatoren für die Aminolyse aktivierter Ester. *Chemische Berichte* **1973,** 106, 3626-3635.

63. Carpino, L. A. 1-Hydroxy-7-azabenzotriazole. An efficient peptide coupling additive. *Journal of the American Chemical Society* **1993,** 115, 4397-4398.

64. Dourtoglou, V.; Ziegler, J.-C.; Gross, B. L'hexafluorophosphate de O-benzotriazolyl-N,N-tetramethyluronium: Un reactif de couplage peptidique nouveau et efficace. *Tetrahedron Letters* **1978,** 19, 1269-1272.

65. Coste, J.; Le-Nguyen, D.; Castro, B. PyBOP®: A new peptide coupling reagent devoid of toxic by-product. *Tetrahedron Letters* **1990,** 31, 205-208.

66. Albericio, F.; Cases, M.; Alsina, J.; Triolo, S. A.; Carpino, L. A.; Kates, S. A. On the use of PyAOP, a phosphonium salt derived from HOAt, in solid-phase peptide synthesis. *Tetrahedron Letters* **1997,** 38, 4853-4856.

67. El-Faham, A.; Albericio, F. Morpholine-Based Immonium and Halogenoamidinium Salts as Coupling Reagents in Peptide Synthesis. *Journal of Organic Chemistry* **2008,** 73, 2731-2737.

68. El-Faham, A.; Funosas, R. S.; Prohens, R.; Albericio, F. COMU: A Safer and More Effective Replacement for Benzotriazole-Based Uronium Coupling Reagents. *Chemistry – A European Journal* **2009,** 15, 9404-9416.

69. Subirós-Funosas, R.; Prohens, R.; Barbas, R.; El-Faham, A.; Albericio, F. Oxyma: An Efficient Additive for Peptide Synthesis to Replace the Benzotriazole-Based HOBt and HOAt with a Lower Risk of Explosion. *Chemistry – A European Journal* **2009,** 15, 9394-9403.

70. El-Faham, A.; Albericio, F. COMU: A third generation of uronium-type coupling reagents. *Journal of Peptide Science* **2010,** 16, 6-9.

71. C. Sherrington, D. Preparation, structure and morphology of polymer supports. *Chem Commun* **1998**, 2275-2286.

72. Meldal, M. [6] Properties of solid supports. In *Methods in Enzymology*, Gregg, B. F., Ed. Academic Press: **1997**; Vol. Volume 289, pp 83-104.

73. García-Martín, F.; Quintanar-Audelo, M.; García-Ramos, Y.; Cruz, L. J.; Gravel, C.; Furic, R.; Côté, S.; Tulla-Puche, J.; Albericio, F. ChemMatrix, a Poly(ethylene glycol)-Based Support for the Solid-Phase Synthesis of Complex Peptides. *Journal of Combinatorial Chemistry* **2006,** 8, 213-220.

74. García-Ramos, Y.; Paradís-Bas, M.; Tulla-Puche, J.; Albericio, F. ChemMatrix® for complex peptides and combinatorial chemistry. *Journal of Peptide Science* **2010,** 16, 675-678.

75. Rink, H. Solid-phase synthesis of protected peptide fragments using a trialkoxy-diphenyl-methylester resin. *Tetrahedron Letters* **1987,** 28, 3787-3790.

76. Kassem, T.; Sabatino, D.; Jia, X.; Zhu, X. X.; Lubell, W. D. To Rink or Not to Rink Amide Link, that is the Question to Address for More Economical and Environmentally Sound Solid-Phase Peptide Synthesis. *International Journal of Peptide Research and Therapeutics* **2009,** 15, 211-218.

77. Madder, A.; Farcy, N.; Hosten, N. G. C.; De Muynck, H.; De Clercq, P. J.; Barry, J.; Davis, A. P. A Novel Sensitive Colorimetric Assay for Visual Detection of Solid-Phase Bound Amines. *European Journal of Organic Chemistry* **1999,** 1999, 2787-2791.

78. Kaiser, E.; Colescott, R. L.; Bossinger, C. D.; Cook, P. I. Color test for detection of free terminal amino groups in the solid-phase synthesis of peptides. *Analytical Biochemistry* **1970,** 34, 595-598.

79. Frank, A. O.; Otto, E.; Mas-Moruno, C.; Schiller, H. B.; Marinelli, L.; Cosconati, S.; Bochen, A.; Vossmeyer, D.; Zahn, G.; Stragies, R.; Novellino, E.; Kessler, H.

Conformational control of integrin-subtype selectivity in isoDGR peptide motifs: a biological switch. *Angewandte Chemie International Edition* **2010,** 49, 9278-9281.

80. Glass, R.; Möller, M.; Spatz, J. P. Block copolymer micelle nanolithography. *Nanotechnology* **2003,** 14, 1153-1160.

81. Boehm, H. Micromechanical Properties and Structure of the Pericellular Coat of Living Cells Modulated by Nanopatterned Substrates. Ruprecht-Karls-Universitaet Heidelberg, **2008**.

82. Blümmel, J.; Perschmann, N.; Aydin, D.; Drinjakovic, J.; Surrey, T.; Lopez-Garcia, M.; Kessler, H.; Spatz, J. P. Protein repellent properties of covalently attached PEG coatings on nanostructured SiO2-based interfaces. *Biomaterials* **2007,** 28, 4739-4747.

83. Corti, A.; Curnis, F. Isoaspartate-dependent molecular switches for integrin–ligand recognition. *Journal of Cell Science* **2011,** 124, 515-522.

84. Curnis, F.; Cattaneo, A.; Longhi, R.; Sacchi, A.; Gasparri, A. M.; Pastorino, F.; Di Matteo, P.; Traversari, C.; Bachi, A.; Ponzoni, M.; Rizzardi, G.-P.; Corti, A. Critical Role of Flanking Residues in NGR-to-isoDGR Transition and CD13/Integrin Receptor Switching. *Journal of Biological Chemistry* **2010,** 285, 9114-9123.

85. Kantlehner, M.; Schaffner, P.; Finsinger, D.; Meyer, J.; Jonczyk, A.; Diefenbach, B.; Nies, B.; Hölzemann, G.; Goodman, S. L.; Kessler, H. Surface Coating with Cyclic RGD Peptides Stimulates Osteoblast Adhesion and Proliferation as well as Bone Formation. *Chembiochem* **2000,** 1, 107-114.

86. Lieb, E.; Hacker, M.; Tessmar, J.; Kunz-Schughart, L. A.; Fiedler, J.; Dahmen, C.; Hersel, U.; Kessler, H.; Schulz, M. B.; Göpferich, A. Mediating specific cell adhesion to low-adhesive diblock copolymers by instant modification with cyclic RGD peptides. *Biomaterials* **2005,** 26, 2333-2341.

87. Mas-Moruno, C.; Dorfner, P. M.; Manzenrieder, F.; Neubauer, S.; Reuning, U.; Burgkart, R.; Kessler, H. Behavior of primary human osteoblasts on trimmed and sandblasted Ti6Al4V surfaces functionalized with integrin αvβ3-selective cyclic RGD peptides. *Journal of Biomedical Materials Research Part A* **2012**, n/a-n/a.

88. Auernheimer, J.; Zukowski, D.; Dahmen, C.; Kantlehner, M.; Enderle, A.; Goodman, S. L.; Kessler, H. Titanium Implant Materials with Improved Biocompatibility through Coating with Phosphonate-Anchored Cyclic RGD Peptides. *Chembiochem* **2005,** 6, 2034-2040.

89. Hersel, U.; Dahmen, C.; Kessler, H. RGD modified polymers: biomaterials for stimulated cell adhesion and beyond. *Biomaterials* **2003,** 24, 4385-4415.

90. Kuemin, M.; Schweizer, S.; Ochsenfeld, C.; Wennemers, H. Effects of Terminal Functional Groups on the Stability of the Polyproline II Structure: A Combined Experimental and Theoretical Study. *J Am Chem Soc* **2009,** 131, 15474-15482.

91. Sato, S.-i.; Kwon, Y.; Kamisuki, S.; Srivastava, N.; Mao, Q.; Kawazoe, Y.; Uesugi, M. Polyproline-Rod Approach to Isolating Protein Targets of Bioactive Small Molecules: Isolation of a New Target of Indomethacin. *J Am Chem Soc* **2007,** 129, 873-880.

92. Crespo, L.; Sanclimens, G.; Montaner, B.; Pérez-Tomás, R.; Royo, M.; Pons, M.; Albericio, F.; Giralt, E. Peptide Dendrimers Based on Polyproline Helices. *J Am Chem Soc* **2002,** 124, 8876-8883.

93. Sanclimens, G.; Crespo, L.; Giralt, E.; Albericio, F.; Royo, M. Preparation of de Novo Globular Proteins Based on Proline Dendrimers. *J Org Chem* **2005,** 70, 6274-6281.

94. Bock, V. D.; Hiemstra, H.; van Maarseveen, J. H. CuI-Catalyzed Alkyne-Azide "Click" Cycloadditions from a Mechanistic and Synthetic Perspective. *European Journal of Organic Chemistry* **2006,** 2006, 51-68.

95. Bock, V. D.; Speijer, D.; Hiemstra, H.; van Maarseveen, J. H. 1,2,3-Triazoles as peptide bond isosteres: synthesis and biological evaluation of cyclotetrapeptide mimics. *Organic and Biomolecular Chemistry* **2007,** 5, 971-975.

96. Ido, T.; Wan, C. N.; Casella, V.; Fowler, J. S.; Wolf, A. P.; Reivich, M.; Kuhl, D. E. Labeled 2-deoxy-D-glucose analogs. 18F-labeled 2-deoxy-2-fluoro-D-glucose, 2-deoxy-2-fluoro-D-mannose and 14C-2-deoxy-2-fluoro-D-glucose. *Journal of Labelled Compounds and Radiopharmaceuticals* **1978,** 14, 175-183.

97. Haubner, R.; Wester, H.-J.; Reuning, U.; Senekowitsch-Schmidtke, R.; Diefenbach, B.; Kessler, H.; Stöcklin, G.; Schwaiger, M. Radiolabeled αvβ3 Integrin Antagonists: A New Class of Tracers for Tumor Targeting. *Journal of Nuclear Medicine* **1999,** 40, 1061-1071.

98. Haubner, R.; Wester, H.-J.; Burkhart, F.; Senekowitsch-Schmidtke, R.; Weber, W.; Goodman, S. L.; Kessler, H.; Schwaiger, M. Glycosylated RGD-Containing Peptides: Tracer for Tumor Targeting and Angiogenesis Imaging with Improved Biokinetics. *Journal of Nuclear Medicine* **2001,** 42, 326-336.

99. Haubner, R.; Wester, H.-J.; Weber, W. A.; Mang, C.; Ziegler, S. I.; Goodman, S. L.; Senekowitsch-Schmidtke, R.; Kessler, H.; Schwaiger, M. Noninvasive Imaging of αvβ3 Integrin Expression Using 18F-labeled RGD-containing Glycopeptide and Positron Emission Tomography. *Cancer Research* **2001,** 61, 1781-1785.

100. Knetsch, P.; Petrik, M.; Griessinger, C.; Rangger, C.; Fani, M.; Kesenheimer, C.; von Guggenberg, E.; Pichler, B.; Virgolini, I.; Decristoforo, C.; Haubner, R. 68Ga-NODAGA-RGD for imaging αvβ3 integrin expression. *European Journal of Nuclear Medicine and Molecular Imaging* **2011,** 38, 1303-1312.

101. Beer, A.; Kessler, H.; Wester, H.; Schwaiger, M. PET Imaging of Integrin αVβ3 Expression. *Theranostics* **2011**, 48-57.

102. Miller, P. W.; Long, N. J.; Vilar, R.; Gee, A. D. Synthesis of 11C, 18F, 15O, and 13N Radiolabels for Positron Emission Tomography. *Angewandte Chemie International Edition* **2008,** 47, 8998-9033.

103. Ntziachristos, V.; Tung, C. H.; Bremer, C.; Weissleder, R. Fluorescence molecular tomography resolves protease activity in vivo. *Nature Medicine* **2002,** 8, 757-760.

104. Santi, P. A. Light sheet fluorescence microscopy: a review. *Journal of Histochemistry & Cytochemistry* **2011,** 59, 129-138.

105. Pfeffer, M. A.; Braunwald, E. Ventricular remodeling after myocardial infarction. Experimental observations and clinical implications. *Circulation* **1990,** 81, 1161-1172.

106. Liehn, E. A.; Postea, O.; Curaj, A.; Marx, N. Repair After Myocardial Infarction, Between Fantasy and Reality: The Role of Chemokines. *Journal of the American College of Cardiology* **2011,** 58, 2357-2362.

107. Sun, M.; Opavsky, M. A.; Stewart, D. J.; Rabinovitch, M.; Dawood, F.; Wen, W.-H.; Liu, P. P. Temporal Response and Localization of Integrins β1 and β3 in the Heart After Myocardial Infarction. *Circulation* **2003,** 107, 1046-1052.

108. Higuchi, T.; Bengel, F. M.; Seidl, S.; Watzlowik, P.; Kessler, H.; Hegenloh, R.; Reder, S.; Nekolla, S. G.; Wester, H. J.; Schwaiger, M. Assessment of αvβ3 integrin expression after myocardial infarction by positron emission tomography. *Cardiovascular Research* **2008,** 78, 395-403.

109. Sherif, H. M.; Saraste, A.; Nekolla, S. G.; Weidl, E.; Reder, S.; Tapfer, A.; Rudelius, M.; Higuchi, T.; Botnar, R. M.; Wester, H.-J.; Schwaiger, M. Molecular Imaging of Early αvβ3 Integrin Expression Predicts Long-Term Left-Ventricle Remodeling After Myocardial Infarction in Rats. *Journal of Nuclear Medicine* **2012,** 53, 318-323.

110. Gao, H.; Lang, L.; Guo, N.; Cao, F.; Quan, Q.; Hu, S.; Kiesewetter, D.; Niu, G.; Chen, X. PET imaging of angiogenesis after myocardial infarction/reperfusion using a one-step labeled integrin-targeted tracer 18F-AlF-NOTA-PRGD2. *European Journal of Nuclear Medicine and Molecular Imaging* **2012,** 39, 683-692.

111. Meoli, D. F.; Sadeghi, M. M.; Krassilnikova, S.; Bourke, B. N.; Giordano, F. J.; Dione, D. P.; Su, H.; Edwards, D. S.; Liu, S.; Harris, T. D.; Madri, J. A.; Zaret, B. L.; Sinusas, A. J. Noninvasive imaging of myocardial angiogenesis following experimental myocardial infarction. *The Journal of Clinical Investigation* **2004,** 113, 1684-1691.

112. Joner, M.; Cheng, Q.; Schönhofer-Merl, S.; Lopez, M.; Neubauer, S.; Mas-Moruno, C.; Laufer, B.; Kolodgie, F. D.; Kessler, H.; Virmani, R. Polymer-free immobilization of a cyclic RGD peptide on a nitinol stent promotes integrin-dependent endothelial coverage of strut surfaces. *Journal of Biomedical Materials Research Part B: Applied Biomaterials* **2012,** 100B, 637-645.

113. Fischman, D. L.; Leon, M. B.; Baim, D. S.; Schatz, R. A.; Savage, M. P.; Penn, I.; Detre, K.; Veltri, L.; Ricci, D.; Nobuyoshi, M.; Cleman, M.; Heuser, R.; Almond, D.; Teirstein, P. S.; Fish, R. D.; Colombo, A.; Brinker, J.; Moses, J.; Shaknovich, A.; Hirshfeld, J.; Bailey, S.; Ellis, S.; Rake, R.; Goldberg, S. A Randomized Comparison of Coronary-Stent Placement and Balloon Angioplasty in the Treatment of Coronary Artery Disease. *New England Journal of Medicine* **1994,** 331, 496-501.

114. Morice, M.-C.; Serruys, P. W.; Sousa, J. E.; Fajadet, J.; Ban Hayashi, E.; Perin, M.; Colombo, A.; Schuler, G.; Barragan, P.; Guagliumi, G.; Molnàr, F.; Falotico, R. A Randomized Comparison of a Sirolimus-Eluting Stent with a Standard Stent for Coronary Revascularization. *New England Journal of Medicine* **2002,** 346, 1773-1780.

115. Wallace, E. L.; Abdel-Latif, A.; Charnigo, R.; Moliterno, D. J.; Brodie, B.; Matnani, R.; Ziada, K. M. Meta-Analysis of Long-Term Outcomes for Drug-Eluting Stents Versus Bare-Metal Stents in Primary Percutaneous Coronary Interventions for ST-Segment Elevation Myocardial Infarction. *The American Journal of Cardiology* **2012,** 109, 932-940.

116. Sigwart, U.; Puel, J.; Mirkovitch, V.; Joffre, F.; Kappenberger, L. Intravascular Stents to Prevent Occlusion and Re-Stenosis after Transluminal Angioplasty. *New England Journal of Medicine* **1987,** 316, 701-706.

117. Finn, A. V.; Joner, M.; Nakazawa, G.; Kolodgie, F.; Newell, J.; John, M. C.; Gold, H. K.; Virmani, R. Pathological Correlates of Late Drug-Eluting Stent Thrombosis. *Circulation* **2007,** 115, 2435-2441.

118. Waksman, R.; Pakala, R. Biodegradable and Bioabsorbable Stents *Current Pharmaceutical Design* **2010,** 16, 4041-4051.

119. Curcio, A.; Torella, D.; Indolfi, C. Mechanisms of Smooth Muscle Cell Proliferation and Endothelial Regeneration After Vascular Injury and Stenting - Approach to Therapy. *Circulation Journal* **2011,** 75, 1287-1296.

120. Chatterjee, J.; Ovadia, O.; Zahn, G.; Marinelli, L.; Hoffman, A.; Gilon, C.; Kessler, H. Multiple N-methylation by a designed approach enhances receptor selectivity. *Journal of Medicinal Chemistry* **2007,** 50, 5878-5881.

121. Mas-Moruno, C.; Beck, J. G.; Doedens, L.; Frank, A. O.; Marinelli, L.; Cosconati, S.; Novellino, E.; Kessler, H. Increasing αvβ3 Selectivity of the Anti-Angiogenic Drug Cilengitide by N-Methylation. *Angewandte Chemie International Edition* **2011,** 50, 9496-9500.

# 8. Appendix

## 8.1. Appendix I:

### Biselectivity of *iso*DGR Peptides for Fibronectin Binding Integrin Subtypes α5β1 and αvβ6: Conformational Control through Flanking Amino Acids

*Alexander Bochen,[1] Udaya Kiran Marelli,[1] Elke Otto,[1] Diego Pallarola,[2] Carles Mas-Moruno,[1] Francesco Saverio Di Leva,[3] Heike Boehm,[2] Joachim P. Spatz,[2] Ettore Novellino,[4] Horst Kessler,[1,5]* and Luciana Marinelli[4]**

[1] Institute for Advanced Study and Center of Integrated Protein Science, Department Chemie, Technische Universität München, Lichtenbergstrasse 4, 85747 Garching, Germany

[2] Department of New Materials and Biosystems, Max Planck Institute for Intelligent Systems, Heisenbergstr. 3, 70569 Stuttgart, Germany & Department of Biophysical Chemistry, University of Heidelberg , INF 253, 69120 Heidelberg, Germany

[3] Department of Drug Discovery and Development, Istituto Italiano di Tecnologia (IIT), Via Morego 30, 16163 Genova, Italy.

[4] Dipartimento di Chimica Farmaceutica e Tossicologica, Università di Napoli “Federico II” Via D. Montesano 49, 80131 Napoli, Italy.

[5] Chemistry Department, Faculty of Science, King Abdulaziz University, P.O. Box 80203, Jeddah 21589, Saudi Arabia

lmarinel@unina.it, kessler@tum.de

*To whom correspondence should be addressed:

* Dept. of Pharmaceutical Chemistry, University of Naples, Via D. Montesano 49, 80131 Napoli, Italy. Phone: + 39 (0) 81 679899. E-mail: lmarinel@unina.it.

*Institute for Advanced Study and Center of Integrated Protein Science, Department Chemie, Technische Universität München, Lichtenbergstrasse 4, 85747 Garching, Germany. Phone: +49 (0) 89 289 13300. Fax: +49 (0) 89 289 13210. Email: kessler@tum.de.

**ABSTRACT**

Integrins are the major class of cell adhesion proteins. Their interaction with different ligands of the extracellular matrix (ECM) is diverse. To reveal these interactions, selective artificial ligands are necessary with a defined activity/selectivity profile. Herein, we describe the development of small, cyclic pentapeptides containing the central *iso*DGR amino acid sequence in which high selectivity and high activity is induced towards fibronectin binding integrins α5β1 and αvβ6 by the flanking amino acids, controlling the conformation of the peptide. A library of cyclic pentapeptides, based on our previously reported peptide motif *c*(-phg-*iso*DGR-X-), has been synthesized, the impact on activity and selectivity of the variable amino acid is screened. The potential effect on binding affinity is characterized by ELISA experiments and the structure of the most promising candidate and its counterpart is determined using NMR and MD simulations. Docking studies elucidate the peptide-integrin interactions on a molecular level. Finally, these results have been verified by cell adhesion experiments on specifically functionalized surfaces, thus paving the way to investigate the fibronectin-integrin interaction pattern within biological systems in the future.

**INTRODUCTION**

Integrins, as one of the most important classes of cell adhesion receptors, play a pivotal role in many physiological processes such as (neo-)angiogenesis, cell adhesion and proliferation[1-3] being key proteins in severe pathological disorders like cancer metastasis, thrombosis, osteoporosis and auto-immune diseases. Consequently, this family of transmembrane glycoproteins has nowadays become a highly studied target in medicinal chemistry.[4] From a structural point of view, integrins are non-covalently linked heterodimers consisting of an α- and a β-subunit.[5] The most prominent motive recognized by integrins is the three amino acid sequence Arg-Gly-Asp (RGD).[1, 6, 7] This tripeptidic sequence has been found in ECM proteins like fibrinogen (Fbg), vitronectin (Vn) and fibronectin (Fn). Using three principles for optimizing peptide structures for

activity and selectivity:[8] cyclization of small peptides, incorporation of D-amino acids and *N*-methylation of a peptide bond in the “spatial screening” procedure, the cyclic pentapeptide *c*(-RGDf(*N*-Me)Val-), Cilengitide,[9] was developed as an anti-angiogenic drug which is currently in clinical phase II and III for treatment of several cancers.[10] Thus artificial RGD-based ligands are not only an important tool to study integrin interactions, but are also of high clinical relevance.[4, 10] Cells differentiate between several ECM proteins to fine-tune their ECM interaction pattern as integrins αvβ3 and αvβ5 primarily recognize Vn as a ligand, while αIIbβ3 targets Fbg. Several integrins recognize also the RGD motive within Fn, which is the main ligand for α5β1, αvβ6 and αvβ8.[4, 11]

Several carcinoma cells, like pancreatic carcinoma, show elevated expression of integrin αvβ6 which was discovered as a Fn-binding protein targeting its RGD binding site, while it is not recognizing Vn or Collagen I as a target.[12] Later, latency-associated peptide (LAP) was discovered as an additional αvβ6 ligand, which is secreted as a complex with transforming growth factor β (TGF-β).[13] RGD peptidomimetic αvβ6 ligands have been developed with good success regarding activity, however these compounds lacked exclusive selectivity for integrin αvβ6 being also active for Vn binding integrin αvβ3.[14] Besides the prominent RGD recognition motif, the non RGD consensus motif DLXXL was discovered as a very strong αvβ6 binder, being inactive for αvβ3, αvβ5 and αIIbβ3.[15] Up to date, this motif is the commonly applied approach to design and synthesize peptide sequences as αvβ6 ligands.[16-18] However, all highly active peptidic αvβ6 ligands synthesized so far consist of longer sequences or apply a multimeric approach to increase affinity,[16, 17] which is unfavorable with respect to synthetic effort, yield and costs compared to smaller peptides.

Fn is also the primary ECM ligand for integrin α5β1.[4] Many attempts have been performed to develop selective ligands for this integrin subtype. Nevertheless, to the best of our knowledge, so far no ligand was discovered addressing integrins α5β1 and αvβ6 exclusively.

Integrin-mediated ECM ligand recognition results in an assembly of a Fn matrix around the cells.[11] Mutating RGD to RGE in the 10$^{th}$ type III repeat Fn module prohibits integrin binding in mice.[19] Despite this fact, Fn containing this mutation can still be assembled into Fn fibrils via αvβ3 integrin binding to an *iso*DGR sequence in 5$^{th}$ type I repeat of Fn.[19] This motif is created after rearrangement by deamidation of the Asn-Gly-Arg (NGR) motif and acts as a novel binding site.[3] This process occurs naturally *in vivo*.[20] Deamidation of the Asn-Gly-Arg (NGR) motive into *iso*DGR forms a new binding site and gain of protein function instead of protein inactivation, as it was shown by Corti et al.[19, 21-

[23] This promising scenario inspired us to investigate the binding capability of the *iso*DGR sequence for Fn binding integrins fostering its integrin binding behavior, if possible.

In a previous work, we grafted the *iso*DGR motive onto a cyclic penta-peptide, *c*(-phg-*iso*DGR-G-), phg is the unnatural amino acid D-phenylglycine, achieving activity enhancement towards α5β1 integrin, compared to the retrosequence *c*(-Vf-isoDGR-)[24] of integrin-binding peptide *c*(-RGDfV-).[25] The development of the *c*(-phg-*iso*DGR-G-) peptide serves as a starting point for the synthesis of small peptides, gaining additional activity for the Fn- (α5β1, αvβ6) system and increased selectivity against Vn-binding integrins (αvβ6, αvβ5). As shown earlier, phg next to *iso*DGR is crucial for α5β1 activity,[25] leaving the glycine residue as the only site for further modifications.

Herein, we describe the systematic screening of our *c*(-phg-*iso*DGR-X-) lead motif aiming to confer to the small lead pentapeptide selectivity towards Fn binding integrins α5β1 and αvβ6 for which few peptides are known to be active and selective. As shown in Table 1, we successfully synthesized peptides exhibiting these features. The ability of these peptides to inhibit the Fn binding to integrin α5β1, αvβ6 and their corresponding natural ligands has been tested by an *in vitro* ELISA assay.[26] The designed *c*(-phg-*iso*DGR-k-) motif represents the first report of a small-sized, highly active, cyclic peptide targeting selectively αvβ6 and α5β1 integrins, which preferentially bind Fn. The structural differences of D- or L-amino acids on 5$^{th}$ position within the sequence, causing the increased activity and selectivity, have been investigated by NMR and docking experiments. The amino group of the lysine side chain gives a position for possible further chemical modifications without losing the activity/selectivity profile. Herein, this has been done by a PEG spacer/thiol anchor for surface functionalization. This allows an additional biological verification of the *iso*DGR sequence in this peptide as an integrin binding sequence by cell adhesion experiments.

**CHEMISTRY**

For the synthesis of peptides standard Fmoc solid phase conditions are used. However, note the importance of starting to load the resin with Arg, as the β-amino acid *iso*Asp turned out to have a strong influence on the peptide conformation. Thus, cyclization could only be achieved if *iso*Asp is located in the middle of the sequence. Attachment of Hegas-MPA at the D-Lys side-chain amino group of **6** yields peptide **13**, suitable for surface coating. Its corresponding reference compound **14** is synthesized using the same methodology, except here Gly is used as a starting amino acid instead of

*iso*Asp. Cyclization of linear penta-peptides occurred in solution. After removal of all protecting groups, peptides are purified by HPLC.

## RESULTS AND DISCUSSION

### *In vitro* inhibition of integrin binding

To investigate the influence of the second exchangeable amino acid (glycine) in *c*(-phg-*iso*DGR-G-) for its influence on integrin binding ability, all compounds of the synthesized library have been examined in a competitive ELISA. Immobilized natural ligand and soluble integrin (Fn/ α5β1, LAP/ αvβ6, Vn/ αvβ3, Vn/ αvβ5, Fbg/ αIIbβ3) are used. As internal controls, highly active penta-peptide Cilengitide, *c*(-RGDf$^{Me}$V-)[10] is used in the case of α5β1, αvβ3 and αvβ5, linear peptide RTDLDSLRT[15] for αvβ6 and Tirofiban[27] for αIIbβ3 (Table 1, $IC_{50}$). Other compounds known in literature (Mol11[14] and *c*(-RGDfK-)[28]) have been included to allow further comparison.

All three different groups of amino acids have been investigated, containing aliphatic or aromatic side-chains. The aliphatic side chains with polar groups are charged under physiological conditions. Two representatives of each group have been selected, both in their L- and D-amino acid configuration. Replacement of glycine by a D-amino acid leads in all cases to higher affinity for α5β1 integrin compared to their corresponding L-amino acid analogs, which are far less active. All compounds of the library show no affinities for integrin αvβ3, except for some L-amino acid analogs remaining a low mid-range affinity for this integrin. Peptides incorporating aliphatic valine and proline residues (**1-4**), only the D-amino acid configuration yields highly active α5β1 inhibitors. Exchanging the aliphatic amino acids by aromatic ones (**9-12**) selectivity of L-amino acids greatly improves, without affecting the excellent activity and selectivity of the analogous D-amino acids as observed before. Last, by using amino acids containing charged side-chains (**5-8**), activity and selectivity retains excellent for the D-amino acids variants.

Remarkably, peptide **12** exhibits a 3.5 times higher activity (5.5 nM vs. 19 nM) for α5β1 integrin and about 10 times higher selectivity (>10000 nM vs. >1000 nM) against αvβ3 integrin than the starting compound *c*(-phg-*iso*DGR-G-)(**0**), resulting in a 35 times increased total selectivity. The most interesting compounds of the library, D-Lys, L-Lys and D-Trp, have been tested for other relevant integrin subtypes (αvβ5, αvβ6 and αIIbβ3, s. Table 2). Lysine can be modified at its side chain in addition to investigate the intriguing differences between D- and L-amino acid configuration. Last, D-Tryptophan as the most active peptide of the library is also included and all compounds are compared in

their activity to the Glycine starting peptide. All selected residues are completely inactive for integrin αvβ5 and αIIbβ3. For integrin αvβ6, only the D-Lys peptide (**6**) remains highly active, whereas the other two compounds (**5** and **12**) do not differ much in their activity compared to the glycine starting peptide (**0**). To further investigate the observed effects of activity and selectivity, most promising peptide **5** was chosen in comparison to its L-amino acid analog **6** using NMR and molecular modeling methods.

**Table 1.** Inhibition of integrin binding to fibronectin (α5β1), vitronectin (αvβ3, αvβ5), LAP (αvβ6) and fibrinogen (αIIbβ3) by head to tail cyclized *iso*DGR pentapeptides with different flanking L- or D-amino acids.

| Peptide | $IC_{50}$[a] α5β1 [nM] | $IC_{50}$[a] αvβ3 [nM] |
|---|---|---|
| **0** *c*(-phg-*iso*DGR-**G-**)[25] | 19 (± 4) | >1000 |
| **1** *c*(-phg-*iso*DGR**V-**) | 115 (± 15) | 576 (± 49) |
| **2** *c*(-phg-*iso*DGR**v**-) | 7.3 (± 0.8) | >10000 |
| **3** *c*(-phg-*iso*DGR**P-**) | 111 (± 9) | 675 (± 104) |
| **4** *c*(-phg-*iso*DGR**p**-) | 7.0 (± 0.1) | >10000 |
| **5** *c*(-phg-*iso*DGR**K-**) | 94 (± 4) | 516 (± 41) |
| **6** *c*(-phg-*iso*DGR**k**-) | 8.7 (± 0.7) | >10000 |
| **7** *c*(-phg-*iso*DGR**E-**) | 92 (± 10) | 3871 (± 435) |
| **8** *c*(-phg-*iso*DGR**e**-) | 11 (± 2) | >10000 |
| **9** *c*(-phg-*iso*DGR**Y-**) | 39 (± 3) | >10000 |
| **10** *c*(-phg-*iso*DGR**y**-) | 8.7 (± 1.6) | >10000 |
| **11** *c*(-phg-*iso*DGR**W-**) | 72 (± 10) | >10000 |
| **12** *c*(-phg-*iso*DGR**w**-) | 5.5 (± 1.2) | >10000 |
| **13** *c*(-phg-*iso*DGR**k** [Hegas-MPA]-) | 27 (± 3.1) | >10000 |
| **14** *c*(-RGDfK[Hegas-MPA]-)[b] | 197 (± 35) | 13.6 (± 3.6) |
| Cilengitide[c] | 15 (± 3) | 0.54 (± 0.15) |
| Mol11[d] | 2807 (± 527) | >10000 |
| *c*(-RGDfK-)[e] | 133 (± 23) | 2.6 (± 0.6) |

[a]$IC_{50}$ values are derived from a competitive ELISA using immobilized ECM protein and soluble integrin. [b]Well known, unselective sequence *c*(-RGDfK-)[28] is included in cell adhesion experiments as a reference compound. [c]Cilengitide, *c*(-RGDf$^{Me}$V-)[10] is used in ELISA as an internal reference compound for αvβ3 and α5β1 assays. [d]Highly active αvβ6 peptidomimetic inhibitor (molecule 11).[14] [e]Frequently used, unselective cyclic pentapeptide, unmodified cyclo-peptide of **14**.[28] Hegas: heptaethylenglycol amino acid, MPA: mercaptopropionic acid, phg: D-phenylglycine

**Table 2.** Inhibition of integrin binding to vitronectin (αvβ5), LAP (αvβ6) and fibrinogen (αIIbβ3) by the most active pentapeptides out of the synthesized library (s. Table 1).

| Peptide | $IC_{50}$ [a] αvβ5 [nM] | $IC_{50}$ [a] αvβ6 [nM] | $IC_{50}$ [a] αIIbβ3 [nM] |
|---|---|---|---|
| **0** *c*(-phg-*iso*DGR-**G-**)[25] | >10000 | 106 (± 19) | >10000 |
| **5** *c*(-phg-*iso*DGR**K-**) | >10000 | 140 (± 9) | >10000 |
| **6** *c*(-phg-*iso*DGR**k**-) | >10000 | 19 (± 2) | >10000 |
| **12** *c*(-phg-*iso*DGR**w**-) | >10000 | 92 (± 14) | >10000 |
| Cilengitide[b] | 7.6 (± 2.3) | 1656 (± 543) | 4208 (± 548) |
| RTDLDSLRT[c] | n.d. | 33 (± 2.8) | n.d. |
| Tirofiban[d] | n.d. | n.d. | 0.95 (± 0.05) |
| Mol11[e] | >10000 | 4.0 (± 0.45) | >10000 |
| *c*(-RGDfK-)[f] | 310 (± 12) | 68 (± 12) | >10000 |

[a] $IC_{50}$ values are derived from a competitive ELISA using immobilized ECM protein and soluble integrin. [b] Cilengitide, *c*(-RGDf$^{Me}$V-)[10] is used in ELISA as an internal reference compound for αvβ5 assay. [c] The linear peptide is used in ELISA as an αvβ6 internal reference compound.[15] [d] Tirofiban is a small molecule, approved drug and used as an internal reference for αIIbβ3 assay.[27] [e] Highly active αvβ6 peptidomimetic inhibitor (molecule 11).[14] [f] Frequently used, unselective cyclic pentapeptide, unmodified cyclo-peptide of **14**.[28] Hegas: heptaethylenglycol amino acid, MPA: mercaptopropionic acid, n.d.: not determined, phg: D-phenylglycine

After determining the influence of the aromatic moiety in cyclic *iso*DGR pentapeptides,[25] *c*(-phg-isoDGR-G-) (**0**) peptide was found as a highly active and selective α5β1 integrin ligand. In *c*(-RGDfV-) peptide valine is well known to be replaced by other amino acids, for example lysine, without affecting the receptor affinity for the αvβ3 integrin binding.[28] Based on this fact, we investigated the influence of the second exchangeable amino acid (glycine) in *c*(-phg-isoDGR-G-) (**0**) peptide on its binding ability to integrins.

Glycine is known to act often as a D-amino acid and its exchange by a D-amino acid might not affect the backbone configuration of the peptide. In fact, replacement of glycine with D-amino acids leads to compounds with higher affinity for α5β1 integrin compared to their L-amino acids analogs.

Remarkably, peptide **12** exhibits the highest activity and highest selectivity for integrin α5β1. To our knowledge, it is the most active and selective small cyclic peptide ligand for α5β1 integrin reported so far. It is even in the range of the best α5β1 mimetics found previously in our group.[29] Additionally, the activity of **6** for integrin αvβ6 is absolutely outstanding for such a small peptide. A general trend in these peptides, gaining activity for the Fn binding integrins α5β1 and αvβ6, is observed. This demonstrates that switching from peptides to mimetics to improve the binding ability is not always necessary. In contrast, the great water solubility of peptides and their very predictable *in vivo* degradation products makes them even more attractive for drug development, circumventing several challenges occurring by use of mimetics like solubility, metabolism and toxicity.

**NMR structure determination**

In order to understand the integrin subtype activity-selectivity profile differences that are brought in by differed stereochemical configuration at one of the amino acid residues in **5** and **6**, the NMR spectroscopic structures of these two compounds in DMSO have been determined by Distance Geometry (DG) calculations and further characterized by Molecular Dynamics (MD) simulations.

Single set of NMR peaks observed in $^{1}$H-1D spectra of both the compounds have indicated the absence of slowly exchanging conformations on NMR time scales. Temperature coefficients for backbone NHs are calculated from variable (295 K to 315 K in 5 K increments) temperature $^{1}$H-1D spectra and the values for the corresponding backbone NHs of the compounds have differed slightly (s. Table 3).

**Table 3.** Temperature coefficient data of **5** and **6** in DMSO.

| **5** *c*(-phg-*iso*DGR**K-**) | | **6** *c*(-phg-*iso*DGR**k**-) | |
|---|---|---|---|
| Name of the NH | Temperature Coefficient (ppb/K) | Name of the NH | Temperature Coefficient (ppb/K) |
| Phg$^{1}$-NH | -6.00 | Phg$^{1}$-NH | -3.33 |
| *iso*Asp$^{2}$-NH | -2.00 | *iso*Asp$^{2}$-NH | -2.00 |
| Gly$^{3}$-NH | -4.30 | Gly$^{3}$-NH | -4.66 |
| Arg$^{4}$-NH | 0.00 | Arg$^{4}$-NH | -2.00 |
| Lys$^{5}$-NH | -4.50 | lys$^{5}$-NH | -4.44 |

For **6**, this data indicated moderate solvent accessibility or hydrogen bonding for phg[1]-NH, *iso*Asp[2]-NH and Arg[4]-NH, while Gly[3]-NH and lys[5]-NH are solvent exposed. In **5**, phg[1]-NH showed a slightly increased and Arg[4]-NH a decreased solvent accessibility tendency compared to the corresponding NHs in **6** whereas the behavior of the other NHs remained unchanged.

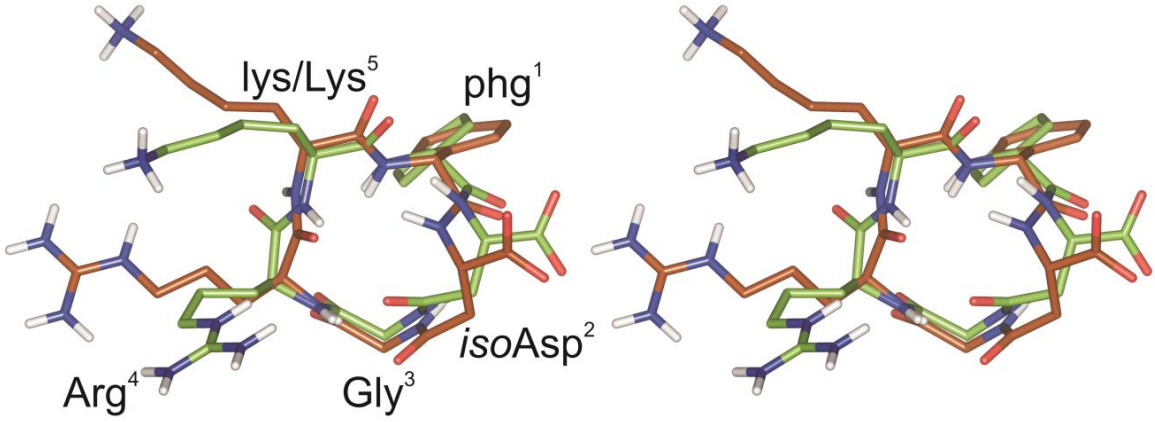


**Figure 1.** Stereo view of the overlaid DG conformers derived for **5** (green) and **6** (brown). For a better view of the conformation, non-polar hydrogens are not shown.

Geometrical structures for both the compounds are derived using DG algorithm in which distance restraints (22 and 24 for **5** and **6**, respectively) calculated from ROESY are used as inputs by imposing 15% relaxed bound limits on them. The derived structures (Figure 1) showed a well-defined gamma turn[30] around the Gly[3] residue of both the compounds, which was also observed for structures earlier reported for cyclopentapeptides containing *iso*DGR motif.[25] The dihedral angles for the said γ-turn ($(\phi_{i+1},\psi_{i+1})$ = (63.9, -65.3) and (84.5, -45.3) for **5** and **6**, respectively) are in close agreement with the theoretical values (70-85, -60 - -70).[31, 32] The structures however showed differences on the other half of the cyclus. **6** showed a β-turn[33] populated around lys[5]-phg[1] whereas **5** exibits a γ-turn $(\phi_{i+1},\psi_{i+1})$ = (91.7, -40.0) centered on phg[1]. The dihedral angles $(\phi_{i+1},\psi_{i+1}, \phi_{i+2},\psi_{i+2})$ = (89.8, 4.7, 121.0, -32.1) around lys[5]-phg[1] in **6** are close to a βI' turn (60, 30, 90, 0).[34] Nevertheless, considering the conformational flexibility in small molecules, a dynamic equilibrium of γ-turn on Gly[3] with β-turn on Gly[3]-Arg[4], γ-turn on phg[1] with β-turn on lys[5] (/Lys[5])- phg[1] in both the compounds cannot be ignored. RMSD over the backbone atoms of the two structures is 0.555 Å. As viewed from Figure 1, a 180° flip in the orientation of Arg[4]-lys[5](Lys[5]) peptide bond is noticeable. This flip, which leads to a significant change in the associated dihedral space along Arg[4]-lys[5](Lys[5]) residues, can be attributed to the preference for a parallel orientation of CO(i) to CαHα(i + 1) bond vectors[35] and the change in the configuration at Lys[5] residue.

The two structures are then taken forward for MD calculations that are performed on GROMACS by using all atom ffcharmm27 force field. MD studies are carried out in DMSO solvent box[36, 37] without using any restraints. Trajectories are then analyzed for interatomic distances and their consistency has been checked by comparison to ROE derived distances, based on which the input DG structures have been derived. The observed violations are within limits that can be accounted for the dynamically averaged NMR experimental data (see SI). The trajectories revealed a well conserved γ-turn positioned at $Gly^3$ residue of the *iso*DGR motif in both molecules. However, more conformational flexibility was observed along the other parts of the molecules as evident from the dihedral angle distribution data given in supporting information. The overall dynamical behavior is more predominant in **5** than **6**. These results are strongly relied upon after their unaltered repetition in multiple MD runs. These conformational and dynamical variations between **5** and **6** might be a reason for the poor activity/selectivity profile of the former than latter.[38]

**Molecular Docking**

To rationalize the influence of the exchangeable amino acid in *c*(-phg-*iso*DGR-X-) peptides on the integrins binding activity, molecular docking studies were performed. Specifically, the DG structures of **5** and **6** were docked in the RGD binding sites of the αvβ3 [39] (PDB code 1L5G), α5β1 [40], αvβ5 [41] and αvβ6 homology models. According to docking results, **5** binds the α5β1 receptor by chelating the metal cation at the MIDAS (metal-ion-dependent adhesion site) with the *iso*Asp carboxylate group and establishing a bidentate salt bridge with (α5)-D227 by the $Arg^4$ guanidinium group. In addition, the phenyl ring of $phg^1$ forms a T-shaped interaction with (β1)-Y127, and the side chain of $Lys^5$ points downwards to set up an ionic bond with (α5)-D228 (see Figure 2a). With regards to **6** in α5β1 receptor, the predicted binding mode is very similar to that adopted by **5** (see Figure 2b) with the only two differences residing in the orientation of the $lys^5$ side chain, which extends onto the dimer interface surface to contact (β1)-E314, and in the formation of an additional H-bond with the (β1)-S221 side chain, which seems to be responsible for the slightly higher potency of **6** compared to **5**. Overall, the interaction patterns observed for both **5** and **6** at the RGD binding domain of the α5β1 integrin are highly consistent with the nanomolar $IC_{50}$ of these peptides.

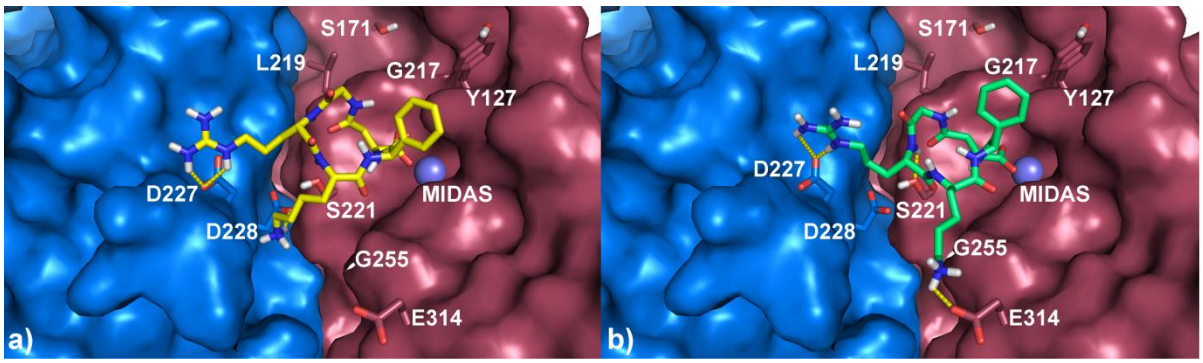


**Figure 2.** Binding modes of **5** (a) and **6** (b) at the **α5β1** integrin. **5** and **6** are shown as yellow and green sticks, respectively. The **α5** and **β1** subunits are depicted as blue and red surfaces, respectively. Receptor amino acid side chains important for the ligand binding are represented as sticks. The metal cation at the MIDAS is represented as a purple sphere.

The αvβ3 integrin, as already pointed out in our previous work [40], mainly differs from α5β1 in two key regions, namely the SDL (Specificity Determining Loop) and a cleft along the dimer interface (herein referred as the downstream pocket). Particularly, the latter pocket consists of some specific amino acids which make this cleft narrower in αvβ3 than in α5β1 (e.g. (β1)-S221 and (β1)-G255 in α5β1 are replaced by (β3)-A218 and (β3)-K253 in αvβ3, respectively). Such substitutions, and primarily the replacement of (β1)-G255 by (β3)-K253, seem to be the reasons for the different binding poses obtained for **5** and **6** in the αvβ3 receptor (see Supporting Information for more details).

As regards the αvβ6 receptor, docking results suggest that both **5** and **6** might adopt a binding mode similar to that observed in α5β1 and αvβ3 with the major difference residing in the orientation of the phg[1] phenyl ring (see Figure 3), which is ascribable to the different amino acidic composition and the 3D shape of the β6 subunit. Indeed, in the αvβ6 receptor a large and more hydrophobic pocket below the SDL region is formed by residues (β6)-K161, (β6)-A208, and (β6)-I210 which replace for instance the bulkier (β3)-Y166, (β3)-R214 and (β3)-R216 present in αvβ3. In addition, the substitution of either (β3)-Y122 in αvβ3 or (β3)-Y127 in α5β1 with (β6)-A117 results in the loss of a key π-stacking interaction by the phg[1] aromatic ring, thus further driving the latter to arrange in a different fashion. Accordingly, both **5** and **6** place the phg[1] phenyl ring within the aforementioned hydrophobic pocket where it establishes multiple favorable interactions with (β6)-A117, (β6)-I174, (β6)-A208 and (β6)-I210, even largely compensating for the lack of the π-stacking interaction observed in both α5β1 and αvβ3. Interestingly, the accommodation of the phg[1] phenyl ring in the larger hydrophobic pocket allows the lys[5] side chain of **6** to adopts an entropically favored conformation extending upwards to form a tight salt bridge with the (β6)-D120 carboxyl group. Clearly, this might be the reason for

the gain in affinity of **6** towards the αvβ6 receptor with respect to αvβ3. The same interaction also seems to be responsible for the gain in αvβ6 affinity of **6** if compared to **5**, having its $Lys^5$ side chain not being involved in any specific interaction with the target.

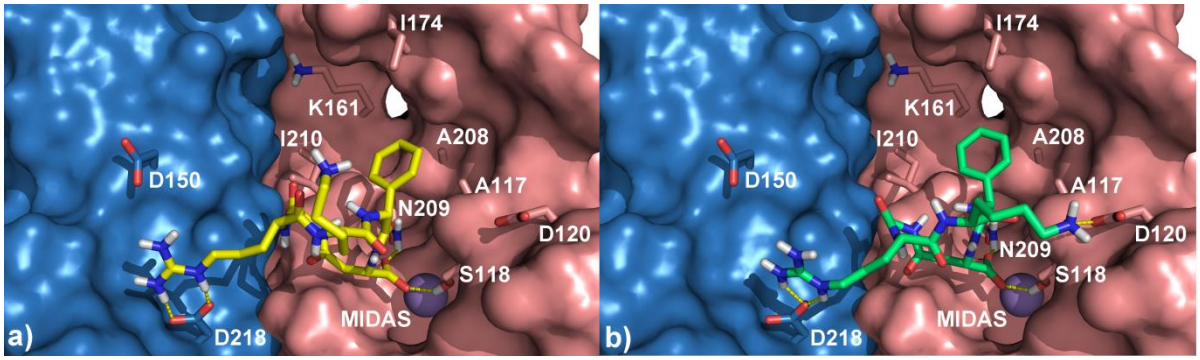


**Figure 3.** Binding modes of **5** (a) and **6** (b) in the **αvβ6** integrin. **5** and **6** are shown as yellow and green sticks, respectively. The **αv** and **β6** subunits are depicted as light blue and pink surfaces, respectively. Receptor amino acid side chains important for the ligand binding are represented as sticks. The metal cation in the MIDAS is represented as a purple sphere.

Accordingly with the high $IC_{50}$ values (> 10 nM) reported for **5** and **6**, docking calculations using the αvβ5 integrin failed to converge, not providing any binding pose with either ligand contacting at the same time both the metal ion and the critical aspartate residues (see Supporting Information for more details). In summary, docking studies performed on **5** and **6** suggest that, the chemical properties and the chirality of the exchangeable amino acid in *c*(-phg-*iso*DGR-X-) combined with the peculiar shape and biochemical features of each integrin RGD binding domain results in slight diverse interaction patterns, thus leading to different activity and selectivity profiles of each peptide towards the distinct integrin subtypes.

**Cell Adhesion Experiments**

Molecular docking experiments performed for compound **5** and **6** were successful to provide a clear insight, at a theoretical level, for the remarkable selectivity towards the α5β1 integrin being barely active for αvβ3 integrin. Selecting a D-amino acid able to be modified at the side-chain, such as compound **6**, allows us to synthesize a fully active derivative (Table 1, **13**) suitable for surface chemistry patterning. This represents a key constituent for the construction of cell-adhesive interfaces.

Upon extracellular binding to ligands, integrins cluster and associate with a variety of submembrane “anchor proteins”, such as paxillin, vinculin and talin, leading to the formation of focal adhesions (FA).[42, 43] These complex multimolecular assemblies are

indirectly linked to the actin cytoskeleton and are the primary structures involved in cell-extracellular matrix (ECM) interactions. Moreover, since FA serve as surface-sensing entities controlling adhesion-mediated signaling,[44, 45] the study of integrin clustering through changes in FA morphology can provide insights into integrin-peptide affinity.

After *in vitro* and theoretical experiments, the next step involves studying the impact of the chemical tuning strategy developed for the *c*(-phg-*iso*DGR-G-) derivatives on a cell-adhesion model system (rat cell line REF52). Specifically for this purpose we selected compound **6** and synthesized its corresponding Hegas-MPA side-chain derivative, yielding compound **13**. As a reference compound, we chose the well-known active but nonselective sequence *c*(-RGDfK-) as a Hegas-MPA derivative (Table 1, **14)**. Cell adhesion behavior studies were conducted on functionalized gold nanoparticle arrays on glass surfaces generated by block-copolymer micelle nanolithography.[46] These hierarchically 68 nm interparticle-distance nano-patterned substrates provide an adequate platform to accurately control the geometrical distribution of integrin-anchoring points, which are essential for cell adhesion (Figure 4b).[47] Substrates were functionalized in a two-step procedure as previously reported.[48] Briefly, glass areas between Au nanoparticles were passivated with PEG-terminated siloxane to prevent non-specific cell binding. Then, gold particles were functionalized with the corresponding thiol-derivative (**13** or **14**).

The molecular assembly of FA and actin fibers in REF52 cells on biofunctionalized-nanopatterned substrates was investigated by immunohistochemical staining for paxillin and actin (Figure 4a). Both surfaces, functionalized with compound **13** or **14**, display a good adhesion behavior characterized by very well spread cells highlighting successful integrin-ligand interactions. However, a closer look at these images reveals striking differences in terms of FA distribution and morphology (Table 4).

At the 4 h time point, cells plated on *c*(-RGDfK[Hegas-MPA]-) (**14**) functionalized surfaces exhibit typical, robust paxillin patches mainly, although not exclusively, along the cell periphery. A minor proportion of these FA are also expressed over the entire ventral surface. Moreover, in the case of surfaces patterned with *c*(-phg-*iso*DGRk[Hegas-MPA]-) (**13)**, FA develop as significant thinner paxillin clusters uniformly distributed at the cell extension and around the nucleus. Under this condition the mean average FA width is 0.51 ± 0.16 $\mu m^2$, significantly less than the value of 1.25 ± 0.39 $\mu m^2$ obtained for the surface functionalized with **14**. Actin fibers are organized as a dense meshwork of peripheral actin filaments and few stress fibers in the case of **14** while cells plated on **13** patterned surfaces exhibit a barely organized actin distribution.

After an 24 h incubation period the overall picture is similar to that described for the 4 h time point. The extent of cell spreading is noticeable and similar on both surfaces displaying paxillin plaques mainly at the cell periphery. A quantitative analysis of the FA indicate growth in FA area of ~20% on *c*(-RGDfK-)-nanopatterns (**14**), whereas cells on *c*(-phg-*iso*DGRk-)-nanopatterns (**13**) show ~100% growth, although still significantly lower in absolute value to that obtained for compound **14** (Table 4). Structural comparison of actin indicates notable differences between functionalizations. *c*(-RGDfK-)-mediated adhesion induce actin stress fibers formation connected to FA, whereas actin filaments in cells plated on *c*(-phg-*iso*DGRk-)-functionalized surfaces, although organized and oriented in the FA direction, do not assembly into mature fibers as in the case of the other compound.

It is evident that activation of different integrins triggered by cell-ligand interactions has a profound effect in the assembly of FA and actin organization. To link the observations described herein with the selective affinity of the evaluated compounds we need to refer to the early stages of cell adhesion. Studies on early events in the migration of endothelial cells have shown that the initial adhesion contacts, namely focal complexes (FX), are nascent adhesion plaques rich in αvβ3 integrin, [49] which transform into FA, rich in α5β1 integrin, following the activation of Rho-A.[49-51] This suggest, considering that *c*(-phg-*iso*DGRk-) is prone to fail αvβ3 activation, that the development of mature FA requires early activation of αvβ3. Although differences in paxillin abundance cannot be entirely attributed to integrin specificity,[52] it is shown by the present studies that this mechanism certainly is involved for the screened peptides. Along these lines, another aspect to consider is the influence over FA maturation by the application of mechanical force by the actin cytoskeleton, and the influence over the actin system assembly by the adhesions growth. The observation that cells plated on *c*(-RGDfK-)-nanopatterns exhibit mature FA and stress fibers while cells plated on *c*(-phg-*iso*DGRk-)-nanopatterns lack these features is in agreement with the ability of adhesion plaques enriched with activated αvβ3 to apply strong traction forces to the substrate during cell migration.[53] The high intracellular tension associated with the stress fibers correlates with the formation and maintenance of high-density αvβ3-integrin FA, which size also increases due to increased intracellular tension.[50] These observations evidence the strong effect that the differential activation of integrins, mainly α5β1 or αvβ3, causes at the cellular adhesion level highlighting the fine-tuned selectivity and activity of the synthesized peptides.

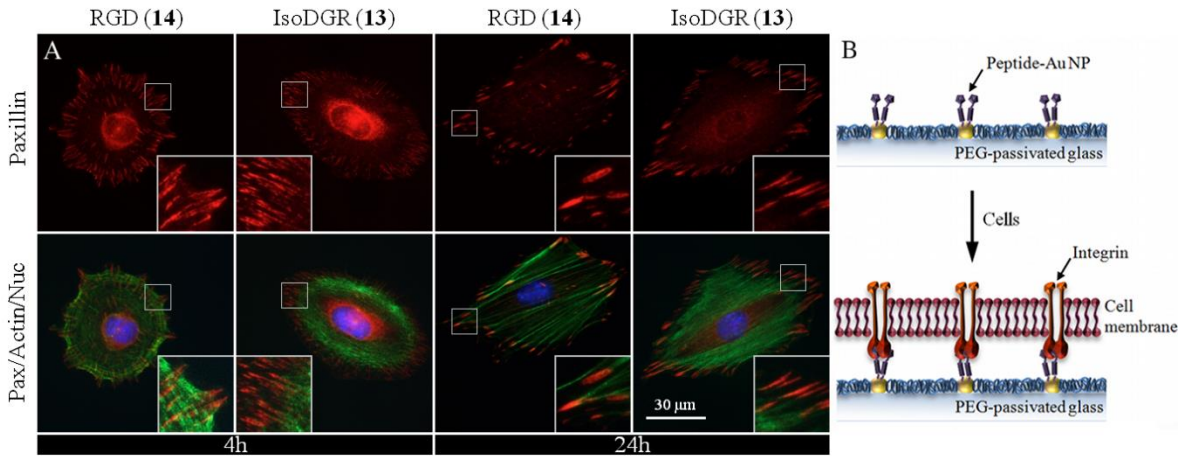


**Figure 4.** a) Immunofluorescence micrographs of REF52 cells plated on 68 nm-nanopatterned surfaces. Cells were fixed and stained for paxillin (red), nuclei (blue) and actin (green) at 4 h and 24 h after plating. The inset at the lower corner of each image is a magnification of a region of the cellular structures. b) Scheme of the biofunctionalized gold patterns employed to study the impact of compound **13** and **14** on FA assembly.

**Table 4.** FA characteristics for REF52 cells plated on 68 nm-nanopatterned surfaces functionalized with compound **13** and **14**.

| Conditions | FA Area [µm$^2$] | Length [µm] | Width [µm] | Axial Ratio (Length/Width) | FA Total Area/Cell Area |
|---|---|---|---|---|---|
| RGD (**14**) 4 h | 3.40 ± 1.66 | 3.78 ± 1.48 | 1.25 ± 0.39 | 3.24 ± 1.46 | 0.093 ± 0.025 |
| *iso*DGR (**13**) 4 h | 1.24 ± 0.58 | 2.92 ± 1.21 | 0.51 ± 0.16 | 6.01 ± 2.63 | 0.070 ± 0.022 |
| RGD (**14**) 24 h | 4.12 ± 1.91 | 4.17 ± 1.55 | 1.31 ± 0.41 | 3.42 ± 1.51 | 0.076 ± 0.027 |
| *iso*DGR (**13**) 24 h | 2.61 ± 1.30 | 3.94 ± 1.50 | 0.90 ± 0.27 | 4.68 ± 2.14 | 0.079 ± 0.022 |

## CONCLUSION

In this work we could introduce the *c*(-phg-*iso*DGR-k-) sequence as a novel peptide, being highly active and biselective for Fn binding integrins α5β1 and αvβ6. The impact of the variable amino acid and their configuration within the *c*(-phg-*iso*DGR-X-) lead motif on integrin binding behavior, mediating cell adhesion *in vivo*, is demonstrated by ELISA experiments and the results verified by NMR structure determination, molecular dynamics and docking experiments as well as cell adhesion experiments. Summarizing these results, the configuration of the amino acid at the variable position is responsible for gain in activity and selectivity towards integrin α5β1 and αvβ6, if a D-amino acid is introduced at this position. Altering this configuration into the L-amino acid analog has a drastic influence on the binding behavior with loss of activity towards the mentioned Fn binding integrins and increased affinity for Vn binding integrin αvβ3 resulting in lower selectivity. MD calculations revealed a higher conformational flexibility in the case of an L-amino acid compared to its D-amino acid analog indicating a first explanation for the activity/selectivity profile. Molecular docking could strengthen the hypothesis of different interaction patterns of the compounds with the different integrins. Precisely, selectivity against αvβ3 is gained by a tighter downstream pocket within this integrin in comparison to integrin α5β1. This disturbs an optimal interaction between one of the two main phamacorphoric groups (*iso*Asp$^2$ and Arg$^4$) of the peptide, the side-chain of Arg$^4$, resulting in a low affinity peptide. This trend follows the sterical demand of the side-chain of the variable amino acid. Discrimination between the D- and L-lysine analogs is mainly derived by the formation of an additional hydrogen bridge by the lysine side chain in its D-amino acid configuration, responsible for gaining activity for integrin α5β1. Cell adhesion experiments confirmed the selectivity for integrin α5β1 and inactivity towards integrin αvβ3. The later integrin is essential during formation of focal complexes, an early step in cell adhesion, and therefore cell adhesion using the *iso*DGR motif is significantly delayed. This *iso*DGR sequence and the c(-phg-*iso*DGRk-) peptide gives a great opportunity for further studies with regards to the different integrin-ECM interactions involved in many biological processes allowing a specific, defined interaction pattern.

## EXPERIMENTAL SECTION

All technical solvents were distilled prior to use. Dry solvents were purchased from *Sigma-Aldrich* or *Fluka*. Protected Fmoc-amino acids and coupling reagents were purchased from *Sigma-Aldrich* (Taufkirchen, Germany) *Novabiochem* (Schwalbach, Germany), *Iris Biotech GmbH* (Marktredwitz, Germany), *PolyPeptide Laboratories* (Strasbourg, France) and *Medalchemy* (Alicante, Spain). TCP-resin was purchased from *PepChem* (Tübingen, Germany). All other chemicals and organic solvents were purchased from commercial suppliers at the highest purity available and used without further purification.

Analytical HPLC was performed using an *Amersham Pharmacia Biotech* Äkta Basic 10F equipment, with a P-900 pump system, a reversed-phase *YMC*-ODS-A $C_{18}$ column (12 nm pore size, 5 µm particle size, 250 mm × 4.6 mm), and UV detection (UV-900, 220 and 254 nm). The system was run at a flow rate of 1.0 mL/min over 30 min using $H_2O$ (0.1% TFA) and MeCN (0.1% TFA) as solvents.

Semi-preparative HPLC was performed using *Waters* equipment: System Breeze; Pump System 1525, UV-Detector 2487 Dual (220 and 254 nm); Driver Software Breeze vers. 3.20; Column material: *YMC*-ODS-A $C_{18}$ (12 nm pore size, 5 µm particle size, 250 mm × 20 mm), *YMC*-ODS-AQ $C_{18}$ (12 nm pore size, 5 µm particle size, 250 mm × 20 mm) or *YMC*basic (proprietary pore size, 5 µm particle size, 250 mm × 20 mm).

HPLC-ESI-MS analyses were performed on a *Hewlett Packard* Series HP 1100 with a *Finnigan* LCQ mass spectrometer using a *YMC*-Hydrosphere $C_{18}$ column (12 nm pore size, 3 µm particle size, 125 mm × 2.1 mm) or *YMC*-Octyl $C_8$ column (20 nm pore size, 5 µm particle size, 250 mm × 2.1 mm). The system uses $H_2O$ (0.1% formic acid) and MeCN (0.1% formic acid) as eluents.

Standard peptide coupling techniques were employed as described below. All yields are not optimized. All tested compounds exhibited ≥ 95% purity determined with RP-HPLC-(MS).

**Solid phase peptide synthesis – general procedures**

Peptide synthesis was carried out using TCP resin following standard Fmoc-strategy.[54]

*Loading of TCP resin:* The amino acid (1.2 eq.) was added to the resin within a syringe equipped with a PP-frit and cannula. DIEA (3.0 eq.) was mixed with anhydrous DCM (8 mL/g resin) and sucked into the syringe. After rotating at rt for 1 h, the remaining tritylchloride groups were capped by addition of a solution of DCM, MeOH, DIEA (17:2:1, v/v/v, 2 mL/g resin) for 15 min. After discarding the solution, the resin was washed thoroughly with DCM (3 × 8 mL), NMP (3 × 8 mL), NMP/MeOH (1:1, v/v, 1 × 8 mL) and MeOH (3 × 8 mL). The loading of the resin was determined gravimetrically after drying overnight, under vacuum in a desiccator and ranged from 0.40-0.65 mmol/g.

*Solid phase Fmoc deprotection*: The resin-bound Fmoc protected peptide was treated with a solution of piperidine in NMP (20%, v/v, 3 × 5 min.) and washed with NMP (3 × 8 mL).

*Solid phase peptide coupling with HOBt/TBTU*: A solution of TBTU, HOBt, Fmoc-Xaa-OH (3.0 eq. each) and DIEA (6.0 eq.) in NMP was added to the resin-bound free amine peptide and rotated for 1 h at rt. The solution was discarded and the resin washed with NMP (3 × 8 mL).

*Cleavage of side-chain protected peptides from TCP resin:* A solution of HFIP in DCM (20%, v/v) was added to the resin attached peptide and rotated for 20 min. (8 mL/g resin). The procedure was repeated twice, washed with DCM (3 × 8 mL) and the collected solutions concentrated in vacuo.

*Peptide backbone cyclization using HATU/HOBt in solution:* The linear, side-chain protected peptide was diluted in DMF to 1 mM. After addition of HATU (2.0 eq.), HOBt (2.0 eq.) and DIEA (10.0 eq.) the mixture was stirred for 12 h. The solvent was removed under reduced pressure and the cyclic peptide precipitated by addition of water. The peptide was spun down in a centrifuge, washed twice with water and dried in a desiccator.

*Removal of Cbz protecting group in solution:* The peptide was dissolved in DMA and 100 mg/mol catalyst (10% Pd/C) was added to the solution. The flask was flushed with hydrogen and the solution stirred at rt and 1 bar $H_2$ pressure for 12 h. The solvent was removed under vacuo, the remaining solid redissolved in a mixture of MeCN/$H_2O$ (9:1), catalyst is filtered off through Celite® and the peptide is obtained by lyophilization.

*Functionalization of cyclic peptides by a linker:* The linker (1.0 eq.) was dissolved in DMF and HATU, HOAt (1.0 eq. each) was added along with DIEA (4.0 eq.). After stirring the solution at rt for 1 h, the partial protected cyclic peptide, containing an unprotected

primary amine, is added and the mixture stirred for one additional hour. The solvent is evaporated and the crude product purified by preparative RP-HPLC.

*Full deprotection of cyclic peptides:* The protected, cyclic peptide was treated with a mixture of TFA, water and TIPS (95:2.5:2.5, v/v/v) for 1 h. The deprotected peptide was precipitated by addition to cold diethylether and spun down in a centrifuge. It is washed twice with cold diethylether, dried under vacuum and purified by preparative RP-HPLC. The peptides are characterized by ESI-MS and analytical HPLC.

**Table 5.** Analytical data of the cyclic peptides.

| Cyclic Peptide | ESI-MS $^{m}/_{z}$ = $[m+H]^{+}$ | RP-HPLC $t_R$ [min](0-100%, 30 min) |
|---|---|---|
| **1** *c*(-phg-*iso*DGR**V-**) | 561.4 | 9.01 |
| **2** *c*(-phg-*iso*DGR**v**-) | 561.4 | 8.33 |
| **3** *c*(-phg-*iso*DGR**P-**) | 559.3 | 9.29 |
| **4** *c*(-phg-*iso*DGR**p**-) | 599.4 | 8.44 |
| **5** *c*(-phg-*iso*DGR**K-**) | 590.4 | 6.43 |
| **6** *c*(-phg-*iso*DGR**k**-) | 590.4 | 5.99 |
| **7** *c*(-phg-*iso*DGR**E-**) | 591.4 | 7.53 |
| **8** *c*(-phg-*iso*DGR**e**-) | 591.4 | 7.18 |
| **9** *c*(-phg-*iso*DGR**Y-**) | 625.4 | 9.10 |
| **10** *c*(-phg-*iso*DGR**y**-) | 625.4 | 9.42 |
| **11** *c*(-phg-*iso*DGR**W-**) | 648.4 | 11.14 |
| **12** *c*(-phg-*iso*DGR**w**-) | 648.4 | 11.28 |
| **13** *c*(-phg-*iso*DGR**k**[Hegas-MPA]-) | 1013.6 | 10.8 (10-100%) |
| **14** *c*(-RGDfK[Hegas-MPA]-) | 1027.7 | 12.0 (10-100%) |

**Integrin binding assay (Fn/ α5β1, LAP/ αvβ6, Vn/ αvβ3, Vn/ αvβ5, Fbg/ αIIbβ3 assay)**

The inhibiting activity and selectivity of the integrin inhibitors was determined in a solid-phase binding assay using coated extracellular matrix proteins and soluble integrins. Binding of the integrins was detected by specific antibodies in an enzyme linked immune sorbent assay (ELISA). The assay was based on a previously reported method with some modifications.[26, 55]

α5β1 assay: Flat-bottom 96-well ELISA plates (*BRAND*, Wertheim, Germany) were coated overnight at 4 °C with 100 µL/well of 0.5 µg/mL fibronectin (*Sigma-Aldrich*, Taufkirchen, Germany) in carbonate-buffer (15 mM $Na_2CO_3$, 35 mM $NaHCO_3$, pH 9.6). Each well was then washed with PBST buffer (137 mM NaCl, 2.7 mM KCl, 10 mM $Na_2HPO_4$, 2 mM $KH_2PO_4$, 0.01% Tween 20, pH 7.4, 3 × 200 µL) and blocked for 1 h at room temperature with 150 µL/well of TSB-buffer (20 mM Tris-HCl, 150 mM NaCl, 1 mM $CaCl_2$, 1 mM $MgCl_2$, 1 mM $MnCl_2$, pH 7.5, 1% BSA). After being washed three times with PBST, equal volumes of internal standard (Cilengitide) or test compounds were mixed with 2.0 µg/mL human integrin α5β1 (*R&D Systems*, Wiesbaden, Germany) giving a final dilution in TSB buffer of 0.00013 to 10 µM for the inhibitors and 1.0 µg/mL for integrin α5β1. These solutions (100 µL/well) were incubated for 1 h at room temperature. The plate was washed three times with PBST buffer and 100 µL/well of 1.0 µg/mL primary antibody (mouse anti-human CD49e, *BD Biosciences*, Heidelberg, Germany) was added to the plate. After incubation for 1 h at room temperature, the plate was washed three times with PBST and 100 µL/well of 2.0 µg/mL of secondary peroxidase-labeled antibody (anti-mouse IgG-POD, *Sigma-Aldrich*, Taufkirchen, Germany) was added to the plate and incubated for 1 h at room temperature. After washing the plate three times with PBST it got developed by adding 50 µL/well of SeramunBlau® fast (*Seramun Diagnostic GmbH*, Heidesee, Germany) and incubated for 5 min at room temperature. The reaction was stopped with 50 µL/well of 3 M $H_2SO_4$ and the absorbance was measured at 450 nm with a plate reader (POLARstar Galaxy, *BMG Labtechnologies*). Each compound concentration was tested in duplicate and the resulting inhibition curves were analyzed using OriginPro 7.5G software, the inflection point describes the $IC_{50}$ value. Each plate contained Cilengitide as internal standard.

αvβ6 assay: Experimental procedure is as described for α5β1 assay, except for the following modifications. The plates are coated with 100 µL/well of 0.4 µg/mL LAP (*R&D Systems*, Wiesbaden, Germany) in carbonate buffer, washed and blocked as described above. Soluble integrin αvβ6 (*R&D Systems*, Wiesbaden, Germany) was mixed with

equal volume of serial diluted inhibitors resulting in a final integrin concentration of 0.25 µg/mL. As a primary antibody 100 µL/well of 1:500 diluted mouse anti-human αv (*Millipore*, Schwalbach/Ts., Germany) was used. Secondary antibody is the same as in integrin α5β1 assay, but 100 µL/well of 2.0 µg/mL were used. Visualization and analysis was performed as described above.

Assays for integrin αvβ3, αvβ5 and αIIbβ3 are described in the supporting information.

**NMR structure determination and molecular dynamics**

DMSO solutions of the two compounds are used and the NMR spectroscopic data (chemical shifts, coupling constants, ROE derived proton-proton internuclear distance restraints and temperature coefficients) required for the studies has been generated by acquiring standard homo and heteronuclear experiments on Bruker 500 MHz NMR spectrometer at 300 K in DMSO-$d_6$ solvent. Additional information on the experimental conditions and details can be found in the supporting information.

**Molecular Modeling**

**Homology Modeling**

The multiple sequence alignment suggested in a previous paper [56] was used to build the homology model of the □$_6$ subunit by means of Schrodinger Prime (version 3.0) [57] software accessible through the Maestro interface.[58] During the model building, Prime keeps the backbone rigid for the cases in which the backbone does not need to be reconstructed due to gaps in the alignment. The loop refinements were carried out using Prime with default parameter settings, if not mentioned otherwise. Prior to refinement, the protein structure was subjected to a protein preparation step to re-orientate side chain hydroxyl groups and alleviate potential steric clashes. The implemented loop modeling protocol consists of several steps.[59] First, large numbers of loops are created by a conformational search in dihedral angle space. Clustering of loop conformations and side chain optimization is used to select representative solutions. On the basis of the user parameters, a limited number of structures are then processed using complete energy minimization. The top ranked solution in terms of Prime energy was considered best. The short loops were refined using default sampling rates in the initial step, while the extended highest sampling rate was chosen for the loop optimization of the SDL region. Side chains were unfrozen within 7.5 Å of the corresponding loop, and the energy cutoff was set to 10 kcal/mol.

**Docking calculations**

Docking calculations of **5** and **6** in the X-ray three-dimensional structure of αvβ3 (PDB code: 1L5G) and in the homology models of α5β1[40], αvβ5[41] and αvβ6 were carried out using the AutoDock 4.2 software, which has been extensively used in the integrin field.[60-63] The conformations of peptides **5** and **6** as experimentally determined by DG were used as docking starting structures. During the docking process the backbone conformation was held fix, while the side chain dihedral angles were free to rotate. The peptides and the receptor structures were converted to AD4 format files using ADT generating automatically all other atom values. The docking area has been defined by a box, centered on the coordinate of the metal in the MIDAS region. Grid points of 70×85×75 with 0.375 Å spacing were calculated around the docking area for all the ligand atom types using AutoGrid 4.2. For each ligand, 100 separate docking calculations were performed. Each docking calculation consisted of 10 million energy evaluations using the Lamarckian genetic algorithm local search (GALS) method. A low frequency local search according to the method of Solis and Wets was applied to docking trials to ensure that the final solution represents a local minimum. Each docking run was performed with a population size of 150, and 300 rounds of Solis and Wets local search were applied with a probability of 0.06. A mutation rate of 0.02 and a crossover rate of 0.8 were used to generate new docking trials for subsequent generations. The GALS method evaluates a population of possible docking solutions and propagates the most successful individuals from each generation into the next one. The docking results from each of the 100 calculations were clustered on the basis of root mean square deviation (rmsd = 2.0 Å) between the Cartesian coordinates of the ligand atoms and were ranked on the basis of the free energy of binding. However, for each ligand, the free energy of binding as well as the consonance with experimental data, (i.e SARs) was taken into account for the choice of the published binding modes. In this regard, it is worth remarking that the difference in the predicted binding free energy (ΔΔG) between the selected binding modes and either the lowest energy solution or the most populated cluster was within the range of 2-3 kcal/mol (except for peptide **5** docked at the **αvβ6** integrin), which is the known error in energy estimation by AD4.[60-63] For a detailed comparative analysis based on the docking predicted ΔΔG, see Table 13 in the Supporting Information.

All of the pictures were rendered using PyMOL (http://www.pymol.org).

**Biofunctionalized nanopatterns**

Gold nanoparticles quasi-hexagonal patterns were prepared on glass coverslips (18 x 18 mm N°1, Carl Roth, Germany) by means of block-copolymer micelle nanolithography as previously described.[46] Briefly, substrates were spin-coated with a solution of polystyrene(1056)-block-poly[2-vinylpyridine($HAuCl_4$)0.25](495) (Polymer Source Inc., Canada) diblock copolymer micelles in *o*-xylene and subsequently subjected to $H_2$:Ar 1:10 plasma treatment (350 W, 0.4 mbar, 90 min). Then, substrates were treated thermally in an oven at 500 °C for 48 h. The interparticle distance between adjacent gold nanoparticles was 68 ± 9 nm as determined by scanning electron microscopy (see Supplementary Information). To prevent non-specific adhesion, the area between gold nanoparticles was passivated with mPEG-triethoxysilane (2000).[48] Finally, passivated surfaces were functionalized with the corresponding integrin-binding molecule **13** or **14** by placing the substrates on top of 50 µL drops of 25 µM solution in MilliQ water for 1 h at room temperature. Physisorbed material was removed by exhaustive rinsing with MilliQ water. Cell experiments were carried out immediately after this step.

**Cell Culture**

REF 52 (rat embryonic fibroblast) wild type cells were cultured in DMEM medium supplemented with 10% FBS and 1% L-glutamin (Invitrogen, Germany) at 37 °C and 5% $CO_2$. For adhesion experiments, cells in culture were rinsed with PBS, released by trypsin-EDTA 0.25% treatment for 5 min at 37 °C, plated at a density of 150 cells/mm$^2$ on the functionalized surfaces in DMEM containing 1% FBS and incubated at 37 °C and 5% $CO_2$ for a given period of time before fixation and immunostaining.

**Immunofluorescence staining**

After 4 or 24 h on the nanopatterned surfaces, cells were washed with PBS at 37 °C and fixed with 2.5% paraformaldehyde in PBS for 10 min. Cells were then permeabilized with 0.1% Triton X-100 in PBS, blocked with 5% goat serum (Invitrogen, Germany) in PBS for 1 h at room temperature and incubated with 1:100 dilution of mouse anti-paxillin (BD Biosciences, Germany) for 1 h at room temperature. Then, cells were labeled with 1:100 dilution of anti-mouse Alexa 594-conjugated secondary antibody (Invitrogen, Germany) in 5% goat serum in PBS for 1 h at room temperature. Filamentous actin and nuclei were labeled with Alexa 488-conjugated phalloidin and DAPI (Invitrogen, Germany) respectively. Cells were visualized at 63x using an Axiovert 200 fluorescent microscope (Carl Zeiss, Germany) equipped with a digital color camera. Image

processing was achieved with the Axiovision Image viewer (Carl Zeiss, Germany). FAs analysis was performed using the image analysis platform WiSoft® (http://www.idea-bio.com). Mean values for different FAs features were obtained from at least 10 cells (≥ 1000 FAs).

## ASSOCIATED CONTENT

**Supporting Information Available**. ELISA assay details for integrins αvβ3, αvβ5 and αIIbβ3, NMR data and structure calculation. This material is available free of charge via the Internet at http://pubs.acs.org.

## AUTHOR INFORMATION

### Corresponding Authors

* Dept. of Pharmaceutical Chemistry, University of Naples, Via D. Montesano 49, 80131 Napoli, Italy. Phone: + 39 (0) 81 679899. E-mail: lmarinel@unina.it.

*Institute for Advanced Study and Center of Integrated Protein Science, Department Chemie, Technische Universität München, Lichtenbergstr. 4, 85747 Garching, Germany. Phone: +49 (0) 89 289 13300. Fax: +49 (0) 89 289 13210. E-mail: Kessler@tum.de.

## ACKNOWLEDGMENT

The authors gratefully acknowledge financial support from the International Graduate School of Science and Engineering (IGSSE), from the TUM Graduate School (TUM GS) and the Max Planck Society. J. P. Spatz is the Weston Visiting Professor at the Weizmann Institute of Science.

## ABBREVIATIONS USED

DAPI, 4',6-diamidino-2-phenylindole; DG, distance geometry; DIEA, diisopropylethylamine; DMEM, Dulbecco's modified Eagle's medium; ECM, extracellular matrix; ELISA, enzyme-linked immunosorbant assay; FA, focal adhesion; Fbg, fibrinogen; FBS, fetal bovine serum; Fn, fibronectin; FX, focal complex; HATU, *O*-(7-

azabenzotriazol-1-yl)-*N*,*N*,*N'*,*N'*,-tetramethyluronium hexafluorophosphate; Hegas, heptaethylenglycol amino acid; HFIP, hexafluoroisopropanol; HOBt, 1-hydroxy-benzotriazole; LAP, latency-associated peptide; MIDAS, metal-ion dependent adhesion site; MPA, mercaptopropionic acid; phg, D-phenylglycine; POD, peroxidase; PP, polypropylene; REF, rat embryonic fibroblast; TBTU, *O*-(Benzotriazol-1-yl)-*N,N,N',N'*-tetramethyluroniumtetrafluoroborat; TCP, tritylchlorid polystyrene; TGF, transforming growth factor; TIPS, triisopropylsilyl; Vn, vitronectin.

## REFERENCES

1. Humphries, J. D.; Byron, A.; Humphries, M. J. Integrin ligands at a glance. *Journal of Cell Science* **2006,** 119, 3901-3903.

2. Meyer, A.; Auernheimer, J.; Modlinger, A.; Kessler, H. Targeting RGD Recognizing Integrins: Drug Development, Biomaterial Research, Tumor Imaging and Targeting. *Current Pharmaceutical Design* **2006,** 12, 2723-2747.

3. Xu, J.; Maurer, L. M.; Hoffmann, B. R.; Annis, D. S.; Mosher, D. F. iso-DGR sequences do not mediate binding of fibronectin N-terminal modules to adherent fibronectin-null fibroblasts. *J Biol Chem* **2010,** 285, 8563-8571.

4. Goodman, S. L.; Picard, M. Integrins as therapeutic targets. *Trends in pharmacological sciences* **2012,** 33, 405-412.

5. Luo, B. H.; Carman, C. V.; Springer, T. A. Structural basis of integrin regulation and signaling. *Annu Rev Immunol* **2007,** 25, 619-647.

6. Ruoslahti, E. RGD and other Recognition Sequences for Integrins. *Annual Review of Cell and Developmental Biology* **1996,** 12, 697-715.

7. Ruoslahti, E.; Pierschbacher, M. New perspectives in cell adhesion: RGD and integrins. *Science* **1987,** 238, 491-497.

8. Weide, T.; Modlinger, A.; Kessler, H. Spatial Screening for the Identification of the Bioactive Conformation of Integrin Ligands. In *Bioactive Conformation I*, Peters, T., Ed. Springer Berlin / Heidelberg: 2007; Vol. 272, pp 1-50.

9. Dechantsreiter, M. A.; Planker, E.; Mathä, B.; Lohof, E.; Hölzemann, G.; Jonczyk, A.; Goodman, S. L.; Kessler, H. N-Methylated Cyclic RGD Peptides as Highly Active and Selective αvβ3 Integrin Antagonists. *Journal of Medicinal Chemistry* **1999,** 42, 3033-3040.

10. Mas-Moruno, C.; Rechenmacher, F.; Kessler, H. Cilengitide: the first anti-angiogenic small molecule drug candidate design, synthesis and clinical evaluation. *Anticancer Agents Med Chem* **2010,** 10, 753-768.

11. Leiss, M.; Beckmann, K.; Giros, A.; Costell, M.; Faessler, R. The role of integrin binding sites in fibronectin matrix assembly in vivo. *Curr Opin Cell Biol* **2008,** 20, 502-507.

12. Busk, M.; Pytela, R.; Sheppard, D. Characterization of the integrin alpha v beta 6 as a fibronectin-binding protein. . *Journal of Biological Chemistry* **1992** 267 5790-5796

13. Munger, J. S.; Huang, X.; Kawakatsu, H.; Griffiths, M. J. D.; Dalton, S. L.; Wu, J.; Pittet, J.-F. o.; Kaminski, N.; Garat, C.; Matthay, M. A.; Rifkin, D. B.; Sheppard, D. A Mechanism for Regulating Pulmonary Inflammation and Fibrosis: The Integrin avb6 Binds and Activates Latent TGF beta1. *Cell* **1999,** 96, 319-328.

14. Goodman, S. L.; Hölzemann, G.; Sulyok, G. A. G.; Kessler, H. Nanomolar Small Molecule Inhibitors for avb6, avb5, and avb3 Integrins. *Journal of Medicinal Chemistry* **2002,** 45, 1045-1051.

15. Kraft, S.; Diefenbach, B.; Mehta, R.; Jonczyk, A.; Luckenbach, G. A.; Goodman, S. L. Definition of an Unexpected Ligand Recognition Motif for avb6 Integrin *Journal of Biological Chemistry* **1999,** 274, 1979-1985.

16. Guan, H.; McGuire, M. J.; Li, S.; Brown, K. C. Peptide-Targeted Polyglutamic Acid Doxorubicin Conjugates for the Treatment of avb6-Positive Cancers. *Bioconjugate Chemistry* **2008,** 19, 1813-1821.

17. Hausner, S. H.; DiCara, D.; Marik, J.; Marshall, J. F.; Sutcliffe, J. L. Use of a Peptide Derived from Foot-and-Mouth Disease Virus for the Noninvasive Imaging of Human Cancer: Generation and Evaluation of 4-[18F]Fluorobenzoyl A20FMDV2 for In vivo Imaging of Integrin avb6 Expression with Positron Emission Tomography. *Cancer Research* **2007** 67 7833-7840

18. Kimura, R. H.; Teed, R.; Hackel, B. J.; Pysz, M. A.; Chuang, C. Z.; Sathirachinda, A.; Willmann, J. K.; Gambhir, S. S. Pharmacokinetically Stabilized Cystine Knot Peptides That Bind Alpha-v-Beta-6 Integrin with Single-Digit Nanomolar Affinities for Detection of Pancreatic Cancer *Clinical Cancer Research* **2012** 18 839-849

19. Takahashi, S.; Leiss, M.; Moser, M.; Ohashi, T.; Kitao, T.; Heckmann, D.; Pfeifer, A.; Kessler, H.; Takagi, J.; Erickson, H. P.; Fässler, R. The RGD motif in fibronectin is essential for development but dispensable for fibril assembly. *The Journal of Cell Biology* **2007,** 178, 167-178.

20. Geiger, T.; Clarke, S. Deamidation, isomerization, and racemization at asparaginyl and aspartyl residues in peptides. Succinimide-linked reactions that contribute to protein degradation. *Journal of Biological Chemistry* **1987,** 262, 785-794.

21. Corti, A.; Curnis, F. Isoaspartate-dependent molecular switches for integrin–ligand recognition. *Journal of Cell Science* **2011,** 124, 515-522.

22. Curnis, F.; Cattaneo, A.; Longhi, R.; Sacchi, A.; Gasparri, A. M.; Pastorino, F.; Di Matteo, P.; Traversari, C.; Bachi, A.; Ponzoni, M.; Rizzardi, G.-P.; Corti, A. Critical Role

of Flanking Residues in NGR-to-isoDGR Transition and CD13/Integrin Receptor Switching. *Journal of Biological Chemistry* **2010,** 285, 9114-9123.

23. Curnis, F.; Longhi, R.; Crippa, L.; Cattaneo, A.; Dondossola, E.; Bachi, A.; Corti, A. Spontaneous Formation of L-Isoaspartate and Gain of Function in Fibronectin. *Journal of Biological Chemistry* **2006,** 281, 36466-36476.

24. Wermuth, J.; Goodman, S. L.; Jonczyk, A.; Kessler, H. Stereoisomerism and Biological Activity of the Selective and Superactive αvβ3 Integrin Inhibitor cyclo(-RGDfV-) and Its Retro-Inverso Peptide. *Journal of the American Chemical Society* **1997,** 119, 1328-1335.

25. Frank, A. O.; Otto, E.; Mas-Moruno, C.; Schiller, H. B.; Marinelli, L.; Cosconati, S.; Bochen, A.; Vossmeyer, D.; Zahn, G.; Stragies, R.; Novellino, E.; Kessler, H. Conformational Control of Integrin-Subtype Selectivity in isoDGR Peptide Motifs: A Biological Switch. *Angewandte Chemie International Edition* **2010,** 49, 9278-9281.

26. Chatterjee, J.; Ovadia, O.; Zahn, G.; Marinelli, L.; Hoffman, A.; Gilon, C.; Kessler, H. Multiple N-methylation by a designed approach enhances receptor selectivity. *J Med Chem* **2007,** 50, 5878-5881.

27. Hartman, G. D.; Egbertson, M. S.; Halczenko, W.; Laswell, W. L.; Duggan, M. E.; Smith, R. L.; Naylor, A. M.; Manno, P. D.; Lynch, R. J. Non-peptide fibrinogen receptor antagonists. 1. Discovery and design of exosite inhibitors. *Journal of Medicinal Chemistry* **1992,** 35, 4640-4642.

28. Haubner, R.; Gratias, R.; Diefenbach, B.; Goodman, S. L.; Jonczyk, A.; Kessler, H. Structural and functional aspects of RGD-containing cyclic pentapeptides as highly potent and selective integrin avb3 antagonists. *J. Am. Chem. Soc.* **1996,** 118, 7461-7472.

29. Heckmann, D.; Meyer, A.; Laufer, B.; Zahn, G.; Stragies, R.; Kessler, H. Rational design of highly active and selective ligands for the a5b1 integrin receptor. *Chembiochem* **2008,** 9, 1397-1407.

30. Matthews, B. W. The γ Turn. Evidence for a New Folded Conformation in Proteins. *Macromolecules* **1972,** 5, 818-819.

31. Rose, G. D.; Glerasch, L. M.; Smith, J. A. Turns in Peptides and Proteins. In *Advances in Protein Chemistry*, Anfinsen, C. B.; Frederic, J. T. E.; Richards, M., Eds. Academic Press: 1985; Vol. 37, pp 1-109.

32. Smith, J. A.; Pease, L. G.; Kopple, K. D. Reverse Turns in Peptides and Protein. *Critical Reviews in Biochemistry and Molecular Biology* **1980,** 8, 315-399.

33. Venkatachalam, C. M. Stereochemical criteria for polypeptides and proteins. V. Conformation of a system of three linked peptide units. *Biopolymers* **1968,** 6, 1425-1436.

34. Richardson, J. S. *Adv Protein Chem.* **1981,** 34, 167-339.

35. Heller, M.; Sukopp, M.; Tsomaia, N.; John, M.; Mierke, D. F.; Reif, B.; Kessler, H. The Conformation of cyclo(−d-Pro−Ala4−) as a Model for Cyclic Pentapeptides of the dL4 Type. *Journal of the American Chemical Society* **2006,** 128, 13806-13814.

36. Mierke, D. F.; Kessler, H. Molecular dynamics with dimethyl sulfoxide as a solvent. Conformation of a cyclic hexapeptide. *Journal of the American Chemical Society* **1991,** 113, 9466-9470.

37. Strader, M. L.; Feller, S. E. A flexible all-atom model of dimethyl sulfoxide for molecular dynamics simulations. *Journal of Physical Chemistry A* **2002,** 106, 1074-1080.

38. Doedens, L.; Opperer, F.; Cai, M.; Beck, J. G.; Dedek, M.; Palmer, E.; Hruby, V. J.; Kessler, H. Multiple N-Methylation of MT-II Backbone Amide Bonds Leads to Melanocortin Receptor Subtype hMC1R Selectivity: Pharmacological and Conformational Studies. *Journal of the American Chemical Society* **2010,** 132, 8115-8128.

39. Adair, B. D.; Xiong, J.-P.; Maddock, C.; Goodman, S. L.; Arnaout, M. A.; Yeager, M. Three-dimensional EM structure of the ectodomain of integrin αvβ3 in a complex with fibronectin. *The Journal of Cell Biology* **2005,** 168, 1109-1118.

40. Marinelli, L.; Meyer, A.; Heckmann, D.; Lavecchia, A.; Novellino, E.; Kessler, H. Ligand Binding Analysis for Human α5β1 Integrin: Strategies for Designing New α5β1 Integrin Antagonists. *Journal of Medicinal Chemistry* **2005,** 48, 4204-4207.

41. Mas-Moruno, C.; Beck, J. G.; Doedens, L.; Frank, A. O.; Marinelli, L.; Cosconati, S.; Novellino, E.; Kessler, H. Increasing αvβ3 Selectivity of the Anti-Angiogenic Drug Cilengitide by N-Methylation. *Angewandte Chemie International Edition* **2011,** 50, 9496-9500.

42. Critchley, D. R. Focal adhesions – the cytoskeletal connection. *Current Opinion in Cell Biology* **2000,** 12, 133-139.

43. Zamir, E.; Geiger, B. Components of cell-matrix adhesions. *Journal of Cell Science* **2001,** 114, 3577-3579.

44. Geiger, B.; Bershadsky, A. Assembly and mechanosensory function of focal contacts. *Current Opinion in Cell Biology* **2001,** 13, 584-592.

45. Zaidel-Bar, R.; Cohen, M.; Addadi, L.; Geiger, B. Hierarchical assembly of cell-matrix adhesion complexes. *Biochem Soc Trans* **2004,** 32, 416-420.

46. Glass, R.; Möller, M.; Spatz, J. P. Block copolymer micelle nanolithography. *Nanotechnology* **2003,** 14, 1153-1160.

47. Arnold, M.; Cavalcanti-Adam, E. A.; Glass, R.; Blümmel, J.; Eck, W.; Kantlehner, M.; Kessler, H.; Spatz, J. P. Activation of Integrin Function by Nanopatterned Adhesive Interfaces. *ChemPhysChem* **2004,** 5, 383-388.

48. Blümmel, J.; Perschmann, N.; Aydin, D.; Drinjakovic, J.; Surrey, T.; Lopez-Garcia, M.; Kessler, H.; Spatz, J. P. Protein repellent properties of covalently attached PEG coatings on nanostructured SiO2-based interfaces. *Biomaterials* **2007,** 28, 4739-4747.

49. Zaidel-Bar, R.; Ballestrem, C.; Kam, Z.; Geiger, B. Early molecular events in the assembly of matrix adhesions at the leading edge of migrating cells. *Journal of Cell Science* **2003,** 116, 4605-4613.

50. Ballestrem, C.; Hinz, B.; Imhof, B. A.; Wehrle-Haller, B. Marching at the front and dragging behind: Differential αvβ3-integrin turnover regulates focal adhesion behavior. *The Journal of Cell Biology* **2001,** 155, 1319-1332.

51. Zamir, E.; Katz, M.; Posen, Y.; Erez, N.; Yamada, K. M.; Katz, B.-Z.; Lin, S.; Lin, D. C.; Bershadsky, A.; Kam, Z.; Geiger, B. Dynamics and segregation of cell-matrix adhesions in cultured fibroblasts. *Nat Cell Biol* **2000,** 2, 191-196.

52. Morgan, M. R.; Byron, A.; Humphries, M. J.; Bass, M. D. Giving off mixed signals - Distinct functions of α5β1 and αvβ3 integrins in regulating cell behaviour. *IUBMB Life* **2009,** 61, 731-738.

53. Beningo, K. A.; Dembo, M.; Kaverina, I.; Small, J. V.; Wang, Y.-l. Nascent Focal Adhesions Are Responsible for the Generation of Strong Propulsive Forces in Migrating Fibroblasts. *The Journal of Cell Biology* **2001,** 153, 881-888.

54. Fields, G. B.; Noble, R. L. Solid phase peptide synthesis utilizing 9-fluorenylmethoxycarbonyl amino acids. *Int J Pept Protein Res* **1990,** 35, 161-214.

55. Mas-Moruno, C.; Beck, J. G.; Doedens, L.; Frank, A. O.; Marinelli, L.; Cosconati, S.; Novellino, E.; Kessler, H. Increasing avb3 Selectivity of the Anti-Angiogenic Drug Cilengitide by *N*-Methylation. *Angew Chem Int Ed Engl* **2011,** 50, 9496-9500.

56. Marinelli, L.; Gottschalk, K.-E.; Meyer, A.; Novellino, E.; Kessler, H. Human Integrin αvβ5: Homology Modeling and Ligand Binding. *Journal of Medicinal Chemistry* **2004,** 47, 4166-4177.

57. *Prime*, 2.0; LLC: New York, 2005.

58. *Maestro*, 8.5; LLC: New York, 2006.

59. Jacobson, M. P.; Pincus, D. L.; Rapp, C. S.; Day, T. J. F.; Honig, B.; Shaw, D. E.; Friesner, R. A. A hierarchical approach to all-atom protein loop prediction. *Proteins: Structure, Function, and Bioinformatics* **2004,** 55, 351-367.

60. Huey, R.; Morris, G. M.; Olson, A. J.; Goodsell, D. S. A semiempirical free energy force field with charge-based desolvation. *Journal of Computational Chemistry* **2007,** 28, 1145-1152.

61. Cosconati, S.; Forli, S.; Perryman, A. L.; Harris, R.; Goodsell, D. S.; Olson, A. J. Virtual screening with AutoDock: theory and practice. *Expert Opinion on Drug Discovery* **2010,** 5, 597-607.

62. Heckmann, D.; Laufer, B.; Marinelli, L.; Limongelli, V.; Novellino, E.; Zahn, G.; Stragies, R.; Kessler, H. Breaking the Dogma of the Metal-Coordinating Carboxylate Group in Integrin Ligands: Introducing Hydroxamic Acids to the MIDAS To Tune Potency and Selectivity. *Angewandte Chemie International Edition* **2009,** 48, 4436-4440.

63. Bollinger, M.; Manzenrieder, F.; Kolb, R.; Bochen, A.; Neubauer, S.; Marinelli, L.; Limongelli, V.; Novellino, E.; Moessmer, G.; Pell, R.; Lindner, W.; Fanous, J.; Hoffman, A.; Kessler, H. Tailoring of Integrin Ligands: Probing the Charge Capability of the Metal Ion-Dependent Adhesion Site. *Journal of Medicinal Chemistry* **2011,** 55, 871-882.

**Table of contents graphic**

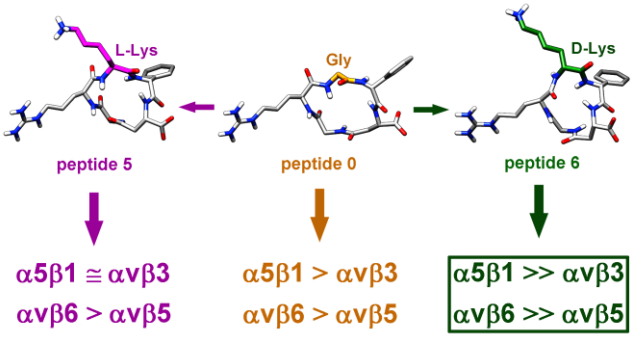

# Supporting Information

## Biselectivity of *iso*DGR Peptides for Fibronectin Binding Integrin Subtypes α5β1 and αvβ6: Conformational Control through Flanking Amino Acids

Alexander Bochen,[1] Udaya Kiran Marelli,[1] Elke Otto,[1] Diego Pallarola,[2] Carles Mas-Moruno,[1] Francesco Saverio Di Leva,[3] Heike Boehm,[2] Joachim P. Spatz,[2] Ettore Novellino,[4] Horst Kessler,[1,5]* and Luciana Marinelli[4]*

[1] *Institute for Advanced Study and Center of Integrated Protein Science, Department Chemie, Technische Universität München, Lichtenbergstrasse 4, 85747 Garching, Germany*

[2] *Department of New Materials and Biosystems, Max Planck Institute for Intelligent Systems, Heisenbergstr. 3, 70569 Stuttgart, Germany & Department of Biophysical Chemistry, University of Heidelberg , INF 253, 69120 Heidelberg, Germany*

[3] *Department of Drug Discovery and Development, Istituto Italiano di Tecnologia (IIT), Via Morego 30, 16163 Genova, Italy.*

[4] *Dipartimento di Chimica Farmaceutica e Tossicologica, Università di Napoli "Federico II" Via D. Montesano 49, 80131 Napoli, Italy.*

[5] *Chemistry Department, Faculty of Science, King Abdulaziz University, P.O. Box 80203, Jeddah 21589, Saudi Arabia*

## Table of Content

## ELISA Assays

**αvβ3 assay:** Experimental procedure is as described for α5β1 assay, except for the following modifications. The plates are coated with 100 µL/well of 1.0 µg/mL vitronectin (Millipore, Schwalbach/Ts., Germany) in carbonate buffer, washed and blocked as described for α5β1. Soluble integrin αvβ3 (Millipore) was mixed with equal amounts of serial diluted inhibitors resulting in a final integrin concentration of 1.0 µg/mL. As a primary antibody 100 µL/well of 2.0 µg/mL mouse anti-human CD51/61 (BD Biosciences, Heidelberg, Germany) was used. Secondary antibody is the same as in integrin $\alpha_5\beta_1$ assay, but 100 µL/well of 1.0 µg/mL were used. Visualization and analysis was performed as described for α5β1.

**αvβ5 assay:** Experimental procedure is as described for α5β1 assay, except for the following modifications. The plates are coated with 100 µL/well of 5.0 µg/mL vitronectin (Millipore, Schwalbach/Ts., Germany) in carbonate buffer, washed and blocked as described for α5β1. Soluble integrin αvβ5 (Millipore) was mixed with equal amounts of serial diluted inhibitors resulting in a final integrin concentration of 1.5 µg/mL. As a primary antibody 100 µL/well of 1:500 diluted mouse anti-human αv (Millipore) was used. Secondary antibody is the same as in integrin α5β1 assay, but 100 µL/well of 1.0 µg/mL were used. Visualization and analysis was performed as described for α5β1.

**αIIbβ3 assay:** Experimental procedure is as described for α5β1 assay, except for the following modifications. The plates are coated with 100 µL/well of 10.0 µg/mL fibrinogen (Millipore, Schwalbach/Ts., Germany) in carbonate buffer, washed and blocked as described for α5β1. Soluble integrin αIIbβ3 (Millipore) was mixed with equal amounts of serial diluted inhibitors resulting in a final integrin concentration of 2.5 µg/mL. As a primary antibody 100 µL/well of 2.0 µg/mL CD41b (BD Biosciences, Heidelberg, Germany) was used. Secondary antibody is the same as in integrin α5β1 assay, but 100 µL/well of 1.0 µg/mL were used. Visualization and analysis was performed as described for α5β1.

## NMR Spectroscopic Studies

The samples for NMR spectroscopic studies were prepared by dissolving the compound in 500 μl of DMSO-$d_6$. The required NMR spectroscopic experiments were recorded at 300K K on Bruker 500 MHz spectrometer equipped with TXI cryoprobe. Single set of signals corresponding to the number of protons in the compounds, observed in $^1$H-1D spectrum indicated the purity and absence of slowly exchanging conformations on time scales of NMR. $^1$H-1D, $^1$H,$^1$H-TOCSY, -ROESY, $^1$H,$^{13}$C-HSQC, and -HMBC NMR experiments have been recorded for each sample. $^1$H-selective homonuclear decoupling experiments were carried out to measure $^3J_H$ couplings. Furthermore, to estimate the solvent shielding or hydrogen bonding strengths of NH protons the temperature dependency of NH chemical shifts was studied by acquiring $^1$H-1D spectra between 295 K and 315 K in steps of 5 K increments. Mixing times for TOCSY spectra were 80 ms, for ROESY spectra 100 ms. HSQC spectra were recorded with a direct proton carbon coupling constant of 140 Hz, and HMBC spectra with a long-range $^1$H-$^{13}$C coupling constant of 7 Hz. For all HSQC spectra, a $^{13}$C composite pulse decoupling was utilized. 8k (except HSQC: 1k) data points were recorded in the direct dimension, 384 and 512 (heteronuclear spectra) in the indirect dimension. For all spectra a 1.5 s relaxation delay was used after every transient. Exponential / square sine window functions were used for spectra apodization.

Chemical shift assignment and $^3J_H$ coupling constant data from different environments has been tabulated in the following sections.

**Proton-proton internuclear distances for structure calculation**: ROE cross peaks in corresponding ROESY spectra recorded in various solvents were integrated by using box method in SPARKY software. These integrated volumes of ROE cross peaks were converted to proton-proton internuclear distances by linear approximation method.

Thus calculated distances were then relaxed by ±10 or ±15 % to generate upper and lower distance bounds to account for experimental and simulation uncertainties.

## Distance Geometry (DG) Calculations

Metric matrix DG calculations were carried out with a home-written distance geometry program utilizing random metrization. The above calculated experimental distance

restraints which are more restrictive than the geometric distance bounds (holonomic restraints) were used to create the final distance matrix. 50 structures were calculated for each system. The structures were then verified and checked for violations if any with respect to the given experimental distance restraint inputs. The structures that best satisfied the distance inputs were then taken forward for MD simulations.

**Supporting Table 1**: Chemical shift assignment of **5** in dimethyl sulfoxide at 300 K.

| Residue | NH | Hα | Hβ | Hγ | Hδ | Hε | Hz |
|---|---|---|---|---|---|---|---|
| phg[1] | 8.689<br>$J_{NH\text{-}H\alpha}$=7.8 Hz | 5.377<br>$J_{NH\text{-}H\alpha}$=7.8 Hz | | | | | |
| *iso*-Asp[2] | 7.660<br>$J_{NH\text{-}H\alpha}$=8.2 Hz | 4.516<br>$J_{NH\text{-}H\alpha}$=8.2 Hz<br>$J_{H\alpha\text{-}H\beta pro\text{-}R}$=6.4 Hz<br>$J_{H\alpha\text{-}H\beta pro\text{-}S}$=4.2 Hz | 2.901 (*pro*-R)<br>2.627 (*pro*-S)<br>$J_{H\alpha\text{-}H\beta pro\text{-}R}$=6.4 Hz<br>$J_{H\alpha\text{-}H\beta pro\text{-}S}$=4.2 Hz<br>$J_{H\beta\ pro\text{-}R\ -H\beta\ pro\text{-}S}$ =15.5 Hz | | | | |
| Gly[3] | 8.363<br>$J_{NH\text{-}H\alpha}$=6.1 Hz<br>$J_{NH\text{-}H\alpha}$=5.1 Hz | 3.799, 3.645<br>$J_{NH\text{-}H\alpha\ pro\text{-}R}$=6.1 Hz<br>$J_{NH\text{-}H\alpha\ pro\text{-}S}$=5.1 Hz<br>$J_{H\alpha\ pro\text{-}R\ -H\alpha\ pro\text{-}S}$ =16.3 Hz | | | | | |
| Arg[4] | 8.339<br>$J_{NH\text{-}H\alpha}$=7.3 Hz | 4.120<br>$J_{NH\text{-}H\alpha}$=7.3 Hz<br>$J_{H\alpha\text{-}H\beta}$=8.6 Hz<br>$J_{H\alpha\text{-}H\beta}$=6.1 Hz | 1.724 (*pro*-R)<br>1.667 (*pro*-S)<br>$J_{H\alpha\text{-}H\beta pro\text{-}R}$=8.6 Hz<br>$J_{H\alpha\text{-}H\beta pro\text{-}S}$=6.1 Hz<br>$J_{H\beta\ pro\text{-}R\ -H\beta\ pro\text{-}S}$ =14.8 Hz | 1.512<br>$J_{H\gamma\text{-}H\delta}$=6.5 Hz | 3.130<br>$J_{H\gamma\text{-}H\delta}$=6.5 Hz<br>$J_{H\delta\text{-}H\varepsilon}$=5.6 Hz | 7.891<br>$J_{H\delta\text{-}H\varepsilon}$=5.6 Hz | |
| Lys[5] | 7.954<br>$J_{NH\text{-}H\alpha}$=7.0 Hz | 4.211<br>$J_{NH\text{-}H\alpha}$=7.0 Hz<br>$J_{H\alpha\text{-}H\beta pro\text{-}R}$=7.0 Hz<br>$J_{H\alpha\text{-}H\beta pro\text{-}S}$=7.0 Hz | 1.747 (*pro*-S)<br>1.644 (*pro*-R)<br>$J_{H\alpha\text{-}H\beta pro\text{-}R}$=7.0 Hz<br>$J_{H\alpha\text{-}H\beta pro\text{-}S}$=7.0 Hz | 1.251 | 1.526 | 2.762 | 7.776 |

**Supporting Table 2**: Chemical shift assignment of **6** in dimethyl sulfoxide at 300 K.

| Residue | NH | Hα | Hβ | Hγ | Hδ | Hε | Hz |
|---|---|---|---|---|---|---|---|
| phg[1] | 8.635 $J_{NH-H\alpha}$=9.6 Hz | 5.618 $J_{NH-H\alpha}$=9.6 Hz | | | | | |
| *iso*-Asp[2] | 7.434 $J_{NH-H\alpha}$=7.2 Hz | 4.401 $J_{NH-H\alpha}$=7.2 Hz $J_{H\alpha-H\beta pro-R}$=9.2 Hz $J_{H\alpha-H\beta pro-S}$=3.8 Hz | 2.766 (*pro*-R) 2.533 (*pro*-S) $J_{H\alpha-H\beta pro-R}$=9.2 Hz $J_{H\alpha-H\beta pro-S}$=3.8 Hz $J_{H\beta\ pro-R\ -H\beta\ pro-S}$ =14.8 Hz | | | | |
| Gly[3] | 8.352 $J_{NH-H\alpha}$=6.8 Hz $J_{NH-H\alpha}$=5.7 Hz | 3.890, 3.531 $J_{NH-H\alpha\ pro-R}$=6.8 Hz $J_{NH-H\alpha\ pro-S}$=5.7 Hz $J_{H\alpha\ pro-R\ -H\alpha\ pro-S}$ =16.2 Hz | | | | | |
| Arg[4] | 8.198 $J_{NH-H\alpha}$=5.3 Hz | 4.072 $J_{NH-H\alpha}$=5.3 Hz $J_{H\alpha-H\beta pro-R}$=7.0 Hz $J_{H\alpha-H\beta pro-S}$=7.0 Hz | 1.680 (*pro*-R) 1.608 (*pro*-S) $J_{H\alpha-H\beta pro-R}$=7.0 Hz $J_{H\alpha-H\beta pro-S}$=7.0 Hz $J_{H\beta\ pro-R\ -H\beta\ pro-S}$ =14.8 Hz | 1.520 1.449 | 3.147 $J_{H\gamma-H\delta}$=7.2 Hz $J_{H\gamma'-H\delta}$=7.2 Hz $J_{H\delta-H\varepsilon}$=5.7 Hz | 7.851 $J_{H\delta-H\varepsilon}$=5.7 Hz | |
| lys[5] | 8.514 $J_{NH-H\alpha}$=7.7 Hz | 4.169 $J_{NH-H\alpha}$=7.7 Hz $J_{H\alpha-H\beta pro-S}$=4.0 Hz $J_{H\alpha-H\beta pro-R}$=10.2 Hz | 1.881 (*pro*-S) 1.521 (*pro*-R) $J_{H\alpha-H\beta pro-S}$=4.0 Hz $J_{H\alpha-H\beta pro-R}$=10.2 Hz | 1.329 | 1.530 1.526 | 2.752 | 7.784 |

**Supporting Table 3**: Temperature coefficient data of **5** and **6** in DMSO.

$^1$H-1D spectra were recorded for both the compounds at variable temperatures ranging from 295 K to 315 K in 5 K intervals and the temperature coefficients were calculated according to $(\Delta\delta*1000)/\Delta T$ where in $\Delta\delta$ and $\Delta T$ are changes in chemical shift of the corresponding NH and the change in sample temperature, respectively.

| Name of the Compound | | | |
|---|---|---|---|
| **5** | | **6** | |
| Name of the NH | Temperature Coefficient (ppb/K) | Name of the NH | Temperature Coefficient (ppb/K) |
| 1(phg)NH | -6.00 | 1(phg)NH | -3.33 |
| 2(*iso*Asp)NH | -2.00 | 2(*iso*Asp)NH | -2.00 |
| 3(Gly)NH | -4.30 | 3(Gly)NH | -4.66 |
| 4(Arg)NH | 0.00 | 4(Arg)NH | -2.00 |
| 5(Lys)NH | -4.50 | 5(lys)NH | -4.44 |

**Supporting Table 4**: Backbone dihedral angles measured from DG structures of **5** and **6**

| Dihedral Angle | Backbone Dihedral Angles in the order **5**/**6** | | | | |
|---|---|---|---|---|---|
| | 1phg | 2*iso*Asp | 3Gly | 4Arg | 5Lys/lys |
| $\phi$ | 91.7 / 121.0 | -77.7 / -67.4 | 63.9 / 84.5 | -67.9 / -118.9 | -116.6 / 89.8 |
| $\theta$ | -- | -19.8 / -56.1 | -- | -- | -- |
| $\psi$ | -39.8 / -32.1 | 100.5 / 99.5 | -65.3 / -45.3 | -68.2 / 112.3 | 58 / 4.7 |

## Molecular Dynamics Studies

All MD simulations were carried out with the GROMACS 4.0.5 version. The above DG structures served as starting conformations for the MD runs. The ffcharmm27 all atom force field was utilized for parameterization of the cyclic pentapeptide and all solvent molecules. The DG structure of Cilengitide was first energy minimized in vacuo, then placed in truncated octahedral boxes with a minimum distance of 2.1 nm between solute atoms and the box walls. After the boxes were filled with solvent molecules, the systems were equilibrated with respect to temperature and pressure in subsequent steps, which are independently performed at increasing temperatures from 50 K to 300 K in 50 K steps. A triple-range cutoff for Coulomb interactions including a reaction-field was used (0.8 and 1.4 nm). Van der Waals interactions were calculated with a short-range cutoff of 0.8 nm and a long-range cutoff of 1.4 nm. An atom pair-list was used with a cutoff of 0.8 nm and was updated each five integration steps. All bonds were constrained with the Shake algorithm. The integration time step was 2 fs. Each of the equilibration steps from 50 K to 250 K had a run time of 50k ps and 0.5 ns for those at 300 K. The MD runs had a

length of 2 ns. The output trajectories were then analyzed for internuclear distances and compared with the experimental data.

**Supporting Figure 1**: Distribution factor histograms of the backbone dihedral angles in **5** fMD (without restraints) trajectory. The vertical blue lines in each graph indicate the corresponding dihedral angle values (ST 4) as measured from the input DG structure.

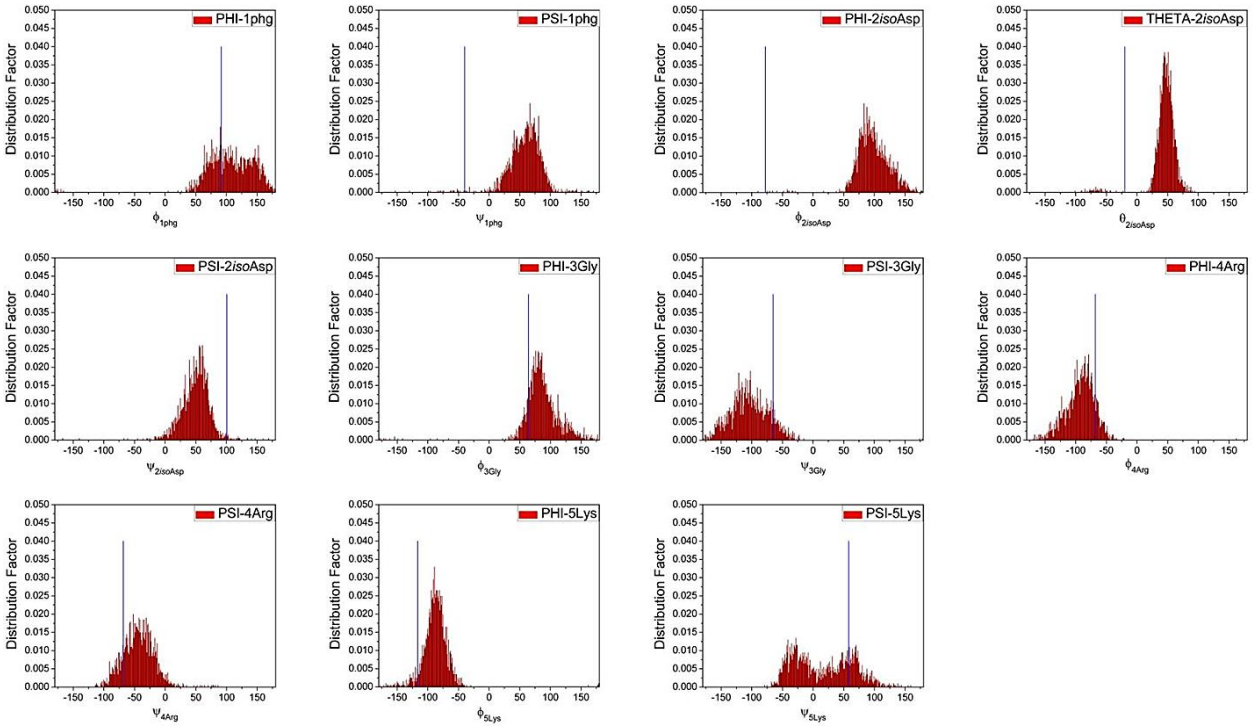


**Supporting Figure 2**: Distribution factor histograms of the backbone dihedral angles in **5** rMD (with restraints) trajectory. The vertical blue lines in each graph indicate the corresponding dihedral angle values (ST 4) as measured from the input DG structure.

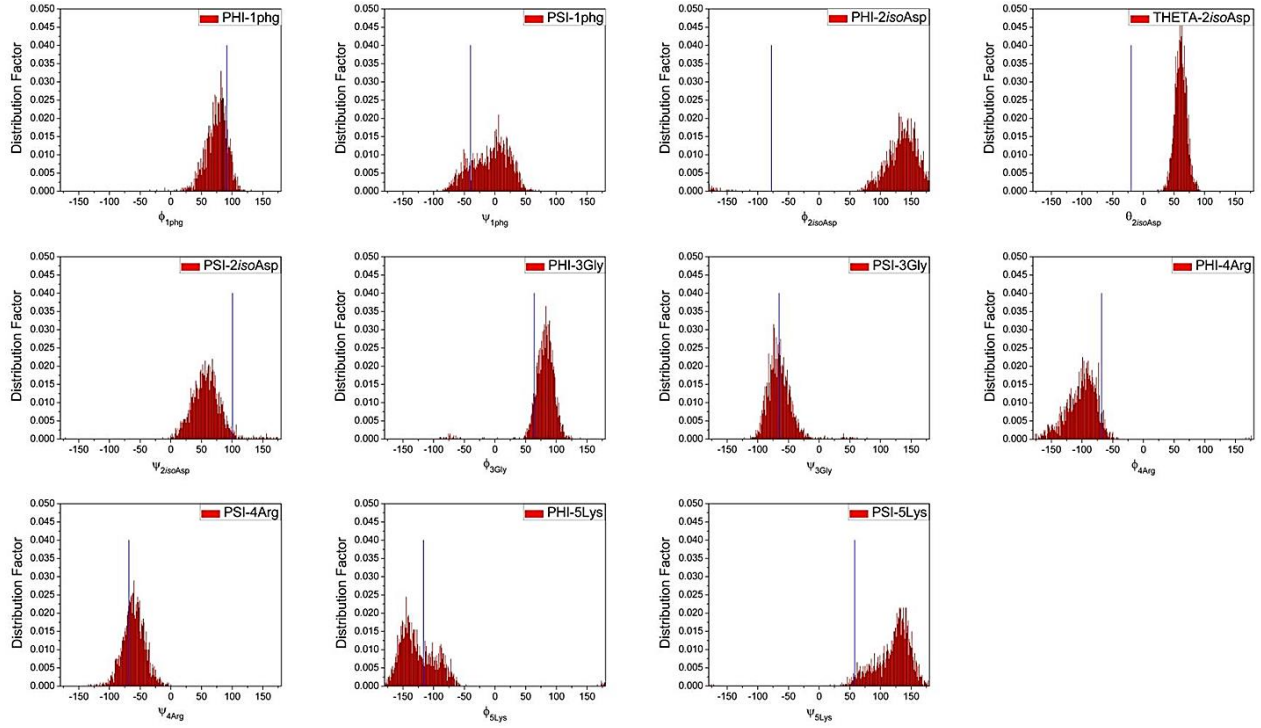


**Supporting Figure 3**: Distribution factor histograms of the backbone dihedral angles in **6** fMD (without restraints) trajectory. The vertical blue lines in each graph indicate the corresponding dihedral angle values (ST 4) as measured from the input DG structure.

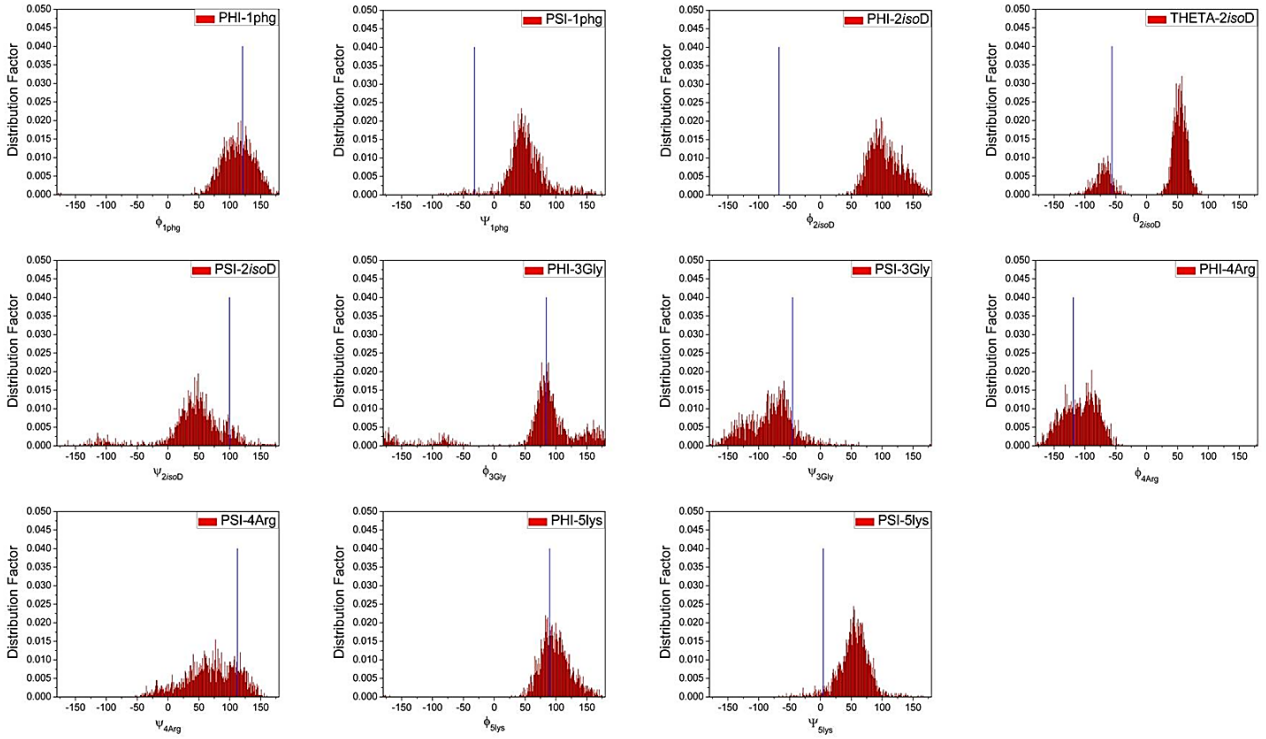


As pointed out in the main text, a structural dissimilarity observed between the DG structures of **5** and **6** is difference in the orientation of 4Arg-5Lys/lys peptide bond. This is

well represented in the correspondingly effected residue dihedral angle distributions, which are around the specific values measured from DG structures.

It is noticeable from the above MD figures that the conformation around the β-turn of 3Gly residue and the respective dihedrals are well conserved. The disagreement between DG and MD structures and therefore the structural dynamics is seen around 2*iso*Asp residue.

**Supporting Table 5**: List of distance restraints that were used to derive the DG structure of **5** and the corresponding violations in fMD trajectory.

| | Residue | Atom | Residue | Atom | Upper Bound | Lower Bound | MD Violations (Å) |
|---|---|---|---|---|---|---|---|
| constraint | 1phg | h | 1phg | ha | 3.34 | 2.48 | |
| constraint | 1phg | ha | 2*iso*Asp | ha | 4.95 | 3.66 | |
| constraint | 1phg | h | 4Arg | ha | 4.62 | 3.41 | |
| constraint | 1phg | h | 5Lys | h | 3.39 | 2.51 | |
| constraint | 1phg | h | 5Lys | ha | 2.65 | 1.96 | +0.37 |
| constraint | 1phg | ha | 5Lys | ha | 4.71 | 3.47 | |
| constraint | 2*iso*Asp | h | 1phg | ha | 3.24 | 2.89 | +0.03 |
| constraint | 2*iso*Asp | h | 2*iso*Asp | ha | 2.67 | 2.26 | +0.15 |
| constraint | 2*iso*Asp | h | 2*iso*Asp | $hb_{pro\text{-}S}$ | 3.79 | 2.81 | |
| constraint | 2*iso*Asp | $hb_{pro\text{-}S}$ | 4Arg | h | 4.18 | 3.09 | +1.17 |
| constraint | 2*iso*Asp | h | 4Arg | h | 5.06 | 3.74 | |
| constraint | 2*iso*Asp | h | 5Lys | ha | 4.85 | 3.58 | +0.28 |
| constraint | 3Gly | h | 2*iso*Asp | h | 4.03 | 2.98 | -0.46 |
| constraint | 3Gly | h | 2*iso*Asp | ha | 4.47 | 3.30 | |
| constraint | 3Gly | h | 2*iso*Asp | $hb_{pro\text{-}R}$ | 2.77 | 2.05 | +0.68 |
| constraint | 3Gly | ha2 | 4Arg | h | 2.96 | 2.19 | +0.33 |
| constraint | 4Arg | h | 4Arg | ha | 3.21 | 2.37 | |
| constraint | 4Arg | h | 5Lys | h | 2.91 | 2.16 | |
| constraint | 5Lys | h | 2*iso*Asp | h | 5.02 | 3.71 | +0.88 |
| constraint | 5Lys | h | 2*iso*Asp | $hb_{pro\text{-}S}$ | 5.00 | 3.70 | |
| constraint | 5Lys | h | 4Arg | ha | 3.51 | 2.59 | +0.06 |
| constraint | 5Lys | h | 5Lys | ha | 3.12 | 2.31 | |

**Supporting Table 6**: List of distance restraints that were used to derive the DG structure of **5** and the corresponding violations in rMD trajectory.

| | Residue | Atom | Residue | Atom | Upper Bound | Lower Bound | MD Violations (Å) |
|---|---|---|---|---|---|---|---|
| constraint | 1phg | h | 1phg | ha | 3.34 | 2.48 | |
| constraint | 1phg | ha | 2*iso*Asp | ha | 4.95 | 3.66 | |
| constraint | 1phg | h | 4Arg | ha | 4.62 | 3.41 | +0.62 |
| constraint | 1phg | h | 5Lys | h | 3.39 | 2.51 | +0.55 |
| constraint | 1phg | h | 5Lys | ha | 2.65 | 1.96 | |
| constraint | 1phg | ha | 5Lys | ha | 4.71 | 3.47 | |
| constraint | 2*iso*Asp | h | 1phg | ha | 3.24 | 2.89 | |
| constraint | 2*iso*Asp | h | 2*iso*Asp | ha | 2.67 | 2.26 | +0.12 |
| constraint | 2*iso*Asp | h | 2*iso*Asp | $hb_{pro\text{-}S}$ | 3.79 | 2.81 | |
| constraint | 2*iso*Asp | $hb_{pro\text{-}S}$ | 4Arg | h | 4.18 | 3.09 | +0.07 |
| constraint | 2*iso*Asp | h | 4Arg | h | 5.06 | 3.74 | |
| constraint | 2*iso*Asp | h | 5Lys | ha | 4.85 | 3.58 | |
| constraint | 3Gly | h | 2*iso*Asp | h | 4.03 | 2.98 | |
| constraint | 3Gly | h | 2*iso*Asp | ha | 4.47 | 3.30 | |
| constraint | 3Gly | h | 2*iso*Asp | $hb_{pro\text{-}R}$ | 2.77 | 2.05 | |
| constraint | 3Gly | ha2 | 4Arg | h | 2.96 | 2.19 | |
| constraint | 4Arg | h | 4Arg | ha | 3.21 | 2.37 | |
| constraint | 4Arg | h | 5Lys | h | 2.91 | 2.16 | |
| constraint | 5Lys | h | 2*iso*Asp | h | 5.02 | 3.71 | -0.27 |
| constraint | 5Lys | h | 2*iso*Asp | $hb_{pro\text{-}S}$ | 5.00 | 3.70 | |
| constraint | 5Lys | h | 4Arg | ha | 3.51 | 2.59 | +0.06 |
| constraint | 5Lys | h | 5Lys | ha | 3.12 | 2.31 | |

**Supporting Table 7**: List of distance restraints that were used to derive the DG structure of **6** and the corresponding violations in fMD trajectory.

| | Residue | Atom | Residue | Atom | Upper Bound | Lower Bound | MD Violations (Å) |
|---|---|---|---|---|---|---|---|
| constraint | 1phg | h | 2*iso*Asp | h | 2.98 | 2.21 | |
| constraint | 1phg | h | 2*iso*Asp | ha | 5.34 | 3.94 | |
| constraint | 1phg | ha | 2*iso*Asp | ha | 4.81 | 3.56 | |
| constraint | 1phg | h | 4Arg | ha | 3.80 | 2.81 | +0.36 |
| constraint | 1phg | h | 5lys | ha | 3.37 | 2.49 | +0.14 |
| constraint | 1phg | ha | 5lys | ha | 4.55 | 3.36 | |
| constraint | 2*iso*Asp | h | 1phg | ha | 3.69 | 2.73 | |
| constraint | 2*iso*Asp | h | 2*iso*Asp | ha | 2.96 | 2.19 | |
| constraint | 2*iso*Asp | h | 2*iso*Asp | $Hb_{pro\text{-}R}$ | 3.61 | 2.66 | |
| constraint | 2*iso*Asp | h | 2*iso*Asp | $hb_{pro\text{-}S}$ | 4.22 | 3.12 | |
| constraint | 2*iso*Asp | ha | 2*iso*Asp | $hb_{pro\text{-}S}$ | 2.74 | 2.02 | |
| constraint | 2*iso*Asp | h | 5lys | ha | 4.68 | 3.46 | +0.57 |
| constraint | 3Gly | h | 2*iso*Asp | h | 4.33 | 3.20 | -0.39 |
| constraint | 3Gly | h | 2*iso*Asp | ha | 4.02 | 2.97 | |
| constraint | 3Gly | h | 2*iso*Asp | $hb_{pro\text{-}R}$ | 2.74 | 2.02 | |
| constraint | 3Gly | h | 2*iso*Asp | $hb_{pro\text{-}S}$ | 3.17 | 2.34 | |
| constraint | 4Arg | h | 2*iso*Asp | $hb_{pro\text{-}S}$ | 4.31 | 3.40 | 0.01 |
| constraint | 4Arg | h | 3Gly | ha2 | 2.85 | 2.10 | |
| constraint | 4Arg | h | 3Gly | ha1 | 3.37 | 2.49 | |
| constraint | 4Arg | h | 4Arg | ha | 3.24 | 2.40 | |
| constraint | 5lys | h | 4Arg | ha | 2.42 | 1.79 | |
| constraint | 5lys | h | 5lys | ha | 2.90 | 2.38 | |
| constraint | 2*iso*Asp | h | 4Arg | h | 4.62 | 3.42 | |
| constraint | 4Arg | h | 2*iso*Asp | ha | 5.55 | 4.04 | |

**Supporting Figure 4**: Stereo view of the overlaid DG conformers derived for **5** (green) and **6**. For a better view of the conformation, non-polar hydrogens are not shown.

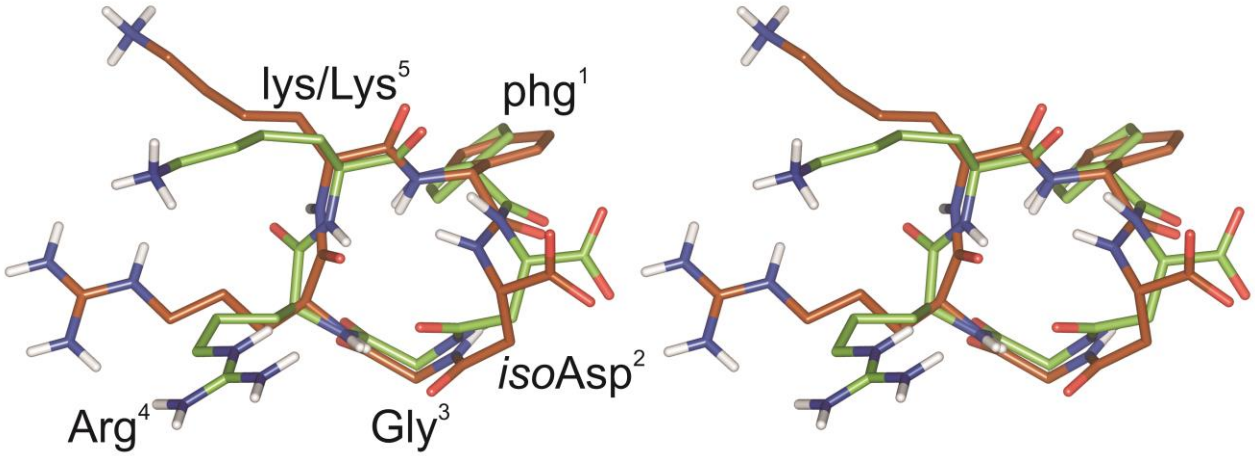


**Supporting Table 8**: Pair wise deviations of backbone atoms in RMSD overlay of DG structures of **5** and **6**.

| S. No. | Residue from **5** | Atom | Residue from **5** | Atom | Deviation |
|---|---|---|---|---|---|
| 1 | 1phg | N | 1phg | N | 0.25 |
| 2 | 1phg | CA | 1phg | CA | 0.27 |
| 3 | 1phg | C | 1phg | C | 0.26 |
| 4 | 2*iso*Asp | N | 2*iso*Asp | N | 0.49 |
| 5 | 2*iso*Asp | CA | 2*iso*Asp | CA | 0.40 |
| 6 | 2*iso*Asp | C | 2*iso*Asp | C | 0.74 |
| 7 | 3Gly | N | 3Gly | N | 0.31 |
| 8 | 3Gly | CA | 3Gly | CA | 0.29 |
| 9 | 3Gly | C | 3Gly | C | 0.28 |
| 10 | 4Arg | N | 4Arg | N | 0.30 |
| 11 | 4Arg | CA | 4Arg | CA | 0.49 |
| 12 | 4Arg | C | 4Arg | C | 1.21 |
| 13 | 5Lys | N | 5lys | N | 0.88 |
| 14 | 5Lys | CA | 5lys | CA | 0.47 |
| 15 | 5Lys | C | 5lys | C | 0.63 |
| Backbone RMSD = 0.5542 | | | | | |

**Supporting Figure 5**: Plot showing the overlay of corresponding backbone dihedral angles measured from the DG structures of **5** and **6**.

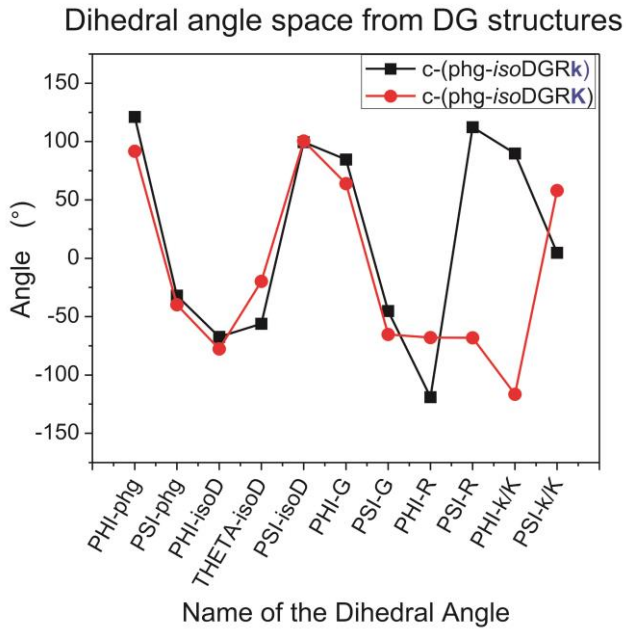


Resemblances and differences in the DG structures derived for **5** and **6** have been represented by an overlay graph of the corresponding backbone dihedral angles. Significant change in the dihedral space observed along $Arg^4$-$lys^5$($Lys^5$) residues can be attributed to a 180° flip in the orientation of $Arg^4$-$lys^5$($Lys^5$) peptide bond which is noticeable from SF **3**.

**Supporting Figure 6**: Stereo view of the overlaid DG structure of **6** (brown) and structure from its most representative cluster (pale blue) in fMD trajectory. For a better view of the conformation, non-polar hydrogens are not shown. The residue alignment is same as that in SF 4.

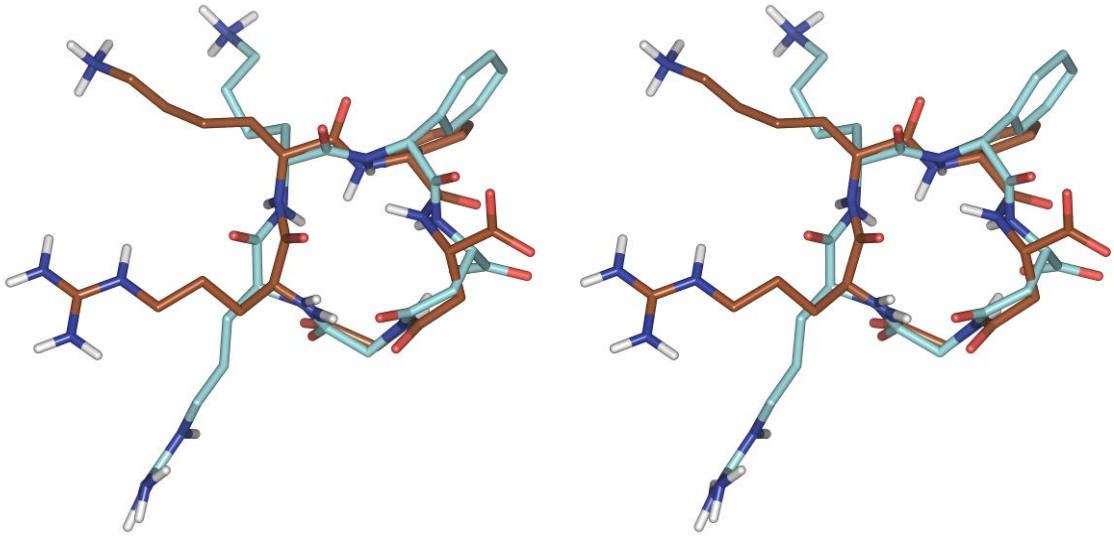

**Supporting Table 9**: Pair wise deviations of backbone atoms in RMSD overlay of DG structure of **6** with the structure from its most representative cluster in fMD trajectory.

| S. No. | Residue | Atom | Residue | Atom | Deviation |
|---|---|---|---|---|---|
| 1 | 1phg | N | 1phg | N | 0.47 |
| 2 | 1phg | CA | 1phg | CA | 1.04 |
| 3 | 1phg | C | 1phg | C | 0.94 |
| 4 | 2*iso*Asp | N | 2*iso*Asp | N | 1.11 |
| 5 | 2*iso*Asp | CA | 2*iso*Asp | CA | 1.76 |
| 6 | 2*iso*Asp | C | 2*iso*Asp | C | 0.48 |
| 7 | 3Gly | N | 3Gly | N | 0.45 |
| 8 | 3Gly | CA | 3Gly | CA | 0.64 |
| 9 | 3Gly | C | 3Gly | C | 0.24 |
| 10 | 4Arg | N | 4Arg | N | 0.33 |
| 11 | 4Arg | CA | 4Arg | CA | 0.51 |
| 12 | 4Arg | C | 4Arg | C | 0.83 |
| 13 | 5lys | N | 5lys | N | 0.44 |
| 14 | 5lys | CA | 5lys | CA | 0.56 |
| 15 | 5lys | C | 5lys | C | 0.52 |
| Backbone RMSD = 0.7859 | | | | | |

**Supporting Figure 7**: Stereo view of the overlaid DG structure of **5** (green) and structure from its most representative cluster (pale pink) in fMD trajectory. For a better view of the conformation, non-polar hydrogens are not shown. The residue alignment is same as that in SF 4.

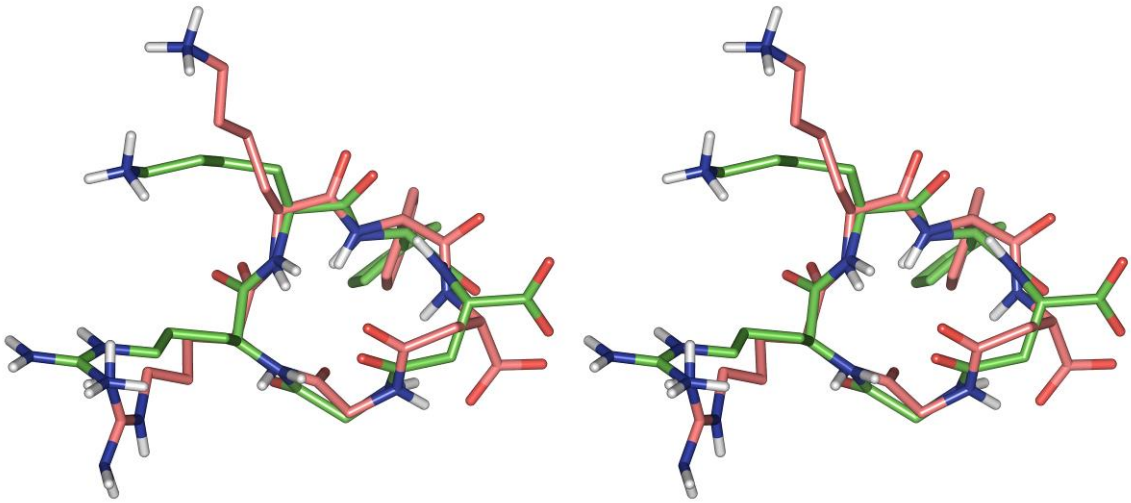

**Supporting Table 10**: Pair wise deviations of backbone atoms in RMSD overlay of DG structure of **5** with the structure from its most representative cluster in fMD trajectory.

| S. No. | Residue | Atom | Residue | Atom | Deviation |
|---|---|---|---|---|---|
| 1 | 1phg | N | 1phg | N | 0.52 |
| 2 | 1phg | CA | 1phg | CA | 0.61 |
| 3 | 1phg | C | 1phg | C | 0.65 |
| 4 | 2*iso*Asp | N | 2*iso*Asp | N | 1.36 |
| 5 | 2*iso*Asp | CA | 2*iso*Asp | CA | 1.50 |
| 6 | 2*iso*Asp | C | 2*iso*Asp | C | 0.49 |
| 7 | 3Gly | N | 3Gly | N | 0.75 |
| 8 | 3Gly | CA | 3Gly | CA | 1.30 |
| 9 | 3Gly | C | 3Gly | C | 0.49 |
| 10 | 4Arg | N | 4Arg | N | 0.38 |
| 11 | 4Arg | CA | 4Arg | CA | 0.92 |
| 12 | 4Arg | C | 4Arg | C | 0.59 |
| 13 | 5Lys | N | 5Lys | N | 0.25 |
| 14 | 5Lys | CA | 5Lys | CA | 0.44 |
| 15 | 5Lys | C | 5Lys | C | 0.44 |
| Backbone RMSD = 0.7760 | | | | | |

**Supporting Figure 8**: Stereo view of the overlaid DG structure of **5** (green) and structure from its most representative cluster (grey) in rMD trajectory. For a better view of the conformation, non-polar hydrogens are not shown. The residue alignment is same as that in SF 4.

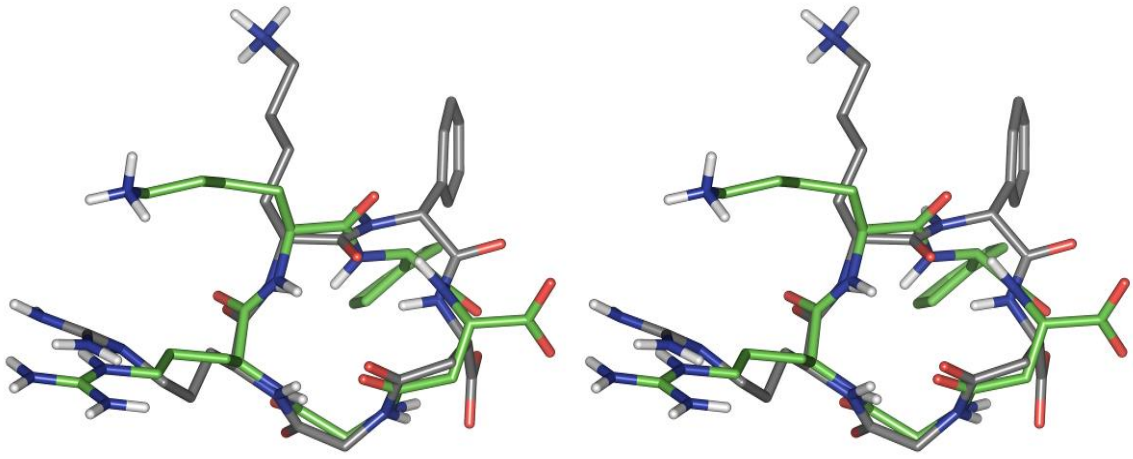

**Supporting Table 11**: Pair wise deviations of backbone atoms in RMSD overlay of DG structure of **5** with the structure from its most representative cluster in rMD trajectory.

| S. No. | Residue | Atom | Residue | Atom | Deviation |
|---|---|---|---|---|---|
| 1 | 1phg | N | 1phg | N | 0.94 |
| 2 | 1phg | CA | 1phg | CA | 1.41 |
| 3 | 1phg | C | 1phg | C | 0.87 |
| 4 | 2*iso*Asp | N | 2*iso*Asp | N | 0.89 |
| 5 | 2*iso*Asp | CA | 2*iso*Asp | CA | 1.57 |
| 6 | 2*iso*Asp | C | 2*iso*Asp | C | 0.22 |
| 7 | 3Gly | N | 3Gly | N | 0.49 |
| 8 | 3Gly | CA | 3Gly | CA | 0.93 |
| 9 | 3Gly | C | 3Gly | C | 0.57 |
| 10 | 4Arg | N | 4Arg | N | 0.21 |
| 11 | 4Arg | CA | 4Arg | CA | 0.30 |
| 12 | 4Arg | C | 4Arg | C | 0.42 |
| 13 | 5Lys | N | 5Lys | N | 0.38 |
| 14 | 5Lys | CA | 5Lys | CA | 0.33 |
| 15 | 5Lys | C | 5Lys | C | 0.45 |
| Backbone RMSD = 0.7809 | | | | | |

**Supporting Figure 9**: Stereo view of the overlaid structures of **5** from its most representative clusters in fMD (pale pink) and rMD (grey) trajectories. For a better view of the conformation, non-polar hydrogens are not shown. The residue alignment is same as that in SF 4.

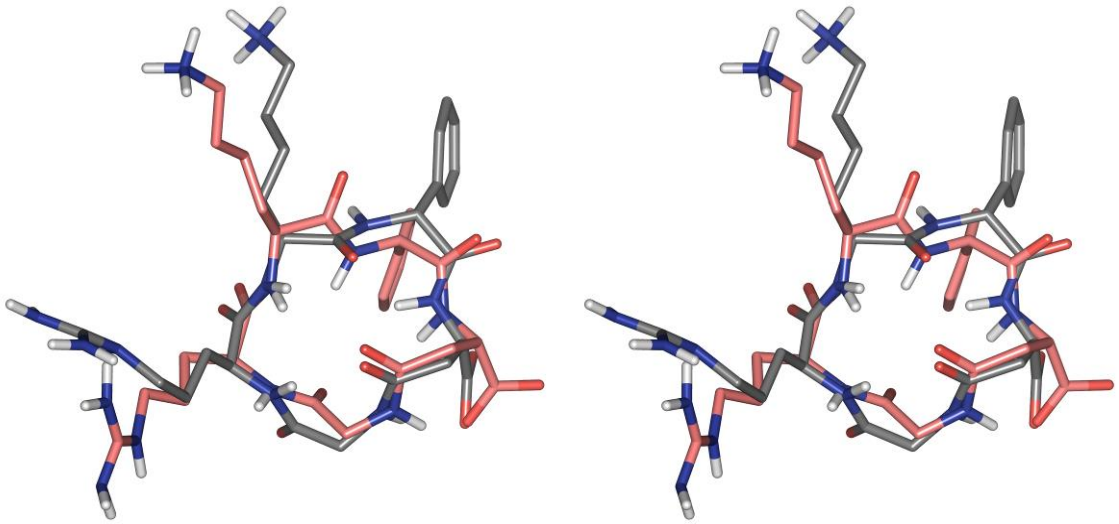

**Supporting Table 12**: Pair wise deviations of backbone atoms in RMSD overlay of structures of **5** from its most representative clusters in fMD and rMD trajectories.

| S. No. | Residue | Atom | Residue | Atom | Deviation |
|---|---|---|---|---|---|
| 1 | 1phg | N | 1phg | N | 0.94 |
| 2 | 1phg | CA | 1phg | CA | 1.00 |
| 3 | 1phg | C | 1phg | C | 0.46 |
| 4 | 2*iso*Asp | N | 2*iso*Asp | N | 0.57 |
| 5 | 2*iso*Asp | CA | 2*iso*Asp | CA | 0.36 |
| 6 | 2*iso*Asp | C | 2*iso*Asp | C | 0.28 |
| 7 | 3Gly | N | 3Gly | N | 0.40 |
| 8 | 3Gly | CA | 3Gly | CA | 0.32 |
| 9 | 3Gly | C | 3Gly | C | 0.77 |
| 10 | 4Arg | N | 4Arg | N | 0.39 |
| 11 | 4Arg | CA | 4Arg | CA | 0.60 |
| 12 | 4Arg | C | 4Arg | C | 0.36 |
| 13 | 5Lys | N | 5Lys | N | 0.21 |
| 14 | 5Lys | CA | 5Lys | CA | 0.71 |
| 15 | 5Lys | C | 5Lys | C | 0.61 |
| Backbone RMSD = 0.5803 | | | | | |

## Molecular Docking of 5 and 6 in αvβ3

Docking of **5** in the αvβ3 integrin results in a binding mode similar to that observed in α5β1 (see Supporting Figure 10a), with a major change in the orientation of $Lys^5$ side chain which assumes a crumpled conformation, although in part counterbalanced by the ionic interaction with (αv)-D218. Such an entropically unfavorable conformation is induced by the presence of the long (β3)-K253 side chain which is kept in place by the neighboring (αv)-R248 and (β3)-A218. The predicted binding is in line with the experimental data indicating that the replacement of $Lys^5$ with either Trp or Tyr in *c*(-phg-*iso*DGR-X-) peptides (assuming that their backbone conformation is similar to that exhibited by **5**) is not well tolerated in αvβ3. In fact, it is likely that the bulky side chains of the latter amino acids would sterically clash within the tight downstream pocket of αvβ3, thus leading to a marked drop in affinity, as observed for peptides **9** and **11**. The aforementioned structural changes between the two integrins together with the inversion of the lysine chirality seem to affect even more the binding of **6** to αvβ3 (see Supporting Figure 10b). In fact, from docking studies, it results that the latter peptide would not be able to insert the $Arg^4$ guanidinium group into the narrow groove at the top of the receptor

propeller domain, thus not establishing a key salt bridge with (αv)-Asp150. On the other hand, the inversion of the lysine chirality does not allow, its side chain to extend into the downstream pocket (as observed for **5**), thus occupying the cavity above the metal where an ionic interaction with (β3)-D251 is formed.

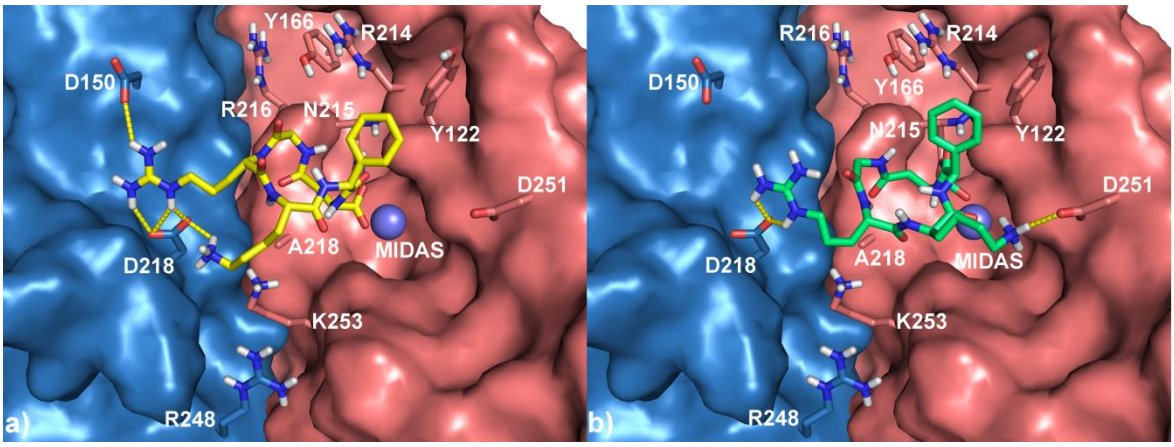


**Supporting Figure 10.** Binding modes of **5** (a) and **6** (b) in the **αvβ3** integrin. **5** and **6** are shown as yellow and green sticks, respectively. The **αv** and **β3** subunits are depicted as light blue and light red surfaces, respectively. Receptor amino acid side chains important for the ligand binding are represented as sticks. The metal cation in the MIDAS is represented as a purple sphere.

## Molecular Docking of 5 and 6 in αvβ5

The poor activity displayed by **5** and **6** against αvβ5 might be explained taking into account the binding modes observed in the aforesaid receptors and the specific features of the αvβ5 RGD binding domain. Indeed, the αvβ5 integrin is affected by a number of significant substitutions making the pocket below the SDL region narrower than in α5β1, αvβ6 and even αvβ3. Particularly, the presence of the bulky amino acid (β5)-L122 (replacing (β3)-Y122 in αvβ3, (β1)-Y127 in α5β1 and (β6)-Y117 in αvβ6, respectively) together with the residues (β5)-Y166, (β5)-R215, (β5)-R217, might barely restrict the available space for the accommodation of the phg[1] phenyl ring, thus sterically hampering the binding of either **5** or **6** to the αvβ5 integrin.

**Supporting Table 13:** Binding free energy difference (ΔΔG) between the published binding modes and the best ranked solutions predicted by AutoDock 4.2.

| | | Receptor | | | |
|---|---|---|---|---|---|
| | | **α5β1** | **αvβ3** | **αvβ6** | |
| **Peptide** | **5** | 1.0 | 3.0 | 4.3 | lowest energy |
| | | 0.8 | 2.1 | 2.9 | largest cluster |
| | **6** | 1.6 | 1.5 | 1.5 | lowest energy |
| | | 1.2 | 1.5 | 1.3 | largest cluster |

## 8.2. Appendix II:

# Impact of RGD-functionalized Polyproline Spacers on Integrin Mediated Cell Adhesion to Gold Nanoparticle Coated Surfaces

Alexander Bochen,[1] Diego Pallarola,[2] Heike Boehm,[2] Joachim P. Spatz,[2] and Horst Kessler,[1,3]*

[1] Institute for Advanced Study and Center of Integrated Protein Science, Department Chemie, Technische Universität München, Lichtenbergstrasse 4, 85747 Garching, Germany

[2] Department of New Materials and Biosystems, Max Planck Institute for Intelligent Systems, Heisenbergstr. 3, 70569 Stuttgart, Germany & Department of Biophysical Chemistry, University of Heidelberg , INF 253, 69120 Heidelberg, Germany

[3] Chemistry Department, Faculty of Science, King Abdulaziz University, P.O. Box 80203, Jeddah 21589, Saudi Arabia

kessler@tum.de

*To whom correspondence should be addressed.

Institute for Advanced Study and Center of Integrated Protein Science, Department Chemie, Technische Universität München, Lichtenbergstrasse 4, 85747 Garching, Germany. Phone: +49 (0) 89 289 13300. Fax: +49 (0) 89 289 13210. Email: kessler@tum.de.

ABSTRACT

Cell adhesion is mediated by a major class of adhesion proteins, termed integrins. They interact with different ligands of the extracellular matrix (ECM), which provide a scaffold the cell can adhere to. By mimicking the natural ligands, designing a defined surrounding and precisely alter this substrate, influences on cell adhesion can be detailed studied. Herein, we describe the development of monovalent and divalent polyproline spacers of different length, being connected to cyclic pentapeptide integrin ligands of the *c*(-RGDfX-) type, and their functionalization for coating of gold nanoparticle structured surfaces. The polyproline sequence as a spacer is compared to peptides using aminohexanoic acid or

PEG based spacers. The implication of the applied spacer system on integrin αvβ3 ligand binding affinity is determined by ELISA experiments. Coating of the peptides to gold nanoparticle structured surfaces and subsequent cell adhesion studies are used to further determine the implication of the used spacer on cell adhesion to these surfaces. The quality of cell adhesion to the surfaces coated with the different peptides is determined by analyzing the cell adhesion dynamics behavior.

## INTRODUCTION

Cell adhesion is a fundamental process for multicellular organisms and one of the most important protein families mediating this process is termed integrins.[1] These transmembrane spanning glycoproteins mediate adhesion of a cell by connecting the cytoskeleton to proteins of the extracellular matrix (ECM). A common feature of all integrins is the assembly out of two different subunits, an α- and a β-subunit.[2] So far 24 different heterodimeric integrins are known and they can be clustered into four subfamilies.[3] One of them are the RGD recognizing integrins, which possess as a common feature recognition of the three amino acids Arg-Gly-Asp (RGD) as a minimum essential binding motif.[4-6] Several proteins of the ECM contain this tripepeptidic binding motif, vitronectin (Vn) being one of the most prominent ones.[7-9] An important specimen of this protein family playing a pivotal role for initial cell adhesion is integrin αvβ3, binding primarily to Vn.[10] As cell adhesion is crucial in several physiological processes and important in the development of diseases like thrombosis (blood coagulation), osteoporosis (insufficient bone matrix remodeling) or cancer (neo-angiogenesis), this class of proteins has been highly investigated.[3, 10-13] Additionally, improvements in the biocompatibility of implants also rely on the understanding of cell processes forming a stable adhesion onto surfaces.[14, 15]

Highly active peptide ligands incorporating the RGD sequence have been designed by using three principles of peptide structure optimization towards activity and selectivity. First, cyclization and thus conformational restriction of short peptide sequences fixing a matched case conformation of the ligand. Second, optimization of the cyclic peptide by screening the peptide in a D-amino acid scan for improvements in binding affinity and last fine-tuning the affinity by *N*-methylation of amide bonds.[16] This whole procedure is a spatial screening of the protein binding pocket aiming to confer activity and selectivity to a linear lead sequence. For integrins, this procedure lead to the development of Cilengitide,[17] *c*(-RGDf(*N*-Me)Val-), an anti-angiogenic drug which is currently in clinical

phase II and III for treatment of several cancers.[18] To functionalize a surface with such a cyclic pentapeptide, an attachment point for modification by an anchor is needed. For the none *N*-methylated stem peptide, *c*(-RGDfV-), it could be shown that the 5$^{th}$ position within this sequence (valine) can be substituted by any other amino acid without affecting the activity of the peptide.[19, 20] Consequently, many studies used *c*(-RGDfK-) or *c*(-RGDfE-) as ligands and these peptides are modified at the side chain of lysine or glutamic acid by aliphatic or polyethyleneglycol (PEG) based spacers.[21-23] However, by modifications of these positions it became evident that alterations also negatively influenced binding affinity of these new ligands as well. To circumvent this obstacle polyvalent ligands have been designed, possessing more than one binding motif.[24-28] Using the multivalent effect binding affinity was increased, but rather large and bulky peptides having four binding motifs were necessary to improve binding affinity compared to the unmodified cyclic stem peptide.[24] Another feature of these spacers is their high flexibility. Consequently, the length of the spacer can only be calculated as an average, without having precise control of its length by means of design. This flexibility could be one reason for the reduced affinity of these ligands as the pharmacophoric groups, crucial for the essential interaction in the integrin binding pocket, might not be ideally exposed.

To precisely study cell-ECM adhesion interactions, it is first necessary to reduce the complexity of the research question to a well-defined model system. Gold nanoparticle structured surfaces allow a precise alignment of gold nanoparticles in a scalable distance. It was shown that an interparticle distance smaller than 68 nm is sufficient to allow stable cell adhesions, which can be characterized by the development of mature focal adhesion points. However, till now only the interparticle distance could be adjusted and highly flexible spacers, which negatively influenced the binding affinity of the ligand, have been used.

Besides well-known α-helices, β-sheets and γ-turns, amino acid sequences can also adopt many different other secondary structures.[29] Collagens, as the most abundant proteins within mammals, form a triple helix out of three different polypeptide strands. Each strand is characterized by a repetitive amino acid pattern of the sequence Gly-Pro-X or Gly-X-Hyp where X may be any other amino acid. Proline (Pro) and hydroxyproline (Hyp) make up to more than 15% of the total amino acid content, being an example for the use of proline for structural supporting proteins in nature.[30] Proline itself, being geometrically constraint between the secondary amine and carboxylic acid by its cyclic structure, tends to form stable, left handed helices. A polyproline sequence

spontaneously forms in aqueous media a rigid helix of the polyproline II type (PPII). Within this helix, three proline residues construct a full turn of the helix and the fourth residue (i+3) being precisely above the first. Three prolines elongate the helix by about 9.3 Å (Figure 1). This helical feature of the polyproline sequences has been used in a wide range of applications.[31-35]

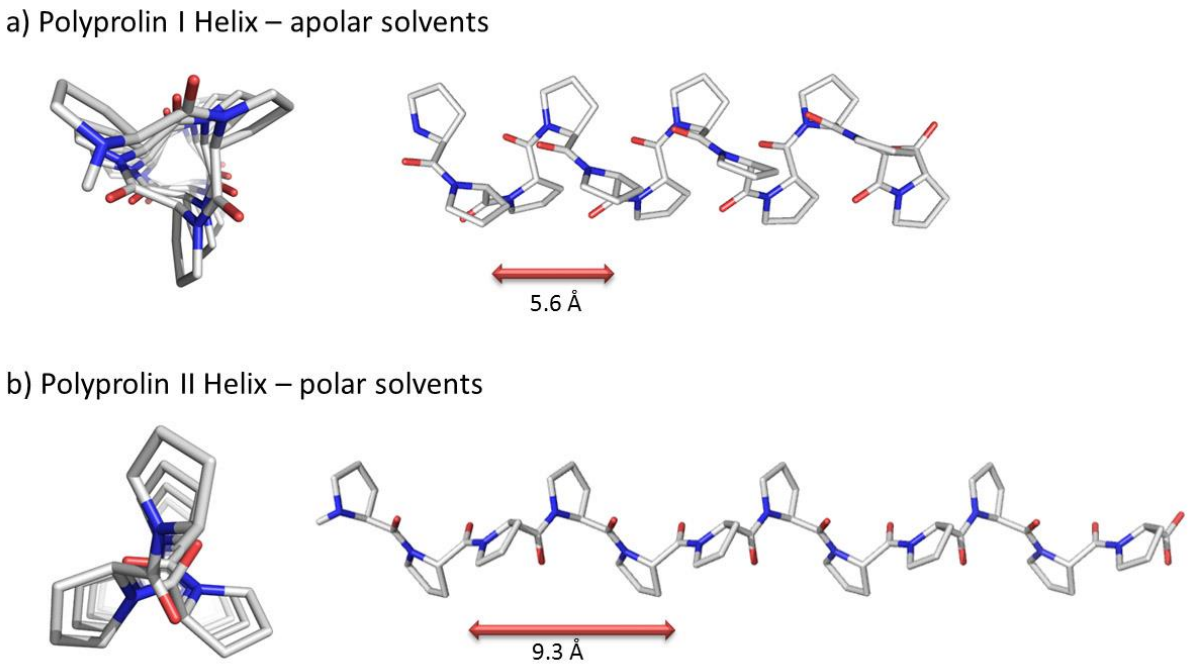


**Figure 1. a)** Calculated structure of the polyproline sequence in apolar solvents forming a polyproline type I helix; **b)** Calculated structure of the polyproline sequence in polar solvents forming a polyproline type II helix.

This study systematically compares the influence of the applied spacer system onto the binding affinity of a ligand to its target. Therefore, cyclic pentapeptides of the *c*(-RGDfX-) type have been used as ligands targeting primarily integrin αvβ3. These ligands have been modified by three kinds of spacers: well used aminohexanoic acid (Ahx) and polyethylenglycole (PEG) type spacers are compared to the polyproline sequence as a spacer system. The former spacers are being examples for flexible and the latter being an example for a rigid spacer. Possible improvements by divalent ligands have additionally been evaluated in the case of the polyproline type spacers (Figure 2). For the assessment of the binding affinity each peptide was tested in an isolated ELISA type receptor assay *in vitro* first, to determine its inhibition constant of Vn binding to integrin αvβ3. All compounds possess a thiol anchor unit to coat them onto gold nanoparticle structured surfaces to allow an investigation of possible differences between the spacer types using a cellular system as a next step. Additionally to the spacer type, the influence

of the spacer length has been examined for spacers of the PEG and polyproline type as well, both *in vitro* and in cellular assays.

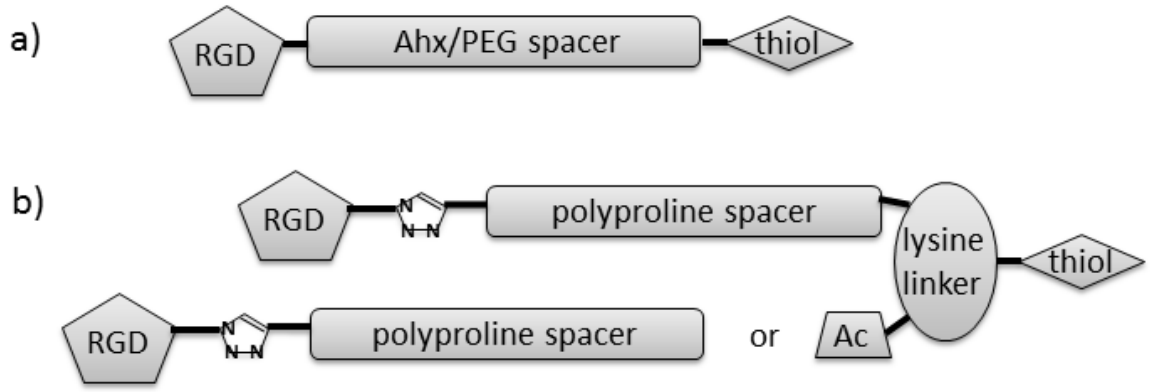


**Figure 2.** General structure of the synthesized peptides. **a)** *cyclo* RGD using aminohexanoic acid (ahx) or polyethyleneglycole (PEG) type spacers, direct attachment of a thiol anchor for surface coating onto the spacer; **b)** *cyclo* RGD ligated by click chemistry to spacers of the polyproline type. Lysine linker was acetylated at Nα position for mono-valent compounds or used as a branching unit for the synthesis of di-valent compounds, spacers starting at both $N^{\alpha}$ and $N^{\varepsilon}$ of the lysine linker possessing a thiol anchor for surface coating.

CHEMISTRY

For the synthesis of peptides two building blocks, the cyclic RGD-peptide and the spacer unit have been synthesized separately first. The linear, side chain protected sequence of the RGD peptide was synthesized on solid phase by Fmoc strategy[36] on tritylchloride polystyrene (TCP) resin, starting with glycine to prevent racemization during the cyclization step later on. As permanent, orthogonal, protecting groups, 2,2,4,6,7-pentamethyldihydrobenzofuran-5-sulfonyl (Pbf) for Arg, *tert.*-butyl for Asp, benzyl (Bz) for Glu and benzyloxycarbonyl (Cbz) for Lys were used. Amino acids (3.0 equiv.) were coupled stepwise with 2-(1*H*-benzotriazole-1-yl)-1,1,3,3-tetramethyluronium tetrafluoroborate (TBTU, 3.0 equiv.) and *N*-hydroxy-benzotriazole (HOBt, 3.0 equiv.) as coupling reagents and *N,N*-diisopropylamine (DIEA, 6.0 equiv.) as a base. Cleavage from the resin by retention of the side-chain protecting groups occurred by a mixture of DCM/acetic acid/trifluorethanol (7:2:1). Cyclization of the linear peptide was done by 2-(7-Aza-1*H*-benzotriazole-1-yl)-1,1,3,3-tetramethyluronium hexafluorophosphate (HATU, 2.0 equiv.), HOBT (2.0 equiv.) and DIEA (10 equiv.) using high dilution to favor intramolecular reaction over the intermolecular reaction. Finally, hydrogenation of the Bz or Cbz group gave the partial protected cyclic peptide. Unprotected glutamic acid of the cyclic peptide was modified by 2-azidoethylamine (4.0 equiv., **11**), HATU (1.05 equiv.)

and DIEA (5.0 equiv.) resulting in the azido modified cyclic peptide **13**, suitable for azide-alkyne 1,3-dipolar cycloaddition (click chemistry) reactions (Scheme 1).[37] 2-azidoethylamine was synthesized from 2-bromoethylamine hydrochloride (1.0 equiv.) and sodium azide (3.0 equiv.).[38]

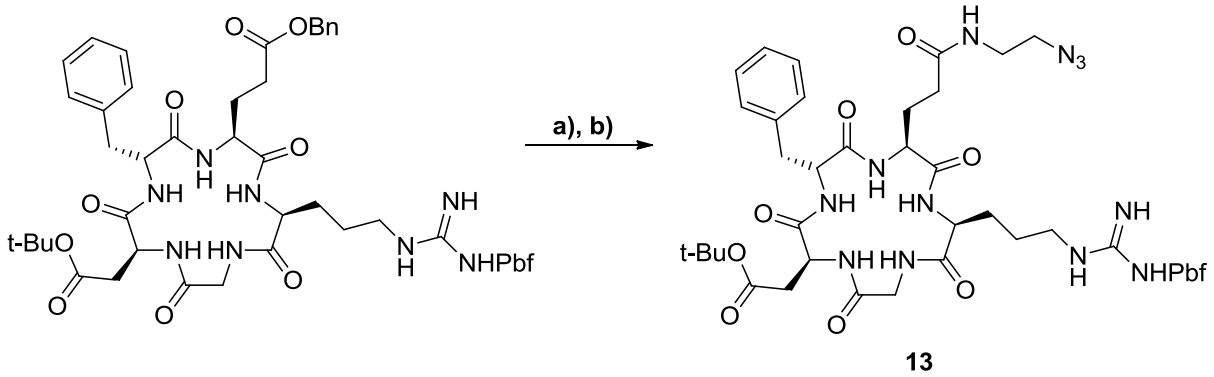


**Scheme 1.** Modification of *cyclo*(-R(Pbf)GD(O$^t$Bu)fE-) for application in click chemistry reactions. **a)** $H_2$, Pd/C, DMA, 12 h; **b)** 2-azidoethylamine, HATU, DMF, 1 h.

PEG and Ahx based spacer systems have been synthesized using the same peptide coupling methodology as described for the synthesis of the linear RGD peptide (s. above). The spacer has been functionalized by trityl protected 3-mercaptopropionic acid (MPA) as a thiol anchor before it is been cleaved from the resin by hexafluorisopropanol (HFIP) (20%/DCM). Each spacer (1.0 equiv.) was reacted with *c*(-R(Pbf)G(O$^t$Bu)fK-) (1.0 equiv.) using HATU (1.0 equiv.) and DIEA (4.0 equiv.). Synthesis of the polyproline based spacers followed a different Fmoc-based synthesis strategy. TCP resin was loaded with Fmoc-Lys(Alloc)-OH, after Fmoc removal the unprotected $N^{\alpha}$ was acetylated by acetic acid anhydride, allyloxycarbonyl protecting group (Alloc) removed by a mixture of *tetrakis*-triphenylphosphinpalladium(0) (0.25 equiv.) and triphenylsilane (10.0 equiv.) in anhydrous DCM. For the synthesis of the polyproline sequence Fmoc-Proline-OH (3.0 equiv.), (1-cyano-2-ethoxy-2-oxoethylidenaminooxy) dimethylamino-morpholino-carbenium hexafluoro-phosphate (COMU,[39, 40] 3.0 equiv.), ethyl(hydroxyimino)cyanoacetate (Oxyma,[41] 3.0 equiv.) and DIEA (6.0 equiv.) were used. Fmoc group was removed by standard conditions and as last step 5-hexynoic acid (3.0 equiv.) coupled by COMU (3.0 equiv.) and DIEA (6.0 equiv.) to the polyproline sequence. In case of the spacer system for divalent peptides, instead of the acetylation step the first polyproline sequence was synthesized at this position as described above. The spacer is cleaved from the solid support by HFIP (20%/DCM), ligated to **13** using $CuSO_4$ (1.0 equiv.) and sodium ascorbate (2.0 equiv.) in a $^t$BuOH/$H_2O$ (1:1-2:1) mixture and purified by RP-HPLC.[37, 42] C-terminal carboxylic acid of the lysine was functionalized as a last step by 2-(tritylthio)ethylamine **12**, 1.0 equiv.), HATU (1.0 equiv.), 1-hydroxy-7-

aza-benzotriazole (HOAt, 1.0 equiv.),DIEA (4.0 equiv.) and finally all remaining protecting groups were removed by trifluoracetic acid/$H_2O$/triisopropylsilane (95:2.5:2.5) treatment and the peptides purified by RP-HPLC (Scheme 2).

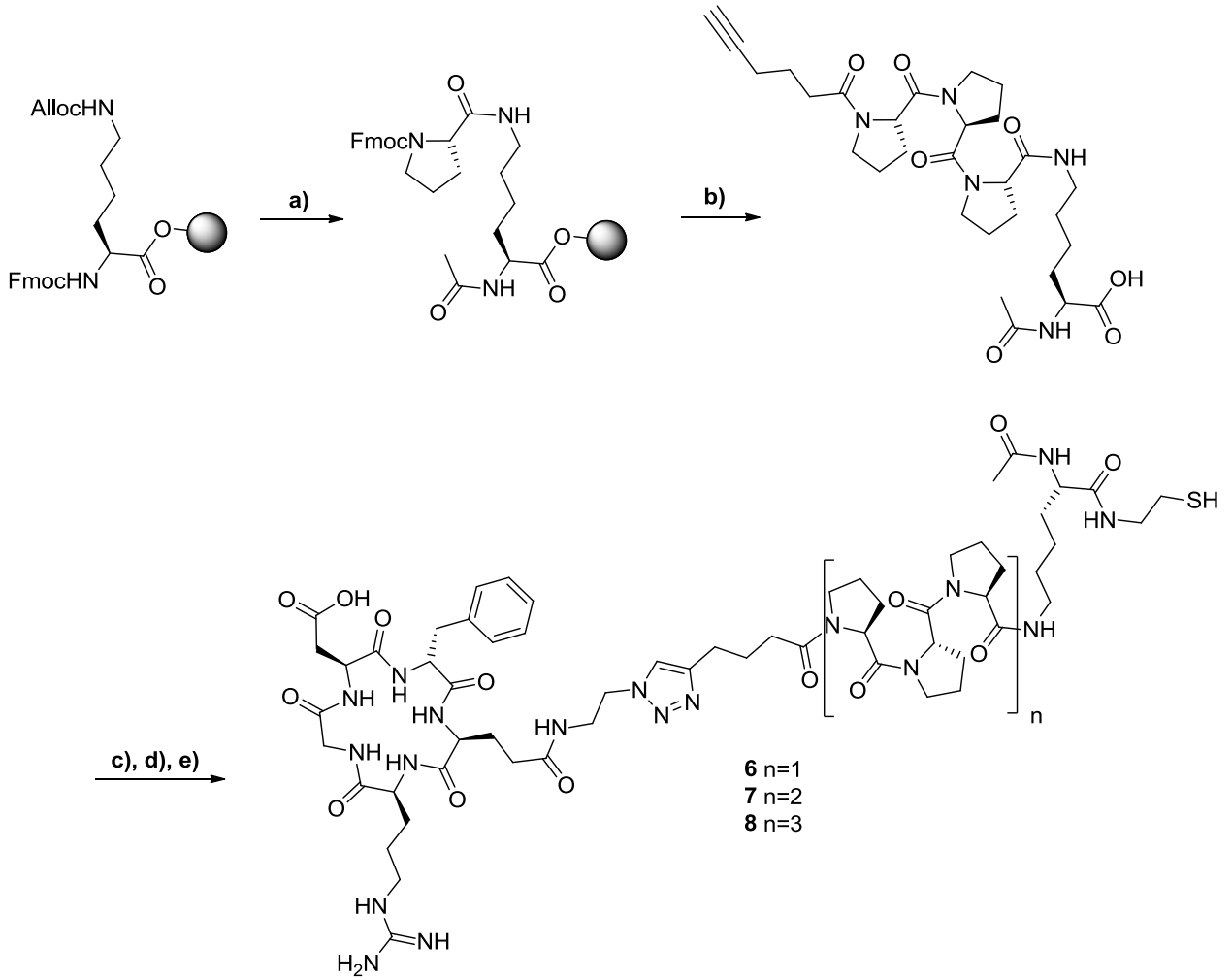


**Scheme 2.** Synthesis of a monomeric proline spacer compound and its ligation with **13**. **a)** *i)* 20% piperidine/NMP (Fmoc dpr.); *ii)* $Ac_2O$, DIEA, NMP; *iii)* $Pd(PPh_3)_4$, phenylsilane, anhydrous DCM, 1 h; *iv)* Fmoc-Pro-OH, COMU, Oxyma, DIEA, NMP, 1 h; (Pro coupling) **b)** *i)* repeats of Fmoc dpr (a *i*) and Pro coupling (a *iv*), 5-hexynoic acid, COMU, DIEA, NMP, 1h, *ii)* 20% HFIP/DCM; **c) 13**, $CuSO_4$, NaAsc., *tert*.-BuOH/$H_2O$, 70 °C, 3 h; **d)** Trt-cystamine, HATU, HOAt, DIEA, DMF, 1 h; **e)** TFA/TIPS/$H_2O$, 1 h.

RESULTS AND DISCUSSION

### *In vitro* inhibition of integrin binding

To evaluate possible differences on integrin binding affinity between the different aliphatic, polyethyleneglycole, proline and proline dimer spacers, all synthesized compounds were tested in a competitive ELISA. Immobilized natural ligand and soluble integrin (Vn/ αvβ3) were used. As internal control, highly active penta-peptide Cilengitide, *c*(-RGDf$^{Me}$V-)[18] was used. Unmodified stem compound known in literature (*c*(-RGDfK-)[19]) has been included to allow further comparison.

Within peptides of the *cyclo*(-RGDfX-) type, the 5$^{th}$ amino acid (X) is known to have no influence on binding affinity.[19] Binding affinity for integrin αvβ3 of monovalent compounds **1-5**, containing only the thiol anchor group (**1**, 3.4 nM), Ahx (**2**, 13.6 nM) and PEG spacers of different lengths (**3**-**5**, 8.4 -16.5 nM), is reduced due to the attachment of the spacer/anchor system when compared to the unmodified peptide *c*(-RGDfK-) (2.6 nM) (Table 1). The binding affinity decreases with increasing spacer length, as it is shown for PEG spacer compounds (**3**-**5**). Remarkably, monovalent compounds (**6**-**8**) are not influenced in their binding affinity towards integrin αvβ3 at all. Their affinity (2.1-2.5 nM) remains unaffected compared to the unmodified *c*(-RGDfK-) (2.6 nM). Although the shortest used polyproline sequence consists only of three consecutive proline residues (**6**), its influence is strikingly. This positive effect towards remained integrin binding affinity is not reduced by increasing polyproline spacer length to six (**7**) or nine (**8**) residues (Figure 3).

Reduced binding affinities for all examined spacer types except for the polyproline spacer might rely on their high flexibility, resulting in a shielding of the pharmacophoric groups. Thus the spacer prevents an ideal interaction with the integrin binding site, as it is not likely for these spacer types to be in a fully extended conformation (all-*trans* conformation). Herein, the incorporation of only three consecutive proline residues stiffens the overall spacer sufficiently to prevent a negative effect of the spacer onto the binding affinity of the peptide.

We then explored the applicability of the polyproline spacer system for divalent ligands, possessing two RGD binding motifs (**9** and **10**). Also for divalent ligands, the polyproline sequence proved to have a positive effect on binding affinity towards integrin αvβ3. Dimerization gave compounds, independent of the polyproline spacer lengths, with subnanomolar activities (0.52 nM, **9**; 0.17 nM, **10**). Compared to the monovalent polyproline peptides (**6**-**8**, 2.1-2.5 nM) binding affinities are increased 4-14 times by

dimerization. Notably, these affinities are in the range of the binding affinity of Cilengitide *c*(-RGDf$^{Me}$V-)[18], the gold standard for integrin αvβ3.

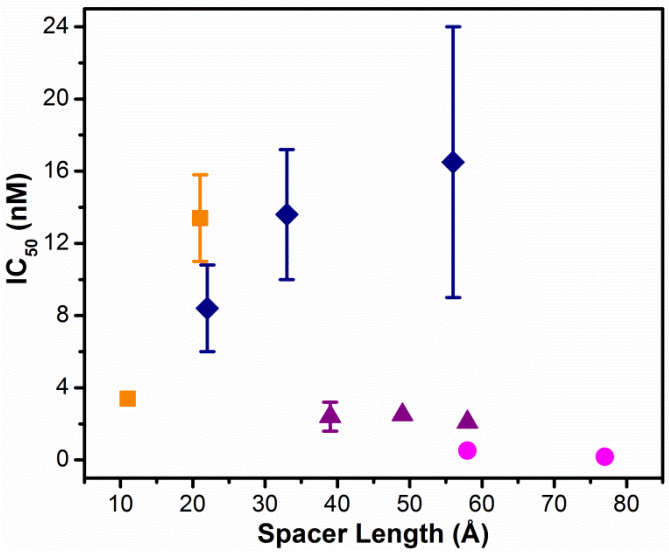


**Figure 28**: Spacer lengths (Å) and types are correlated to the integrin binding affinity ($IC_{50}$). Square: **1-2**, diamonds: **3-5**, triangles: **6-8**, circles: **9-10**.

Multivalent compounds are known for a long time in literature.[43-46] Multivalent compounds have been developed using aminohexanoic acid and PEG based spacers.[24, 26] However, so far this concept had several drawbacks. Either the applied spacers had been very short[47, 48] or tetrameric compounds were needed to regain the activity of the unmodified cyclic peptide, increasing its activity for octamers onwards.[25] In some cases, the polyvalent approach did not work out at all, leading to a decreasing binding affinity in a series from mono-, di- to tetravalent compounds[49] or binding affinity was reduced by increasing spacer length.[27] Herein, we systematically investigated three different spacers in their influence towards the binding affinity of a cyclic RGD ligand. A comparison of Ahx, PEG and polyproline spacers is reported here for the first time. We could clearly confirm the negative influence of the Ahx and PEG spacers with regards to ligand binding affinities, demonstrated the retained binding affinity by using the polyproline sequence and further advancements by dimerization.

**Table 1.** Inhibition of integrin binding to vitronectin (αvβ3) by monovalent and divalent cyclic RGD pentapeptides using different kinds of spacer/anchor systems.

| Peptide | $IC_{50}$ [a] αvβ3 [nM] |
|---|---|
| **1** *c*(-RGDfK[MPA]-) [b] | 3.4 (± 0.4) |
| **2** *c*(-RGDfK[Ahx-MPA]-) | 13.6 (± 2.4) |
| **3** *c*(-RGDfK[Trigas-MPA]-) | 8.4 (± 2.4) |
| **4** *c*(-RGDfK[Hegas-MPA]-) | 13.6 (± 3.6) |
| **5** *c*(-RGDfK[HegasHegas-MPA]-) | 16.5 (± 7.5) |
| **6** Ac-K-[*c*(-RGDfE[HexPPP]-)]-cta | 2.4 (± 0.8) |
| **7** Ac-K-[*c*(-RGDfE[HexPPPPPP]-)]-cta | 2.5 (± 0.4) |
| **8** Ac-K-[*c*(-RGDfE[HexPPPPPPPPP]-)]-cta | 2.1 (± 0.2) |
| **9** [*c*(-RGDfE[HexPPP]-)]$_2$K-cta | 0.52 (± 0.04) |
| **10** [*c*(-RGDfE[HexPPPPP]-)]$_2$K-cta | 0.17 (± 0.03) |
| *c*(-RGDfK-)[b] | 2.6 (± 0.6) |
| Cilengitide[c] | 0.54 (± 0.15) |

[a] $IC_{50}$ values are derived from a competitive ELISA using immobilized ECM protein and soluble integrin. [b] Frequently used, unselective cyclic pentapeptide, unmodified cyclic-peptide of **1-5**.[19] [c] Cilengitide, *c*(-RGDf$^{Me}$V-)[18] is used in ELISA as an internal reference compound for integrin αvβ3 assay. Ahx: 6-amino-hexanoic acid, cta: cystamin, Hegas: heptaethylenglycol amino acid, Hex: 4-(1-(2-aminoethyl)-1*H*-1,2,3-triazol-4-yl)butanoic acid, MPA: mercaptopropionic acid, Trigas: triethylenglycol.

## Cell Adhesion Experiments

To evaluate, if the observed *in vitro* results can be transferred to a cellular system we developed a platform enable us to screen all the ten compounds on one single surface. The effects of the three different kinds of spacers, the influence of PEG and proline spacer length as well as the effect of divalent polyproline spacer systems on cell adhesion behavior have been further examined. The multiwell nanoarray employed for this purpose was constructed on the basis of an already established technique,[50] which allows to pattern onto the glass surface 8 nm gold nanoparticles in a quasi-hexagonal structure with an average interparticle distance of 68 nm. These hierarchically nano-patterned substrates provide an adequate platform to accurately control the geometrical distribution of integrin-anchoring points, which are essential for cell adhesion. Substrates were functionalized in a two-step procedure as previously reported.[51] Briefly, glass areas

between gold nanoparticles were passivated with PEG-terminated siloxane to prevent non-specific cell binding. Then, gold particles inside each identical array, separated by an individual chamber, were functionalized with the corresponding integrin-binding compound as depicted in Fig. 4. Cell adhesion behavior studies were conducted with a rat embryonic fibroblast (REF 52) cell line expressing yellow fluorescent protein (YFP)-paxillin.[52] Cell spreading and focal adhesions (FA) dynamics were followed by fluorescence visualization employing the high throughput microscopy system Hermes Wiscan$^{TM}$. By this approach, the total time required per compound was significantly shortened thus achieving multi-analyte screening with an additional benefit in terms of reproducibility and reduction of variability.

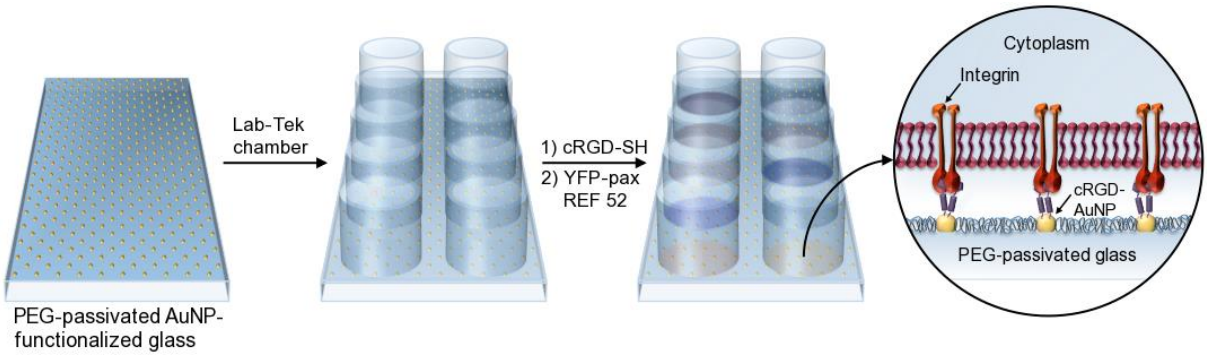


**Figure 4.** Drawing describing the steps involved in the assembly of the multiwell array employed for cell adhesion dynamics studies. Each different color inside the wells represents a different *c*(-RGDfK-)-based compound.

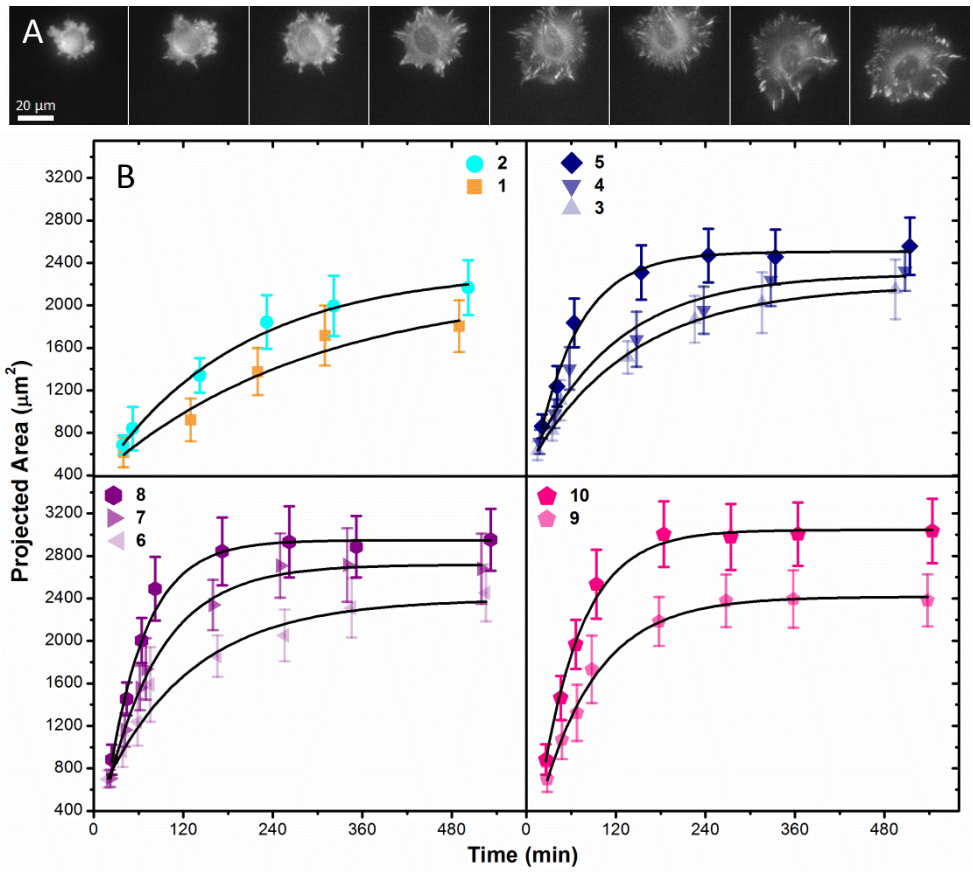


**Figure 5. A)** Visualization of cell spreading dynamics exemplified by YFP-paxillin REF 52 cells onto gold nanopatterned surfaces functionalized with compound **6**. **B)** Cell spreading dynamics followed by fluorescence visualization of YFP-paxillin at 535 nm. Solid line in each plot represents the outcome of fitting the time-resolved spreading area data to a one-phase exponential association function.

Fig. 5 shows the spreading profiles of YFP-paxillin REF 52 cells onto the different peptide-functionalized arrays. Quantitative analysis of spreading rates and projected areas was addressed after cell contact initiation by following YFP fluorescence at 535 nm. For all compounds an isotropic growth following a power-law behavior was observed, similar to previous findings.[53] However, striking differences are evident along the multiwell array. Quantification of the influence of the different compounds on cell spreading dynamics is summarized in Table 2. Peptides containing short hydrophobic spacers, such as compounds **1** and **2** display the slowest spreading rate of the whole set of compounds, being cell growth onto nanopatterns functionalized with compound **2** slightly sharper than for compound **1**. Both, PEG- and proline (monovalent and divalent) *c*(-RGDfK-) peptides evidence faster spreading rates than the previous compounds. Interestingly, spreading rate was observed to increase with the increasing spacer length. This feature was shared for all the compounds in contrast with the *in vitro* behavior findings (Table 1). In those assays, monovalent compounds **1**-**5**, containing alkanethiol

and PEG-thiol as spacer, suffer from a reduction of activity by increasing the spacer length. Presumably, this behavior can be associated with the ability of the spacer to fold, thus shielding the active moiety. The situation is quite different on the surface, where the Au-thiol bond and the interchain van der Waals interactions limit the movement of the molecule.[54] These observations suggest that the spacer length, over its flexibility, plays a dominant role in integrin-mediated adhesion. In the same terms, the behavior of the mono- and divalent compounds **6**-**10** was straightforward. The stiffer polyproline spacers exhibited a remarkable ability for binding-motif presentation, which improved with increasing spacer length and dimerization. Lag time for spreading initiation was also influenced by the nature and length of the spacers. Cells plated onto nanopatterns coated with compounds **6**-**10** (polyproline spacers) and compound **5** (longest PEG-spacer) exhibited flattening and spreading initiation between 15 and 20 min after plating. However, compounds **3**-**4** (shorter PEG spacers) and compound **1**-**2** (short hydrophobic spacers) induced cell flattening around 25 and 40 min, respectively.

**Table 2.** Characterization of cell spreading dynamics. Maximum projected area and time constant values were obtained by fitting the data from each array to a one-phase exponential association function. For the sake of comparison, the spacer length of each compound was included.

| Peptide | Spacer length [Å] | Max. projected area [$\mu m^2$] | Time constant [s] |
|---|---|---|---|
| **1** *c*(-RGDfK[MPA]-) | 11 | 2182 (± 363) | 0.21 (± 0.11) |
| **2** *c*(-RGDfK[Ahx-MPA]-) | 21 | 2334 (± 322) | 0.32 (± 0.05) |
| **3** *c*(-RGDfK[Trigas-MPA]-) | 22 | 2189 (± 330) | 0.44 (± 0.09) |
| **4** *c*(-RGDfK[Hegas-MPA]-) | 33 | 2297 (± 305) | 0.53 (± 0.14) |
| **5** *c*(-RGDfK[Hegas-MPA]-) | 56 | 2491 (± 268) | 1.04 (± 0.14) |
| **6** Ac-K-[*c*(-RGDfE[HexPPP]-)]-cta | 39 | 2394 (± 252) | 0.50 (± 0.08) |
| **7** Ac-K-[*c*(-RGDfE[HexPPPPPP]-)]-cta | 49 | 2718 (± 275) | 0.81 (± 0.05) |
| **8** Ac-K-[*c*(-RGDfE[HexPPPPPPPPP]-)]-cta | 58 | 2949 (± 273) | 1.18 (± 0.12) |
| **9** [*c*(-RGDfE[HexPPP]-)]$_2$K-cta | 39 | 2416 (± 245) | 0.79 (± 0.06) |
| **10** [*c*(-RGDfE[HexPPPPP]-)]$_2$K-cta | 49 | 3046 (± 285) | 1.09 (± 0.08) |

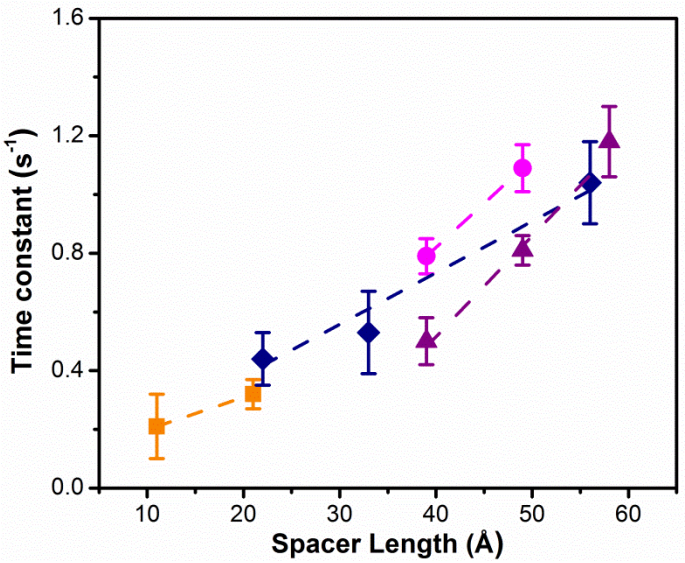


**Figure 6.** Influence of spacer length on cell spreading rate. Orange: **1**-**2**; Blue: **3**-**5**; Purple: **6**-**8**; Pink: **9**-**10**.

**Table 3.** Contribution of equal spacer elongation to the spreading rate of YFP-paxillin REF 52.

| Spacer series | Slope $\Delta k/\Delta L$ [$Å^{-1}$ $s^{-1}$] |
|---|---|
| Hydrophobic | 0.011 |
| Polyethyleneglycol | 0.017 ± 0.005 |
| Polyproline monomer | 0.034 ± 0.006 |
| Polyproline dimer | 0.031 |

To quantitatively assess the impact of the spacer length along the different compounds series we plotted the time constant values for each fitted curve against the maximum spacer length (Fig. 6). Peptides containing hydrophobic (**1**-**2**) and PEG (**3**-**5**) spacers provide similar contribution to the cell spreading, at least within the limited range analyzed for the hydrophobic compounds. Significant differences were observed for the peptides containing polyproline spacers. The enhancement observed on cell adhesion affinity towards these peptides by equal spacer elongation proved to be twice stronger than with the PEG series. Interestingly, increasing the polyproline content led to equivalent contribution for monomers (**6**-**8**) and dimers (**9**-**10**), but with a trend shifted to higher values for the latter, demonstrating the influence of the multimeric effect on cell affinity.

To further characterize the behavior of cell adhesion onto the nanopatterns coated with the different integrin-binding molecules we studied the dynamics of the development of FA. Upon extracellular binding to ligands, integrins cluster and associate with a variety of

submembrane “anchor proteins”, such as paxillin, vinculin and talin, leading to the formation of FA.[9, 55] These complex multimolecular assemblies are the primary structures involved in cell-ECM interactions, serving as surface-sensing entities controlling adhesion-mediated signaling.[56, 57] Therefore the study of FA dynamics can provide a comprehensive insigth into integrin-peptide affinity.

Fig. 7 shows the evolution of the area of FA, relative to the projected area of the cell, as a function of time. Similar to the observation for the spreading initiation, the evolution of FA was significantly affected by the nature of the coating. Cells on surfaces functionalized with short spacer compounds (**1**-**3**) evidenced well-defined FA 2.5 h after seeding. This behavior was even more pronounced in the case of compound **1** where only 50% of the cells exhibited robust paxillin patches at that time point. In contrast, nanopatterns coated with compounds containing longer spacers (**4**-**10**) induced similar features only 60-80 min after cells were plated, showing no significant differences between conditions except for compound **4**. In this case, 60% of the cells displayed mature FA within that time interval. It is worthwhile to mention that this difference cannot be explained only in terms of a spreading initiation delay. We observed that, by subtracting the lag time for spreading initiation, the growth rate of FA on surfaces functionalized with these compounds was higher than for the surfaces functionalized with compounds containing alkane- and short PEG-based spacers. Another notable difference between these two groups of compounds, shorter (**1**-**3**) and longer (**4**-**10**) spacers, was the shape of the obtained curves. While for the compounds **4**-**10**, cells displayed a sustained increase in FA area followed by a slowly declination towards an asymptotic value, cells plated on surfaces coated with compounds **1**-**3** exhibited a nearly constant value (meaning that FA area grows by the same proportion as cell area rises). Further analysis of the maximum values of the corresponding curves revealed that cells coated onto nanopatterns with polyproline-based compounds induced the highest expression of FA of the whole series (Fig. 8). These results highlight the ability of polyproline-based spacers, over alkane and PEG spacers, to efficiently present the active moiety to the cell, thus triggering strong integrin-ligand interactions.

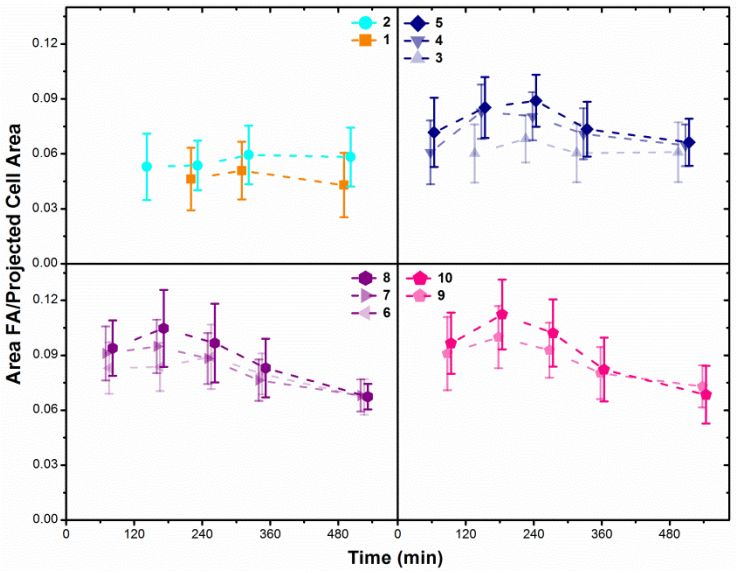


**Figure 7.** FA expression dynamics followed by fluorescence visualization of YFP-paxillin at 535 nm.

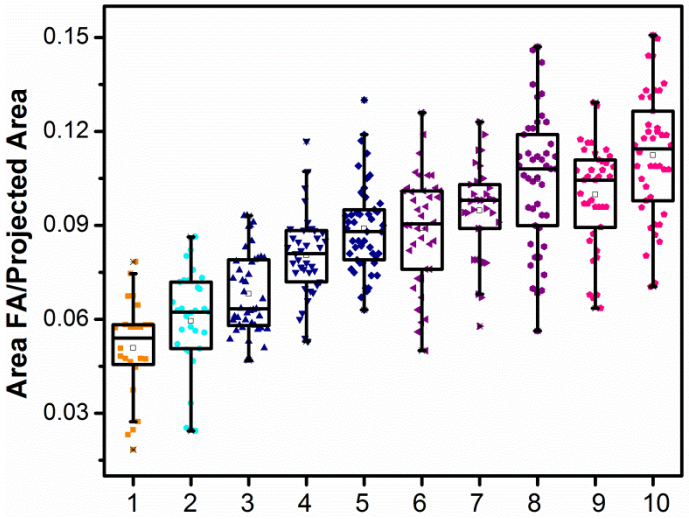


**Figure 8.** Maximum values for FA expression corresponding to the curves in Fig. 7.

## CONCLUSION

In this work we could demonstrate advantages of the polyproline sequence as a spacer over ahx and PEG based spacers connecting RGD peptides to surfaces for integrin mediated cell adhesion. In both, isolated receptor assays of the ELISA type and cell adhesion studies to gold nanoparticle structured surfaces, the compounds being connected by the polyproline spacer to a thiol anchor resulted in ligands with a higher integrin binding affinity and improved cell adhesion properties compared to ligands using spacers of the ahx or PEG type. In detail, functionalization of the ligand by the ahx spacer drastically decreased the ligand binding affinity *in vitro*. Altering the spacer type to a PEG spacer of comparable length as the ahx spacer, ligand binding affinity was not

hampered as much as before. Nevertheless, increasing the length of the PEG spacer further reduces the ligand binding affinity. In contrast, the use of the polyproline sequences as a spacer did not alter the ligands binding affinity towards the targeted integrin αvβ3, independent of its length. Divalent ligands using the polyproline spacer, being connected by a lysine linker, further improved ligand binding affinity 5-14 fold. Coating these peptides to gold nanoparticle structured surfaces and subsequent cell adhesion revealed a similar trend as observed before in the ELISA experiments. The quality of cell adhesion is the lowest, if no spacer or ahx spacer is used and increases by increasing length of the PEG spacer. These results are exceeded, if a monovalent ligand combined with a polyproline spacer is used. Cell adhesion further improves by elongating the proline spacer. Additional benefits can be achieved, if polyproline spacers are used in divalent ligands. Besides the quality of the formed focal adhesion points at the end of the experiment, additionally the cell adhesion dynamics is the fastest by using polyproline spacers compared to the other spacer types. This systematic screening on the influence of the spacer type and spacer length on cell adhesion demonstrates the advantages of the polyproline sequence as a spacer compared to the widespread use of ahx and PEG spacers. This might stimulate the future development of surfaces possessing a higher biocompatibility as well as the possibility to more precisely control the display of a ligand on a surface, thus enabling the study of cell adhesion processes in a more defined surrounding.

## EXPERIMENTAL SECTION

All technical solvents were distilled prior to use. Dry solvents were purchased from *Sigma-Aldrich* or *Fluka*. Protected Fmoc-amino acids and coupling reagents were purchased from *Sigma-Aldrich* (Taufkirchen, Germany) *Novabiochem* (Schwalbach, Germany), *Iris Biotech GmbH* (Marktredwitz, Germany), *PolyPeptide Laboratories* (Strasbourg, France) and *Medalchemy* (Alicante, Spain). TCP-resin was purchased from *PepChem* (Tübingen, Germany). All other chemicals and organic solvents were purchased from commercial suppliers at the highest purity available and used without further purification.

Analytical HPLC was performed using an *Amersham Pharmacia Biotech* Äkta Basic 10F equipment, with a P-900 pump system, a reversed-phase *YMC*-ODS-A $C_{18}$ column (12 nm pore size, 5 µm particle size, 250 mm × 4.6 mm), and UV detection (UV-900, 220 and

254 nm). The system was run at a flow rate of 1.0 mL/min over 30 min using $H_2O$ (0.1% TFA) and MeCN (0.1% TFA) as solvents.

Semi-preparative HPLC was performed using *Waters* equipment: System Breeze; Pump System 1525, UV-Detector 2487 Dual (220 and 254 nm); Driver Software Breeze vers. 3.20; Column material: *YMC*-ODS-A $C_{18}$ (12 nm pore size, 5 µm particle size, 250 mm × 20 mm), *YMC*-ODS-AQ $C_{18}$ (12 nm pore size, 5 µm particle size, 250 mm × 20 mm) or *YMC*basic (proprietary pore size, 5 µm particle size, 250 mm × 20 mm).

HPLC-ESI-MS analyses were performed on a *Hewlett Packard* Series HP 1100 with a *Finnigan* LCQ mass spectrometer using a *YMC*-Hydrosphere $C_{18}$ column (12 nm pore size, 3 µm particle size, 125 mm × 2.1 mm) or *YMC*-Octyl $C_8$ column (20 nm pore size, 5 µm particle size, 250 mm × 2.1 mm). The system uses $H_2O$ (0.1% formic acid) and MeCN (0.1% formic acid) as eluents.

Standard peptide coupling techniques were employed as described below. All yields are not optimized. All tested compounds exhibited ≥ 95% purity determined by RP-HPLC-(MS).

**General procedures**

Peptide synthesis was carried out using TCP resin following standard Fmoc-strategy.[36]

*General procedure I - Loading of TCP resin*: The amino acid (1.2 equiv.) was added to the resin within a syringe equipped with a PP-frit and cannula. DIEA (3.0 equiv.) was mixed with anhydrous DCM (8 mL/g resin) and sucked into the syringe. After rotating at ambient temperature for 1 h, the remaining tritylchloride groups were capped by addition of DCM, MeOH, DIEA (17:2:1, v/v/v, 2 mL/g resin) and rotated for 15 min. After discarding the solution, the resin was washed thoroughly with DCM (3 × 8 mL), NMP (3 × 8 mL), NMP/MeOH (1:1, v/v, 1 × 8 mL) and MeOH (3 × 8 mL). The loading of the resin was determined gravimetrically after drying overnight in a desiccator and ranged from 0.40-0.65 mmol/g.

*General procedure II - Solid phase Fmoc deprotection*: The resin-bound Fmoc protected peptide was treated with a solution of 20% piperidine in NMP (v/v, 3 × 5 min.) and washed with NMP (3 × 8 mL).

*General procedure III - Solid phase peptide coupling using TBTU/HOBt*: TBTU (3.0 equiv.) and HOBt (3.0 equiv.) were dissolved in NMP (0.12 mM). DIEA (6.0 equiv.) was added and the resulting solution transferred to a vial containing the AA (3.0 equiv.). After complete dissolving the solution was sucked into the syringe and rotated for 1 h at ambient temperature. The mixture was discarded and the resin thoroughly washed with NMP (5 × 10 mL/g resin).

*General procedure IV - Solid phase peptide coupling using COMU/Oxyma*: COMU (3.0 equiv.) and Oxyma (3.0 equiv.) were dissolved in NMP (0.12 mM). DIEA (6.0 equiv.) was added and the resulting solution transferred to a vial containing the AA (3.0 equiv.). After complete dissolving the solution was sucked into the syringe containing the resin and rotated for 1 h at ambient temperature. The mixture was discarded and the resin thoroughly washed with NMP (5 × 10 mL/g resin).

*General procedure V - Acylation of amines on solid phase*: The swollen resin was treated 2 × 5 min by a mixture of $Ac_2O$, DIEA and NMP (1:2:7, v/v/v) and washed 5 times with NMP.

*General procedure VI - Removal of Alloc group on solid phase*: The resin was washed three times with DCM and three times with anhydrous DCM. T*etrakis*(triphenylphosphin)palladium(0) (0.25 equiv.) was dissolved together with phenylsilane (10.0 equiv.) in anhydrous DCM. The solution was sucked onto the syringe and rotated at ambient temperature for 1 h. Care had to be taken due to gas formation and the pressure was released from time to time. The resin was washed 2 × 3 min with 0.5% DDTC/DMF and 2 × 3 min with 0.5% DIEA/DMF. The procedure was repeated once or twice, till the resin obtained its original color and washed 5 times with NMP as a last step.

*General procedure VII- Cleavage of side-chain protected peptides from TCP-resin by acetic acid*: The swollen resin was washed 3 times with DCM and 8 mL/g resin of DCM/AcOH/TFE (7:2:1, v/v/v) mixture were added to the resin. After rotating for 30 min the mixture was collected in a round bottom flask and the procedure repeated twice. The resin was washed with DCM (3×) and the washing solution was added to the flask. The mixture is concentrated in vacuo and the acetic acid co-evaporated by addition of toluene. The crude product was dissolved in a mixture of MeCN/$H_2O$, lyophilized and used without further purification.

*General procedure VIII - Cleavage of side-chain protected peptides from TCP resin by HFIP*: A solution of 20% HFIP in DCM (v/v) was added to the resin bound peptide and rotated for 20 min (8 mL/g resin). The procedure was repeated twice, washed with DCM (3 × 8 mL), the collected solutions concentrated in vacuo and the crude product purified by RP-HPLC.

*General procedure IX - Peptide backbone cyclization in solution using HATU/HOBt*: The linear, side-chain protected peptide was diluted in DMF to 1 mM. After addition of HATU (2.0 equiv.), HOBt (2.0 equiv.) and DIEA (10.0 equiv.) the mixture was stirred for 12 h. The solvent was removed under reduced pressure and the cyclic peptide precipitated by addition of water. The peptide was spun down in a centrifuge, washed twice with water and dried in a desiccator.

*General procedure X - Removal of Bz/Cbz protecting group*: The peptide was dissolved in DMA and 100 mg/mol catalyst (10% Pd/C) was added to the solution. The flask was flushed with hydrogen and the solution stirred at ambient temperature and 1 bar $H_2$ pressure for 12 h. The solvent was removed in vacuo, the remaining solid redissolved in a mixture of MeCN/$H_2O$ (9:1), catalyst is filtered off through Celite® and the peptide is obtained by lyophilization.

*General procedure XI - Ligation of peptides using click-chemistry*: Alkyne peptide (1.0 equiv.) and azide peptide (1.0 equiv. per alkyne moiety) were dissolved separately in a mixture of warm $^t$BuOH/$H_2O$ (1:1 – 2:1). 1.0 equiv. (referred to the alkyne) of an aqueous 0.1 M $CuSO_4$ solution was added. The flask was flushed thoroughly by argon and under argon flow 2.0 equiv. (referred to the azide) of freshly prepared aqueous 0.1 M sodium ascorbate solution was added to the mixture. The flask was sealed, equipped with a pressure outlet, heated to 70 °C and stirred for 3 h. The solvent was removed after completion of the reaction by freeze drying and the crude product purified by RP-HPLC.

*General procedure XII – Anchor modification of peptides*: The spacer peptide (1.0 equiv.) was dissolved in DMF and HATU, HOAt (1.0 equiv. each) was added along with DIEA (4.0 equiv.). After stirring the solution at ambient temperature for 1 h, the corresponding amino functionalized molecule was added to the mixture and stirred for one additional hour. The solvent was evaporated and the crude product purified by RP-HPLC.

*General procedure XIII - Full deprotection of cyclic peptides*: The protected, cyclic peptide was treated with a mixture of TFA, water and TIPS (95:2.5:2.5, v/v/v) for 1 h. The deprotected peptide was precipitated by addition to cold diethylether and spun down in a

centrifuge. It is washed twice with cold diethylether, dried under vacuum and purified by RP-HPLC.

**Synthesis of the compounds**

**1** *c(-RGDfK[MPA]-):* The peptide was synthesized by reaction of **14** (1.0 equiv.) and Trt-mercaptopropionic acid (1.05 equiv.) according to *General Procedure XII* and *General Procedure XIII* (2.7 mg, 3.9 µmol, 27%). MS (ESI): 692.5 $(M+H)^+$, 714.5 $(M+Na)^+$, 730.4 $(M+K)^+$. RP-HPLC (10-100%): 11.1 min.

**2** *c(-RGDfK[Ahx-MPA]-):* The compound was synthesized starting from 6-(Trt-3-mercaptopropanamido)hexanoic acid and **14** according to *General Procedure XII* and *General Procedure XIII* (1.0 mg, 1.3 µmol, 9%). MS (ESI): 805.6 $(M+H)^+$, 827.6 $(M+Na)^+$, 843.6 $(M+K)^+$. RP-HPLC (10-100%): 11.6 min.

**3** *c(-RGDfK[Trigas-MPA]-):* Following *General Procedure XII* **14** and **15** are ligated and protecting groups removed (*General Procedure XIII*) to give the product (1.7 mg, 2.0 µmol, 5%). MS (ESI): 837.6 $(M+H)^+$, 859.6 $(M+Na)^+$, 875.6 $(M+K)^+$. RP-HPLC (10-100%): 11.7 min.

**4** *c(-RGDfK[Hegas-MPA]-):* The peptide was synthesized as described for **3** (1.2 mg, 1.2 µmol, 16%). MS (ESI): 1027.7 $(M+H)^+$, 1049.9 $(M+Na)^+$, 1065.5 $(M+K)^+$. RP-HPLC (10-100%): 12.0 min.

**5** *c(-RGDfK[HegasHegas-MPA]-):* The peptide was synthesized as described for **3** (2.5 mg, 1.8 µmol, 30%). MS (ESI): 682.3 $(M+2H)^{2+}$, 693.1 $(M+H+Na)^{2+}$, 1362.8 $(M+H)^+$, 1384.9 $(M+Na)^+$, 1400.9 $(M+K)^+$. RP-HPLC (10-100%): 12.2 min.

**6** Ac-K-[c(-RGDfE[HexPPP]-)]-cta: **18** and **13** are ligated following *General Procedure XI*. Synthesis was continued without RP-HPLC purification by addition of **12** according to *General Procedure XII*. After intermediate RP-HPLC workup protecting groups are removed (*General Procedure XIII*) to yield the final product (1.8 mg, 1.3 µmol, 72%). MS (ESI): 1305.9 $(M+H)^+$, 1327.9 $(M+Na)^+$, 1343.9 $(M+K)^+$. RP-HPLC (10-60%): 14.8 min.

**7** Ac-*K-[c(-RGDfE[HexPPPPPP]-)]-cta:* **13** and **19** are ligated and modified following the same procedures as described for **6** (2.0 mg, 1.3 µmol, 38%). MS (ESI): 533.0 $(M+3H)^{3+}$, 799.0 $(M+2H)^{2+}$, 810.3 $(M+H+Na)^{2+}$, 1597.0 $(M+H)^+$, 1619.9 $(M+Na)^+$. RP-HPLC (10-100%): 10.7 min.

**8** Ac-*K-[c(-RGDfE[HexPPPPPPPPP]-)]-cta:* **13** and **20** are ligated and modified following the same procedures as described for **6** (1.6 mg, 0.9 µmol, 52%). MS (ESI): 944.7 $(M+2H)^{2+}$, 956.6 $(M+H+Na)^{2+}$, 963.9 $(M+H+K)^{2+}$, 1888.0 $(M+H)^{+}$, 1910.0 $(M+Na)^{+}$. RP-HPLC (10-100%): 11.7 min.

**9** *[c(-RGDfE[HexPPP]-)]$_2$K-cta***: 13** and **21** are ligated and modified following the same procedures as described for **6** (0.8 mg, 0.4 µmol, 24%). MS (ESI): 783.0 $(M+2H+Na)^{3+}$, 1161.5 $(M+2H)^{2+}$, 1173.0 $(M+H+Na)^{2+}$, 1180.5 $(M+H+K)^{2+}$. RP-HPLC (10-100%): 11.1 min.

**10** *[c(-RGDfE[HexPPPPPP]-)]$_2$K-cta***: 13** and **22** are ligated and modified following the same procedures as described for **6** (0.7 mg, 0.2 µmol, 19%). MS (ESI): 968.9 $(M+3H)^{3+}$, 976.6 $(M+2H+Na)^{3+}$, 981.6 $(M+2H+K)^{3+}$, 1452.7 $(M+2H)^{2+}$, 1463.8 $(M+H+Na)^{2+}$. RP-HPLC (10-100%): 12.6 min.

**11** *2-Azidoethylamine*: 2-Bromoethylamine hydrochloride (10.0 g, 48.8 mmol, 1.0 equiv.) was dissolved in 30 mL $H_2O$. $NaN_3$ (9.5 g, 146.4 mmol, 3.0 equiv.) was added and the solution stirred at 75 °C for 18 h. NaOH (1.9 g, 48.8 mmol, 1.0 equiv.) was added slowly under stirring, the aqueous phase extracted with DCM (3 × 50 mL), the organic phase dried by $MgSO_4$ and the solvent removed in vacuo to give the product as a pale yellow oil (3.7 g, 42.6 mmol, 87%). Note, the product also evaporates, if the pressure is reduced below 80 mbar and 40 °C heating bath temperature. $^1$H-NMR (250 MHz, DMSO-$d_6$): δ (ppm) = 3.25 (t, $^3J$ = 6.0 Hz, 2H), 2.70 (t, $^3J$ = 6.0 Hz, 2H).

**12** *2-(Tritylthio)ethylamine hydrochloride*: 2-Aminoethylthiol (3.0 g, 38.9 mmol, 1.4 equiv.) and triphenylmethanol (7.23 g, 27.8 mmol, 1.0 equiv.) were dissolved in 50 mL TFA and stirred for 15 min. The solvent was removed in vacuo and the residue redissolved in ethyl acetate (180 mL), being extracted by sat. $NaHCO_3$ (3 × 100 mL) and dried by $MgSO_4$. 30 g silica gel was added after filtration and the solvent removed in vacuo. The product was purified from triphenylmethanol by column chromatography, eluent mixture of hexane/ ethyl acetate = 9:1. The product was eluted by chloroform/methanol (4:1) and the solvent removed in vacuo. The residue was redissolved in *tert.*-butanol and acidified by addition of 1*N* HCl to pH 1.5. The mixture was freeze dried to yield the final product (6.94 g, 19.5 mmol, 70%). $^1$H NMR (250 MHz, DMSO-$d_6$): δ (ppm) = 7.95 (s, 2H), 7.41 – 7.17 (m, 15H), 3.34 (s, 2H), 2.47 (s, 2H). $^{13}$C-NMR (63 MHz, DMSO-$d_6$): δ (ppm) = 144.0, 129.0, 128.2, 126.9, 99.5, 66.4, 37.6. MS (ESI): 243.0 $(Trt)^{+}$. RP-HPLC (10-100%): 18.8 min.

**13** *cyclo[-R(Pbf)GD(O$^t$Bu)fE(Et$N_3$)-]:* TCP resin was loaded with Fmoc-Gly-OH (*General Procedure I*) and the peptide synthesized by following procedure: Repetitive steps of *General Procedure II* and *General Procedure III* until the linear, Fmoc deprotected peptide is obtained, continued by *General Procedure VII*, *General Procedure IX* and *General Procedure X*. Partial protected cyclic peptide *c*(-R(Pbf)GD(O$^t$Bu)fE-) was modified using HATU (1.05 equiv.), **11** (4.0 equiv.) and DIEA (5.0 equiv.) in DMF (0.5 M). This solution was stirred for 1 h at ambient temperature and the solvent removed in vacuo. The crude product is purified by RP-HPLC (333 mg, 380 µmol, 58%). MS (ESI): 925.4 (M-$^t$Bu+H)$^+$, 981.3 (M+H)$^+$, 1003.4 (M+Na)$^+$, 1961.4 (2M+H)$^+$, 1983.6 (2M+Na)$^+$. RP-HPLC (10-100%): 25.7 min.

**14** *cyclo[-RGDfK-]:* TCP resin was loaded with Fmoc-Gly-OH (*General Procedure I*) and the peptide synthesized by following procedure: Repetitive steps of *General Procedure II* and *General Procedure III* were performed till the linear, Fmoc deprotected peptide is obtained, continued by *General Procedure VII*, *General Procedure IX* and *General Procedure XIII*. MS (ESI): 604.5 (M+H)$^+$, 626.5 (M+Na)$^+$, 1207.3 (2M+H)$^+$, 1229.4 (2M+Na)$^+$, 1810.6 (3M+H)$^+$.

**15** *5-Oxo-1,1,1-triphenyl-9,12-dioxa-2-thia-6-azatetradecan-14-oic acid*: 1 g TCP resin was loaded with 2-(2-(Fmoc-2-aminoethoxy)ethoxy)acetic acid (*General Procedure I*) and Fmoc deprotected (*General Procedure II*). 3-(tritylthio)propanoic acid (450 mg, 1.3 mmol, 1.3 equiv.) was added to a solution of TBTU (562 mg, 1.8 mmol, 1.75 equiv.) and DIEA (772 µL, 4.55 mmol, 6.5 equiv.) in 5 mL NMP. The solution was sucked into the syringe, rotated for 1.5 h, washed 5 times thoroughly with NMP. The product is cleaved from the solid support (*General Procedure VII*) and purified by RP-HPLC to give the product (252 mg, 0.51 mmol, 80%). MS (ESI): 243.2 (Trt)$^+$, 516.2 (M+H)$^+$, 987.1 (2M+H)$^+$, 1009.3 (2M+Na)$^+$, 1025.4 (2M+K)$^+$. RP-HPLC (10-100%): 21.6 min.

**16** *5-Oxo-1,1,1-triphenyl-9,12,15,18,21,24-hexaoxa-2-thia-6-azaheptacosan-27-oic acid*: 30 mg TCP resin was loaded with Fmoc-$PEG_6$-OH (2-(2-(2-(2-(2-(2-Fmoc-aminoethoxy)ethoxy) ethoxy)ethoxy)ethoxy)ethoxy)propionic acid) (*General Procedure I*) and Fmoc removed (*General Procedure II*). 3-(tritylthio)propanoic acid (36 mg, 104 µmol, 3.0 equiv.) was added to a solution of COMU (45 mg, 104 µmol, 3.0 equiv.) and DIEA (35.3 µL, 208 µmol, 6.0 equiv.) dissolved in NMP, sucked onto the syringe, rotated for 1 h at ambient temperature and the resin was washed with NMP (5×) and DCM (3×). The product was cleaved from the solid support (*General Procedure VII*) and purified by RP-

HPLC (9.8 mg, 14.3 µmol, 79%). MS (ESI): 243.2 $(Trt)^+$, 684.1 $(M+H)^+$, 706.4 $(M+Na)^+$, 722.4 $(M+K)^+$, 1367.1 $(2M+H)^+$, 1391.7 $(2M+Na)^+$. RP-HPLC (10-100%): 26.2 min.

**17** *5,27-Dioxo-1,1,1-triphenyl-9,12,15,18,21,24,31,34,37,40,43,46-dodecaoxa-2-thia-6,28-diazanonatetracontan-49-oic acid*: The synthesis was performed as described for **16**), except one additional Fmoc deprotection and Fmoc-PEG-OH coupling step (12.3 mg, 12.1 µmol, 67%). MS (ESI): 243.2 $(Trt)^+$, 777.4 $(M+H-Trt)^+$, 799.4 $(M+Na-Trt)^+$, 1019.5 $(M+H)^+$, 1041.7 $(M+Na)^+$, 1057.5 $(M+K)^+$. RP-HPLC (10-100%): 25.9 min.

**18** *Ac-K[PPP(5-hexynoic acid)]-OH:* 333 mg TCP resin was loaded with Fmoc-Lys(Alloc)-OH (*General Procedure I*), Fmoc deprotected (*General Procedure II*), acetylated (*General Procedure V*) and alloc group removed (*General Procedure VI*). The polyproline sequence and its functionalization by 5-hexynoic acid was synthesized by repetitive steps of *General Procedure II* and *General Procedure IV*. The peptide was cleaved from the resin (*General Procedure VIII*) and purified by RP-HPLC (102 mg, 0.18 mmol, 78%). MS (ESI): 574.3 $(M+H)^+$, 596.4 $(M+Na)^+$, 612.4 $(M+K)^+$, 1147.0 $(2M+H)^+$, 1171.5 $(2M+Na)^+$, 1185.4 $(2M+K)^+$. RP-HPLC (10-100%): 10.4 min.

**19** *Ac-K[PPPPPP(5-hexynoic acid)]-OH:* The peptide was synthesized using the same methodology as described for **18** (107 mg, 0.12 mmol, 52%). MS (ESI): 865.4 $(M+H)^+$, 887.7 $(M+Na)^+$, 903.6 $(M+K)^+$, 1730.3 $(2M+H)^+$, 1752.3 $(2M+Na)^+$, 1768.5 $(2M+K)^+$. RP-HPLC (10-50%): 11.6 min.

**20** *Ac-K[PPPPPPPPP(5-hexynoic acid)]-OH:* The peptide was synthesized using the same methodology as described for **18** (183 mg, 0.16 mmol, 68%). MS (ESI): 1156.7 $(M+H)^+$, 1178.9 $(M+Na)^+$, 1196.6 $(M+K)^+$. RP-HPLC (10-100%): 10.2 min.

**21** *(5-hexynoic acid)PPP-K[PPP(5-hexynoic acid)]-OH:* The peptide was synthesized using the same methodology as described for **18**, except for the following modifications: After initial Fmoc removal (*General Procedure II*) of Fmoc-Lys(Alloc)-OH loaded TCP resin, the first polyproline spacer moiety was synthesized by repetitive steps of *General Procedure II* and *General Procedure IV*. The synthesis was continued as described for **18** (213 mg, 0.23 mmol, 38%). MS (ESI): 917.5 $(M+H)^+$, 939.6 $(M+Na)^+$, 955.7 $(M+K)^+$, 1855.5 $(2M+Na)^+$. RP-HPLC (10-100%): 12.5 min.

**22** *(5-hexynoic acid)PPPPPP-K[PPPPPP(5-hexynoic acid)]-OH:* The peptide was synthesized using the same methodology as described for **21** (324 mg, 0.22 mmol, 37%).

MS (ESI): 750.6 $(M+2H)^{2+}$, 1499.5 $(M+H)^{+}$, 1521.8 $(M+Na)^{+}$. RP-HPLC (10-100%): 12.1 min.

**Integrin binding assay (Vn/ αvβ3)**

The inhibiting activity of the integrin ligands was determined in a solid-phase binding assay using coated extracellular matrix protein and soluble integrin. Binding of the integrin was detected by a specific antibody in an enzyme linked immune sorbent assay (ELISA). The assay was based on a previously reported method with some modifications.[58, 59]

αvβ3 assay: Flat-bottom 96-well ELISA plates (*BRAND*, Wertheim, Germany) were coated overnight at 4 °C with 100 µL/well of 1.0 µg/mL vitronectin (Millipore, Schwalbach/Ts., Germany) in carbonate-buffer (15 mM $Na_2CO_3$, 35 mM $NaHCO_3$, pH 9.6). Each well was then washed with PBST buffer (137 mM NaCl, 2.7 mM KCl, 10 mM $Na_2HPO_4$, 2 mM $KH_2PO_4$, 0.01% Tween 20, pH 7.4, 3 × 200 µL) and blocked for 1 h at room temperature with 150 µL/well of TSB-buffer (20 mM Tris-HCl, 150 mM NaCl, 1 mM $CaCl_2$, 1 mM $MgCl_2$, 1 mM $MnCl_2$, pH 7.5, 1% BSA). After being washed three times with PBST, equal volumes of internal standard (Cilengitide) or test compounds were mixed with 2.0 µg/mL human integrin αvβ3 (Millipore, Schwalbach/Ts., Germany) giving a final dilution in TSB buffer of 0.00013 to 10 µM for the inhibitors and 1.0 µg/mL for integrin αvβ3. These solutions (100 µL/well) were incubated for 1 h at room temperature. The plate was washed three times with PBST buffer and 100 µL/well of 2.0 µg/mL primary antibody mouse anti-human CD51/61 (BD Biosciences, Heidelberg, Germany) was added to the plate. After incubation for 1 h at room temperature, the plate was washed three times with PBST and 100 µL/well of 1.0 µg/mL of secondary peroxidase-labeled antibody (anti-mouse IgG-POD, *Sigma-Aldrich*, Taufkirchen, Germany) was added to the plate and incubated for 1 h at room temperature. After washing the plate three times with PBST it got developed by adding 50 µL/well of SeramunBlau® fast (*Seramun Diagnostic GmbH*, Heidesee, Germany) and incubated for 5 min at room temperature. The reaction was stopped with 50 µL/well of 3 M $H_2SO_4$ and the absorbance was measured at 450 nm with a plate reader (POLARstar Galaxy, *BMG Labtechnologies*). Each compound concentration was tested in duplicate and the resulting inhibition curves were analyzed using OriginPro 7.5G software, the inflection point describes the $IC_{50}$ value. Each plate contained Cilengitide as internal standard.

**Biofunctionalized nanopatterns**

Gold nanoparticle quasi-hexagonal patterns were prepared on glass coverslips by means of diblock-copolymer micelle nanolithography as previously described.[50] Briefly, substrates were dip-coated with a solution of polystyrene(1056)-block-poly[2-vinylpyridine($HAuCl_4$)0.25](495) (Polymer Source Inc., Canada) diblock copolymer micelles in *o*-xylene at a constant pulling rate of 1 mm/s and subsequently subjected to $H_2$:Ar 1:10 plasma treatment (350 W, 0.4 mbar, 90 min). Then, substrates were treated thermally in an oven at 500 °C for 48 h. The interparticle distance between adjacent gold nanoparticles was 68 ± 9 nm as determined by scanning electron microscopy. Subsequently, the area between gold nanoparticles was passivated with mPEG-triethoxysilane (2000) to prevent non-specific adhesion according to a procedure described elsewhere.[51] For immunohistochemical experiments, gold nanopatterns on 20 x 20 mm N°1 glass coverslips (Carl Roth, Germany) were employed while cell dynamics experiments were performed on 26 x 76 mm N°1 glass coverslips (Thermo Scientific, Germany). In the latter case, a 16-well Lab-Tek chamber was glued onto the nanopatterned surface with a biocompatible adhesive, Twinsil (Picodent, Germany). This configuration allowed high throughput screening of the whole set of *c*(-RGDfX-)-based molecules with one single surface. Each well, in the case of the multiple-well array, or each 20 x 20 mm surface was functionalized with the corresponding integrin-binding molecule at a concentration of 25 µM in MilliQ water for 1 h at room temperature. Physisorbed material was removed by exhaustive rinsing with MilliQ water and PBS. Cell experiments were carried out immediately after this step.

**Cell culture**

REF 52 (rat embryonic fibroblast) wild type cells and REF 52 expressing yellow fluorescent protein (YFP)-paxillin[52] were cultured in DMEM medium supplemented with 10 % FBS and 1 % L-glutamin (Invitrogen, Germany) at 37 °C and 5 % $CO_2$. For adhesion experiments, cells in culture were rinsed with PBS, released by trypsin-EDTA 0.25% treatment for 5 min at 37 °C, plated at a density of 150 cells/mm$^2$ on the functionalized surfaces in DMEM containing 1% FBS, 1 % L-glutamin and 100 units/mL penicillin-streptomycin (Invitrogen, Germany) and incubated at 37 °C and 5% $CO_2$.

**Immunofluorescence staining**

After 4 h on the nanopatterned surfaces, REF 52 WT cells were washed with PBS at 37 °C and fixed with 2.5% paraformaldehyde in PBS for 10 min. Cells were then

permeabilized with 0.1% Triton X-100 in PBS, blocked with 5% goat serum (Invitrogen, Germany) in PBS for 1 h at room temperature and incubated with 1:100 dilution of rabbit anti-paxillin (Abcam, USA) for 1 h at room temperature. Then, cells were labeled with 1:100 dilution of anti-rabbit Alexa 594-conjugated secondary antibody (Invitrogen, Germany) in 5% goat serum in PBS for 1 h at room temperature. Filamentous actin, membrane and nuclei were labeled with Alexa 488-conjugated phalloidin, Alexa 647-conjugated WGA and DAPI (Invitrogen, Germany), respectively. Cells were examined with a 63/1.25 Oil Ph3 Antiflex Plan-Neofluar objective (Carl Zeiss, Germany) using an Axiovert 200 fluorescent microscope (Carl Zeiss, Germany) equipped with a Hamamatsu (model C10600-10B-H) digital CCD camera (Hamamatsu Photonics, Germany). Image processing was achieved with the Axiovision Image viewer (Carl Zeiss, Germany). FA and Cell area analysis was performed on the 594 and 647 nm channels (16-bit TIF images), respectively, using the image analysis platform WiSoft$^{TM}$ (Idea Bio-Medical, Israel). Briefly, images were first subjected to a low-pass filtration to smooth non-uniformities in intensity and secondly to a high-pass filtration to flatten the image and enhance edges. Finally, the resulting processed images were employed to tune the parameters (threshold, maximum and minimum size of the patches, etc.) for the segmentation module, which defines objects based on their intensity and morphological attributes. For each *c*(-RGDfX-)-based compound at least 50 cells from at least two independent experiments were evaluated.

**Cell dynamics experiments**

YFP-paxillin REF 52 cells were plated on the multiple-well array and immediately mounted on the thermostatized stage of the microscope at 37 °C under 5 % $CO_2$ and controlled humidity. Immunofluorescence visualization of cells was performed with a Hermes WiScan$^{TM}$ (Idea Bio-Medical, Israel) system equipped with an Andor (model iXon 897) digital CCD camera (Andor Technology, USA), a fast AutoFocus device[60] and an automated stage. Cells were examined with a U Plan FL N 60x/0.9 objective (Olympus, Japan) at different time intervals starting 10 min after plating. Each visualization round consisted in the acquisition of 180 images per well with an average acquisition time per image of 0.6 s. Image processing was performed using the image analysis platform WiSoft$^{TM}$ (Idea Bio-Medical, Israel) similarly to that described for the fixed samples using the YFP channel for both FA and Cell area characterization. Each time point of the corresponding *c*(-RGDfX-)-based compound consisted in the evaluation of 50 cells from at least two different multiple-well arrays.

ACKNOWLEDGMENT

The authors gratefully acknowledge financial support from the International Graduate School of Science and Engineering (IGSSE), from the TUM Graduate School (TUM GS) and the Max Planck Society. J. P. Spatz is the Weston Visiting Professor at the Weizmann Institute of Science.

ABBREVIATIONS USED

COMU, (1-cyano-2-ethoxy-2-oxoethylidenaminooxy) dimethylamino-morpholinocarbenium hexafluorophosphate; DAPI, 4',6-diamidino-2-phenylindole; DIEA, diisopropylethylamine; DMEM, Dulbecco's modified Eagle's medium; ECM, extracellular matrix; ELISA, enzyme-linked immunosorbant assay; FA, focal adhesion; FBS, fetal bovine serum; HATU, *O*-(7-azabenzotriazol-1-yl)-*N*,*N*,*N'*,*N'*,-tetramethyluronium hexafluorophosphate; Hegas, heptaethylenglycol amino acid; HFIP, hexafluoroisopropanol; HOAt, 1-hydroxy-7-aza-benzotriazole; HOBt, 1-hydroxy-benzotriazole; MPA, mercaptopropionic acid; Oxyma, ethyl(hydroxyimino)cyanoacetate; POD, peroxidase; PP, polypropylene; REF, rat embryonic fibroblast; TBTU, *O*-(Benzotriazol-1-yl)-*N,N,N',N'*-tetramethyluroniumtetrafluoroborat; TCP, tritylchlorid polystyrene; TIPS, triisopropylsilyl; Vn, vitronectin; YFP, yellow fluorescence protein.

REFERENCES

1. Lowell, C. A.; Mayadas, T. N. Overview: Studying Integrins In Vivo. In *Integrin and Cell Adhesion Molecules*, Shimaoka, M., Ed. Humana Press: **2012**; Vol. 757, pp 369-397.

2. Luo, B. H.; Carman, C. V.; Springer, T. A. Structural basis of integrin regulation and signaling. *Annu Rev Immunol* **2007,** 25, 619-647.

3. Barczyk, M.; Carracedo, S.; Gullberg, D. Integrins. *Cell and Tissue Research* **2010,** Volume 339, 269-280.

4. Ruoslahti, E. RGD and other recognition sequences for integrins. *Annu Rev Cell Dev Biol* **1996,** 12, 697-715.

5. Humphries, J. D.; Byron, A.; Humphries, M. J. Integrin ligands at a glance. *Journal of Cell Science* **2006,** 119, 3901-3903.

6. Ruoslahti, E.; Pierschbacher, M. New perspectives in cell adhesion: RGD and integrins. *Science* **1987,** 238, 491-497.

7. Hynes, R. O. Integrins: Versatility, modulation, and signaling in cell adhesion. *Cell* **1992,** 69, 11-25.

8. Hynes, R. O. The Extracellular Matrix: Not Just Pretty Fibrils. *Science* **2009,** 326, 1216-1219.

9. Zamir, E.; Geiger, B. Components of cell-matrix adhesions. *Journal of Cell Science* **2001,** 114, 3577-3579.

10. Goodman, S. L.; Picard, M. Integrins as therapeutic targets. *Trends in pharmacological sciences* **2012,** 33, 405-412.

11. Cox, D.; Brennan, M.; Moran, N. Integrins as therapeutic targets: lessons and opportunities. *Nature Reviews Drug Discovery* **2010,** 9, 804-820.

12. Liu, Z.; Wang, F.; Chen, X. Integrin alpha(v)beta(3)-Targeted Cancer Therapy. *Drug Dev Res* **2008,** 69, 329-339.

13. Meyer, A.; Auernheimer, J.; Modlinger, A.; Kessler, H. Targeting RGD Recognizing Integrins: Drug Development, Biomaterial Research, Tumor Imaging and Targeting. *Current Pharmaceutical Design* **2006,** 12, 2723-2747.

14. Kantlehner, M.; Finsinger, D.; Meyer, J.; Schaffner, P.; Jonczyk, A.; Diefenbach, B.; Nies, B.; Kessler, H. Selective RGD-Mediated Adhesion of Osteoblasts at Surfaces of Implants. *Angewandte Chemie International Edition* **1999,** 38, 560-562.

15. Kantlehner, M.; Schaffner, P.; Finsinger, D.; Meyer, J.; Jonczyk, A.; Diefenbach, B.; Nies, B.; Hölzemann, G.; Goodman, S. L.; Kessler, H. Surface Coating with Cyclic RGD Peptides Stimulates Osteoblast Adhesion and Proliferation as well as Bone Formation. *Chembiochem* **2000,** 1, 107-114.

16. Weide, T.; Modlinger, A.; Kessler, H. Spatial Screening for the Identification of the Bioactive Conformation of Integrin Ligands. In *Bioactive Conformation I*, Peters, T., Ed. Springer Berlin / Heidelberg: 2007; Vol. 272, pp 1-50.

17. Dechantsreiter, M. A.; Planker, E.; Mathä, B.; Lohof, E.; Hölzemann, G.; Jonczyk, A.; Goodman, S. L.; Kessler, H. N-Methylated Cyclic RGD Peptides as Highly Active and Selective αvβ3 Integrin Antagonists. *Journal of Medicinal Chemistry* **1999,** 42, 3033-3040.

18. Mas-Moruno, C.; Rechenmacher, F.; Kessler, H. Cilengitide: the first anti-angiogenic small molecule drug candidate design, synthesis and clinical evaluation. *Anticancer Agents in Medicinal Chemistry* **2010,** 10, 753-768.

19. Haubner, R.; Gratias, R.; Diefenbach, B.; Goodman, S. L.; Jonczyk, A.; Kessler, H. Structural and functional aspects of RGD-containing cyclic pentapeptides as highly potent and selective integrin avb3 antagonists. *Journal of the American Chemical Society* **1996,** 118, 7461-7472.

20. Laufer, B.; Frank, A. O.; Chatterjee, J.; Neubauer, T.; Mas-Moruno, C.; Kummerlöwe, G.; Kessler, H. The Impact of Amino Acid Side Chain Mutations in Conformational Design of Peptides and Proteins. *Chemistry – A European Journal* **2010,** 16, 5385-5390.

21. Auernheimer, J.; Zukowski, D.; Dahmen, C.; Kantlehner, M.; Enderle, A.; Goodman, S. L.; Kessler, H. Titanium Implant Materials with Improved Biocompatibility through Coating with Phosphonate-Anchored Cyclic RGD Peptides. *Chembiochem* **2005,** 6, 2034-2040.

22. Lieb, E.; Hacker, M.; Tessmar, J.; Kunz-Schughart, L. A.; Fiedler, J.; Dahmen, C.; Hersel, U.; Kessler, H.; Schulz, M. B.; Göpferich, A. Mediating specific cell adhesion to low-adhesive diblock copolymers by instant modification with cyclic RGD peptides. *Biomaterials* **2005,** 26, 2333-2341.

23. Kalinina, S.; Gliemann, H.; López-García, M.; Petershans, A.; Auernheimer, J.; Schimmel, T.; Bruns, M.; Schambony, A.; Kessler, H.; Wedlich, D. Isothiocyanate-functionalized RGD peptides for tailoring cell-adhesive surface patterns. *Biomaterials* **2008,** 29, 3004-3013.

24. Thumshirn, G.; Hersel, U.; Goodman, S. L.; Kessler, H. Multimeric cyclic RGD peptides as potential tools for tumor targeting: solid-phase peptide synthesis and chemoselective oxime ligation. *Chemistry* **2003,** 9, 2717-2725.

25. Wängler , C.; Maschauer, S.; Prante, O.; Schäfer, M.; Schirrmacher, R.; Bartenstein, P.; Eisenhut, M.; Wängler , B. Multimerization of cRGD Peptides by Click Chemistry: Synthetic Strategies, Chemical Limitations, and Influence on Biological Properties. *Chembiochem* **2010,** 11, 2168-2181.

26. Lössner, D.; Kessler, H.; Thumshirn, G.; Dahmen, C.; Wiltschi, B.; Tanaka, M.; Knoll, W.; Sinner, E.-K.; Reuning, U. Binding of Small Mono- and Oligomeric Integrin Ligands to Membrane-Embedded Integrins Monitored by Surface Plasmon-Enhanced Fluorescence Spectroscopy. *Analytical Chemistry* **2006,** 78, 4524-4533.

27. Kubas, H.; Schäfer, M.; Bauder-Wüst, U.; Eder, M.; Oltmanns, D.; Haberkorn, U.; Mier, W.; Eisenhut, M. Multivalent cyclic RGD ligands: influence of linker lengths on receptor binding. *Nuclear Medicine and Biology* **2010,** 37, 885-891.

28. Li, Z. B.; Cai, W.; Cao, Q.; Chen, K.; Wu, Z.; He, L.; Chen, X. (64)Cu-labeled tetrameric and octameric RGD peptides for small-animal PET of tumor alpha(v)beta(3) integrin expression. *J Nucl Med* **2007,** 48, 1162-1171.

29. Liskamp, R. M. J.; Rijkers, D. T. S.; Kruijtzer, J. A. W.; Kemmink, J. Peptides and Proteins as a Continuing Exciting Source of Inspiration for Peptidomimetics. *Chembiochem* **2011,** 12, 1626-1653.

30. Krane, S. The importance of proline residues in the structure, stability and susceptibility to proteolytic degradation of collagens. *Amino Acids* **2008,** 35, 703-710.

31. Kuemin, M.; Schweizer, S.; Ochsenfeld, C.; Wennemers, H. Effects of Terminal Functional Groups on the Stability of the Polyproline II Structure: A Combined Experimental and Theoretical Study. *J Am Chem Soc* **2009,** 131, 15474-15482.

32. Sato, S.-i.; Kwon, Y.; Kamisuki, S.; Srivastava, N.; Mao, Q.; Kawazoe, Y.; Uesugi, M. Polyproline-Rod Approach to Isolating Protein Targets of Bioactive Small Molecules: Isolation of a New Target of Indomethacin. *J Am Chem Soc* **2007,** 129, 873-880.

33. Crespo, L.; Sanclimens, G.; Montaner, B.; Pérez-Tomás, R.; Royo, M.; Pons, M.; Albericio, F.; Giralt, E. Peptide Dendrimers Based on Polyproline Helices. *J Am Chem Soc* **2002,** 124, 8876-8883.

34. Sanclimens, G.; Crespo, L.; Giralt, E.; Albericio, F.; Royo, M. Preparation of de Novo Globular Proteins Based on Proline Dendrimers. *J Org Chem* **2005,** 70, 6274-6281.

35. Fillon, Y. A.; Anderson, J. P.; Chmielewski, J. Cell Penetrating Agents Based on a Polyproline Helix Scaffold. *J Am Chem Soc* **2005,** 127, 11798-11803.

36. Fields, G. B.; Noble, R. L. Solid phase peptide synthesis utilizing 9-fluorenylmethoxycarbonyl amino acids. *International Journal of Peptide and Protein Research* **1990,** 35, 161-214.

37. Meldal, M.; Tornøe, C. W. Cu-Catalyzed Azide−Alkyne Cycloaddition. *Chem Rev* **2008,** 108, 2952-3015.

38. Angelos, S.; Yang, Y.-W.; Patel, K.; Stoddart, J. F.; Zink, J. I. pH-Responsive Supramolecular Nanovalves Based on Cucurbit[6]uril Pseudorotaxanes. *Angewandte Chemie International Edition* **2008,** 47, 2222-2226.

39. El-Faham, A.; Albericio, F. Morpholine-Based Immonium and Halogenoamidinium Salts as Coupling Reagents in Peptide Synthesis. *Journal of Organic Chemistry* **2008,** 73, 2731-2737.

40. El-Faham, A.; Funosas, R. S.; Prohens, R.; Albericio, F. COMU: A Safer and More Effective Replacement for Benzotriazole-Based Uronium Coupling Reagents. *Chemistry – A European Journal* **2009,** 15, 9404-9416.

41. Subirós-Funosas, R.; Prohens, R.; Barbas, R.; El-Faham, A.; Albericio, F. Oxyma: An Efficient Additive for Peptide Synthesis to Replace the Benzotriazole-Based HOBt and HOAt with a Lower Risk of Explosion. *Chemistry – A European Journal* **2009,** 15, 9394-9403.

42. Rostovtsev, V. V.; Green, L. G.; Fokin, V. V.; Sharpless, K. B. A Stepwise Huisgen Cycloaddition Process: Copper(I)-Catalyzed Regioselective “Ligation” of Azides and Terminal Alkynes. *Angewandte Chemie International Edition* **2002,** 41, 2596-2599.

43. Mammen, M.; Choi, S.-K.; Whitesides, G. M. Polyvalent Interactions in Biological Systems: Implications for Design and Use of Multivalent Ligands and Inhibitors. *Angewandte Chemie International Edition* **1998,** 37, 2754-2794.

44. Kessler, H.; Schudok, M.; Haupt, A. In *Dimerization of Cyclic Hexapeptides: Strong Increase of Biological Activity*, Peptides 1988: Procedings of the 20th European Peptide Symposium, Tübingen, 1988; Jung, G.; Bayer, E., Eds. Walter de Gruyter, Berlin, New York: Tübingen, 1988; pp 664-666.

45. Gestwicki, J. E.; Cairo, C. W.; Strong, L. E.; Oetjen, K. A.; Kiessling, L. L. Influencing Receptor−Ligand Binding Mechanisms with Multivalent Ligand Architecture. *Journal of the American Chemical Society* **2002,** 124, 14922-14933.

46. Kiessling, L. L.; Gestwicki, J. E.; Strong, L. E. Synthetic multivalent ligands in the exploration of cell-surface interactions. *Current Opinion in Chemical Biology* **2000,** 4, 696-703.

47. Li, Z.-b.; Cai, W.; Cao, Q.; Chen, K.; Wu, Z.; He, L.; Chen, X. 64Cu-Labeled Tetrameric and Octameric RGD Peptides for Small-Animal PET of Tumor αvβ3 Integrin Expression. *Journal of Nuclear Medicine* **2007,** 48, 1162-1171.

48. Wu, Y.; Zhang, X.; Xiong, Z.; Cheng, Z.; Fisher, D. R.; Liu, S.; Gambhir, S. S.; Chen, X. microPET Imaging of Glioma Integrin αvβ3 Expression Using 64Cu-Labeled Tetrameric RGD Peptide. *Journal of Nuclear Medicine* **2005,** 46, 1707-1718.

49. Yim, C. B.; Dijkgraaf, I.; Merkx, R.; Versluis, C.; Eek, A.; Mulder, G. E.; Rijkers, D. T.; Boerman, O. C.; Liskamp, R. M. Synthesis of DOTA-conjugated multimeric [Tyr3]octreotide peptides via a combination of Cu(I)-catalyzed "click" cycloaddition and thio acid/sulfonyl azide "sulfo-click" amidation and their in vivo evaluation. *Journal of Medicinal Chemistry* **2010,** 53, 3944-3953.

50. Glass, R.; Möller, M.; Spatz, J. P. Block copolymer micelle nanolithography. *Nanotechnology* **2003,** 14, 1153-1160.

51. Blümmel, J.; Perschmann, N.; Aydin, D.; Drinjakovic, J.; Surrey, T.; Lopez-Garcia, M.; Kessler, H.; Spatz, J. P. Protein repellent properties of covalently attached PEG coatings on nanostructured SiO2-based interfaces. *Biomaterials* **2007,** 28, 4739-4747.

52. Zamir, E.; Katz, B. Z.; Aota, S.; Yamada, K. M.; Geiger, B.; Kam, Z. Molecular diversity of cell-matrix adhesions. *Journal of Cell Science* **1999,** 112, 1655-1669.

53. Chang, F.; Lemmon, C. A.; Park, D.; Romer, L. H. FAK Potentiates Rac1 Activation and Localization to Matrix Adhesion Sites: A Role for βPIX. *Molecular Biology of the Cell* **2007,** 18, 253-264.

54. Vericat, C.; Vela, M. E.; Benitez, G.; Carro, P.; Salvarezza, R. C. Self-assembled monolayers of thiols and dithiols on gold: new challenges for a well-known system. *Chemical Society Reviews* **2010,** 39, 1805-1834.

55. Critchley, D. R. Focal adhesions – the cytoskeletal connection. *Current Opinion in Cell Biology* **2000,** 12, 133-139.

56. Geiger, B.; Bershadsky, A. Assembly and mechanosensory function of focal contacts. *Current Opinion in Cell Biology* **2001,** 13, 584-592.

57. Zaidel-Bar, R.; Cohen, M.; Addadi, L.; Geiger, B. Hierarchical assembly of cell-matrix adhesion complexes. *Biochem Soc Trans* **2004,** 32, 416-420.

58. Mas-Moruno, C.; Beck, J. G.; Doedens, L.; Frank, A. O.; Marinelli, L.; Cosconati, S.; Novellino, E.; Kessler, H. Increasing avb3 Selectivity of the Anti-Angiogenic Drug Cilengitide by *N*-Methylation. *Angew Chem Int Ed Engl* **2011,** 50, 9496-9500.

59. Chatterjee, J.; Ovadia, O.; Zahn, G.; Marinelli, L.; Hoffman, A.; Gilon, C.; Kessler, H. Multiple N-methylation by a designed approach enhances receptor selectivity. *Journal of Medicinal Chemistry* **2007,** 50, 5878-5881.

60. Liron, Y.; Paran, Y.; Zatorsky, N. G.; Geiger, B.; Kam, Z. Laser autofocusing system for high-resolution cell biological imaging. *Journal of Microscopy* **2006,** 221, 145-151.